WOOD RESEARCH doi.org/10.37763/wr.1336-4561/66.5.700710
e-ISSN 2729-8906
66(5): 2021 700-710 pp.

EFFECT OF NATURAL AND ACCELERATED AGING ON THE PROPERTIES OF WOOD-PLASTIC COMPOSITES

LIYUAN ZHAO, BIN LV, XIAORUI PENG, YUEJIN FU
CHINESE ACADEMY OF FORESTRY
P.R.CHINA

(RECEIVED DECEMBER 2020)

ABSTRACT

The correspondence of natural and laboratory-accelerated aging of WPC has long been a highly important problem discussed by many scholars. In this work, the changes in moisture content (MC), modulus of rupture (MOR), modulus of elasticity (MOE), screw holding force and creep recovery rates of two groups of wood-plastic composites (WPC) after natural and accelerated aging (high-low temperature cycles and freeze-thaw cycles) were studied to provide guidance for the use of WPC in outdoor applications. The results showed that, after the natural aging and freeze-thaw cycles treatments, MC increased significantly with both 167% of the untreated value of wood-HDPE composites with 30% wood fiber content and a thickness of 25 mm (W_{25}), while 67% and 133% of the wood-HDPE composites with 30% wood fiber content and a thickness of 20 mm (W_{20}), but is almost unchanged after the treatment with high-low temperature cycles. The mechanical strength, including MOR, MOE, screw holding force and creep recovery rate, decreased after natural and accelerated aging. The greatest decreases of MOR, MOE, screw holding force and creep recovery rate were 14%, 13%, 21%, and 7% for W_{25}, while 5%, 8%, 8%, and 14% for W_{20} respectively. Environmental aging can reduce the strength of WPC, but the bending strength retention rate is more than 85%, showing that performance of WPC is relatively stable compared to wood materials, which is one of the reasons for the widely use of WPC in outdoor applications.

KEYWORDS: Natural aging, high-low temperature cycles, freeze-thaw cycles, creep performance.

INTRODUCTION

Wood-plastic composites (WPC) are composites that contain wood fiber and thermosets or thermoplastics. WPCs are environmentally-friendly materials because they reduces

the deforestation and the negative impact of large-scale use of plastics on the environment. Wood-thermoset composites were first developed in the early 1900s. An early commercial composite composed of phenol-formaldehyde and wood fiber was reported in 1916 and was used as a gearshift knob for the Rolls Royce automobile (Clemons 2002). Because thermosets are plastics that cannot be melted by reheating once cured, wood-plastic composites are generally materials consisting of wood fiber mixed with thermoplastic and additives in a certain proportion. The WPC industry has experienced tremendous growth in recent years because WPC combine the desirable durability of plastics with the cost-effectiveness of wood fibers as a filler or reinforcing agent (Mengeloglu et al. 2000, Clemons 2002, Pilarski and Matuana 2005, Zini et al. 2011). The addition of wood to unfilled plastic can greatly stiffen the plastic but often makes it more brittle (Clemons 2002). WPC can be used for floors, decking, fencing, landscape timbers, plank roads, leisure chairs, and decorative boards (Pilarski and Matuana 2005, Badji et al. 2017).

The influence of wood species, wood flour content and other additives such as tinder fungus on the physical and mechanical properties of WPC has long been studied in the previous research (Stark et al. 2004, Kaymakci et al. 2016, Chen et al. 2017, Xu et al. 2017). Although the durability of WPC is better than that of the solid wood (Albrektas et al. 2020), researches on the durability are very important because of the wildly use of WPC in exterior applications. Pilarski and Matuana (2005, 2006) examined the effects of accelerated freeze-thaw actions on the durability of wood fiber-plastic composites and showed that the stiffness of the composites decreased significantly after only two freeze-thaw cycles, regardless of both the wood species and content.

Temperature and exposure time have important effects on the mechanical properties of WPC (La Mantia and Morreale 2008). Wang and Morrel (2005) studied the effects of moisture and temperature cycling on the properties of WPC and showed that moisture sorption tends to increase with the number of wet/dry cycles and is associated with a significant reduction in MOR and MOE.

The correspondence of natural and laboratory-accelerated aging of WPC has always been a highly important problem investigated by many scholars in order to enable accurate prediction of the long-term properties of WPCs. However, previous studies did not include investigations of the difference between wet and dry state with various treatments. In this work, the properties such as moisture content (MC), modulus of rupture (MOR), modulus of elasticity (MOE), screw holding force and creep performance of WPC after the natural aging, high-low temperature cycles and freeze-thaw cycles are studied in order to providing guidance for the use of WPC in outdoor applications.

MATERIALS AND METHODS

Materials

Two groups of WPC samples containing poplar flour, plastics and processing aids in the proportions of 30:65:5, were used for the experiments. The samples thicknesses were 25 mm and 20 mm, respectively.

40 mesh flours and high density polyethylene (HDPE) were mixed in a co-rotating twin-screw extruder. The densities of the two specimens were 1.15 and 1.10 g.cm^{-3}, respectively. Tab. 1 shows the designations of the specimens.

Treatments for natural aging

The specimens are exposed in an outdoor natural site for 1 year on a galvanized steel rack in Beijing, China. The exposure conditions included four annual seasons (January 10th, 2019 to January 10th, 2020) allowing us to consider the contribution of each season and examine the long-term degradation effects. In 2019, the average temperature in Beijing was 12.5°C, while the annual precipitation was 511.1 mm.

Treatments for high-low temperature cycles

According to the GB/T 24508: 2009, the specimens were placed at room temperature 23 ± 2°C for 1 h, then were placed in a low-temperature test chamber at -20 ± 2°C for 6 h, and then were placed in a dry oven at 60 ± 2°C for 16 h after storing at room temperature 23 ± 2°C for 1 h. This was designated as a single treatment cycle. In this work, the specimens were treated by 3 high-low temperature cycles.

Treatments for freeze-thaw cycles

Freeze-thaw cycles were carried out according to GB/T 24508: 2009. One complete freeze-thaw cycle consisted of three stages: *(1)* water soaking; *(2)* freezing for 24 h; *(3)* thawing for 24 h. The specimens were immersed in the water (20°C) for 24 h, then placed in a low-temperature test chamber at a temperature of -30 ± 2°C for 24 h, and then were removed and placed at room temperature 23 ± 2°C for 24 h. This was designated as single treatment cycle. In this work, the specimens were treated by 3 freeze-thaw cycles. Tab. 1 shows the treatment conditions and testing parameters of the materials.

Tab. 1: Designations, treatment conditions and testing parameters of materials.

Des.	Thickness (mm)	Density (g·cm^{-3})	HDPE (wt%)	Wood flour (wt%)	Treatment conditions	Testing parameters
W_{25}	25	1.15	65	30	Untreated	M_0, MOR_0, MOE_0, S_0, C_0
					natural aging	M_1, MOR_1, MOE_1, S_1, C_1
					high-low temperature cycles (for 3)	M_2, MOR_2, MOE_2, S_2, C_2
					freeze-thaw cycles (for 3)	M_3, MOR_3, MOE_3, S_3, C_3
W_{20}	20	1.10	65	30	Untreated	M_0, MOR_0, MOE_0, S_0, C_0
					natural aging	M_1, MOR_1, MOE_1, S_1, C_1
					high-low temperature cycles (for 3)	M_2, MOR_2, MOE_2, S_2, C_2
					freeze-thaw cycles (for 3)	M_3, MOR_3, MOE_3, S_3, C_3
One complete high-low temperature cycle: 23°C for 1 h, -20°C for 6 h, 23°C for 1 h, 60°C for 16 h; One complete freeze-thaw cycle: 20°C (in water) for 24 h, -3°C for 24 h, 2°C (room temperature) for 16 h.						

Measurement of MC

MCs for two groups of untreated specimens (M_0), specimens after natural aging (M_1), specimens after 3 high-low temperature cycles (M_2), and specimens after 3 freeze-thaw cycles (M_3) were examined according to ISO 16979: 2003. MC values were calculated using Eq. 1:

$$MC = \frac{M_n - m}{m} \times 100\%, \quad (1)$$

where: M_n - the initial mass of the specimen with different treatments at 23 ± 2°C and a humidity of 50% for 24 h (kg), m - the mass after drying at 103°C for 24 h (kg).

Measurement of MOR and MOE

Mechanical characterizations were carried out at 20 ± 2°C and 65 ± 5% RH. The MOR and MOE values for the untreated specimens (MOR_0 and MOE_0), specimens after natural aging (MOR_1 and MOE_1), specimens after 3 high-low temperature cycles (MOR_2 and MOE_2), and specimens after 3 freeze-thaw cycles (MOR_3 and MOE_3) were obtained according to ISO 16978: 2003.

A Universal Mechanical Testing Machine (SHIMADZU AG-IS 50KN, Japan) with the maximum load of 50 kN was used for the measurements. The bending load was applied at a rate of 10 mm·min^{-1} until the failure of the specimen. MOR and MOE were calculated using Eqs. 2 and 3:

$$MOR = \frac{3F_{max}L}{2bh^2} \quad (2)$$

$$MOE = \frac{FL^3}{4bh^3s} \quad (3)$$

where: F_{max} - the maximum load (N), L - the length of span (mm), b - the width of the specimen (mm), h - the thickness of the specimen (mm), F - the load increment on the straight-line portion of the load-deformation curve (N), s - the deformation corresponding to F (mm).

Measurement of screw holding force

The screw holding force for the untreated specimens (S_0), specimens after natural aging (S_1), specimens after 3 high-low temperature cycles (S_2), and specimens after 3 freeze-thaw cycles (S_3) were examined according to ISO 27528: 2009.

Measurement of creep performance

The creep recovery rate for the untreated specimens (C_0), specimens after natural aging (C_1), specimens after 3 high-low temperature cycles (C_2), and specimens after 3 freeze-thaw cycles (C_3) were examined according to GB/T 29418: 2012. These values were obtained using Eq. 4:

$$C = \frac{d_1 - d_2}{d_1 - d_0} \times 100\% \quad (4)$$

where: d_0 - deformation before loading (mm), d_1 - deformation after loading for 24 h (mm), d_2 - deformation after taking off loading for 24 h (mm).

Data analysis

The SPSS statistical software, (SPSS Inc, Chicago, IL, USA), was used for data analysis. Duncan multiple comparison tests were carried out to analyze whether the effect of natural aging or artificial aging was significant.

RESULTS AND DISCUSSION

Effects of aging on MC

Fig. 1 shows the MC results for the two groups of WPC specimens including untreated, treated by natural aging, high-low temperature cycles and freeze-thaw cycles. MC values increased significantly after the natural aging and freeze-thaw cycles. Compared to that of the untreated sample, the MC of W_{25} and W_{20} increased by 167% and 67% after the natural aging, and by 167% and 133% after the freeze-thaw cycles, respectively. However, it is almost unchanged after the treatment with the high-low temperature cycles.

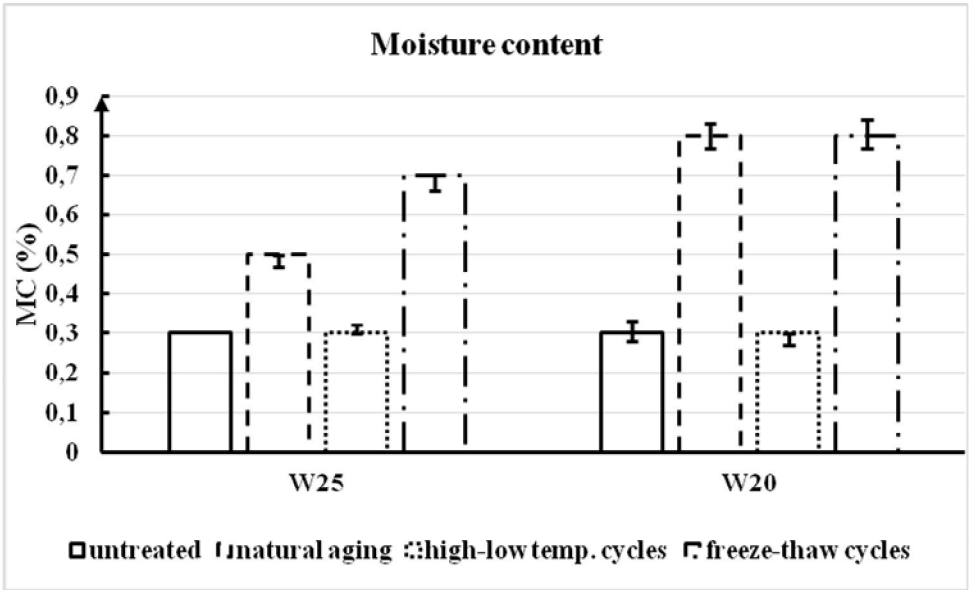

Fig. 1: MC of W_{25} and W_{20} specimens for untreated one, after treatments of natural aging, high-low temperature cycles and freeze-thaw cycles.

The weight of WPC is mainly related to wood fiber or powder and is not affected by PE, PP and PVC (Pilarski and Matuana 2005, Xiao 2010). In the process of natural aging, WPC experienced the effect of rain and snow. Due to the effect of hydroxyl (-OH) in wood fiber, WPC will be accompanied by the breaking and recombination of the hydrogen bond in the process of natural aging (Xiao 2010, Zhao et al. 2015a), resulting in the mass increase after aging that leads to the increase in the MC value. The weight of WPC increases after freeze-thaw cycles due to the existence of water (Pilarski and Matuana 2005). However, when it undergoes high-low temperature cycles, the material does not involve the condensation and melting of water, and therefore the MC value was not changed after the treatment by high-low temperature cycles.

Effects of aging on MOR and MOE

Fig. 2 and 3 shows the MOR and MOE of two groups of WPC specimens for the untreated case, and specimens after treatments of natural aging, high-low temperature cycles and freeze-thaw cycles. The MOR and MOE values of the two groups of WPC decreased after the treatment. This is consistent with the results of previous studies (Badji et al. 2017). Relative to that of the untreated specimen, the MOR values of W_{25} after the treatments of natural aging, high-low temperature cycles and freeze-thaw cycles decreased by 14%, 8%, and 4%, respectively. The corresponding MOR values of W_{20} decreased by 3%, 5%, and 0%, respectively, relative to the MOR of the untreated specimen. The MOE of WPC showed similar changes after the treatment. The MOE of W_{25} decreased by 13%, 8%, and 5%, while it decreased by 8%, 6%, and 3% for W_{20}. These results suggest that these artificial weathering conditions degrade lead to a weaker degradation of the mechanical properties than natural aging, in agreement with the results of Badji et al. (2017).

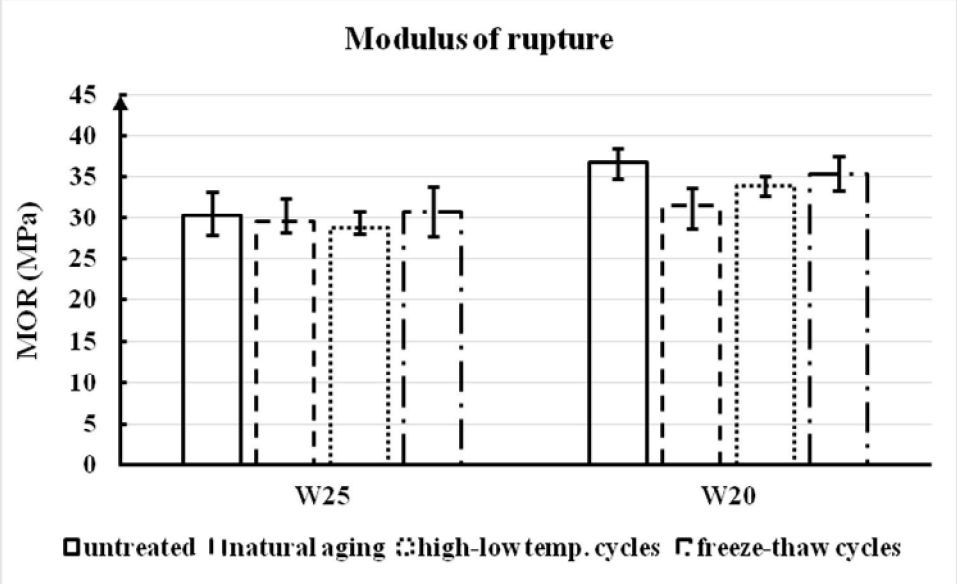

Fig. 2: MOR for untreated specimens, and specimens after treatments of natural aging, high-low temperature cycles and freeze-thaw cycles.

When the material undergoes high-low temperature cycles, the plastic produces larger thermal deformation due to the different expansion of wood fiber and plastic (Chatterji 1999a, Clemons 2002), resulting in the decrease of the adhesion strength between the fiber and plastic. This leads to the lower MOR and MOE values of WPC after the high-low temperature cycles.

Both MOR and MOE also decreased when the material underwent the freeze-thaw cycles. Pilarski and Matuana (2005) showed that the observed property loss was primarily due to the effect of water during the cycling that appears to have led to the decreased interfacial adhesion between the wood flour and the rigid PVC matrix. Freeze-thaw actions had no apparent effect on the density of the composites after exposure. However, these changes led to a moisture uptake that decreased the interfacial adhesion and increased the amount and size of the pores in the composites, resulting in a significant degradation of the flexural properties (Pilarski and

Matuana 2005). However, this mechanism is different from that of the degradation due to the high-low temperature cycles. In the process of freeze-thaw cycles, wood fiber soaks up moisture to expand its volume. At the same time, water molecules destroyed the interface between the wood fiber and the matrix, weakening the original effect of the wood fiber and resulting in the decrease of MOR and MOE (Xiao 2010). The effects on the mechanical strength of WPC after two treatments (high-low temperature cycles in dry state and freeze-thaw cycles in wet state) are different because of their different mechanisms. The water in the cell cavity and micropores of the cell wall freezes at low temperature. The condensation of water at low temperature is a process of breaking the original ice layer followed by the formation of a new ice layer until all of the water freezes (Chatterji 1999a,b). As a kind of porous material, the high bonding strength between ice and wood surface makes the mechanical properties of WPC tend to increase because the hydroxyl group on the molecular chain of wood is a hydrophilic group (Ayrilmis 2007, Zhao et al. 2015a,b). Therefore, the strength of WPC after freeze-thaw cycles is higher than that of WPC after the high-low temperature cycles.

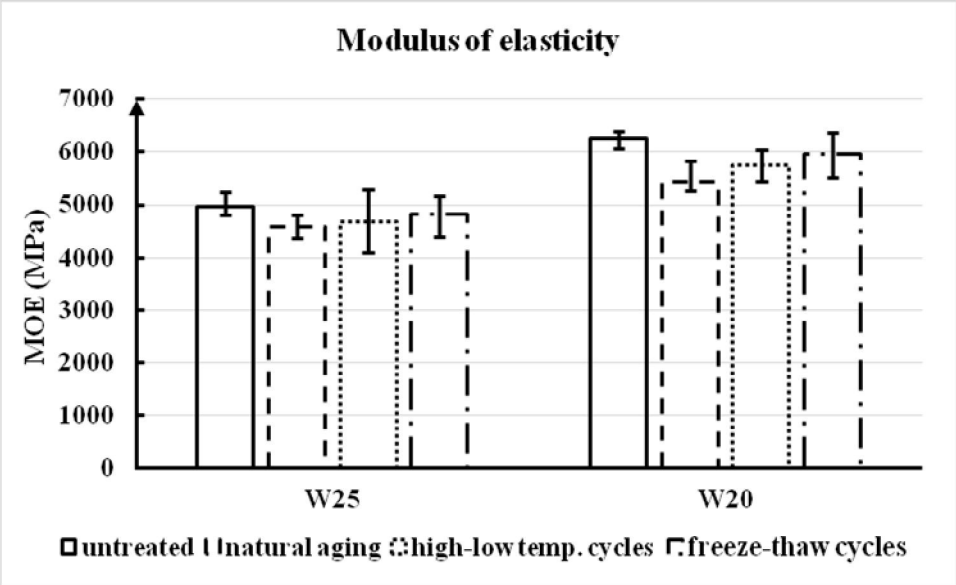

Fig. 3: MOE for untreated specimens, and specimens after treatments of natural aging, high-low temperature cycles and freeze-thaw cycles.

On the other hand, the retention values of MOR for W_{25} after the natural aging, high-low temperature cycles and freeze-thaw cycles were 86%, 92%, and 96%, while they were 97%, 95%, and 100% for W_{20}, demonstrating that the performance of WPC was relatively stable despite the decrease of MOR after the treatments. Therefore, WPC is widely used in outdoor applications.

Effects of aging on screw holding force

Fig. 4 shows the screw holding force of the two untreated WPC specimens, and the specimens after treatments by natural aging, high-low temperature cycles and freeze-thaw cycles. The screw holding force decreased after each of the three treatments. Compared to

the untreated specimen, the screw holding force of W_{25} after the natural aging, high-low temperature cycles and freeze-thaw cycles decreased by 11%, 21%, and 8%, while the corresponding decreases were 6%, 8%, and 2% for W_{20}, respectively.

Due to the different shrinkage of fiber and plastic at different temperatures, the adhesion force will decrease with temperature changes, leading to the decrease of the screw withdrawal force. The screw holding force after the freeze-thaw cycle is greater than that of the material after the high-low temperature cycle, which is consistent with the MOR and MOE results discussed above.

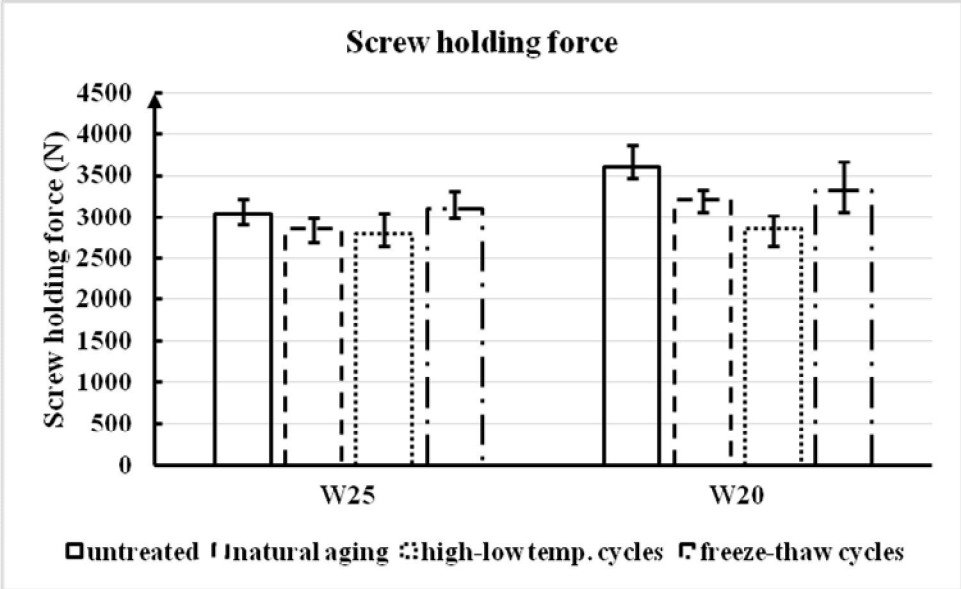

Fig. 4: Screw holding force for untreated specimens, and specimens after treatments of natural aging, high-low temperature cycles and freeze-thaw cycles.

Effects of aging on creep performance

Creep performance is an important factor for the use of WPC materials for long-term loading. The long-term load-bearing capacity of materials can be predicted by the creep performance, and thus, creep performance also describes the material's safety.

Fig. 5 shows the creep recovery rate of two groups of WPC specimens for different treatments. The creep recovery rates for the untreated specimens of W_{25} and W_{20} were 89% and 93%. After natural aging, high-low temperature cycles and freeze-thaw cycles, the rates decreased by 6%, 7%, and 1% for W_{25}, and by 9%, 14%, and 10% for W_{20}, respectively.

The creep recovery rate can reach more than 80% even though it decreases slightly after the treatments, indicating that aging has little effect on the creep performance of WPC. Therefore, WPC is a relatively safe material when it is used for building planks or other structural load-bearing materials.

Correspondence of natural aging and accelerated aging

The type of weathering appears to affect the WPC properties. The correspondence of natural aging and laboratory accelerated aging of WPC has been a problem discussed by many

scholars. It was shown that DMA can be used to measure a series of short-term creep or relaxation rates at constant temperature utilizing the time-temperature-transformation software to convert the short-term test results at high temperature into the long-term actual results at room temperature that enable the prediction of the mechanical properties of WPC at room temperature over the time period of several years (Maiti 2016, Lu et al. 2018). This is also an important means for predicting the long-term performance of WPC.

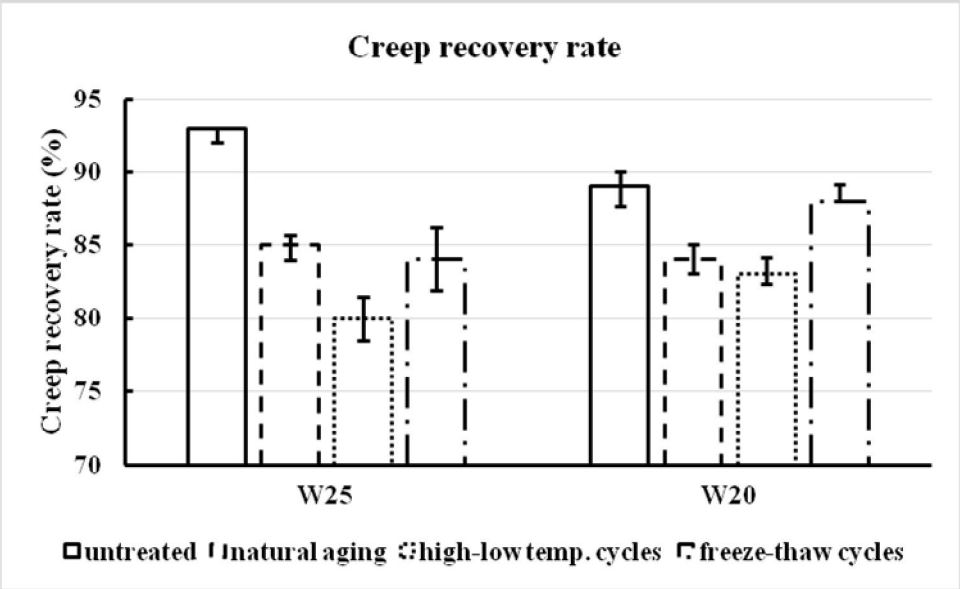

Fig. 5: Creep recovery rates for untreated specimens, and specimens after treatments of natural aging, high-low temperature cycles and freeze-thaw cycles.

CONCLUSIONS

This study evaluated the mechanical properties of WPC after the natural aging and accelerated laboratory aging. The following conclusions were reached: *(1)* After aging treatment, *i.e.*, natural aging and accelerated aging, MC of WPC increased, and mechanical properties such as MOR, MOE, screw holding force and creep recovery rate decreased as well. *(2)* The retention of MOR is greater than 86% after natural aging, high-low temperature cycles and freeze-thaw cycles. *(3)* The creep recovery rate can reach more than 80% after aging, showing that WPC is a relatively safe material for use in building floors or other structural load-bearing materials. *(4)* The mechanical properties of WPC after freeze-thaw cycles are better than those of WPC after high-low temperature cycles. *(5)* The time-temperature- transformation software of the DMA analyzer can be used to convert the short-term test results at high temperature into the long-term actual results at room temperature, so as to predict the long-term performance of WPC.

ACKNOWLEDGMENTS

This work was financially supported by the National Key Research and Development Plan Key Special Projects (2016YFF0201903).

REFERENCES

1. Albrektas, D., Jucienė, M., Dobilaitė, V., 2020: The influence of thermal modification on the resistance to water impact properties and strength of wood used in outdoor conditions. Wood Research 65(3): 353-364.
2. Ayrilmis, N., 2007: Effect of panel density on dimensional stability of medium and high density fiberboards. Journal of Materials Science 42(20): 8551-8557.
3. Badji, C., Soccalingame, L., Garay, H., Bergeret, A., Benezet, J.C., 2017: Influence of weathering on visual and surface aspect of wood plastic composites: Correlation approach with mechanical properties and microstructure. Polymer Degradation and Stability 137(3): 162-172.
4. Chatterji, S., 1999a: Aspects of the freezing process in a porous material–water system: Part 1. Freezing and the properties of water and ice. Cement and Concrete Research 29(4): 627-630.
5. Chatterji S., 1999b: Aspects of freezing process in porous material-water system: Part 2. Freezing and properties of frozen porous materials. Cement and Concrete Research 29(5): 781-784.
6. Chen, L., Han, J.Q., Huang, R.Z., Xu, X.W., Wu, Q.L., 2017: Thermal decomposition properties of recycled tire rubber filled wood/high density polyethylene composites. Wood Research 62(5): 701-714.
7. Clemons, C., 2002: Wood-plastic composites in the United States: The interfacing of two industries. Forest Products Journal 52(6): 10-18.
8. GB/T 24508, 2009: Wood-plastic composite flooring.
9. GB/T 29418, 2012: The methods for mechanical and physical properties of wood-plastic composite product.
10. ISO 16978, 2003: Wood-based panels. Determination of modulus of elasticity in bending and of bending strength.
11. ISO 16979, 2003: Wood-based panels. Determination of moisture content.
12. ISO 27528, 2009: Wood-based panels. Determination of resistance to axial withdrawal of screws.
13. Kaymakci, A., Badji, N., Akkilic, H., 2016: Utilization of tinder fungus as filler in production of HDPE/wood composite. Wood Research 61(6): 885-894.
14. La Mantia, F.P., Morreale, M., 2008: Accelerated weathering of polypropylene/wood flour composites. Polymer Degradation and Stability 93(7): 1252-1258.

15. Lu, J.X., Peng, H., Cai, J.Z., Jiang, J.L., Zhao, R.J., Gao, Y.L., 2018: Application of dynamic mechanical analysis in wood science research. Journal of Forestry Engineering 3(5): 1-11.
16. Maiti, A.A., 2016: Geometry-based approach to determining time-temperature superposition shifts in aging experiments. Rheologica Acta 55(1): 83-90.
17. Mengeloglu, F., Matuana, L.M., King, J.A., 2000: Effects of impact modifiers on the properties of rigid pvc/wood-fiber composites. Journal of Vinyl and Additive Technology 6(3): 153-157.
18. Pilarski, J.M., Matuana, L.M., 2005: Durability of wood flour-plastic composites exposed to accelerated freeze-thaw cycling. Part I. Rigid PVC matrix. Journal of Vinyl and Additive Technology 11(1): 1-8.
19. Pilarski, J.M., Matuana, L.M., 2006: Durability of wood flour-plastic composites exposed to accelerated freeze-thaw cycling. Part II. High density polyethylene matrix. Journal of Applied Polymer Science 100(1): 35-39
20. Stark, N.M., Matuana, L.M., Clemons, C.M., 2004: Effect of processing method on surface and weathering characteristics of wood-flour/HDPE composites. Journal of Applied Polymer Science 93(3): 1021-1030.
21. Xiao, W., 2010: The influence of accelerated aging on the properties of wood-plastic composite materials - freeze-thaw, xenon accelerated aging. Pp 34-40, Master's thesis of NanJing Forestry University. China.
22. Xu, K.M., Kang, K.Y., Liu, C., Huang, Y.B., Zhu, G., Zheng, Z.F., Li, W.L., 2017: The effects of expoxidized soybean oil on the mechanical, water absorption thermal stability and melting processing properties of wood plastic composites. Wood Research 62(5): 795-806.
23. Wang, W.H., Morrell, J.J., 2005: Effects of moisture and temperature cycling on material properties of a wood/plastic composite. Forest Products Journal 55(10): 81-83.
24. Zhao, L.Y., Jiang, J.H., Lu, J.X., Zhan, T.Y., 2015a: Flexural properties of wood in low temperature environment. Cold Regions Science and Technology 116: 65-69.
25. Zhao, L.Y., Jiang, J.H., Lu, J.X. Zhou, Y.D., 2015b: Effect of low temperature cyclic treatments on modulus of elasticity of birch wood. Bioresources 10(2): 2318-2327.
26. Zini, E., Scandola, M., 2011: Green composites: an overview. Polymer Composites 32(12): 1905-1915.

LIYUAN ZHAO, BIN LV, XIAORUI PENG,YUEJIN FU*
CHINESE ACADEMY OF FORESTRY
RESEARCH INSTITUTE OF WOOD INDUSTRY
BEIJING 100091
P.R.CHINA
*Corresponding author: bj-fyj@163.com

WOOD RESEARCH doi.org/10.37763/wr.1336-4561/66.5.711720
e-ISSN 2729-8906
66(5): 2021 711-720 pp.

RATIO ANALYSIS BETWEEN COMPRESSION AND SHEARING OF 72 BRAZILIAN WOOD SPECIES

FRANCISCO ANTONIO ROCCO LAHR
UNIVERSITY OF SAO PAULO
BRAZIL

EDUARDO CHAHUD
FEDERAL UNIVERSITY OF MINAS GERAIS
BRAZIL

FELIPE NASCIMENTO ARROYO, ANDRÉ LUIS CHRISTOFORO, EDSON FERNANDO CASTANHEIRA RODRIGUES, JOÃO PAULO BOFF ALMEIDA
FEDERAL UNIVERSITY OF SAO CARLOS
BRAZIL

VINICIUS BORGES DE MOURA AQUINO
FEDERAL UNIVERSITY OF SOUTH AND SOUTHEAST PARA ARAGUAIA
BRAZIL

HERISSON FERREIRA DOS SANTOS
FEDERAL INSTITUTE OF EDUCATION SCIENCE AND TECHNOLOGY OF RONDONIA
BRAZIL

(RECEIVED NOVEMBER 2020)

ABSTRACT

The Brazilian standard ABNT NBR 7190 (1997) governs the premises for the wood structure sizing through a table and the simplified method. Thus, this research aims to analyze whether the simplified method shown in the standard matches the resistance values of 72 Brazilian species, separated from class C20 to C60. In the end, it was possible to conclude that the value displayed by the standard between the ratio of shear and compression in the direction parallel to the fibers is half of what actually happens in Brazilian species, showing an urgent review in the standard premises.

KEYWORDS: Wooden structures, simplified characterization, Brazilian standard, sizing.

INTRODUCTION

Wood, being abundant in Brazil, can be considered an excellent structural material, in addition to having good resistance in traction and compression (Lahr et al. 2021, Almeida et al. 2019). Precisely because of this resistance in either efforts, wood is indicated for both small and large structures (Poleto et al. 2020, Silva et al. 2020). However, it is necessary to carry out reforestation in order not to harm the environment (Pigozzo et al. 2018a, Wolenski et al. 2020). In addition, with reforestation its source is renewable, another important point and should be highlighted, unlike the other structures usually used: reinforced concrete and metal (Pigozzo et al. 2018b, Oliveira et al. 2019).

According to Alves (2020), Brazil had 493.5 million hectares of forests in 2017, equivalent to 12% of all world forests. With a government incentive on the reforestation wood production, whether to recover deforested areas or for structural purposes, these trees can store up to 200 tons of CO_2 throughout their lives, thus showing their importance against environmental impacts (Christoforo et al. 2017, Santos et al. 2020). According to Gomes (2016), the steel structure emits more than 1600 kg of CO_2 per ton of steel produced. Concrete, on the other hand, emits around 1100 kg of CO_2 per ton of clinker produced (Felix and Possan 2018).

In Brazil, the Brazilian Association of Technical Standards (ABNT) which governs the premises for the design of structures: wood, concrete and steel, with NBR 7190 (1997) being the current standard for wooden structures (Nascimento et al. 2021). Tab. 1 below presents the strength classes with the respective properties stipulated by the standard, helping the engineer in structural calculation with only the wood strength class, without needing to carry out laboratory tests to determine physical and mechanical properties.

Tab. 1: Strength class with its respective physical and mechanical properties of hardwoods according to ABNT NBR 7190 (1997).

Classes	$f_{c0,k}$ (MPa)	$f_{v0,k}$ (MPa)	$E_{c0,m}$ (MPa)	$\rho_{12\%}$ (kg·m^{-3})
C20	20	4	9500	650
C30	30	5	14500	800
C40	40	6	19500	950
C60	60	8	24500	1000

In addition to this table, the current standard shows a simplified characterization of wood species according to the type: conifer or dicotyledonous (hardwood) (Christoforo et al. 2020, Almeida et al. 2020). With this simplified characterization and Tab. 1, the civil engineer is able to estimate other properties required for dimensioning, using relationships between the wood resistances. As an example, Tab. 1 shows only the compressive strength parallel to the fibers ($f_{c0,k}$), shear parallel to the fibers ($f_{v0,k}$), modulus of elasticity ($E_{c0,m}$) and the apparent density ($\rho_{12\%}$), these values being characteristic (Nogueira et al. 2020, Duarte et al. 2020). If the engineer needs the normal compressive strength to fibers ($f_{c90,k}$), he can adopt $f_{c0,k}$ as an estimator of this property ($f_{c90,k} = f_{c0,k} \cdot 0.25$).

For a correct and safe sizing of a structure, it is ideal to know all the properties of resistance and rigidity (Pigozzo et al. 2018c,d). However, according to Couto et al. (2020), these

relations shown in the Brazilian standard (simplified method) may not match reality. In its study, 10 species of Brazilian wood were used, covering all resistance classes (C20 to C60) shown in Tab. 1. With the analysis, it was possible to conclude that no species had the relationship between the shear parallel to the fibers and the compression parallel to the fibers equal to the value shown in the standard. The average value obtained between this relationship was 0.22, while the Brazilian standard displays it as being 0.12.

Matos and Molina (2016) also analyzed the relationship between $f_{v0,k}$ and $f_{c0,k}$ of two Brazilian species: *Pinus elliotti* and *Eucalyptus saligna*. In his study it was possible to notice a greater discrepancy of this relationship in the pine species, since the relationship was 0.29 and the standard displays as being 0.15. For the eucalyptus species, the ratio was 0.13, very close to the standard (0.12).

In view of this, this research aims to assess whether the ratio between the shear parallel to the characteristic fibers ($f_{v0,k}$) and the parallel compression to the characteristic fibers ($f_{c0,k}$) of 72 Brazilian wood species are equivalent with those shown by the Brazilian standard NBR 7190 (1997). For that, the 72 species were divided between the four normative resistance classes (Tab. 1). At the end, he analyzed the ratio between these two properties by resistance class and considering all species together, besides using a linear regression model to stipulate which would be the best ratio value.

MATERIAL AND METHODS

The 72 species used in this research are shown in Tab. 2 below, with their respective resistance classes (RC) according to ABNT NBR 7190 (1997).

Tab. 2: Wood species evaluated.

Common name	RC	Common name	RC	Common name	RC	Common name	RC
Amescla	C20	Angelim Amargoso	C40	Angelim Saia	C60	Breu Vermelho	C60
Caixeta	C20	Angelim Araroba	C40	Casca Grossa	C60	Champanhe	C60
Cajueiro	C20	Angico Branco	C40	Castelo	C60	Cutiúba	C60
Cambará	C20	Bicuíba	C40	Catanudo	C60	Garrote	C60
Cambará Rosa	C20	Branquilho	C40	Envira Branca	C60	Guajará	C60
Cedro Doce	C20	Cafearana	C40	Envira	C60	Ipê	C60
Cedro	C20	Canafistula	C40	Garapa	C60	Angelim Vermelho	C60
Cedroarana	C20	Canela Parda	C40	Guaiçara	C60	Itaúba	C60
Marupá	C20	Canelão	C40	Guanandi	C60	Angico Preto	C60
Quarubarana	C20	Casca Grossa	C40	Guarucaia	C60	Jatobá	C60
Cambará	C30	Copaíba	C40	Ipê	C60	Tatajuba	C60
Castanheira	C30	Cupiúba	C40	Louro Preto	C60	Maçaranduba	C60
Cedro Amazonense	C30	Goiabão	C40	Oiticica Amarela	C60	Mandioqueira	C60
Cedro	C30	Louro Verde	C40	Parinari	C60	Oiuchu	C60
Cupiúba	C30	Mirarema	C40	Peroba Mica	C60	Quina Rosa	C60
Embireira	C30	Piolho	C40	Umirana	C60	Roxinho	C60
Tauari	C30	Quaruba Rosinha	C40	Angelim Pedra	C60	Sucupira	C60
Abiú	C40	Rabo de Arraia	C40	Angelim Ferro	C60	Tachi	C60

The wood from homogeneous lots was properly stored, resulting in a moisture content close to 12%, according to the premises of ABNT NBR 7190 (1997). The test methods of

the Brazilian standard were also followed to obtain the mechanical properties.

Also, as recommended by the Brazilian standard, twelve specimens per species were manufactured and tested for compressive strength parallel to the fibers and shear strength (Fig. 1), resulting in 1896 experimental determinations altogether.

(a) (b)

Fig. 1: a) apparatus used to perform the compression tests parallel to the grain; b) apparatus used to perform the shear parallel to the fibers.

The specimens were broken in the universal testing machine (AMSLER with load capacity of 25 tons). Their moisture content (U) at the time of the tests was obtained using the Marrari M5 contact moisture meter (10.76 ≤ U ≤ 12.96%). With the samples moisture content, the resistance values (f_U) were corrected to the moisture content of 12%, as indicated by ABNT NBR 7190 (1997), with the aid of equation 1 below, in which f_U consists in the samples resistance associated with the moisture content U, while $f_{12\%}$ consists of the resistance to 12% moisture:

$$f_{12\%} = f_U \cdot \left[1 + \frac{2 \cdot (U - 12)}{100}\right] \quad (1)$$

Based on the corrected values for 12% moisture content ($f_{c0,12\%}$ and $f_{v0,12\%}$), Eq. 2 was used to determine the characteristic value ($f_{c0,k}$ and $f_{v0,k}$) for the woods categorization, in which f_1, f_2 to f_n denote the values of resistance in ascending order of the 12 (n) specimens tested, according to ABNT NBR 7190 (1997):

$$f_k \geq \begin{cases} 0.70 \cdot \dfrac{\sum_{i=1}^{n} f_i}{n} \\ 1.10 \cdot \left[2 \cdot \left(\dfrac{f_1 + f_2 + \cdots + f_{(n/2)-1}}{(n/2) - 1}\right) - f_{n/2}\right] \end{cases} \quad (2)$$

Statistical analysis

The ratio between the characteristic shear strength in the direction parallel to the fibers ($f_{v0,k}$) and the compressive strength in the direction parallel to the fibers ($f_{c0,k}$) established by the Brazilian standard ABNT 7190 (1997) is expressed by Eq. 3:

$$\frac{f_{v0k}}{f_{c0,k}} = 0.12 \quad (3)$$

To evaluate the optimal ratio between the two properties by resistance classes and also for the set composed of all species, a linear regression model with one parameter was used (Eq. 4), with β_0 being the parameter (coefficient of the relationship between $f_{v0,k}$ and $f_{c0,k}$ using the least squares method:

$$f_{v0k} = \beta_0 \cdot f_{c0,k} \quad (4)$$

The average absolute percentage error (MAPE, Eq. 5) and the regression variation coefficient (CV) were used as measures of error and variability in the results obtained using Eq. 4, and the adjustment quality was determined using determination coefficient (R^2, Eq. 7).

$$MAPE\,(\%) = 100 \cdot \frac{1}{n} \cdot \sum_{i=1}^{n} \frac{|Ypredito_i - Ydados_i|}{|Ydados_i|} \quad (5)$$

$$CV\,(\%) = 100 \cdot \frac{\sqrt{\sum_{i=1}^{n} \frac{(Ypredito_i - Ydados_i)^2}{n}}}{\bar{Y}dados} \quad (6)$$

$$R^2\,(\%) = 100 \cdot \left(1 - \frac{\sum_{i=1}^{n}(Ypredito_i - Ydados_i)^2}{\sum_{i=1}^{n}(Ydados_i - \bar{Y}dados)^2}\right) \quad (7)$$

From Eqs. 5 to 7, n is the samples number considered, $Ypredict_i$ is the value estimated by the regression model, $Ydata_i$ is the experimentally determined value and $\bar{Y}data$ is the average value of the results determined experimentally.

RESULTS AND DISCUSSION

Fig. 2 shows the result of the strengths obtained in the compression and shear strength tests in the direction parallel to the fibers by strength class (SC).

From this figure, it is possible to observe that the greater the compressive strength of the wood, the greater the shear strength. The standard deviations, and consequently the coefficients of variation (CV), were low. ABNT NBR 7190 (1997) advises that the CV must be less than 18% to demonstrate quality in the tests performed. The maximum CV obtained from the samples was 11.84% and 18.29% for compression and shear, respectively, showing this quality.

Tab. 3 shows the results of the ratio between shear and compression in the direction parallel to the fibers of the 4 strength classes, as well as the ratio considering all species together.

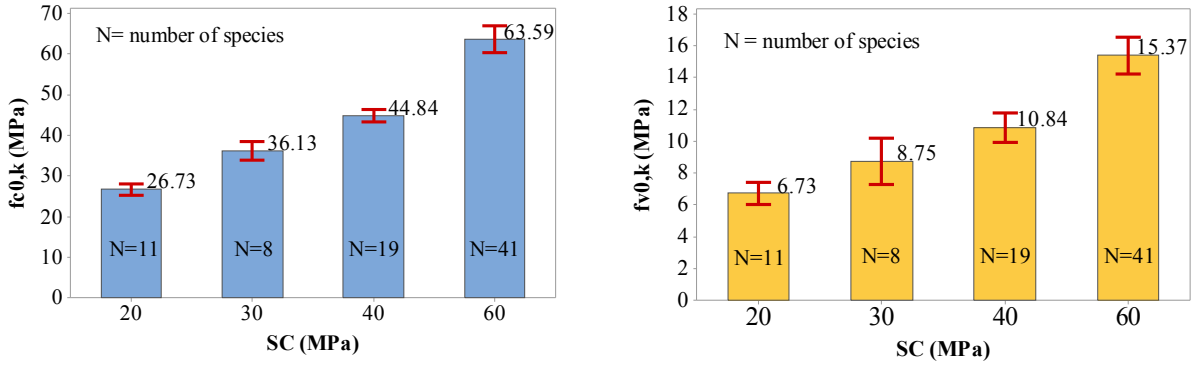

(a) (b)

Fig. 2: Synthesis of the characteristic values of compressive strength (a) and shear (b) in the direction parallel to the fibers of the studied wood species.

Tab. 1: Linear models results ($f_{v0,k} = \beta_0 \cdot f_{c0,k}$).

Groups	Coefficient (β_0)	CV (%)	MAPE (%)	R^2 (%)
C20	0.25	13.44	10.08	11.73
C30	0.24	18.72	16.01	6.24
C40	0.24	18.01	15.82	15.89
C60	0.24	17.27	14.62	43.14
All species	0.24	17.97	14.22	73.30

As can be seen, the ideal ratio between shear and compression in compression parallel to the fibers is 0.25 for class C20 and 0.24 for the rest. The standard displays a value of 0.12, regardless of the resistance class. Considering all species together, also from the NBR 7190 (1997) standard, this ratio should be 0.24. The determination coefficient for this relationship considering all species was 73.30%, higher than the 70% required by Montgomery (2013), indicating the quality of the chosen regression model. With this difference of 100% (double), the structural engineer would have a resistance 50% lower than what the wood actually resists, causing the structure to be oversized if it uses compression to estimate the shear. If using shear to estimate compression, the standard would be doubling the value of what actually resists, causing the structure to be undersized, which can cause pathologies and compromise the structure (Andrade Jr et al. 2014).

Thus, it is evident that the Brazilian standard for wooden structures (NBR 7190, 1997) needs to undergo revision, since civil engineers are carrying out structural design with data that does not match reality. This failure was also evidenced in the work of Matos and Molina (2016) and Couto et al. (2020), in which they found a discrepancy of 83% in 10 species studied (Couto et al. 2020) and a difference of 93% for the species of *Pinus elliotti* (Matos and Molina 2016). The only work that obtained a small difference in relation to the norm was in the work of Couto et al. (2020) for the species of *Eucalyptus saligna*, being only 8%.

CONCLUSIONS

The results obtained from this research made it possible to conclude that: *(1)* Although the quantity of samples taken (1896) is high, the variation CV obtained met the limit imposed by the Brazilian standard for wooden structures (NBR 7190, 1997) of 18%, showing the quality of the tests carried out. *(2)* The ideal value for the ratio between shear strength and compression, both in the direction parallel to the fibers, should be 0.25 for class C20 and 0.24 for the others, instead of the value imposed by the standard. *(3)* The ideal ratio value, considering all species, should be 0.24 and not 0.12, showing that the Brazilian standard needs to be revised because it is oversizing or under-sizing wooden structures in Brazil. With this correction, the engineers would adopt the value that the wood really resists, making the sizing is correct and don't occur pathologies or over-sizing in the structure. *(4)* The linear regression model adopted showed excellent quality, as it was higher than the 70% required by Montgomery (2013), showing that the relationship should be 0.24.

REFERENCES

1. Almeida, T.H., Almeida, D.H., Arroyo, F.N., Araújo, V.A., Chahud, E., Branco, L.A.M.N., Christoforo, A.L., Lahr, F.A.R., 2019: Time of exposure at 60°C service temperature: influence on strength and modulus of elasticity in compression parallel to the grain of hardwood species. BioResources 14(1): 207-219.
2. Almeida, T.H., Almeida, D.H., Moritani, F.Y., Pereira, M.C.M., Christoforo, A.L., Lahr, F.A.R., 2020: Analytical study of the curve of static bending test for wood specimens. Ambiente Construído 20(1): 325-332.
3. Andrade Jr, J.R., Almeida, D.H., Almeida, T.H., Christoforo, A.L., Stamato, G.C., Lahr, F.A., 2014: Avaliação das estruturas de cobertura em madeira de um galpão de estoque de produtos químicos (Evaluation of wooden roof structures in a chemical storage shed). Ambiente Construído 14(3): 75-85.
4. ABNT NBR 7190, 1997: Projeto de Estruturas de Madeira (Wooden structures design).
5. Alves, R.S.C, 2020: Efeito da quantidade de floresta na predação de sementes e frugivoria em diferentes tipos de ambientes (Effect of the amount of forest on seed predation and frugivory in different types of environments). Dissertação (Mestrado em Ecologia e Biodiversidade). Universidade Estadual Paulista (UNESP), Rio Claro, 48 pp.
6. Christoforo, A.L., Arroyo, F.N., Silva, D.A., Panzera, T.H., Lahr, F.A., 2017: Full characterization of *Calycophyllum multiflorum* wood specie. Engenharia Agrícola 37(4): 637-643.
7. Christoforo, A.L., Couto, N.G., Almeida, J.P.B., Aquino, V.B. De M., Lahr, F.A.R., 2020: Apparent density as an estimator of wood properties obtained in tests where failure is fragile. Engenharia Agrícola 40: 105-112.
8. Couto, N.G., Almeida, J.P., Govone, J.S., Christoforo, A.L., Lahr, F.A., 2020: Relação entre a resistência ao cisalhamento e a resistência à compressão paralela às fibras de

madeiras folhosas (Relationship between shear strength and compressive strength parallel to hardwood fibers). Ambiente Construído 20(4): 319-327.
9. Duarte, B.B., Lahr, F.A.R., Nascimento, M.F., Christoforo, A.L., 2020: Correlation between density and porosity from ten species of tropical wood. International Journal of Engineering Research And Applications (IJERA)10(3): 30-32.
10. Felix, E.F., Possan, E., 2018: Balanço das emissões e da captura de CO_2 em estruturas de concreto: simulação em função do consumo e tipo de cimento (Balance of emissions and capture of CO_2 in concrete structures: simulation according to consumption and type of cement). Revista IBRACON de Estruturas e Materiais 11(1): 1-14.
11. Gomes, R.D., 2016: Análise dos Impactos Ambientais e da Sustentabilidade em Usinas Siderúrgicas Integradas a Coque (Analysis of environmental impacts and sustainability in steel plants integrated with coke). Dissertação (Graduaçaõ em Engenharia Metalúrgica). DEMM/POLI/UFRJ, Rio de Janeiro, 62 pp.
12. Lahr, F.A.R., Arroyo, F.N., Rodrigues, E.F.C., Almeida, J.P.B., Aquino, V.B.M., Wolenski, A.R.V., Santos, H.F., Ferraz, A.L.N., Chahud, E., Molina, J.C., Pinheiro, R.V., Christoforo, A.L., 2021: Models to estimate longitudinal compressive strength of Brazilian hardwood based on apparent density. BioResources 16(1): 1373-1381.
13. Matos, G.D., Molina, J.C., 2016: Resistência da madeira ao cisalhamento paralelo às fibras segundo as normas ABNT NBR 7190:1997 e ISO 13910:2005 (Resistance of wood to shear parallel to fibers according to ABNT NBR 7190: 1997 and ISO 13910: 2005). Matéria 21(4): 1069-1079.
14. Montgomery, D.C., 2013: Design and analysis of experiments (8 ed.). Arizona State University: John Wiley & Sons, Inc, 757 pp.
15. Nascimento, M.L., Rodrigues, E.F.C., Balanco, G.G., Christoforo, A.L., Rocco Lahr, F.A., 2021: Structural analysis of a stress-laminated-timber bridge deck using hardwood. Journal of Bridge Engineering 26(3): 04021005.
16. Nogueira, M.C.J.A., Araujo, V.A., Vasconcelos, J.S., Christoforo, A.L., Lahr, F.A.R., 2020: Sixteen properties of *Eucalyptus tereticornis* wood for structural uses. Bioscience Journal 36: 449-457.
17. Oliveira, G.O.B., Pinheiro, R.V., Arroyo, F.N., Almeida, D.H., Almeida, T.H., Silva, D.A.L., Christoforo, A.L., Lahr, F.A.R., 2019: Technical feasibility study of the use of softwoods in lattice structure. Howe. Type for roofing (Gaps between 8-18 meters). Current Journal of Applied Science and Technology 35(4): 1-8.
18. Pigozzo, J.C., Chahud, E., Arroyo, F.N., Christoforo, A.L., Almeida, D.H., Lahr, F.A., 2018a: Comparison of anchorage strength of bonded-in steel bars with epoxy resin, varying the superficial treatments and moisture after bonding, using *Corymbia citriodora* wood. Current Journal of Applied Science and Technology 28(5): 1-6.
19. Pigozzo, J.C., Arroyo, F.N., Christoforo, A.L., Almeida, D.H., Calil Jr, C., Lahr, F.A., 2018b: Design and execution of wood-concrete deck bridge. Current Journal of Applied Science and Technology 28(3): 1-10.

20. Pigozzo, J.C., Arroyo, F.N., Christoforo, A.L., Almeida, D.H., Calil Jr, C., Lahr, F.A., 2018c: Behavior of shear connectors formed by bonded-in "X" type steel bars in wood-concrete specimens. Current Journal of Applied Science and Technology 28(5): 1-8.
21. Pigozzo, J.C., Arroyo, F.N., Christoforo, A.L., Calil Junior, C., Almeida, D.H., Lahr, F.A.R., 2018d: Pull out strength of bonded-in steel bars behavior in *Pinus oocarpa* shiede timber. Current Journal of Applied Science and Technology 28: 1-9.
22. Poleto, S.F.S., Aquino, V.B M., Chahud, E., Pinheiro, R.V., Branco, L.A.M.N., Silva, D.A.L., Campos, C.I., Molina, J.C., Carvalho, C.M., Christoforo, A.L., Lahr, F.A.R., 2020: Evaluation of CCB-preserved medium density particleboards. BioResources 15: 3678-3687.
23. Santos, S.N.C., Almeida, T.H., Sardela, M.R., Lahr, F.A.R., Gonçalves, D., 2020: Surface properties and crystallinity of *Pinus taeda* and *Hymenaea stilbocarpa* treated at low temperatures in different grain directions. Journal Of The Indian Academy Of Wood Science 17(1): 1-8.
24. Silva, D.A.L., Aquino, V.B.M., Lahr, F.A.R., Christoforo, A.L., 2020: Influência dos parâmetros de fabricação nas Propriedades Físicas e Mecânicas de Paineis de Partícula de Média Densidade (Influence of manufacturing parameters on the physical and mechanical properties of medium density particle boards). Materia-Rio de Janeiro 25: e-12580.
25. Wolenski, A.R.V., Dias, F.M. Peixoto, R.G., Christoforo, A.L., Lahr, F.A.R., 2020: Modelos para estimativa das propriedades mecânicas de compressão e tração na direção paralela às fibras (Models for estimating the mechanical properties of compression and tension in the direction parallel to the fibers). Ambiente Construído 20(1): 263-276.

FRANCISCO ANTONIO ROCCO LAHR
UNIVERSIDADE DE SÃO PAULO - SÃO CARLOS
DEPARTAMENTO DE ENGENHARIA ESTRUTURAL
AV. TRABALHADOR SÃOCARLENSE, N. 400 – 13.566-590
SÃO CARLOS, BRAZIL

EDUARDO CHAHUD
UNIVERSIDADE FEDERAL DE MINAS GERAIS - BELO HORIZONTE
DEPARTAMENTO DE ENGENHARIA CIVIL
AV. ANTÔNIO CARLOS, N. 6627 – 31.270-901
BELO HORIZONTE, BRAZIL

FELIPE NASCIMENTO ARROYO*, ANDRÉ LUIS CHRISTOFORO, EDSON FERNANDO CASTANHEIRA RODRIGUES, JOÃO PAULO BOFF ALMEIDA
UNIVERSIDADE FEDERAL DE SÃO CARLOS - SÃO CARLOS
DEPARTAMENTO DE ENGENHARIA CIVIL
RODOVIA WASHINGTON LUÍS – 36.307-352
SÃO CARLOS, BRAZIL
*Corresponding author: lipe.arroyo@gmail.com

VINICIUS BORGES DE MOURA AQUINO
UNIVERSIDADE FEDERAL DO SUL E SUDESTE DO PARÁ - SANTANA DO ARAGUAIA
DEPARTAMENTO DE ENGENHARIA CIVIL
RUA GERALDO RAMALHO, N. 33 – 68.560-000
SANTANA DO ARAGUAIA, BRAZIL

HERISSON FERREIRA DOS SANTOS
INSTITUTO FEDERAL DE EDUCAÇÃO CIÊNCIA E TECNOLOGIA DE RONDÔNIA – ARIQUEMES
DEPARTAMENTO DE ENGENHARIA DE MATERIAIS
AV. JUSCELINO KUBITSCHEK, N. 2717 A 2853 – 76.872-847
ARIQUEMES, BRAZIL

WOOD RESEARCH doi.org/10.37763/wr.1336-4561/66.5.721731
e-ISSN 2729-8906
66(5): 2021 721-731 pp.

STUDY ON PERMEABILITY OF *CUNNINGHAMIA LANCEOLATA* BASED ON STEAM TREATMENT AND FREEZE TREATMENT

YUEQIAN YANG, WEI XU, XIA LIU
NANJING FORESTRY UNIVERSITY
CHINA

XIAODONG (ALICE) WANG
LAVAL UNIVERSITY
CANADA

(RECEIVED NOVEMBER 2020)

ABSTRACT

In order to improve the permeability of *Cunninghamia lanceolata,* the weight gain rate of *C. lanceolata* was taken as index. The effect of time, temperature and water content on the weight gain rate of impregnated wood was analyzed by frozen and steaming treatment. By comparing the weight gain rate under different modification methods, the optimal modification process was determined. The results indicate that the optimum parameters of *C. lanceolata* were saturated water content (-25°C and 8 h) at this time, the three-day gain rate of silica sol impregnated at normal temperature and pressure was 15.058%. After *C. lanceolata* is pre-treated by superheated steam, the weight gain rate of *C. lanceolata*, which in oven-dried specimen (120°C and 3 h) contents was the highest, at this time, the three-day gain rate of silica sol impregnated at normal temperature and pressure was 15.291%. By comparing the results of pre-freezing with the results of superheated steam treatment of *C. lanceolata*, the latter will increase the permeability of *C. lanceolata* better. Therefore superheated steam treatment should be chosen as an effective method for the pretreatment.

KEYWORDS: *Cunninghamia lanceolata,* fast-growing, freezing treatment, modification treatment, ANOVA, optimization.

INTRODUCTION

The traditional natural trees, as the main material of furniture production, have a long growth cycle while the market demand for furniture is increasing, causing the situation of

shortage of supply gradually (Fahrenhorst and Altan 1992). Start with the source of materials and improve the performance of quick-growing materials. let it can meet the demand of furniture production, so as to improve the capacity of qualified wood and alleviate the problem of insufficient wood supply (Pittau et al. 2018).

Based on literature review, it was found that permeability is an important index to measure wood properties, so improving the permeability of wood was the key to improve the effect of wood modification (Zlem et al. 2018, Emaminasab et al. 2015). In order to improve the permeability of wood, the number and size of the micropores of the effective pore membrane, the content and distribution of amorphous material deposited in the inner wall and cell wall, and the content and distribution of resin in the cell cavity were the main factors affecting the permeability of wood (Bao 1992). As two commonly used methods of wood treatment, freezing treatment and steam treatment have a significant effect on improving the permeability of wood (Seo et al. 2015, Ogawa et al. 2016).

The principle of pre-freezing treatment on improving wood permeability is that The water in the saturated wood is frozen into ice. When the volume of water molecules increases, the cell wall and pore wall are squeezed, and part of the pore membrane is destroyed, which expands the pores of wood to a certain extent, so as to improve the permeability of wood (Lan et al. 2016, Lisiewska et al. 2007). In addition, according to the research, the pre-freezing treatment can also migrate part of the wood extracts to the cell wall, which can not only fill the cell wall, but also improve the elasticity of the cell wall, so as to improve the shrinkage phenomenon of wood during drying. (Abd-Elhady 2014, Tomas et al. 2013, Zhang et al. 2011).

Steam treatment improves wood permeability, as well. High temperature steam in steam pretreatment produces persistent pressure on wood, which destroys the pore film on the cell wall inside the wood, thus allowing liquid molecules to pass more smoothly through the pores and enter into the cell space and cell cavity, thus increasing the permeability of wood (Awoyemi et al. 2010, Missio et al. 2016). In addition, the free hydroxyl groups of cellulose and hemicellulose in the wood react to such reactions as cross linking during steam treatment heating, which results in a reduction in the number of hydrophilic groups, thus reducing the moisture absorption of wood and enhancing the dimensional stability of wood, so the moisture content uniformity of wood was higher and the dry shrinkage ratio was lower after steam treatment (Poonia et al. 2015, Bao and Zhou 2017).

It was understood that there are few reports on the effects of freezing and steam treatment on the permeability of *Cunninghamia lanceolata*. Steam treatment and pre freezing treatment can expand some internal pores of wood, improve the permeability of wood, improve the performance of fast-growing wood and relieve the pressure of wood energy shortage (Cortez and Roberto 2012, Tao 2006).

Thus, in this work, improving the permeability of *C. lanceolata* was in focus. Through the freezing and steam treatment of *C. lanceolata*, analyzes the impregnation weight gain rate under different parameters, and clarifies the optimal modification parameters of *C. lanceolata*, in order to provide theoretical guidance for advanced wood improvement technology.

MATERIAL AND METHODS

Test materials and equipment

Samples of fast-growing *Cunninghamia lanceolata* 20 × 20 × 100 mm (T × R × L) were used in this study. In each group, 8 repeated tests were arranged, that is, 8 pieces of test materials were tested under the same conditions, and the average value was finally taken. The equipment (Vlosky and Shupe 2004, Zhu et al. 2020) used in the test is shown in Tab. 1.

Tab. 1: Laboratory equipment.

Name of equipment	Model	Manufacturers
Electric blast dryer	DHG-9245A Type	Shanghai - Heng Scientific Instruments Co., Ltd.
Electronic balance (0.001g)	EL-3KJ Type	Changzhou Tianzhiping Instrument Equipment Co., Ltd.
Refrigerators	BC-101KT1Type	Guangdong Rongsheng Electric Co., Ltd.

Steam treatment test design

The three factors of temperature, time and moisture content were taken as the main experimental research parameters (Tab. 2). The orthogonal test of three levels was carried out (Tab. 3). Each group carries out eight repeated tests, and the final result takes its average value.

Tab. 2: Table of variable factors for ordinary superheated pre-stemming.

Level	Temperature (°C)	The moisture content (%)	Time (h)
1	100	Wet specimen	1
2	120	Oven-dried specimen	2
3	140	Air-dried specimen	3

Tab. 3: The weight gain rate of impregnation of untreated and superheated pre-steaming treatment C. lanceolata.

N°.	Temperature (%)	Moisture content (%)	Time (h)	WPG (%)	The improve of WPG (%)
1	100	Wet specimen	1	13.321	5.87
2	100	Oven-dried specimen	2	12.863	2.23
3	100	Air-dried specimen	3	15.072	19.78
4	120	Wet specimen	2	14.832	17.87
5	120	Oven-dried specimen	3	15.291	21.52
6	120	Air-dried specimen	1	14.530	15.47
7	140	Wet specimen	3	13.531	7.53
8	140	Oven-dried specimen	1	11.963	-4.93
9	140	Air-dried specimen	2	12.642	0.47
Untreated	——	——	——	12.583	——

The *C. lanceolata* with the same size and specification have been Pre-frozen treated in the orthogonal experiment, The process was as follows: *(1)* The oven-dried specimen was obtained by drying *C. lanceolata*; The air-dried specimen with moisture content about 15% was obtained under relative humidity 65 ± 3%, 20 ± 2°C; Soak *C. lanceolata* to saturated water content to get wet specimen. *(2)* The wood with different moisture content was placed in

the steaming environment at a certain temperature for a period of time, and the relative humidity was maintained at 100%. *(3)* The steamed wood was placed at room temperature for a period of time until it is at normal temperature. *(4)* Dry the steam-treated wood until it was fully dry and wait for impregnation. *(5)* The steam-treated wood was impregnated at normal temperature and pressure. Combined with the impregnated condition of the fast-growing wood at normal temperature and pressure and the pre-freezing treatment test, the same impregnating time was used for three days and nights in the test. Then the weight gain rate of the steam-treated wood impregnated with silica sol was compared. *(6)* The weight gain rate of the impregnated wood reflects the permeability of the pre-treated wood to some extent. Therefore, the optimum steam treatment scheme and test parameters can be concluded by comparing the weight gain rate of the pretreated material with untreated material and comparing the increase of the permeability of steamed materials

Freeze treatment test design

Three factors of temperature, time and moisture content, were taken as the main experimental research parameters (Tab. 4). The orthogonal test of three factors and three levels was carried out (Tab. 5). Each group carries out eight repeated tests, and then the average value was calculated as the final result (Dong et al. 2018).

Tab. 4: Table of variable factors for pre-freezing process.

Level	Temperature (°C)	Time (h)	Moisture content (%)
1	-10	8	Oven-dried specimen
2	-15	12	Air-dried specimen
3	-20	16	Wet specimen

Tab. 5: The weight gain rate of impregnation and untreated of pre-freezing C. lanceolata.

N°.	Temperature (°C)	Time (h)	Moisture content (%)	WPG (%)	The improve of WPG (%)
1	-10	8	Oven-dried specimen	13.670	8.64
2	-10	12	Air-dried specimen	10.085	-19.85
3	-10	16	Wet specimen	13.204	4.93
4	-15	8	Air-dried specimen	7.429	-40.96
5	-15	12	Wet specimen	11.009	-12.51
6	-15	16	Oven-dried specimen	8.594	-31.70
7	-20	8	Wet specimen	14.758	17.28
8	-20	12	Oven-dried specimen	14.481	15.08
9	-20	16	Air-dried specimen	12.007	-4.58
Untreated	-	-	-	12.583	-

The *C. lanceolata* with the same size and specification have been Pre-frozen treated in the orthogonal experiment, The process was as follows: *(1)* The oven-dried specimen was obtained by drying *C. lanceolata*; The air-dried specimen with moisture content about 15% was obtained under relative humidity 65 ± 3%, 20 ± 2°C; Soak *C. lanceolata* to saturated water content to get wet specimen. *(2)* The wood with different moisture content was placed in the refrigerator with temperature of -10°C, -15°C and -20°C for some time. *(3)* The frozen

wood was placed at room temperature for a period of time until it thawed. *(4)* Dry the pre-frozen wood until it was fully dry and wait for impregnation; *(5)* The wood that have been pre-treated was impregnated at normal temperature and pressure. Because the change of weight gain rate of two kinds of quick-growing materials was observed before, in order to compare the weight gain rate of each group of test materials after impregnation of silica sol, the same impregnation time was used for three days and nights (72 h). *(6)* The weight gain rate of the impregnated material reflects the permeability of the pre-treated *C. lanceolata* to some extent. Therefore, compare the weight gain rate of the pre-treated material with untreated material and compare the increase of the permeability of pre-frozen materials to find the optimum pre-frozen method and experiment parameter.

RESULTS AND DISCUSSION

Effect of steam treatment on the permeability

Experimental results of steam treatment on weight gain rate

According to the data in Tab. 4, the weight gain rate of *C. lanceolata* impregnated at normal temperature and pressure after three days without pretreatment was 12.583%, and the weight gain rate of *C. lanceolata* impregnated silica sol after three days after superheated steam treatment ranged from 11.963% to 15.291%, and the weight gain rate was - 4.93 - 21.52% over untreated wood. By comparing the weight gain rate between the superheated steam pretreatment and the untreated material, it was found that the permeability of most *C. lanceolata* was enhanced after superheated steam treatment, and a few was decreased. The permeability of *C. lanceolata* was best in the 5th group. That is, specimen was oven-dried, steam temperature was 120°C and steam treatment time was 3 h.

Range analysis (Cadambi et al. 2012) of weight gain rate of C. lanceolata treated by steam

Tab. 6 is an intuitive analysis of the weight gain rate of *C. lanceolata* impregnated material after superheated steam pretreatment. According to the data in the table, the range value, which mean the influence of superheated steam pretreatment on *C. lanceolata*, is temperature > time > moisture content. This shows that the temperature have the greatest influence on the permeability of *C. lanceolata,* followed by time, and the effect of moisture content was the least. With the increase of temperature, the weight gain rate of *C. lanceolata* impregnated material after superheated steam pretreatment increased first and then decreased, and the effect was the best when the temperature was 120°C. With the increase of treatment time, the weight gain rate of *C. lanceolata* impregnated material after superheated steam pretreatment increased first and then decreased, and the effect was the best when the treatment time was 3 h. The weight gain rate of material superheated steam treatment manifested as air-dried specimen > wet specimen > oven-dried specimen. When the temperature was 120°C ,the time was 3 h and moisture content was air dried condition the weight gain rate of *C. lanceolata* impregnated material after superheated steam pretreatment was the best, that is, the permeability of *C. lanceolata* after superheated steam pretreatment was the best.

Tab. 6: Maximum analysis of variables on weight gain rate of impregnation of superheated pre-steanming treatment C. lanceolata.

Properties	Level	Temperature (°C)	Moisture content (%)	Time (h)
WPG (%)	Mean1	13.752	13.895	13.271
	Mean2	14.884	13.372	13.446
	Mean3	12.712	14.081	14.631
	Range	2.172	0.709	1.360

ANOVA analysis (Didier et al. 2002) of weight gain rate of C. lanceolata steam treatment

Tab. 7 is the variance analysis and significance test of the influence of variable factors on the weight gain rate of *C. lanceolata* superheated steam impregnated material. From the data in the table, we can see that temperature and time have a significant effect on the weight gain rate of *C. lanceolata* after superheated steam pretreatment, and the moisture content during superheated steam pretreatment has little effect on the permeability of *C. lanceolata* after pretreatment.

Tab. 7: Variance analysis and significance test of designed parameters on WPG of impregnation of superheated pre-steaming treatment C. lanceolata.

Factor	Sum of squares	DF	F value	F critical value	Pr > F
Temperature	7.083	2	46.294	19	*
Water content	0.810	2	5.294	19	
Time	3.286	2	21.477	19	*
Error	0.15	2			

$\alpha = 0.05$.

Optimization and verification of steam treatment process of C. lanceolata

According to the results of orthogonal test of steam treatment of *C. lanceolate* (Alizadeh and Fujita 2010), the optimum parameters of steam treatment of *C. lanceolata* were 120°C, 3 h and air-dried. The weight gain rate of *C. lanceolata* impregnated material after superheated steam pretreatment was best in this condition. Among them, only moisture content had no significant effect on the weight gain rate of *C. lanceolata*. In the actual utilization of wood, the moisture content of wood was close to the air-dried, considering the actual use of wood and the cost of drying treatment (Kadam et al. 2011), under the condition that the temperature was 120°C, the time was 3 h and the moisture content was air-dried, the permeability of *C. lanceolata* was the best after superheated steam pretreatment.

Effects of freezing treatment on the permeability

Experimental results of freeze-treated C. lanceolata

Tab. 5 shows the weight gain rate of *C. lanceolata* after pretreatment and material impregnated with silica sol. From the data in the table, the weight gain rate of *C. lanceolata* without pretreatment was 12.583% after three days of normal temperature and pressure impregnation. The weight gain rate of *C. lanceolata* impregnated with silica sol after three days after pretreatment ranged from 7.429% to 14.758%, and the weight gain rate was in range

-40.96% to 17.28% over untreated wood. By comparing the weight gain rate of *C. lanceolata* impregnated with silica gel after pre-freezing treatment, it was found that the permeability of some *C. lanceolata* was enhanced after pre-freezing treatment, and the some was decreased, and the group 7 under the condition that *C. lanceolata* was wet specimen, the pre-freezing temperature of -20°C and pre-freezing of 8 h resulted in the best permeability of *C. lanceolata.*

Range analysis of weight gain rate of C. lanceolata frozen treatment

Tab. 8 is an intuitive analysis of the weight gain rate of *C. lanceolata* pretreated impregnated materials after pre-freezing treatment. According to the data in the table, the range values of three factors of pre-freezing treatment were: temperature > moisture content > time, so the influence of three factors in the pre-freezing treatment test was: temperature > moisture content > time. With the decrease of temperature, the weight gain rate of *C. lanceolata* after pre-freezing treatment first decreased and then increased. With the increase of pre-freezing treatment time, the weight gain rate of *C. lanceolata* gradually decreased, the weight gain rate after pre-freezing treatment manifested as wet specimen > oven-dried specimen> air-dried specimen. The weight gain rate of *C. lanceolata* impregnated material was the highest when the temperature was -20°C, treatment time was 8 h and under the condition of wet specimen, that is, the permeability of *C. lanceolata* was the best.

Tab. 8: Maximum analysis of variables on weight gain rate of impregnation of pre-freezing C. lanceolata.

Properties	Level	Temperature (°C)	Time (h)	Moisture content (%)
WPG（%）	Mean1	12.320	11.952	12.248
	Mean2	9.011	11.858	9.840
	Mean3	13.749	11.268	12.990
	Range	4.738	0.684	3.150

ANOVA of weight gain rate of C. lanceolata treated by freezing

Tab. 9 is the variance analysis of the weight gain rate of *C. lanceolata* impregnated materials after pre-freezing treatment. From the variance and significance analysis of factors, it can be seen that the temperature of pre-freezing treatment has a significant effect on the weight gain rate of *C. lanceolata* impregnated silica sol, and the moisture content of *C. lanceolata* also has an effect on the weight gain rate of *C. lanceolata* impregnated after pre-freezing treatment, that is, the moisture content and pre-freezing treatment temperature of *C. lanceolata* have an effect on improving the permeability of *C. lanceolata*, and the time of pre-freezing treatment had little effect on the improvement of *C. lanceolata* permeability.

Tab. 9: Variance analysis and significance test of designed parameters on WPG of impregnation of pre-freezing C. lanceolata.

Factor	Sum of squares	DF	F value	F critical value	Pr > F
Temperature	35.440	2	20.136	19	*
Time	0.825	2	0.469	19	
Water content	16.272	2	9.245	19	
Error	1.76	2			

α =0.05.

Optimization and verification of freezing treatment process of C. lanceolata

In the orthogonal test, the pre-freezing results of *C. lanceolata* under wet material condition are the best, all the specimens of *C. lanceolata* in single factor test were saturated water content state. According to the results of orthogonal test, the best pretreatment time of pre-freezing treatment was 8 hours. Since the temperature was the most significant to the increment rate of *C. lanceolata*, the treatment temperature in the test was selected as: -25°C, -30°C, -35°C, -40°C, and then the pretreated material was impregnated with silica sol at normal temperature and pressure for three days, and each group was repeated eight tests, and the average value was calculated as the final result to compare its weight gain rate.

Tab. 10 shows the change of weight gain rate of *C. lanceolata* pretreated under normal temperature and pressure after dipping silica sol. Through comparing the results of pretreated specimens at different temperatures, we can see that in the range from -40°C to -25°C, the change of weight gain rate of *C. lanceolata* decreases gradually, and the maximum value of 15.058% was obtained when the pretreated temperature was -25°C, that is, the penetration of *C. lanceolata* was the best when the pretreated temperature was -25°C, and the impregnating effect of the modifier is the best.

Based on the results of orthogonal test and single factor test of *C. lanceolata* pre-freezing treatment. The optimum parameters of pre-freezing treatment were as follows: moisture content was saturated, temperature was -25°C, time was 8 h, that is, when the *C. lanceolata* was under saturated condition, treatment temperature was -25°C and treatment time was 8 h, the best penetration and impregnation were obtained.

Tab. 10: Effect of pre-freezing temperature on weight gain rate of C. lanceolata.

No.	Temperature (°C)	WPG (%)
1	-25	15.058
2	-30	14.154
3	-35	13.649
4	-40	13.458

CONCLUSIONS

The impregnation performance of the modified *Cunninghamia lanceolata* were studied by orthogonal test by freezing and steam treatment. The following conclusions could be drawn from this work. The changes of weight gain of *C. lanceolata* under different parameters were studied by freezing and steam treatment, and the optimum steam modification technology was defined. The results from this work showed that when the water content was saturated, temperature was -25°C and time was 8 h, the optimum parameters of pre-freezing treatment of *C. lanceolata* was obtained, at this time, the three-day gain rate of silica sol impregnated at normal temperature and pressure was 15.058%. When the temperature was 120°C, treatment time was 3 h and the moisture content was air-dried specimen, the weight gain rate of *C. lanceolata* impregnated with superheated steam was the highest, at this time, the three-day gain rate of silica sol impregnated at normal temperature and pressure was 15.291%. Compared with the results of

pre-freezing and superheated steam treatment of *C. lanceolata*, it was found that the permeability of *C. lanceolata* increased significantly after superheated steam pretreatment, therefore, the superheated steam treatment should be chosen.

ACKNOWLEDGMENTS

The authors are grateful for the support from the Project from International Cooperation Joint Laboratory for Production, Education, Research and Application of Ecological Health Care on Home Furnishing.

REFERENCES

1. Abd-Elhady, M., 2014: Effect of citric acid, calcium lactate and low temperature prefreezing treatment on the quality of frozen strawberry. Annals of Agricultural Sciences 59(1): 69-75.
2. Alizadeh, B., Fujita, M.,, 2010: Modular datapath optimization and verification based on modular-HED. Ieee Transactions On Computer-Aided Design Of Integrated Circuits And Systems 29(9): 1422-1435.
3. Awoyemi, L., Femi-Ola, T.O., Aderibigbe, E.Y., 2010: Pre-freezing as a pre-treatment for thermal modification of wood. Part 2: surface properties and termite resistance. Journal of the Indian Academy of Wood Science 7(1-2): 19-24.
4. Bao, F., 1992: A study on the principle of permeability control of wood. Scientia Silvae Sinicae 28(4): 336-342.
5. Bao, Y., Zhou, Y., 2017: Comparative study of moisture absorption and dimensional stability of Chinese cedar wood with conventional drying and superheated steam drying. Drying Technology 35(5/8): 860-866.
6. Cortez, D.V., Roberto, I.C., 2012: CTAB, Triton X-100 and freezing-thawing treatments of *Candida guilliermondii*: Effects on permeability and accessibility of the glucose-6-phosphate dehydrogenase, xylose reductase and xylitol dehydrogenase enzymes. New Biotechnology 29(2): 192-198.
7. Didier, G., Brezellec, P., Remy, E., Henaut, A., 2002: GeneANOVA - gene expression analysis of variance. Bioinformatics 18(3): 490-491.
8. Dong, Y., Wang, Y.J., Wang, W., Cao, J.Z., 2018: Preparation and properties of emulsified water repellent made from paraffin wax and silane for wood modification. China Wood Industry 32(04): 18-21.
9. Emaminasab, M., Tarmian, A., Pourtahmasi, K., 2015: Permeability of poplar normal wood and tension wood bioincised by *Physisporinus vitreus* and *Xylaria longipes*. International Biodeterioration & Biodegradation 105: 178-184.
10. Kadam, D.M., Nangare, D.D., Singh, R., Kumar, S., 2011. Low-cost greenhouse technology for drying onion (*Allium cepa* L.) slices. Journal of Food Process Engineering 34(1): 67-82.

11. Lan, Y.Y., Tao, Y.S., Tian, T., Hu, Z.Y., Peng, C.T., 2016: The effect of pre-fermentative freezing treatment on the sensory quality of 'Meili' rosé wine. South African Journal for Enology & Viticulture 35(2): 257-263.
12. Lisiewska, Z., Bczyński, P.G., Kmiecik, W., 2007: Effects of the methods of pre-treatment before freezing on the retention of chlorophylls in frozen leaf vegetables prepared for consumption. European Food Research & Technology 226(1-2): 25-31.
13. Missio., André, L., Mattos., Bruno, D., Cademartori, D., Pedro, H.G., 2015: Effects of two-step freezing-heat treatments on Japanese raisintree (*Hovenia Dulcis* Thunb.) Wood properties. Journal of Wood Chemistry & Technology 36(1): 16-26.
14. Ogawa, T., Chikashige, K., Araki, H., Kitagawa, M., Azuma, K., 2016: Effects of drying methods and pre-treatment conditions on the functional component contents and antioxidant activities in Egoma (*Perilla frutescens* (L.) Bitt. var. frutescens) leaves. Nippon Shokuhin Kagaku Kogaku Kaishi 63(5): 217-224.
15. Pittau, F., Krause, F., Lumia, G., Habert, G., 2018: Fast-growing bio-based materials as an opportunity for storing carbon in exterior walls. Building & Environment 129: 117-129.
16. Poonia, P.K., Hom, S. K., Sihag, K., Tripathi, S., 2016: Effect of microwave treatment on longitudinal air permeability and preservative uptake characteristics of chir pine wood. Maderas Ciencia Y Tecnología 18(1): 125-134.
17. Seo, J.H., Kim, K.I., Hwang, I.G., Yoo, S.M., Choi, M.J., 2015: Effects of thermal treatment and freezing storage period on physicochemical and nutritional characteristics of Shiitake mushrooms. Korean Journal of Food Science & Technology 47(3): 350-358.
18. Tao, J., 2006: Effects of intensive microwave irradiation on the permeability of larch wood. Scientia Silvae Sinicae 42(11): 87-92.
19. Tomas, C., Blanch, E., Fazeli, A., Moce, E., 2013: Effect of a pre-freezing treatment with cholesterol-loaded cyclodextrins on boar sperm longevity, capacitation dynamics, ability to adhere to porcine oviductal epithelial cells in vitro and DNA fragmentation dynamics. Reproduction Fertility and Development 25 (6): 935-946.
20. Tonye, J., Meke-Me-Ze, C., Titi-Nwel, P., 1993: Implications of national land legislation and customary land and tree tenure on the adoption of alley farming. Agroforestry Systems 22(2): 153-160.
21. Vlosky, R.P., Shupe, T.F., 2004: Buyer perceptions and purchasing patterns related to treated wood use in children's playground equipment 54(10): 41-48.
22. Zhang, Y., Miao, P., Zhuang, S., Wang X., Xia, J., Limin, W.U., 2011: Improving the dry-ability of eucalyptus by pre-microwave or pre-freezing treatment. Journal of Nanjing Forestry University (Natural Science Edition)35(02): 61-64.
23. Zlem., Gezici-Ko., Sebastiaan, J.F., Erich, Hendrik, P., Huinink., Leendert, G.J., 2018: Understanding the influence of wood as a substrate on the permeability of coatings by NMR imaging and wet-cup. Progress in Organic Coatings 114: 135-144.
24. Zhu, Z.L., Dietrich, B., Guo, X.L., Cao, P.X., 2020: High-quality and high-efficiency machining of stone-plastic composite with diamond helical cutters. Journal of Manufacturing Processes 58: 914-922.

YUEQIAN YANG, WEI XU*, XIA LIU
CO-INNOVATION CENTER OF EFFICIENT PROCESSING AND UTILIZATION OF FOREST RESOURCES
NANJING FORESTRY UNIVERSITY
NANJING 210037
CHINA
*Corresponding author: xuwei@njfu.edu.cn

XIAODONG (ALICE) WANG
LAVAL UNIVERSITY
DEPARTMENT OF WOOD AND FOREST SCIENCES
QUEBEC
CANADA

WOOD RESEARCH doi.org/10.37763/wr.1336-4561/66.5.732745
e-ISSN 2729-8906
66(5): 2021 732-745 pp.

IMPACT OF THE ELECTRIC CABLES INSTALLATION ON THE IGNITION PARAMETERS OF THE SPRUCE WOOD SURFACE

ALEŠ NEČAS, JOZEF MARTINKA, PETER RANTUCH, IGOR WACHTER, TOMÁŠ ŠTEFKO
SLOVAK UNIVERSITY OF TECHNOLOGY IN BRATISLAVA
SLOVAKIA

(RECEIVED FEBRUARY 2021)

ABSTRACT

This study is aimed to investigate of an impact of electrical cables installed on Norway spruce (*Picea abies* (L.) Karst.) wood board surface on main ignition parameters (mainly critical heat flux, ignition temperature, thermal response parameter and thermal inertia). Ignition parameters have been determined by dependence of ignition times (raised to the power of -1, -1/2 and -0.547) on heat flux. Initiation times have been measured for three configurations of spruce wood boards with surface dimensions of 100 x 100 mm ± 1 mm (the first configuration: board without cables on surface, the second configuration: board with three electrical cables on surface - spacing between cables was equal to their diameter and the third configuration: board with five electrical cables - spacing between cables was equal to their diameter) at five heat fluxes (30, 35, 40, 45 and 50 $kW \cdot m^{-2}$). Obtained results proved that installation of the electrical cables on the spruce wood board surface has a significant impact on the ignition parameters. The critical heat flux (8.5 $kW \cdot m^{-2}$), apparent thermal inertia 0.20 ± 0.02 $kJ^2 \cdot m^{-4} \cdot K^{-2} \cdot s^{-1}$ and ignition temperature 324 ± 105°C of spruce wood board increased up to 18 ± 3 $kW \cdot m^{-2}$ (critical heat flux), 0.68 ± 0.03 $kJ^2 \cdot m^{-4} \cdot K^{-2} \cdot s^{-1}$ (apparent thermal inertia) and 475 ± 27°C (ignition temperature) by the installation of electrical cables on the surface of spruce wood board.

KEYWORDS: Critical heat flux, electrical cables, ignition parameters, thermal inertia, thermal response parameter, spruce wood.

INTRODUCTION

The critical heat flux is the lowest value of the heat flux that still initiates the material. In terms of initiation, a distinction is made between piloted ignition (decomposition products are acted upon by an auxiliary initiation source, e.g. an electric spark) and spontaneous ignition (thermal

decomposition products are initiated by thermal radiation without an auxiliary initiation source). From the point of view of the method of determination, a distinction is made between critical heat flux and minimum heat flux. The critical heat flux is according to Mikkola and Wichman (1989), Janssens (1991), Delichatsios et al. (1991), Tewarson (2002), Spearpoint and Quintiere (2001) determined by the dependence of the initiation time raised to the power of -1, -1/2 or -0.547 on the heat flux. The value of the exponent depends on the chosen calculation method and the thermal thickness of the material. In the equation of statistical dependence compiled in this way, a value of time to ignition (after the exponentiation) is substituted by a value of zero (theoretically corresponds to infinite initiation time) and the critical heat flux is expressed from it. Lawson and Simms (1952) determined the critical heat flux from the dependence of the heat flux on the ratio of heat flux to ignition time raised to 1/2. The minimum heat flux is defined by Babrauskas (2003) as the average value of the highest value of the heat flux that does not yet cause initiation and the lowest value that already causes initiation.

The second important initiation parameter is the thermal inertia, which e.g. Patel et al. (2011) defines as the product of the coefficient of thermal conductivity, heat capacity and density of a material. The thermal inertia determines the resistance of the material to ignition and flame propagation over the surface (with increasing thermal inertia, the resistance of the material increases). The thermal inertia is calculated according to Eq. 1, which is given e.g. Tewarson and Ogden (1992):

$$k \cdot \rho \cdot c = \left(\frac{TRP}{T_i - T_0}\right)^2 \tag{1}$$

where: $k \cdot \rho \cdot c$ is product of thermal conductivity k (kW·m^{-1}·K^{-1}) with density ρ (kg·m^{-3}) and specific heat (kJ·kg^{-1}·K^{-1}) called thermal inertia (kJ^2·m^{-4}·K^{-2}·s^{-1}), TRP is thermal response parameter (kW·s$^{1/2}$·m^{-2}) computed according to Eq. 2, that is stated by Fateh et al. (2014), T_i is ignition temperature (K) and T_0 is ambient temperature (K):

$$TRP = \sqrt{\frac{4}{\pi}} \cdot \frac{1}{Sl} \tag{2}$$

where: Sl is the slope of line that express the dependence of time to ignition to heat flux (-), the time to ignition can be powered on -1, -1/2, -0,547 or on other value (in dependency on used calculation method).

The thermal inertia can also be calculated according to Eq. 3 reported by Lawson and Simms (1952). Eq. 3 is in the original source given for Centimetres – gram – second system of units, so in this study it is modified to the form valid for SI system units:

$$k \cdot \rho \cdot c = 0.00175 \cdot \left(\frac{(q - q_{cr})}{1046} \cdot t_{ig}^{\frac{2}{5}} - 68\right) \tag{3}$$

where: q_{cr} is critical heat flux ($W \cdot m^{-2}$), q is heat flux for which thermal inertia is computed ($W \cdot m^{-2}$) and t_{ig} is time to ignition (s).

The third important initiation parameter is the ignition temperature on the surface of the material at the moment of initiation (hereinafter referred to as ignition temperature). Ignition temperature has a higher informative value than auto-ignition or spontaneous ignition temperature, which were determined by e.g. Zachar et al. (2012) and Vandlickova et al. (2020). The advantage of ignition temperature over auto-ignition or spontaneous ignition temperatures is the fact that ignition temperature is directly applicable in fire modeling and fire hazard assessment of materials. The ignition temperature of the material is calculated according to Eq. 4 given by Spearpoint and Quintiere (2001). A simplified form of Eq. 4 in the form of Eq. 5 is given by Xu et al (2015).

$$q_{cr} = \sigma\left(T_{ig} - T_0\right)^4 + h_c\left(T_{ig} - T_0\right) \quad (4)$$

$$T_{ig} = \left(\frac{q_{cr}}{\sigma}\right)^{1/4} \quad (5)$$

where: σ is the Stefan-Boltzmann constant ($5.67 \cdot 10^{-8}$ $W \cdot m^{-2} \cdot K^{-4}$), T_{ig} is ignition temperature (K), T_0 is the ambient temperature (293 K) and h_c is the natural convective heat transfer coefficient (normally assumed 5 $W \cdot m^{-2} \cdot K^{-1}$).

A large number of works (Su et al. 2019) have dealt with the research of critical heat flux, thermal inertia, ignition temperature and charring depth of wood, wood-based materials and synthetic polymers. Significantly less attention was paid to the stated initiation parameters of elements consisting of different materials, e.g. Furst et al. (2021) investigated the fire resistance of textile-reinforced concrete). The influence of the installation of electrical cables in the grooves in the surface of OSB boards has so far been investigated by only one scientific work by Martinka and Stefko et al. (2020). The published results prove a significant influence of the installation of electrical cables in the grooves in the surface of OSB boards on the initiation parameters. In addition, Martinka and Rantuch et al. (2020) investigated the effect of the installation of a power cable (conducting electric current) in the surface of OSB boards on the surface temperature of the board. So far, however, no scientific work has been published examining the effect of electric cable installation (on the surface of wood or wood material) on the initiation parameters of the resulting composition.

The aim of this paper is to determine the effect of the installation of a power cable on the surface of a Norway spruce wood board (*Picea abies* (L.) Karst.) on the initiation parameters (critical heat flux, ignition temperature, thermal response parameter and apparent thermal inertia) of the final composition.

MATERIALS AND METHODS

Norway spruce wood (*Picea abies* (L.) Karst.) samples were examined on the surface of which a CHKE-R J3x1.5, B2ca, s1, d1, a1 power cable (hereinafter only CHKE-R) was installed.

The configuration of the samples is shown in Fig. 1. Physical properties of spruce wood and electric cable samples are in Tabs. 1 and 2. Water content in the Tab. 1 have been determined from mass of wet sample and mass of sample dried at temperature of 103 ± 2°C (to constant mass). Cross-section of the used electric cable is shown in Fig. 2.

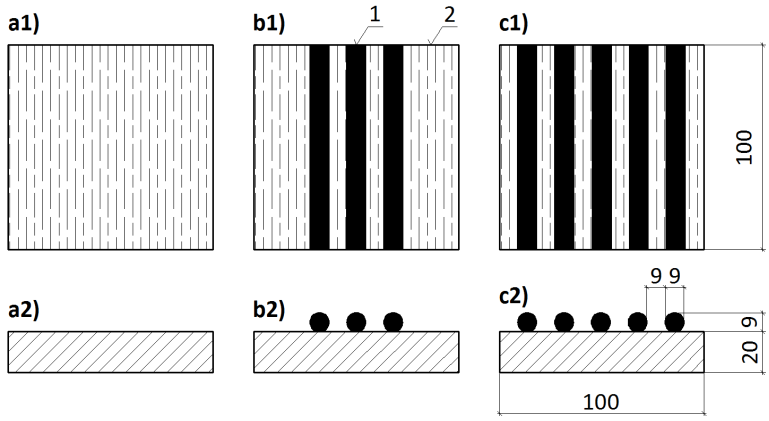

1: Electrical cable; 2: Spruce wood board (dimensions in mm).

Fig. 1: Configuration of the investigated material composition: a) spruce wood board without electrical cables on the surface, b) spruce wood board with three electrical cables on the surface, c) spruce wood board with five electrical cables on the surface (1 - view from the above and 2 - cross-section).

Tab. 1: Physical properties of spruce wood boards.

Thickness (mm)	20 ± 0.1
Water content (mass %)	8 - 10
Density (kg·m^{-3})	422 ± 22

Tab. 2: Physical and fire properties of CHKE-R electrical cable.

Cable diameter (mm)	9
Number of conductors (-)	3
Conductors cross section (mm^2)	1.5
Conductor material (-)	Copper
Material of conductor insulation (-)	Polyethylene
Sheath material (-)	Polyethylene filled with $Al(OH)_3$ + $Mg(OH)_2$
Rated voltage DC (V)	1000
Rated voltage AC (V)	600
Reaction to fire class (-)	$B2_{ca}$, s1, d1, a1

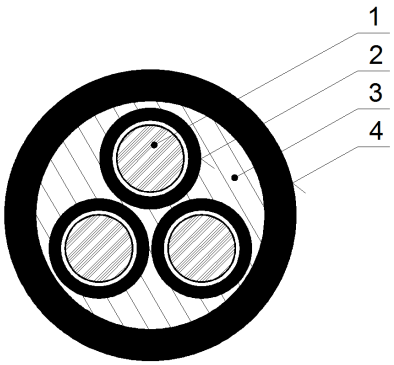

1: Copper wire; 2: wire insulation (polyethylene copolymer); 3: bedding (polyethylene copolymer filled with $Al(OH)_3 + Mg(OH)_2$); 4: sheath (polyethylene copolymer filled with $Al(OH)_3 + Mg(OH)_2$).

Fig. 2: Cross-section of CHKE-R electrical cable.

Critical heat flux (CHF), thermal response parameter (TRP) and apparent thermal inertia (ATI) have been computed from time to ignitions measured at heat fluxes of 30, 35, 40, 45 and 50 $kW \cdot m^{-2}$. Temperature of the cone calorimeter heater has been from 862 K (correspond to the heat flux of 30 $kW \cdot m^{-2}$) to 998 K (correspond to the heat flux of 50 $kW \cdot m^{-2}$). Ignition times at the indicated heat fluxes were determined using a cone calorimeter according to ISO 5660-1: 2015. Critical heat flux have been computed according to Lawson and Simms (1952), Mikkola and Wichman (1989), Janssens (1991), Tewarson (1994, 2002), Spearpoint and Quintiere (2001). Lawson and Simms (1952) computed critical heat flux from the dependency of heat flux to ratio of heat flux to ignition time powered to 1/2. Mikkola and Wichman (1989), Tewarson (1994, 2002), Spearpoint and Quintiere (2001) computed critical heat flux from the dependency of ignition time powered to -1 (thermally think materials) or -1/2 (thermally thick materials) on the heat flux. Mikkola and Wichman (1989) computed the final critical heat flux as a sum of computed critical heat fluxes (from dependence of ignition time on the heat flux) with constant value of 3 $kW \cdot m^{-2}$ (this constant covers heat loses during ignition). Spearpoint and Quintiere (2001) computed the final critical heat flux as a ratio of the critical heat flux (from dependence of ignition time on heat flux) and a constant value of 0.76 (this constant covers heat loses during ignition). Janssens (1991) computed the critical heat flux from the dependence of ignition time (powered to -0.547) on the heat flux. According to the cited author, this method is especially suitable for wood and wood based products.

Ignition temperatures were calculated from critical heat fluxes by procedures according to Spearpoint and Quintiere (2001) and Xu et al. (2015).

RESULTS AND DISCUSSION

Dependence of ignition times (powered on -1, -1/2 and -0.547) on heat flux for investigated materials are shown in the Fig. 3 to 5. Dependence of heat flux on ratio of heat flux to time to ignition powered on 1/2 is in the Fig. 6. Critical heat fluxes (calculated from data in Fig. 3 to 6) are in the Tab. 3. Due to the thickness of the spruce wood samples (20 mm), these behave as thermally thick. Therefore, the heat fluxes in Tab. 3 were calculated for assumption that the examined samples were thermally thick materials.

Tab. 3: Critical heat flux for spruce wood boards with installed electrical cables on their surfaces (configuration is according to Fig. 1).

	Critical heat flux ($kW \cdot m^{-2}$)		
Method (-) / Configuration (-)	1st	2nd	3rd
Lawson and Simms (1952)	21	24	21
Mikkola and Wichman (1989)	6.5	17.5	10
Janssens (1991)	7	16	9
Spearpoint and Quintiere (2001)	4.5	19	9
Tewarson (2002)	3.5	14.5	7
Average	8.5 ± 6	18 ± 3	11 ± 5

In the 3rd configuration, for all the examined heat fluxes (30 to 50 $kW \cdot m^{-2}$), the electric cable installed on the surface was ignited first and the spruce wood was ignited subsequently. The 2nd configuration showed different behaviour: at heat fluxes of 30 and 35 $kW \cdot m^{-2}$ the electric cable was ignited first; at heat fluxes of 40, 45 and 50 $kW \cdot m^{-2}$ spruce wood was ignited first.

The effect of electric cable installed on the surface of the spruce wood board was assessed by one-way analysis of variance (ANOVA) at the significance level of $\alpha = 0.05$. The calculated values ($p = 0.048$; $F = 3.94$ and $F_{crit} = 3.89$) prove that the installation of an electric cable on the surface of the spruce wood board has a significant effect on the change (increase) of the critical heat flux of the resulting composition. This is because wood and wood-based materials have a lower critical heat flux (higher tendency to initiation) than electric cables. This conclusion is also confirmed by the results of scientific work of Scudamore et al. (1991), Babrauskas (2003), Rantuch et al. (2018a,b). Under the test conditions, an electric cable with a diameter of 9 mm was installed on a spruce board (2nd and 3rd configuration according to Fig. 1). Since the heat flux decreases with the square of the distance, the heat flux incident on the surface of the wood board was thus slightly lower in the 2nd and 3rd configuration than in the 1st configuration. Thus, in the 1st configuration, the highest heat flux fell on the surface of the spruce board, while in the 2nd and 3rd configuration, the higher heat flux irradiates the surface of the electric cables.

Comparison of the data in Tab. 3 with the data published by Scudamore et al. (1991), Babrauskas (2003), Rantuch 2018a,b shows that the average critical heat flux (in Tab. 3) reaches similar values as the critical heat flux of organic polymers (natural and synthetic) and electrical cables published in most scientific papers.

Ignition temperatures of the examined samples are shown in Tab. 4. As ignition temperatures are calculated from critical heat flux (according to Eqs. 4 and 5), results from the ANOVA show a statistically significant effect of electric cable installation on spruce wood board surface not only on critical heat flux but also on ignition temperatures.

A comparison of the data in Tab. 4 with the data published by Babrauskas (2003) proves that more realistic values of ignition temperatures are provided by the method according to Xu et al. (2015). Ignition temperatures calculated according to Spearpoint and Quintiere (2001) are too high.

Tab. 4: Ignition temperatures of spruce wood boards with installed electrical cables on their surfaces (configuration is according to Fig. 1).

	Ignition temperature (°C)		
Method (-) / Configuration (-)	1st	2nd	3rd
Spearpoint and Quintiere (2001)	544 ± 135	729 ± 29	619 ± 77
Xu et al. (2015)	324 ± 105	475 ± 27	381 ± 65

Thermal response parameter (TRP) is in the Tab. 5 and apparent thermal inertia is in the Tab. 6.

Tab. 5: Thermal response parameters of spruce wood boards with installed electrical cables on their surfaces (configuration is according to Fig. 1).

Configuration (-)	Thermal response parameter ($kW \cdot s^{1/2} \cdot m^{-2}$)
1st	159
2nd	198
3rd	313

Tab. 6: Apparent thermal inertia of spruce wood boards with installed electrical cables on their surfaces (configuration is according to Fig. 1).

	Thermal inertia ($kJ^2 \cdot m^{-4} \cdot K^{-2} \cdot s^{-1}$)		
Method (-) / Configuration (-)	1st	2nd	3rd
Lawson and Simms (1952)	0.20 ± 0.02	0.36 ± 0.01	0.68 ± 0.03
Tewarson and Ogden (1992)	0.11 ± 0.05	0.08 ± 0.01	0.28 ± 0.06

Comparison of TRP in Tab 5 with the results of scientific work of Babrauskas (1992) and Khan et al. (2016) and ASTM E1321-13 (2013) demonstrate that the TRP of the investigated material compositions is comparable to the average TRP of ordinary polymers ($257 \pm 15\ kW \cdot s^{1/2} \cdot m^{-2}$).

The values of thermal inertia (Tab. 6) are comparable with the values ($0.54 \pm 0.38\ kJ^2 \cdot m^{-4} \cdot K^{-2} \cdot s^{-1}$) determined by Spearpoint and Quintiere (2001) for along grain orientation of selected wood species.

Increasing values of TRP (Tab. 5) and thermal inertia (Tab. 6) indicate increasing resistance of the 2nd and 3rd configuration to initiation and flame propagation (compared to the 1st configuration). This conclusion roughly corresponds to the critical heat flux (Tab. 3) and ignition temperature (Tab. 4).

Comparison of the coefficients of determination (R^2) in Fig. 3 to 6, as well as the data in Tab. 3 (critical heat flux above $20\ kW \cdot m^{-2}$ is unrealistic for the investigated compositions) proves that, for wood and wood-based materials (20 mm thick) with installed electric cables on the surface (if the spacing is equal to the diameter of electric cables), the best explanatory value is the dependence of the initiation time raised to -1/2 or -0.547 on the heat flux for the purpose of calculation of the initiation parameters.

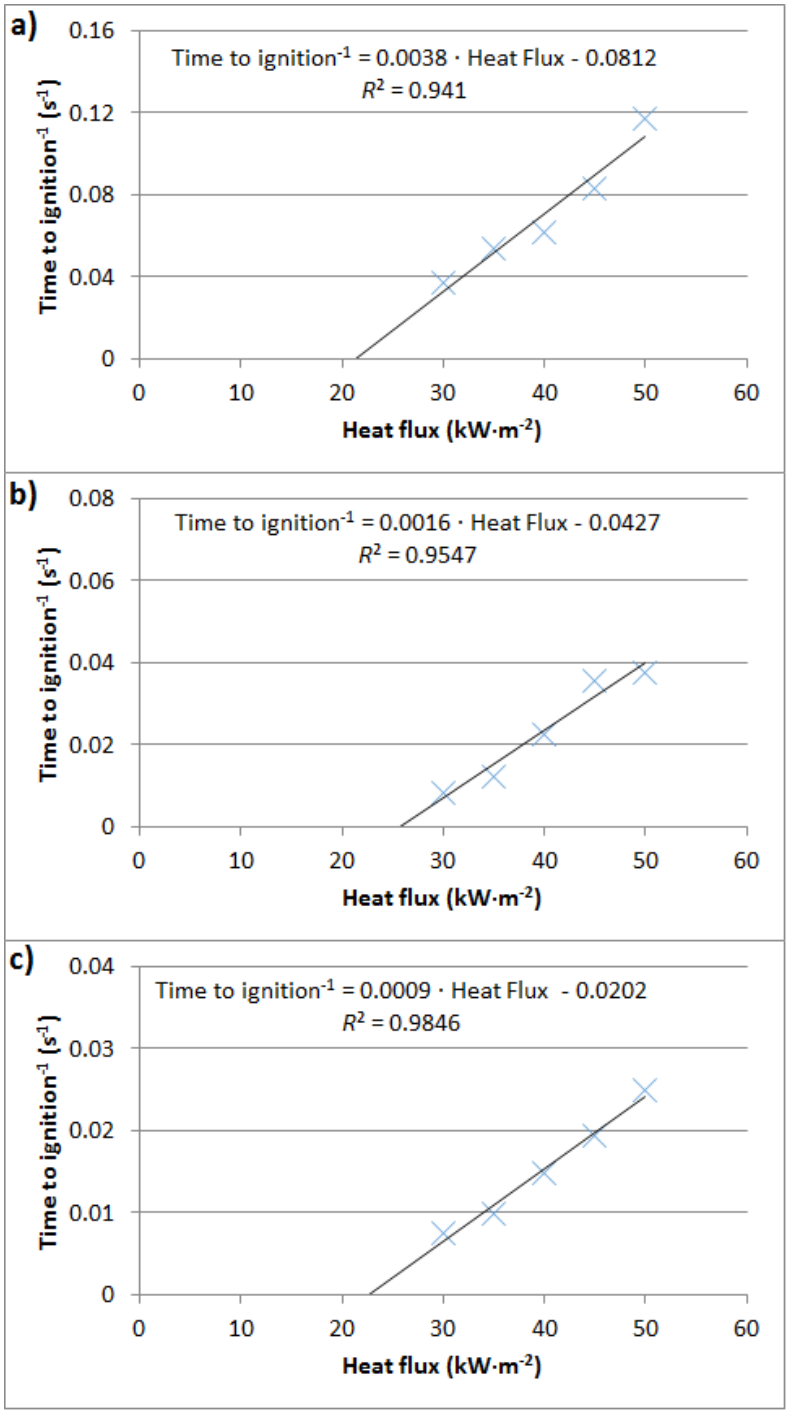

Fig. 3: Dependence of ignition time^{-1} on heat flux for three configurations of spruce wood board and electrical cable a) configuration according to Fig. 1a; b) configuration according to Fig. 1b; c) configuration according to Fig. 1c (assumption of thermally thin material).

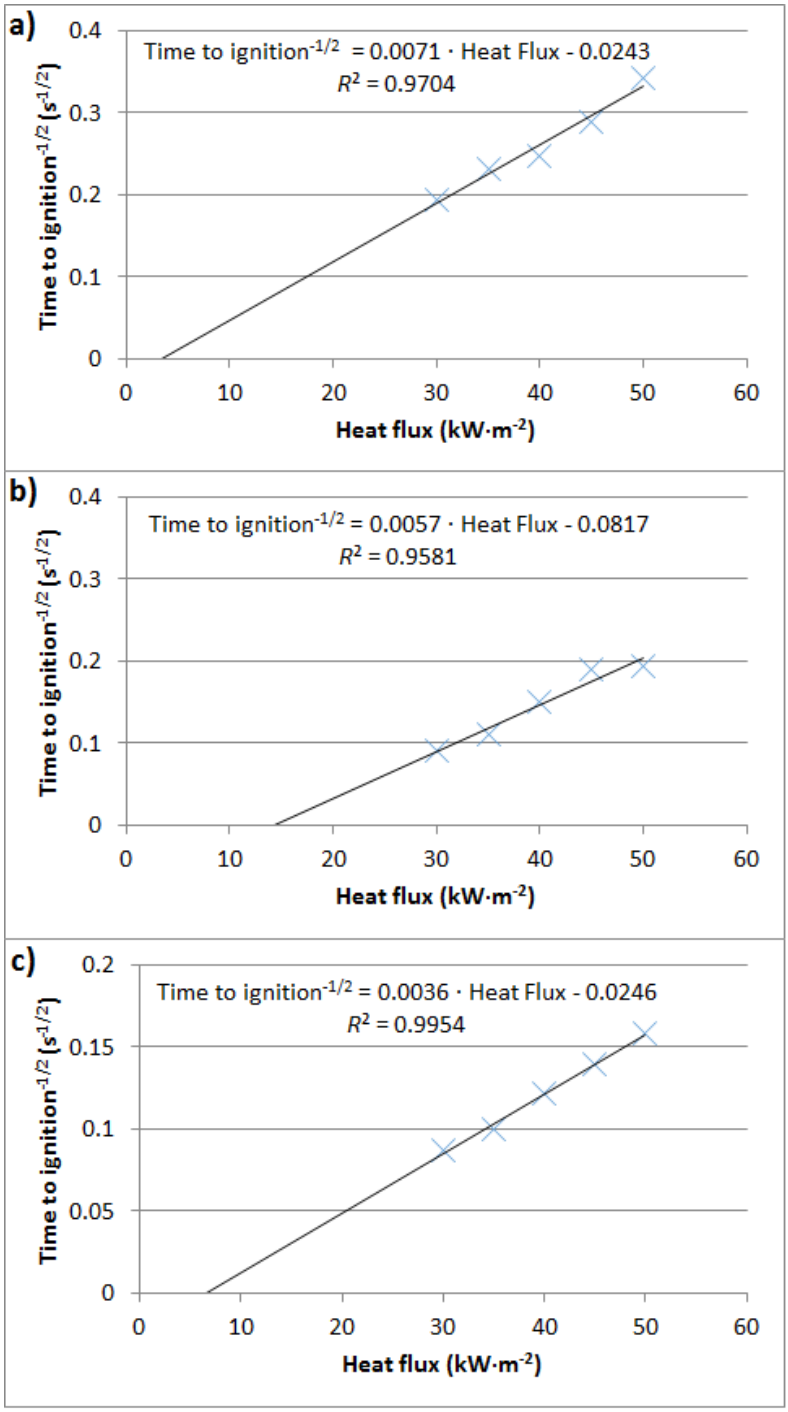

Fig. 4: Dependence of ignition time$^{-1/2}$ on heat flux for three configurations of spruce wood board and electrical cable a) configuration according to Fig. 1a; b) configuration according to Fig. 1b; c) configuration according to Fig. 1c (assumption of thermally thick material).

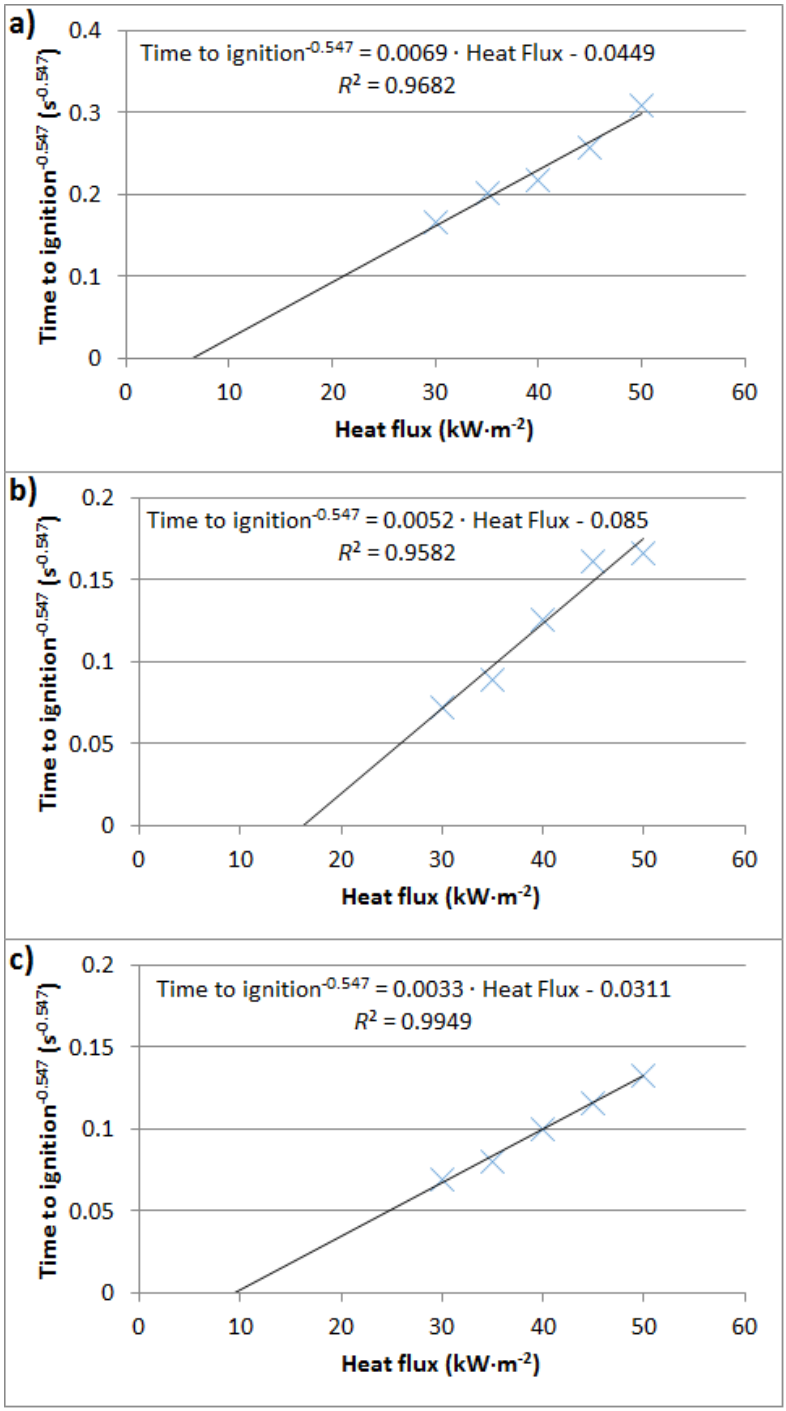

Fig. 5: Dependence of ignition time$^{-0.547}$ on heat flux for three configurations of spruce wood board and electrical cable a) configuration according to Fig. 1a; b) configuration according to Fig. 1b; c) configuration according to Fig. 1c (assumption of thermally thick material, calculation procedure is according to Janssens 1991).

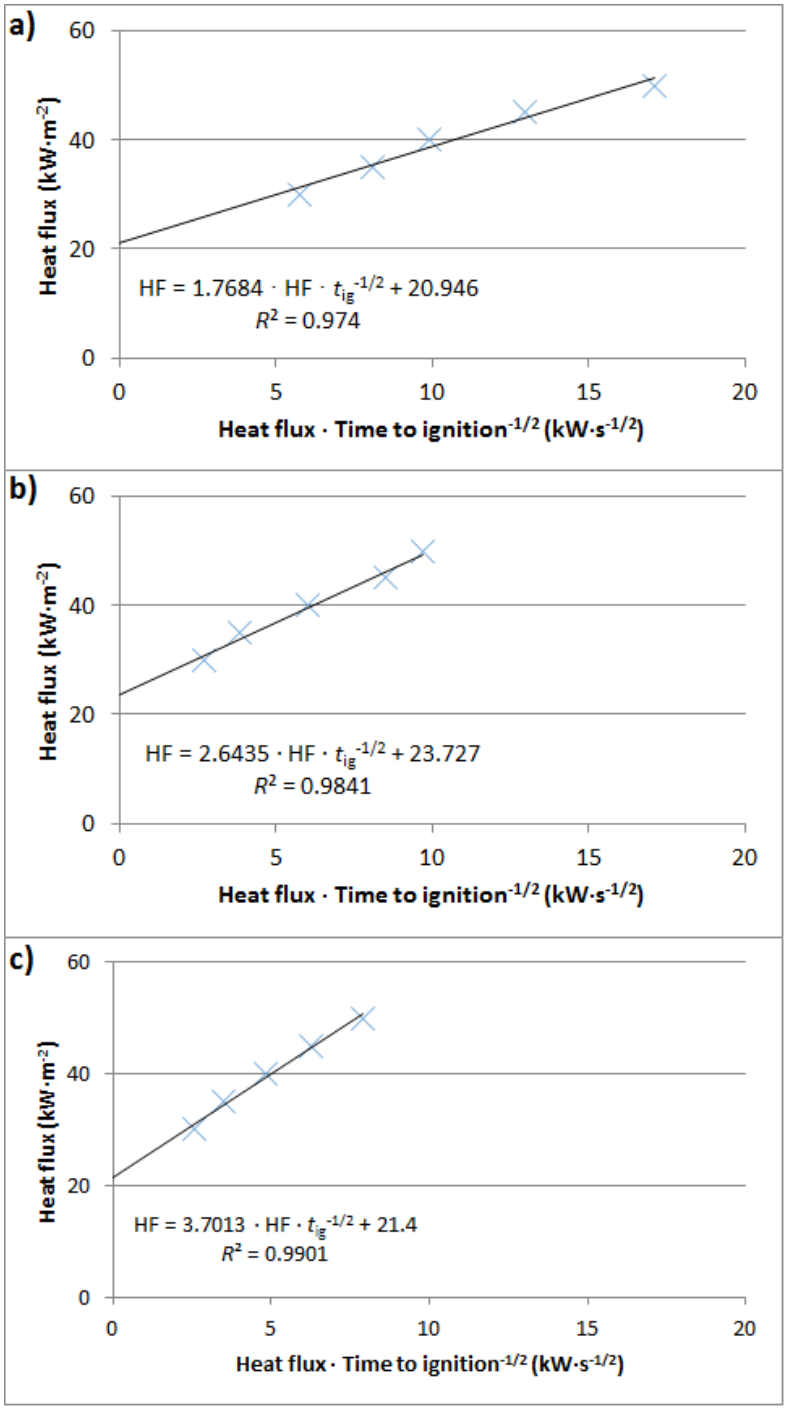

Fig. 6: Dependence of heat flux on ratio of heat flux to time to ignition (powered on 1/2) for three configurations of spruce wood board and electrical cable a) configuration according to Fig. 1a; b) configuration according to Fig. 1b; c) configuration according to Fig. 1c (HF denote heat flux and t_{ig} denote time to ignition, calculation procedure is according to Lawson and Simms 1952).

CONCLUSIONS

This paper deals with the influence of installation of power electric cable (reaction to fire class B_{2ca}, s_1, d_1, a_1), installed on the surface of a spruce wood board, on the initiation parameters (critical heat flux, apparent thermal inertia, ignition temperature and thermal response parameter). The data obtained show that the installation of an electric cable on the surface of a spruce wood board will significantly increase the critical heat flux (from 8.5 ± 6 $kW \cdot m^{-2}$ to 18 ± 3 $kW \cdot m^{-2}$), ignition temperature (from 324 ± 105°C to 475 ± 27°C) thermal response parameter (from 159 $kW \cdot s^{1/2} \cdot m^{-2}$ to 313 $kW \cdot s^{1/2} \cdot m^{-2}$) and apparent thermal inertia (from 0.20 ± 0.02 $kJ^2 \cdot m^{-4} \cdot K^{-2} \cdot s^{-1}$ to 0.68 ± 0.03 0.02 $kJ^2 \cdot m^{-4} \cdot K^{-2} \cdot s^{-1}$). These values prove that the installation of electrical cables on the surface of wood and wood-based materials must be taken into account when evaluating the initiation parameters of the resulting material compositions. The recorded increase is so significant that it must be considered in modelling the flame spread over the surface (the key parameter for modelling flame spread is apparent thermal inertia) or modelling the development of fire in fire compartments with the presence of wooden elements with electric cables installed on their surface.

ACKNOWLEDGEMENTS

This work was supported by the Slovak Research and Development Agency under the contract No. APVV-16-0223. This work also supported by the KEGA agency under the contracts No 001TU Z-4/2020 and 016STU-4/2021.

REFERENCES

1. ASTM E1321-13, 2013: Standard test method for determining material ignition and flame spread properties.
2. Babrauskas, V., 1992: The cone calorimeter. In: Heat release in fires (eds. Babrauskas, V., Grayson, S.J.). Pp 61-92, Elsevier Publishing Company, London.
3. Babrauskas, V., 2003: Ignition handbook. Fire Science Publishers. Issaquah, 1128 pp.
4. Delichatsios, M.A., Panagiotou, Th., Kiley, F., 1991: The use of time to ignition data for characterizing the thermal inertia and the minimum (critical) heat flux for ignition or pyrolysis. Combustion and Flame 84(3-4): 323-332.
5. Fateh, T., Rogaume, T., Luche, J., Richard, F., Jabouille, F., 2014: Characterization of the thermal decomposition of two kinds of plywood with a cone calorimeter – FTIR apparatus. Journal of Analytical and Applied Pyrolysis 107(1): 87-100.
6. Furst, R., Vlach, T., Pokorny, M., Mozer, V., 2021: Study of behavior of textile-reinforced concrete with epoxy resin matrix in fire. Fire and Technology 14: 22.
7. ISO 5660-1:2015, 2015: Reaction to fire tests. Heat release, smoke production and mass loss rate. Part 1: Heat release rate (cone calorimeter method) and smoke production rate (dynamic measurement).

8. Janssens, M.L., 1991: A thermal model for piloted ignition of wood including variable thermophysical properties. In: Fire Safety Science – proceedings of the third international symposium (eds. Cox, D., Langford, B.). Pp 167-176, International Association for Fire Safety Science, London.
9. Khan, M.M., Tewarson, A., Chaos, M., 2016: Combustion characteristics of materials and generation of fire products. In: SFPE Handbook of Fire Protection Engineering (ed. Hurley, M.J.). Pp 1143-1232, Springer. New York.
10. Lawson, D.I., Simms, D.L., 1952: The ignition of wood by radiation. British Journal of Applied Physics 3(9): 288-292.
11. Martinka J., Rantuch P., Stefko T., Wachter I., 2020: Electric cables installed in OSB boards surfaces and their temperature. In: Wood and Fire Safety (eds. Osvaldova, L., Markert, F., Zelinka, S.). Pp 426-431, Springer. Cham.
12. Martinka, J., Stefko, T., Wachter, I., Rantuch, P., 2020: Impact of electrical cables embedded into oriented strand board on critical heat flux. Wood Research 65(2): 257-270.
13. Mikkola E., Wichman, I.S., 1989: On the thermal ignition of combustible materials. Fire and Materials 14(3): 87-96.
14. Patel, P., Hull, T.R., Stec, A.A., Lyon, R.E., 2011: Influence of physical properties on polymerflammability in the cone calorimeter. Polymers Advanced Technologies 22(1): 1100-1107.
15. Rantuch, P., Štefko, T., Martinka, J., 2018a: Critical heat flux determination of electric cable insulation. Research papers Faculty of Materials Science and Technology Slovak University of Technology in Trnava 26(42): 11-20.
16. Rantuch, P., Štefko, T., Martinka, J., Wachter, I., Kobetičová, H., 2018b: Impact of initiator placement on ignition of the vertically positioned electrical cable. In: SGEM Proceedings of the 18th International Multidisciplinary Scientific GeoConference Nano, Bio and Green - Technologies for a Sustainable Future. Pp 419-426, STEF 92 Technology. Vienna.
17. Scudamore, M.J., Briggs, P.J., Prager, F.H., 1991: Cone calorimetry—a review of tests carried out on plastics for the association of plastic manufacturers in Europe. Fire and Materials 15(2): 65-84.
18. Spearpoint, M.J., Quintiere, J.G., 2001: Predicting the piloted ignition of wood in the cone calorimeter using an integral model - effect of species, grain orientation and heat flux. Fire Safety Journal 36(4): 391-415.
19. Su, H.C., Tung, S.F., Tzeng, C.T., Lai, C.M., 2019: Variation in the charring depth of wood studs inside wood-frame walls with time in a fire. Wood Research 64(3): 449-460.
20. Tewarson, A., 1994: Flammability parameters of materials: ignition, combustion, and fire propagation. Journal of Fire Sciences 12(4): 329-356.
21. Tewarson, A., 2002: Generation of heat and chemical compounds in fires. In: The SFPE Handbook of Fire Protection Engineering (ed. DiNenno PJ). Pp 618-697, National Fire Protection Association. Quincy.
22. Tewarson, A., Ogden, S.D. 1992: Fire behavior of polymethylmethacrylate. Combustion and Flame 89(3-4): 237-259.

23. Vandlickova, M., Markova, I., Osvaldova, L.M., Gaspercova, S., Svetlik, J., Vraniak, J., 2020: Tropical wood dusts - granulometry, morfology and ignition temperature. Applied Sciences 10(21): 1-15.
24. Xu, Q., Chen, L., Harries, K.A., Zhang, F., Liu, Q., Feng, J., 2015: Combustion and charring properties of five common constructional wood species from cone calorimeter tests. Construction and Building Materials 96(1): 416-427.
25. Zachar, M., Mitterova, I., Xu, Q., Majlingova, A., Cong, J., Galla S., 2012: Determination of fire and burning properties of spruce wood. Drvna Industrija 63(3): 217-223.

ALEŠ NEČAS, *JOZEF MARTINKA, PETER RANTUCH, IGOR WACHTER,
TOMÁŠ ŠTEFKO
SLOVAK UNIVERSITY OF TECHNOLOGY IN BRATISLAVA
FACULTY OF MATERIALS SCIENCE AND TECHNOLOGY IN TRNAVA
JANA BOTTU 2781/25
917 24 TRNAVA
SLOVAKIA
*Corresponding author: jozef.martinka@stuba.sk

WOOD RESEARCH doi.org/10.37763/wr.1336-4561/66.5.746761
e-ISSN 2729-8906
66(5): 2021 746-761 pp.

A COMPARISON OF METABOLITES IN WOOD-FORMING TISSUES FROM EIGHT COMMERCIAL TIMBER TREE SPECIES OF HEILONGJIANG PROVINCE IN CHINA

JIANGTAO SHI, JUNYI PENG, CHONGYANG XIA
NANJING FORESTRY UNIVERISTY
CHINA

JIAN LI
NOTHEAST FORESTRY UNIVERISTY
CHINA

(RECEIVED JANUARY 2021)

ABSTRACT

Four coniferous and four deciduous commercial tree species from Northeastern of China were selected to investigate the differences of metabolites in wood-forming tissues by gas chromatography-mass spectrometry. The results showed that the identified metabolites mainly consisted of neutral sugars, lipids, and organic acids. The mean contents of both arabinofuranose and 1-cyclohexene-1-carboxylic acid were higher in coniferous trees than in deciduous ones. Similarly, the D-fructose and D-glucose content was significantly higher in coniferous trees than deciduous trees, but the total contents of these two sugars was roughly equal among most tree species. The mean content of lactic acid, glycerol and malic acid was lower in coniferous trees than deciduous trees. The malic acid content decreased in later-stages of wood formation than in early-stage for all tree species. The content of L-proline and myo-inositol was greater in later-stage of wood formation than early-stage. The content of octadecanoic acid, D-fructose and D-glucose decreased in later-stage of wood formation for most tree species. All of this suggested that the metabolites in wood-forming tissues showed the significance of species-specific and seasonal dynamic differences among the eight tree species.

KEYWORDS: Metabolic profiling, early wood, latewood, wood formation, sugars.

INTRODUCTION

Wood formation is controlled by both endogenous and exogenous factors. Endogenous factors such as tree genotype or physiological processes (Schrader et al. 2004), can be termed as

different genus and different tree species, e.g. coniferous trees and deciduous trees. Generally Coniferous trees produce softwood where hardwoods come from deciduous trees. It is known that softwoods mainly consist of uniform wood cells (tracheids), whereas multitudinous cells (vessels, fibers, rays) make up the structure of hardwoods. Furthermore, softwoods possess a higher lignin content than hardwoods, whereas hardwoods contain a greater concentrations of hemicellulose. It is due to these differences and variation in the anatomy and chemistry of woods that result in the difficulties that softwoods and hardwoods face for many applications. On the other hand, temperature, light and water availability (Deslauriers and Morin 2005) also serve as important exogenous factors that affect the development of wood characteristics, like early-wood, later-wood, and growth rings. From a biochemistry perspective, wood formation is the results of a tree converting free carbon dioxide to organic carbon via photosynthesis and through the complex and efficient biosynthesis, which is a process of energy metabolic and substance transformation. During wood forming there are there are many precursors, intermediates and enzymes, which influence the metabolites present and participate in the physiological activity of the wood forming. The metabolization of wood formation is a dynamic life function. However, the knowledge of the metabolites present during wood formation and their difference within tree species is limited.

Because of the large variation and differences in metabolites, the metabolism was employed as the basic analytical method to understand the wood forming. By focusing on the metabolites, molecular weight less than 1000 Da, all participated in organism or physiology histocyte. Morris et al found that the relationship between the cellulose content and metabolites in the wood forming tissues from various genotypes of Loblolly pine, as well as showing that the metabolic level can be used as tool for the study of wood formation (Morris et al. 2004). Robinson reported that the metabolites in wood-forming tissues of *Pseudotsuga menziesii* showed a strong dependence on phenotypic characteristic and growing location, rather than hereditary constitution (Robinson et al. 2007). Compared to normal wood, the relative contents of shikimic acid and coniferin, which serve as important intermediates in lignin biosynthesis, significantly increased in accordance with the higher lignin content present in compression wood (Yeh et al. 2006). Andersson-Gunneras et al. (2006) measured metabolites present in wood-forming tissues of *Populus davidiana* Dode using GC-MS combined with the gene expression analysis, the results suggested that the cell wall polymer biosynthesis undergoes de novo programmed regulation. Saccharides and lipids content was greater in *Pinus koraiensis* compression wood-forming tissues compared to normal wood tissues and the changes were related to inclination angle and degree (Shi and Li 2012). However, the analysis of the metabolic process of wood formation and simultaneous comparison among several tree species has never been reported or found in any literature review.

Herein, eight tree species, *Pinus koraiensis*, *Pinus sylvestris*, *Abies nephrolepis*, *Larix gmelini*, *Betula platyphylla*, *Fraxinus mandshurica*, *Populus simonii* and *Ulmus propinqua* were selected. These tree species are economically and ecologically important species in the timberline of northeastern of China, where they play an important role in forestry ecology and wood supply. In our previous studies (Shi and Li 2016), the early-stage

wood-forming tissues were analyzed by Fourier Transformed Infrared spectroscopy method to distinguish the differences among tree species. Thus, the objective of this work aimed to understand: *(1)* the differences between the metabolites in wood-forming tissue of coniferous and deciduous trees species, *(2)* the changes of metabolites in early-stages and later-stages of wood formation in one growth season. The differences in the metabolites present in wood-forming tissue of the different tree species were determined and compared based on the differences between coniferous and deciduous trees, as well as early-stage and late-stage wood formation.

MATERIAL AND METHODS

Plant materials and collection

Eight important coniferous and deciduous trees growing under the same climatic conditions, which were healthy stands with three replicates for each tree species, were selected from the forestry land, Harbin, China. The ages and diameters of the trees are presented in Tab. 1. The wood forming-tissues were collected in June and September 2016 according to the former publishes (Shi and Li 2012, Paiva et al. 2008). To collect the wood-forming tissues, the bark of each tree (three trees each species) was removed at chest height (above ground 1.25 m) and the differentiating xylem tissues were scraped with a razor blade from the outermost side of the exposing stem. The harvested tissues were frozen in the liquid N_2 immediately. Wood samples were well grinded in the liquid nitrogen and stored at -80°C.

Tab. 1: Information of sampling trees.

Species	Average diameter at breast high (cm)	Average tree age (year)
Pinus sylvestris	26.8	55
Pinus koraiensis	16.5	52
Abies nephrolepis	25.3	58
Larix gmelini	21.6	46
Fraxinus mandshurica	21.3	59
Populus simonii	13.5	9
Ulmus propinqua	13.5	28
Betula platyphylla	14.5	35

Metabolites extraction and GC-MS examination

The metabolites of wood-forming tissues were extracted according to our previous reports (Shi and Li 2012, Lisec et al. 2006). In brief, about 50 mg of frozen wood powder was placed in a 1.5 mL tube and mixed with 1 mL of precooled methanol and 45 µL Ribitol (Sigma, USA) (dissolution in ddH_2O and 2 $mg \cdot mL^{-1}$, according to an internal standard). The mixture was incubated at 70°C and 950 rpm for 15 min then for centrifuged 10 min at 12000 rpm. The supernatant was then mixed with equal parts volume of precooled chloroform and incubated at 37°C and centrifuged 950 rpm for 5 min. Then 500 µL of ddH_2O at 4°C was added and centrifuged at 4000 rpm for 15 min. The 200 µL supernatant was vacuum-dried at -60°C for 4 hours and then re-dissolved in 50 µL Solution A [20 $mg \cdot mL^{-1}$ Methoxyamine hydrochloride

(Sigma, USA) dissolved in Pyridine (Sigma, USA)]. The mixture was incubated at 37°C for 2 hours and then 100 μL of Solution B [20 $\mu L \cdot ml^{-1}$ Alkanes (Sigma, USA) dissolved in MSTFA (Sigma, USA)] was added at the same temperature and incubated for 30 min. After 24 hours at room temperature, one micro liter extraction was injected into the GC-MS (Varian450GC-240MS, USA), which has a VF-5 ms column (30 m × 0.25 mm × 0.25 μm). Injection port temperature was 250°C, with a flow rate of 1.0 $ml \cdot min^{-1}$, initial temperature of 70°C and heating rate of 5°C$\cdot min^{-1}$ until a 300°C and cooled for 5 min until 70°C was reached. Helium (99.99%) was used as a carrier gas and a flow rate of 2 $ml \cdot min^{-1}$ was maintained with a split-flow of 50 : 1000. The electron bombardment of the MS ionization was at 70eV with an ion source temperature of 300°C and mass range of 50-1000 $m \cdot z^{-1}$.

Data acquisition and analyze

The gas chromatogram was observed using MS Workstation version 6.9.3 and the online results were searched with the NIST (National Institute of Standard and Technology, USA) mass spectrum data with a similarity ≥ 75%, and referred to related literature for metabolites identification and classification (Yeh et al. 2006, Shi and Li 2012, 2015). The metabolites relative contents were expressed by the equation of:

$$C_x = [(A_x/A_i) \times 0.045 \times 2 \text{ mg mL}^{-1}] / m_0 \ (\text{mg} \cdot \text{g}^{-1}) \quad (1)$$

where: C_x is the relative content of identified metabolite; A_x is the peak area of identified metabolite; A_i is the peak area of internal standard; and m_0 is the dry weight of wood-forming tissue (Shi and Li 2012).

RESULTS AND DISCUSSION

Overall of metabolites in wood forming-tissue of coniferous and deciduous trees

The comprehensive comparison of chromatograms in the eight tree species and 45 peaks were selected. Based on the mass spectrum database reported by (Yeh et al. 2006, Shi and Li 2012), 34 peaks were identified and 11 peaks were unknown. Figs. 1 and 2 show the categories and varieties of metabolites in wood-forming tissue from the eight-tree species. In these figures, it can be observed that metabolites were different between tree species. The identified metabolites were mainly classified into neutral sugars, lipids, organic acid, amino acid, *N*-compounds. Neutral sugars, which are the foundation of energy and substance metabolism in trees, are the most predominant metabolites. D-fructose, D-glucose and a-d-glucopyranoside were the most abundant sugars in the wood-forming tissue, but their contents varied by tree species and the growth season (Tabs. 2 and 3). The percentage of total sugars in coniferous tree metabolites was usually from 43.74% - 84.04%, but was 31.22% - 87.95% in deciduous trees (Figs. 1 and 2). The total percentage of sugars present was lowest at 31.22% and highest at 87.95% in *F. mandshurica* early-stage and *P. simonii* late-stage of the growth season, respectively. In all eight species, the total sugar concentration increased in

the later-stages compared to the early-stages of the growth season. This seasonal trend of total sugar content was consistent with the former reports (Budzinski et al. 2016, Gruber et al. 2013, Dietze et al. 2014), which suggested that, during later-stages of wood formation, low temperature and water availably caused a reduction of wood cell wall biosynthesis. More carbohydrates were able to be mobilized for the next growing season when there was more supply respiration during low photosynthesis (Ögren 2000), better response to cold acclimation (Welling and Palva 2006, Bonhomme et al. 2009, Turhan and Ergin 2012) and early spring growth (Barbaroux and Breda 2002). D-xylose was only detected in deciduous species, which corresponded to higher xylose content in hardwood hemicellulose.

The lipids were the second most abundant metabolites and were comprised of hexadecanoic acid, octadecanoic acid and monostearin. Similar to sugar metabolites, the percentage of lipids was commonly lower in coniferous woods (0.92%-7.14%) than in deciduous woods (1.19%-12.52%). However, the lipids concentration in all tree species sharply decreased in later-stage of the growth season than in the early-stage. Obst (1998) defined hexadecanoic acid and octadecanoic acid as cutin, which plays an important role in protecting woods (Obst 1998).

The result indicated that when living at boreal and temperate regions, higher of levels of lipid present in the wood tissue is beneficial for trees during colder temperatures and trends to slow wood formation.

In addition, many organic acids, such as malic acid and lactic acid, were detected in wood-forming tissues of all the tree species. The organic acid was commonly intermediate of the tricarboxylic acid (TCA) cycle and incorporated in the TCA cycle to generate energy (Fernie et al. 2004, Hijza and Killiny 2017). The percentage of organic acid was much higher in deciduous trees (4.8% - 6.13%) than in coniferous trees (1.23% - 2.17%) at the early-stage of wood formation (Fig. 1). This was maybe due to greater photosynthesis effectiveness of deciduous trees over conifer trees. However, at late-stage wood formation the organic acid percentages was almost the same (Fig. 2). In *A. nephrolepis* and *L. gmelini,* organic acid concentration increased more in winter than in summer, whereas *P. koraiensis* and *P. sylvestris* showed the inverse change. Interestingly, the organic acid concentration in all deciduous woods significantly decreased in winter compared to the summer. The defoliation in deciduous trees is responsible for the decrease in organic acid concentrations in the winter.

Low quantities of alcohol metabolites were also detected, of which myo-inositol and glycerol were the most predominant in the wood-forming tissues. The percentage of alcohol was lower in coniferous trees than in deciduous trees (Figs.1 and 2). The variation of total alcohols during the change in seasons was different for each tree species. Contrary to the Budzinski's report (Budzinski et al. 2016), most amino acid metabolites were more abundant in the later-stage of wood formation for all tree species (Figs.1 and 2).

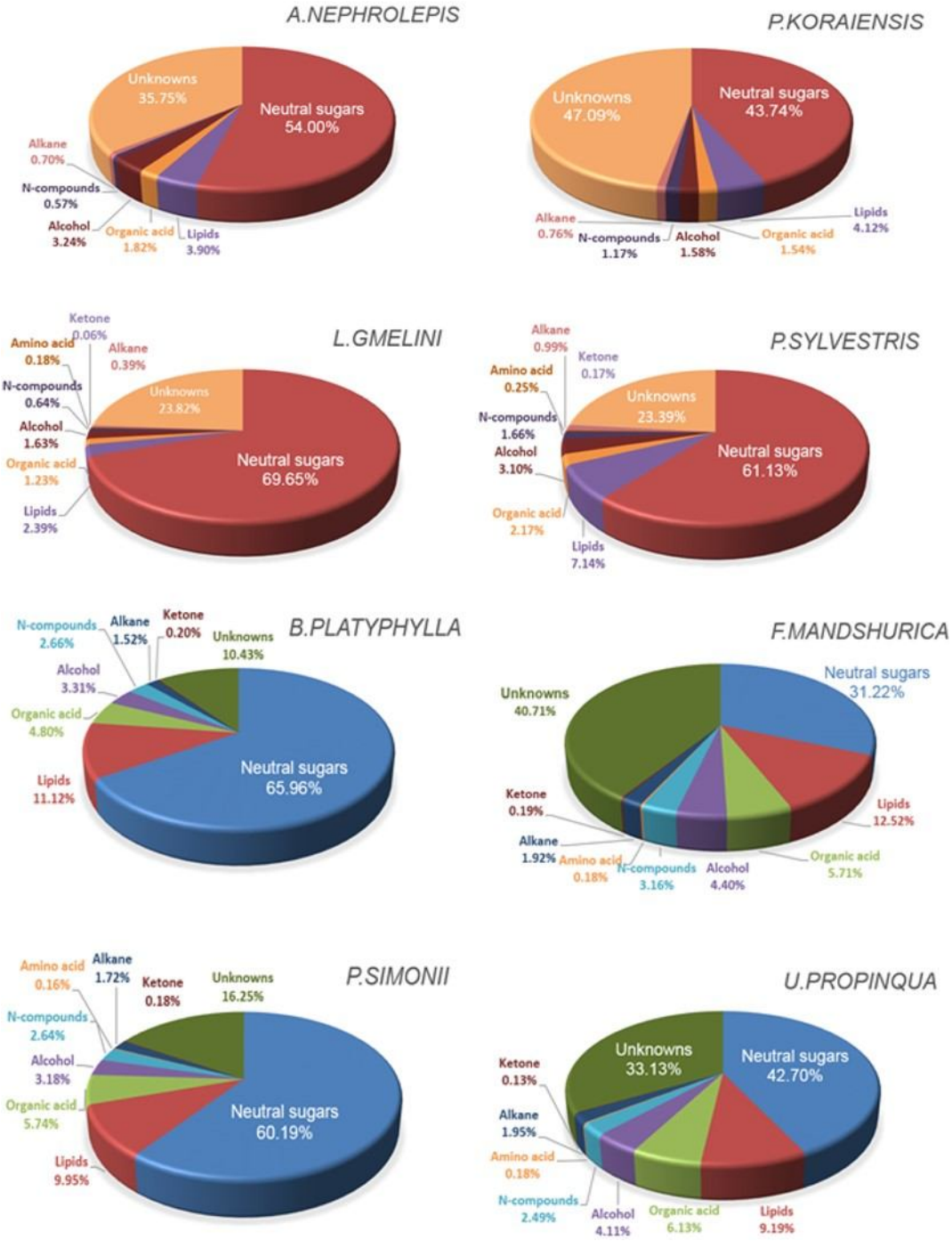

Fig. 1: Percentage composition of metabolites in the wood forming-tissue from 8 tree species at early-stage of growth season.

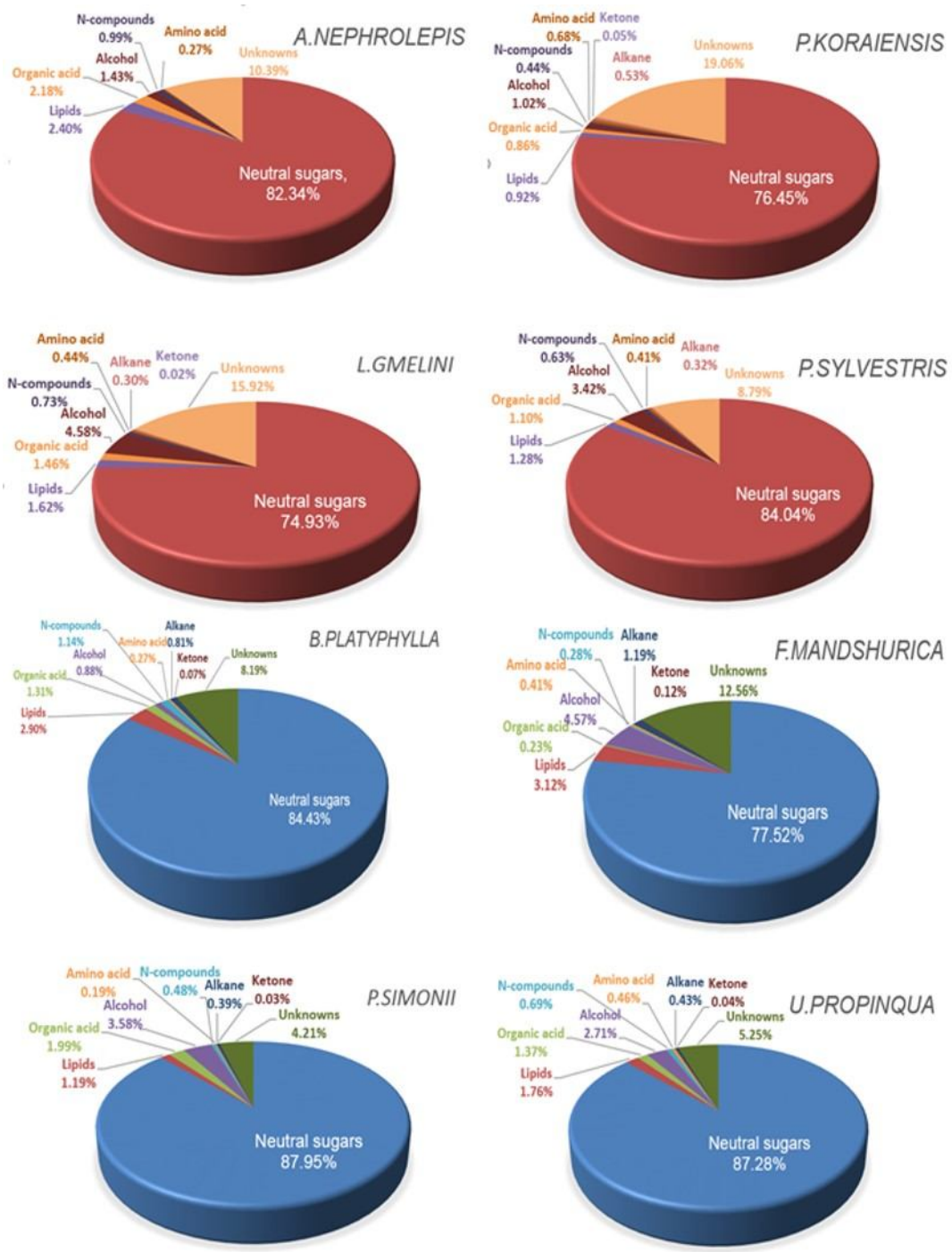

Fig. 2: Percentage composition of metabolites in the wood forming-tissue from 8 tree species at late-stage of growth season.

Metabolites changes in early-stage and late-stage of wood formation

The composition of most metabolites in the wood-forming tissues changed between the early-stage and late-stage of wood formation within tree species (Tabs. 2 and 3).

Sugars

Owing to the stability and reproducible derivatives for many sugars and organic acids,

trimethylsilyl (TMS) derivatization method was chosen to investigate the sugar content in wood-forming tissues. A-d-glucopyranoside was the most abundant sugar and its concentration notably increased in the late-stage of the growth season for all tree species. The greater increment of A-d-glucopyranoside content was present in *P. koraiensis* (from 11.591 $mg \cdot g^{-1}$ to 55.924 $mg \cdot g^{-1}$) and *U. propinqua* (from 9.474 $mg \cdot g^{-1}$ to 58.038 $mg \cdot g^{-1}$). D-fructose and D-glucose were the other most predominant sugars, but their concentrations decreased during late-stage wood formation in most trees besides *B. platyphylla* and *F. mandshurica*. In general, UDP-Glucose was regarded as the precursor for cellulose biosynthesis (Coleman et al. 2007, Kqczkowshi 2003). The relative glucose content decreased in the wood-forming tissues and lead to a lower yield of UDP-glucose. The fructose reduction also indicated that the conversion efficiency from sucrose to UDP-glucose declined. It was indicated that the cellulose synthesis efficiency decreased in latewood compared to early wood. In deciduous trees xylose content was higher during the summer, which may be caused by cell wall division and expansion during tree growth (Budzinski et al. 2016, Ko et al. 2011). **S**mall amounts of D-xylofuranose, arabinofuranose, D-turanose and lactose were detected, in most case the content increased or was only detected in later-stages of the growth season (Tabs. 2 and 3). It shows that the glucose and fructose could be converted to other monosaccharides and used as a source of energy in various biological processes. Although the composition of sugar metabolites varied in summer and winter seasons, the total sugar concentration was roughly equal among tree species. Budzinski et al (2016) investigated metabolites in Eucalyptus cambial tissue and reported that the total sugar concentration increased in the winter when identified by GC-MS; but their concentrations were similar in summer and winter seasons when measured by HPLC.

Organic acids

Organic acids served as important intermediates participant in several plant biochemical pathways, such as energy production, amino acid biosynthesis, and secondary metabolites biosynthesis (López-Bucio et al. 2000). The Malic acid concentration was more abundant during the early-stage of the growth season in all tree species (Tabs. 2 and 3), especially in deciduous trees (1.036 $mg \cdot g^{-1}$ to 2.246 $mg \cdot g^{-1}$). The acid content was reduced by 86.2% in *B. platyphylla* and not detected in *F. mandshurica* during the late-stage of the growth season. Apart from *A. nephrolepis* and *L. gmelini*, the other tree species showed lower lactic acid concentration in the late-stage of the growth season. Ethanedioic acid and 1-cyclohexene-1-carboxylic acid concentrations were higher in coniferous trees at the late-stage of the growth season, but it was the inverse in deciduous trees. Butanoic acid had a greater presence in coniferous trees (0.09 $mg \cdot g^{-1}$ to 0.345 $mg \cdot g^{-1}$) than in deciduous trees (0.017 $mg \cdot g^{-1}$ to 0.278 $mg \cdot g^{-1}$), however the content differs from species to species. Previous studies (Budzinski et al. 2016, Chia et al. 2000) showed that the more abundant organic compounds during summer was a result of vigorous activity of TCA cycle and metabolized to produce more other energy and carbon compounds.

Lipids and alcohols

The hexadecanoic acid, octadecanoic acid and monostearin were the most prominent lipids in the wood-forming tissues, and their concentrations were higher in deciduous trees. The hexadecanoic acid concentration ranged from 0.751 $mg \cdot g^{-1}$ to 1.46 $mg \cdot g^{-1}$ in coniferous trees, but up to 1.689 $mg \cdot g^{-1}$ to 2.844 $mg \cdot g^{-1}$ in deciduous trees during the early-stage of the growth season. The octadecanoic acid concentration was between 0.501 mg g^{-1} to 0.952 $mg \cdot g^{-1}$ in coniferous trees and was between 1.094 $mg \cdot g^{-1}$ to 1.900 $mg \cdot g^{-1}$ in deciduous trees during the early-stage of the growth season. Commonly, the lipid concentrations were more abundant during the early of growth season. Octadecanoic acid content was reduced by 98.5% in *P. simonii* and 97.1% in *P. koraiensis* during the late-stage of the growth season, respectively. According to former reports, the hexadecanoic acid and octadecanoic acid content significantly decreased in latewood and the former was the first production via fatty acid synthesis, which was benign from acetyl-CoA and then the latter was produced based on malonyl-CoA (Blerchert et al. 1995). The fatty acids served as the precursor for some of the secondary metabolite synthesis and its changes suggested the decline of the secondary metabolites accumulation rate in the later-stages of wood formation.

Myo-inositol is generally known as an important sugar alcohol in various cellular processes of plant physiology, such as stress response, cell wall biogenesis and growth regulation and so forth (Irvine and Schell 2001, Abid et al. 2009, Valluru and Van den Ende 2001). Myo-inositol total concentration was higher in coniferous than deciduous trees. Furthermore, myo-inositol concentration changed during the early and late growth seasons and was different in all eight tree species. At the late-stage of the growth season, the myo-inositol concentration decreased in *A. nephrolepis* (from 1.198 $mg \cdot g^{-1}$ dropped to 0.508 $mg \cdot g^{-1}$), *P. koraiensis* (from 0.567 $mg \cdot g^{-1}$ dropped to 0.441 $mg \cdot g^{-1}$) and *B. platyhylla* (from 0.409 $mg \cdot g^{-1}$ dropped to 0.074 $mg \cdot g^{-1}$). However, it increased in the other five tree species, especially in *F. mandshurica* (from 0.614 $mg \cdot g^{-1}$ to 4.418 $mg \cdot g^{-1}$) and *L. gmelini* (from 0.758 $mg \cdot g^{-1}$ to 3.434 $mg \cdot g^{-1}$). This finding means that the content of myo-inositol was tree species specific. Glucitol decreased in content from early-stage to late-stage in coniferous but it was the inverse in deciduous species. Another detected alcohol, glycerol, which is an intermediate of 3-phosphoglyceric acid metabolic, was more abundant in the early-stage of the growth season, especially in deciduous trees. This was a result of the reduction of glucose content during the late-stage of wood formation.

Amino acids and N-compounds

Small amounts of amino acids, such as L-proline, L-aspartic acid and serine were detected in the wood-forming tissues. Based on our previous results (Shi and Li 2012, 2015), amino acids were more abundant in the later-stage of the growth season and proline was the most prominent of the amino acids. The highest (0.486 $mg \cdot g^{-1}$) L-proline concentration was in late-stage *P. koraienis* wood-forming tissue. The proline primarily existed in cytoplasm solution and was produced from 2-oxoglutarate metabolism of the TCA. It was found that the Proline-rich protein not only participated in xylem cell differentiate but also being related to lignification, in which, the initial and reactive site for monolignol polymerization were likely provided (Zhang et al. 2000). Many reports showed that the content increased in compression wood formation

compared to the normal wood, indicating the proline responded to abiotic stress (Yeh et al. 2006, Shi and Li 2012, Kusano et al. 2008). The L-aspartic acid and serine were detected in the late-stage of all tree species and it had the highest concentration in *U. propinqua* (0.246 $mg \cdot g^{-1}$) and *F. mandshurica* (0.462 $mg \cdot g^{-1}$).

CONCLUSIONS

Metabolites in wood-forming tissues from eight important commercial tree species were extracted and 34 peaks were identified by GC-MS after being derivatized by TMS. The wood-forming tissues were rich in natural sugars, organic acids and lipids. Metabolites contents were determined to be tree species-specific and the changes in the early-stage and late-stage of growth the seasons. The percentage of natural sugars and lipids were higher in deciduous trees than in coniferous trees. D-xylose was detected only in deciduous trees. The total natural sugar content was more abundant in the late-stage than that in the early-stage and the a-d-glucopyranoside notably increased at the late-stage in all tree species. However, the lipids content sharply dropped in the late-stage of the growth season. The percentage of organic acid was much higher in deciduous trees than in coniferous trees at the early-stage of the growth season. The results suggested that the metabolic substance allocation in wood formation varied by tree species and growth seasons.

ACKNOWLEDGMENTS

We appreciate the financial Support by the Key Laboratory of Bio-based Material Science and Technology (Northeast Forestry University) Ministry of Education (SWZCL2016-09), National Natural Science Foundation of China (31971585, 31600454), and Jiangsu Co-Innovation Center for Efficient Processing and Utilization of Forest Resources. The authors also thanks Lee M. Smith (University of North Texas, USA) for his help in language editing.

Tab. 2: Metabolites in wood forming-tissue of four coniferous trees. Note: the values are given as mean ± SD (n=3). "---"in the table was not detected. EW: early wood; LW: late wood.

Retention time (min)	Metabolites	Relative amount ($mg \cdot g^{-1}$)							
		A.nephrolepis		*P. koraiensis*		*L. gmelini*		*P. sylvestris*	
		EW	LW	EW	LW	EW	LW	EW	LW
7.04-7.08	Lactic acid	0.121±0.012	0.210±0.008	0.136±0.007	0.064±0.009	0.057±0.013	0.141±0.031	0.133±0.027	0.096±0.015
9.141-9.181	Ethanedioic acid	0.090±0.005	0.358±0.037	0.103±0.003	0.168±0.011	0.06±0.003	0.237±0.032	0.053±0.008	0.117±0.012
12.590-12.613	Glycerol	0.598±0.081	0.488±0.091	0.431±0.053	0.348±0.045	0.298±0.071	0.474±0.039	0.411±0.068	0.349±0.055
14.778-14.892	Serine	---	---	0.031±0.011	---	---	---	---	
18.182-18.197	Malic acid	0.574±0.042	0.386±0.049	0.324±0.062	0.109±0.008	0.225±0.023	0.118±0.016	0.398±0.061	0.191±0.020
18.942-18.954	L-Aspartic acid	---	0.096±0.048	---	0.039±0.007	---	0.145±0.022	---	---
19.059-19.065	L-proline	---	0.118±0.019	---	0.486±0.047	0.118±0.021	0.232±0.026	0.102±0.033	0.262±0.056
19.166-19.176	Butanoic acid	---	0.224±0.068	0.132±0.006	0.116±0.017	0.158±0.030	0.345±0.056	---	0.09±0.011
19.457-19.468	Silane	0.306±0.061	0.368±0.064	0.412±0.046	0.175±0.041	0.193±0.012	0.301±0.033	0.330±0.052	0.226±0.036
21.188-21.207	D-Xylofuranose	---	0.174±0.012	---	0.129±0.035	---	0.141±0.068	0.046±0.012	0.124±0.027
24.355-24.362	Arabinofuranose	---	0.184±0.018	---	0.142±0.036	---	0.132±0.031	---	0.149±0.009
25.341-25.358	D-Fructose	0.176±0.033	---	0.348±0.079	---	0.103±0.026	---	---	---
25.454-25.493	1-Cyclohexene -1-carboxylic acid	0.302±0.022	0.482±0.094	0.192±0.021	0.211±0.029	0.13±0.026	0.285±0.039	0.188±0.028	0.157±0.016
26.526-26.555	D-Fructose	4.508±0.077	1.978±0.167	5.539±0.549	1.758±0.193	6.091±0.613	3.225±0.372	4.644±0.973	2.227±0.428
26.733-26.752	D-Fructose	3.792±0.051	1.414±0.831	4.366±0.336	1.324±0.118	4.631±0.728	2.387±0.269	3.406±0.521	2.227±0.351
26.898-26.912	Glucitol	0.142±0.007	0.07±0.042	0.122±0.033	0.026±0.006	---	---	---	0.034±0.005
27.038-27.053	D-Glucose	3.112±0.029	2.932±0.907	6.935±0.499	2.437±0.162	6.367±0.637	5.966±0.519	6.567±0.012	3.06±0.236
27.407-27.426	D-Glucose	0.790±0.016	0.648±0.051	1.932±0.088	0.574±0.035	1.835±0.232	1.471±0.662	1.538±0.189	0.742±0.048
28.283-28.296	Myo-Inositol	0.302±0.039	0.068±0.009	0.273±0.037	0.105±0.023	0.47±0.069	2.284±0.810	0.146±0.029	0.206±0.043
28.816-28.823	a-D-Glucopyranose	---	---	0.263±0.027	0.268±0.041	---	---	---	---
29.725-29.734	Gluconic acid	---	0.044±0.009	0.202±0.012	0.036±0.003	0.167±0.035	0.121±0.027	0.101±0.015	0.042±0.008
29.859-29.870	2-Ethoxyethanol	---	0.048±0.020	---	0.022±0.004	---	---	---	0.022±0.000
30.273-30.288	Hexadecanoic acid	1.124±0.062	1.272±0.139	1.346±0.102	0.514±0.035	0.751±0.067	1.005±0.093	1.460±0.112	0.548±0.039

30.742-30.752	Myo-Inositol	0.896±0.112	0.440±0.073	0.294±0.045	0.336±0.073	0.288±0.048	1.150±0.704	0.693±0.072	1.551±0.912
33.281-33.292	Androst-2-en-17 -amine	0.342±0.056	0.418±0.054	0.457±0.049	0.197±0.029	0.237±0.031	0.348±0.055	0.391±0.062	0.223±0.047
33.833-33.845	Octadecanoic acid	0.762±0.053	0.060±0.021	0.952±0.061	0.027±0.008	0.501±0.041	---	0.942±0.083	0.032±0.011
36.477-36.493	2-Trifluoromethyl-N,N-diundecylbenzylamine	---	0.184±0.033	0.185±0.026	0.092±0.012	0.09±0.016	0.149±0.042	0.143±0.020	0.098±0.018
37.519-37.538	4-Methylthio-N-phenyl-1,2-carbazoledicarboximide	---	0.166±0.028	0.185±0.039	0.074±0.017	0.088±0.022	0.127±0.035	0.135±0.016	0.079±0.025
39.313-39.332	Silane	0.112±0.026	0.134±0.037	0.124±0.022	0.092±0.013	0.058±0.017	0.095±0.024	0.069±0.014	0.047±0.009
39.643-39.658	a-D-Glucopyranoside	19.906±0.144	56.756±3.279	11.591±2.019	55.924±6.338	26.03±3.279	49.935±5.015	8.429±1.015	44.439±5.189
42.132-42.145	Monostearine	0.448±0.034	0.494±0.037	0.616±0.033	0.214±0.019	0.295±0.048	0.379±0.061	0.476±0.067	0.231±0.032

Tab. 3: Metabolites in wood forming-tissue of four deciduous trees. Note: the values are given as mean ± SD (n=3). "---"in the table was not detected. EW: early wood; LW: late wood.

Retention time (min)	Metabolites	Relative amount ($mg \cdot g^{-1}$)							
		B. platyphylla		*F. mandshurica*		*P. simonii*		*U. propinqua*	
		EW	LW	EW	LW	EW	LW	EW	LW
7.04-7.08	Lactic acid	0.141±0.021	0.189±0.045	0.314±0.044	0.138±0.026	0.146±0.037	0.056±0.008	0.139±0.012	0.122±0.006
9.141-9.181	Ethanedioic acid	0.215±0.047	0.273±0.050	0.14±0.029	---	0.165±0.033	0.112±0.024	0.135±0.041	0.142±0.029
12.590-12.613	Glycerol	0.490±0.077	0.321±0.059	1.202±0.118	0.712±0.083	0.684±0.075	0.858±0.082	0.849±0.099	0.432±0.048
14.778-14.892	Serine	---	0.013±0.005	---	0.462±0.047	---	0.013±0.002	---	0.024±0.007
18.182-18.197	Malic acid	1.036±0.128	0.234±0.036	2.246±0.215	---	1.735±0.139	0.716±0.067	1.689±0.151	0.542±0.062
18.942-18.954	L-Aspartic acid	---	0.077±0.015	---	---	---	0.043±0.009	---	0.246±0.069
19.059-19.065	L-Proline	---	0.08±0.012	0.09±0.010	0.182±0.023	0.065±0.015	0.039±0.021	0.067±0.024	0.076±0.033
19.166-19.176	Butanoic acid	---	0.028±0.006	---	---	0.075±0.011	0.047±0.005	0.278±0.047	0.121±0.035
19.457-19.468	Silane	0.101±0.042	0.116±0.057	0.146±0.022	0.35±0.036	0.162±0.035	0.075±0.018	0.100±0.011	0.052±0.006
21.188-21.207	D-Xylofuranose	0.049±0.012	0.136±0.037	---	---	0.041±0.008	0.115±0.025	0.041±0.011	0.158±0.042
23.288-23.3	D-Xylose	0.031±0.005	0.037±0.011	0.062±0.027	0.023±0.004	0.043±0.010	---	0.037±0.009	0.032±0.012
24.355-24.362	Arabinofuranose	---	0.126±0.033	---	0.072±0.016	---	0.124±0.025	---	0.171±0.031

25.341-25.358	D-Fructose	---	---	---	---	0.093±0.025	---	0.077±0.014	---
25.454-25.493	1-Cyclohexene-1-carboxylic acid	0.038±0.009	0.052±0.015	0.096±0.012	0.22±0.042	0.109±0.033	0.059±0.008	0.051±0.010	0.030±0.002
26.526-26.555	D-Fructose	0.917±0.102	1.626±0.236	0.402±0.087	2.136±0.318	3.222±0.525	1.033±0.272	1.835±0.321	1.686±0.442
26.733-26.752	D-Fructose	0.683±0.083	1.163±0.159	0.272±0.051	1.57±0.233	2.43±0.261	0.752±0.049	1.438±0.136	1.212±0.208
26.898-26.912	Glucitol	0.024±0.006	0.062±0.017	0.23±0.042	2.064±0.349	0.034±0.010	0.045±0.013	0.041±0.012	0.088±0.025
27.038-27.053	D-Glucose	1.374±0.182	2.420±0.219	2.034±0.256	10.942±2.014	5.322±1.389	1.719±0.306	2.667±0.285	2.698±0.312
27.407-27.426	D-Glucose	0.278±0.042	0.545±0.066	0.452±0.048	2.538±0.252	1.269±0.127	0.426±0.072	0.607±0.093	0.642±0.085
28.816-28.823	a-D-Glucopyranose	---	0.026±0.006	0.092±0.025	0.181±0.042	0.176±0.033	---	0.139±0.029	0.016±0.005
29.725-29.734	Gluconic acid	---	0.042±0.015	---	---	0.102±0.032	0.029±0.006	0.067±0.028	0.068±0.022
29.859-29.870	2-Ethoxyethanol	0.064±0.013	0.044±0.007	0.108±0.032	---	0.081±0.018	---	0.075±0.013	0.034±0.009
30.273-30.288	Hexadecanoic acid	1.763±0.134	1.207±0.099	2.844±0.253	0.8±0.059	1.883±0.193	0.414±0.052	1.689±0.207	0.876±0.085
30.742-30.752	Myo-Inositol	0.409±0.082	0.121±0.037	0.614±0.058	4.418±0.618	0.495±0.094	0.931±0.173	0.618±0.062	1.466±0.203
33.281-33.292	Androst-2-en-17-amine	0.477±0.078	0.397±0.045	0.868±0.093	---	0.606±0.061	0.138±0.027	0.54±0.082	0.288±0.042
33.833-33.845	Octadecanoic acid	1.094±0.179	0.059±0.006	1.900±0.215	0.41±0.056	1.330±0.168	0.019±0.003	1.172±0.123	0.038±0.007
36.477-36.493	2-Trifluoromethyl-N,N-diundecylbenzylamine	0.172±0.033	0.167±0.029	0.344±0.012	0.444±0.048	0.236±0.029	0.057±0.007	0.208±0.037	0.124±0.022
37.519-37.538	4-Methylthio-N-phenyl-1,2-carbazoledicarboximide	0.146±0.050	0.151±0.038	0.336±0.062	---	0.232±0.034	0.050±0.004	0.210±0.022	0.106±0.035
39.313-39.332	Silane	0.352±0.075	0.389±0.069	0.794±0.101	1.534±0.233	0.538±0.060	0.124±0.027	0.446±0.055	0.266±0.031
39.643-39.658	a-D-Glucopyranoside	16.222±2.025	46.582±5.317	11.758±1.843	48.435±6.336	11.698±2.119	39.695±4.627	9.474±1.501	58.038±7.910
41.612-41.639	2-Monostearine	0.035±0.008	0.054±0.011	0.122±0.024	0.402±0.051	0.061±0.012	---	0.116±0.018	0.03±0.004
42.132-42.145	Monostearine	0.427±0.057	0.492±0.081	1.266±0.103	3.318±0.318	0.776±0.067	0.173±0.032	0.624±0.063	0.372±0.039
42.918-42.923	D-Turanose	0.091±0.028	0.057±0.016	0.120±0.031	0.494±0.059	0.09±0.008	1.011±0.134	0.149±0.037	0.046±0.012
44.491-44.503	Lactose	---	0.109±0.012	---	5.368±0.318	---	0.093±0.017	---	0.342±0.041

REFERENCES

1. Abid, G., Silue, S., Muhovshi, Y., Jacquemin, J.M., Toussaint, A., Baudoin, J.P., 2009: Role of myo inositol phosphate synthase and sucrose synthase genes in plant seed development. Gene 439: 1-10.
2. Andersson-Gunnerås, S., Mellerowicz, E.J., Love, J., Segerman, B., Ohmiya, Y., Coutinho, P.M., Nilsson, P., Henrissat, B., Moritz, T., Sundberg, B., 2006: Biosynthesis of cellulose-enriched tension wood in *Populus*: Global analysis of transcripts and metabolites identified biochemical and developmental regulators in secondary wall biosynthesis. The Plant Journal 45(2): 144-165.
3. Barbaroux, C., Breda, N., 2002: Contrasting distribution and seasonal dynamics of carbohydrate reserves in stem wood of adult-ring porous sessile oak and diffuse-porous beech trees. Tree Physiology 22: 1201-1210.
4. Blerchert, S., Brodchelm, W., Holder, S., Kammerer, L., Kutchan, T.M., Mueller, M.J., Xia, Z.Q., Zenk, M.H., 1995: The octadecanoid pathway: signal molecules for the regulation of secondary pathways. Proceedings of the National Academy of Sciences of the United States of America. USA 92(10): 4099-4105.
5. Bonhomme, M., Peuch, M., Ameglio, T., Rageau, R., Guilliot, A., Decourteix, M., Alves, G., Sakr, S., Lacointe, A., 2009: Carbohydrate uptake from xylem vessels and its distribution among stem tissues and buds in walnut (*Juglans regia* L.). Tree Physiology 30: 89-102.
6. Budzinski, I.G.F., Moon, D.H., Lindén, P., Moritz, T., Labate, C.A., 2016: Seasonal variation of carbon metabolism in the cambial zone of *Eucalyptus grandis*. Frontiers in Plant Science 7: 932.
7. Chia, D.W., Yoder, T.J., Reiter, W.D., Gibson, S.L., 2000: Fumaric acid: an overlooked form of fixed carbon in Arabidopsis and other plant species. Planta 211: 743-751.
8. Coleman, H.D., Canam, T., Kang, K.Y., Ellis, D.D., Mansfield, S.D., 2007: Over-expression of UDP-glucose pyrophosphorylase in hybrid poplar affects carbon allocation. Journal of Experimental Botany 58: 4257-4268.
9. Deslauriers, A., Morin, H., 2005: Intra-annual tracheid production in balsam fir stems and the effect of meteorological variables. Trees 19: 402-408.
10. Dietze, M.C., Sala, A., Carbone, M.S., Czimczik, C.I., Mantooth, J.A., Richardson, A.D., Vargas, R., 2014: Nonstructural carbon in woody plants. Annual Review of Plant Biology 65: 667-687.
11. Fernie, A.R., Carrari, F., Sweetlove, L.J., 2004: Respiratory metabolism: glycolysis, the TCA cycle and mitochondrial electron transport. Current Opinion in Plant Biology 7: 254-261.
12. Fiehn, O., Kopka, J., Dörmann, P., Altmann, T., Trethewey, R.N., Willmitzer, L., 2000: Metabolite Profiling for Plant Functional Genomics. Nature Biotechnology 18(11): 1157-1161.
13. Gruber, A., Pirkebner, D., Oberhuber, W., 2013: Seasonal dynamics of mobile carbohydrate pools in phloem and xylem of two alpine timberline conifers. Tree Physiology

33: 1076-1083.
14. Hijza, F., Killiny, N., 2017: Collection and chemical composition of phloem sap from *Citrus sinensis* L. osbeck (sweet orange). Plos one 9(7): 1-11.
15. Irvine, R.F., Schell, M.J., 2001: Back in the water: the return of the inositol phosphates. Nature Reviews Molecular Cell Biology 2: 327-338.
16. Kachroo, A., Kachroo, P., 2006: Salicylic acid-, jasmonic acid- and ethylene-mediated regulation of plant defense signaling. In: Genetic Regulation of Plant Defense Mechanisms, J Setlow, ed (New York Springer) 28. Pp 55-83.
17. Ko, J.H., Prassinos, C., Keathley, D., Han, K.H., 2011: Novel aspects of transcriptional regulation in the winter survival and maintenance mechanism of poplar. Tree Physiology 31: 208-225.
18. Kqczkowshi, J., 2003: Structure function and metabolism of plant cell wall. Acta Physiologiae Plantarum 25(3): 287-305.
19. Kusano, T., Berberich, T., Tateda, C., Takahashi, Y., 2008: Polyamine: essential factors for growth and survival. Planta 228: 367-381.
20. Lisec, J., Schauer, N., Kopka, J., Willmitzer, L., Fernie, A.R., 2006: Gas chromatography mass spectrometry-based metabolite profiling in plants. Nature. Protocols 1: 387-396.
21. López-Bucio, J., Nieto-Jacobo, M.F., Ramírez-Rodríguez, V., Herrera-Estrella, L., 2000: Organic acid metabolism in plant: from adaptive physiology to transgenic varieties for cultivation in extreme soils. Plant Science 160: 1-13.
22. Morris, C.R., Scott, J.T., Chang, H.M., Sederoff, R.R., O'Malley, D., Kadla, J.F., 2004: Metabolic profiling: a new tool in the study of wood formation. Journal. Agricultural and Food Chemistry 52: 1427-1434.
23. Obst, J.R., 1998: Special (secondary) metabolites from wood. Bruce A, Palfreyman J.W. eds. Pp 151-165, Forest Products Biotechnology, London, Great Britain.
24. Ögren, E., 2000: Maintenance respiration correlates with sugar but not nitrogen concentration in dormant plants. Physiologia Plantarum 108: 295-299.
25. Paiva, J.A.P., Garcés, M., Akves, A., Garnier-Géré, P., Rodrigues, J.C., Lalanne, C., Porcon, S., Le, Provost, G., Perez, D.S., Brach, J., Frigerio, J.M., Claverol, S., Barré, A., Fevereiro, P., Plomion, C., 2008: Molecular and phenotypic profiling from the base to the crown in maritime pine wood-forming tissue. New Phytologist 178: 283-301.
26. Robinson, A.R., Ukrainetz, N.K., Kang, K.Y., Mansfield, S.D., 2007: Metabolite profiling of Douglas-fir (*Pseudotsuga menziesii*) field trials reveals strong environmental and weak genetic variation. New Phytologist 174: 762-773.
27. Schrader, J., Nilsson, J., Mellerowicz, E., Berglund, A., Nilsson, P., Hertzberg, M., Sandberg, G., 2004: A high-resolution transcript profile across the wood-forming meristem of poplar identifies potential regulators of cambial stem identity. Plant Cell 16: 2278-2292.
28. Shi, J.T., Li, J., 2016: Comparative analysis of spectroscopy features of early-stage wood forming tissue in common tree species in Northeast, China. Scientia Silvae Sinicae 52(6): 115-121.
29. Shi, J.T., Li, J., 2015: Metabolic profiles in wood forming tissue during tension wood

formation. Wood Research 60(4): 531-542.
30. Shi, J.T., Li, J., 2012: Metabolites and chemical group changes in the wood-forming tissue of *Pinus koraiensis* under inclined conditions. BioResources 7(3): 3463-3475.
31. Turhan, E., Ergin, S., 2012: Soluble sugars and sucrose-metabolizing enzymes related to cold acclimation of sweet cherry cultivars grafted on different rootstocks. The Scientific World Journal 2012: 1-7.
32. Valluru, R., Van den Ende, W., 2001: Myo-inositol and beyond-emerging networks under stress. Plant Science 181: 387-400.
33. Villas-Bôas, S.G., Noel, S., Lane, G.A., Attwood, G., Cookson, A., 2006: Extracellular metabolomics: a metabolic footprinting approach to assess fiber degradation in complex media. Analytical. Biochemistry 349: 297-305.
34. Welling, A., Palva, E.T., 2006: Molecular control of cold acclimation in trees. Physiologia Plantarum 127: 167-181.
35. Yeh, T.F., Morris, C.R., Goldfarb, B., Chang, H.M., Kadla, J.F., 2006: Utilization of polar metabolite profiling in the comparison of juvenile wood and compression wood in loblolly pine (*Pinus taeda*). Tree Physiology 26: 1497-1503.
36. Zhang, Y., Sederoff, R.R., Allona, I., 2000: Differential expression of genes encoding cell wall proteins in vascular tissues from vertical and bent Loblolly pine trees. Tree Physiology 20: 457-466.

JIANGTAO SHI*, JUNYI PENG, CHONGYANG XIA
NANJING FORESTRY UNIVERSITY
COLLEGE OF MATERIALS SCIENCE AND ENGINEERING
NO.159 LONGPAN RD. XUANWU D.
NANJING, 210037
P. R. CHINA
*Corresponding author: shijiangtao128@163.com

JIAN LI
NORTHEAST FORESTRY UNIVERSITY
KEY LABORATORY OF BIO-BASED MATERIAL SCIENCE AND TECHNOLOGY
MINISTRY OF EDUCATION
NO. 26 HEXING RD. XIANGFANG D.
HARBIN, 150040
P. R. CHINA

WOOD RESEARCH doi.org/10.37763/wr.1336-4561/66.5.762776
e-ISSN 2729-8906
66(5): 2021 762-776 pp.

SELECTED PROPERTIES OF COMPREGNATED WOOD USING LOW MOLECULAR WEIGHT PHENOL FORMALDEHYDE AND SUCCINIC ANHYDRIDE

SARAH AUGUSTINA[1], IMAM WAHYUDI[1], WAYAN DARMAWAN[1], JAMALUDIN MALIK[2], NAOKI OKANO[3], TAIYO OKADA[3], KAZUSHIGE MURAYAMA[4], HIKARU KOBORI[3], YOICHI KOJIMA[3], SHIGEHIKO SUZUKI[5]

[1]IPB UNIVERSITY, INDONESIA
[2]FOREST PRODUCTS RESEARCH AND DEVELOPMENT CENTER, INDONESIA
[3]SHIZUOKA UNIVERSITY, JAPAN
[4]FORESTRY AND FOREST PRODUCTS RESEARCH INSTITUTE, JAPAN
[5]SHIZUOKA PROFESIONAL UNIVERSITY OF AGRICULTURE, JAPAN

(RECEIVED DECEMBER 2020)

ABSTRACT

The aim of this study was to investigate the effect of impregnating materials (low molecular weight phenol formaldehyde or LmwPF and succinic anhydride or SA), their concentrations (5 and 10%), and compression ratios (20 and 40% from initial thickness) on improvement of specific gravity (SG) and dimensional stability on nyatoh, sepetir, and pisang putih wood; and then compared them to control and densified wood. The results showed that SG and dimensional stability of compregnated wood were affected by all parameters studied. Higher compression ratio and concentration will result in a greater improvement. In general, SG and dimensional stability of compregnated wood were better than the control. SG of LmwPF- and SA-compregnated wood increased by 10.69–22.31% and 6.96–23.09%, respectively. Utilization of LmwPF and SA has significantly reduced the spring-back, but the latter is better. The compression-set recovery after compregnation was 18.34–33.99%, while after densification was 47.86–71.49%.

KEYWORDS: Compregnation, compression ratio, lesser-used wood species, low molecular of phenol formaldehyde, succinic anhydride, spring-back.

INTRODUCTION

Densification is a process that has been widely applied to modify the properties of wood. After processing, the wood becomes denser and its specific gravity (SG) increases significantly (Inoue et al. 1991, Kutnar et al. 2009, Tu et al. 2014, Pelit and Yalçin 2017). This process in general can be divided into four stages: starting with softening of cell wall or plasticizing, then flattening the wood constituents due to compression, followed by setting in deformed condition, and ending with fixation which prevents the wood from returning to its original shape and size (Morsing and Hoffmeyer 1998). The effectiveness of densification is influenced and depends on internal and external factors. Anatomical characteristics and moisture content are the main internal factors to be considered (Tabarsa and Chui 2000, Nairn 2005, Kamke and Kutnar 2010, Darwis et al. 2017), while pre-treatment, direction of compression, compression ratio (CR), temperature, as well as closing and holding time during treatment are the external factors (Shams et al. 2006, Rautkari et al. 2011).

Hot immersion before pressing is commonly used as a pre-treatment because it can accelerate the softening of the lignin so that the wood is easily flattened and compacted (Navi and Sandberg 2012, Khalil et al. 2014). According to Kutnar and Sernek (2007), Kamke and Kutnar (2010), lignin begins to soften when the wood temperature is above its glass transition temperature (Tg). According to Kelley et al. (1987), Furuta et al. (1997), Kong et al. (2017), Tg of lignin is between 50°C to 100°C depending on the species and age of the wood.

Apart from pre-treatment, the applied compression ratio must also be considered. An appropriate compression ratio level will significantly increase the strength, SG, and dimensional stability of the wood; conversely, too high a compression ratio level will not only cause excessive deformation but also cause severe damage to the wood, thereby reducing its strength and dimensional stability (Bao et al. 2017). The correct compression ratio levels can also reduce the ability of the wood to return to its original shape and size (spring-back), especially if wood is put into the room with high humidity. According to Sadatnezhad et al. (2017), spring-back is related to the hygroscopicity of wood and the release of internal stresses that occur during densification. Its value will increase as the compression ratio increases. There is severe spring-back, up to 75%, on poplar wood after the wood is processed using techno-hydro-mechanical (THM) at 50% compression ratio (Bao et al. 2017), while according to Pelit et al. (2016), the set recovery produced by 25% compression ratio was lower than 50% compression ratio on densified Uludağ fir wood (4–8% versus 18–24%).

In order to reduce the spring-back phenomenon in densified wood, the wood must be impregnated with proper materials prior to compaction. This process is called compregnation which is a combination of densification (compaction) and impregnation. Impregnated with synthetic resins such as low molecular weight phenol formaldehyde (LmwPF) or with anhydride such as succinic anhydride (SA) will increase the hydrophobicity of wood and at the same time strengthen its fixation (Shams et al. 2004, Khalil et al. 2014). Apart from being a bulking agent, the presence of impregnation materials also plays a role in the formation of covalent bonds between wood components so that internal stresses remain stored in the microfibrils and the cell wall matrix (Morsing and Hoffmeyer 1998). According to Wan and Kim (2006), Gabrielli

(2009), Lahtela and Karki (2014), Bao et al. (2016), compregnated wood has better strength and dimensional stability than compacted wood without impregnation (densified wood).

Studies on compregnated wood especially using the lesser-used tropical species are very limited. Therefore, this study aims to analyze nyatoh (*Palaquium* spp.), sepetir (*Sindora* spp.) and pisang putih (*Mezzettia* spp.) wood which had been impregnated with LmwPF or SA prior to pressing. The main focus of this study is on the changes occurred in SG and dimensional stability due to the treatment applied and the phenomenon of spring-back. Comparison of similar characteristics to those of densified wood and control wood are also discussed.

MATERIAL AND METHODS

Logs 120 cm in length and 50 cm in diameter at breast height from the bottom of the trunk of nyatoh, sepetir, and pisang putih trees was used as the main samples. The trees came from a forest concession area in North Kalimantan Province, Indonesia. The logs were cut into 3 cm thick boards and air-dried for 2 months before converting into wood samples in eleven treatment categories. Sample size for each category is presented in Tab. 1. Only the clear wood samples namely free from knots, mold, fungi, and visible defects were tested.

Tab. 1: Sample size of each treatment category.

Treatments		Size (cm)
Category	Code	
1. Untreated	C	2 x 2 x 2
2. Hot immersion without impregnating material but densified at 20% CR	WR–0–20	2 x 2 x 2.4
3. Impregnated and hot immersion within 5% LmwPF and densified at 20% CR	PF–5–20	2 x 2 x 2.4
4. Impregnated and hot immersion within 10% LmwPF and densified at 20% CR	PF–10–20	2 x 2 x 2.4
5. Impregnated and hot immersion within 5% SA and densified at 20% CR	SA–5–20	2 x 2 x 2.4
6. Impregnated and hot immersion within 10% SA and densified at 20% CR	SA–10–20	2 x 2 x 2.4
7. Hot immersion without impregnating material but densified at 40% CR	WR–0–40	2 x 2 x 2.8
8. Impregnated and hot immersion within 5% LmwPF and densified at 40% CR	PF–5–40	2 x 2 x 2.8
9. Impregnated and hot immersion within 10% LmwPF and densified at 40% CR	PF–10–40	2 x 2 x 2.8
10. Impregnated and hot immersion within 5% SA and densified at 40% CR	SA–5–40	2 x 2 x 2.8
11. Impregnated and hot immersion within 10% SA and densified at 40% CR	SA–10–40	2 x 2 x 2.8

The number of samples for densification without impregnation at 20 and 40% compression ratio was 18 pieces (2 levels of compression ratio x 3 replications x 3 species), meanwhile for compregnation they were 360 pieces (8 categories x 15 replications x 3 species).

Densification and compregnation process

Before proceed into the next steps, sample dimensions were measured to obtain its volume and then weighed. For densification treatment (without impregnation), after hot soaking within water at 80°C for 3 hours the samples were directly compacted using machine at 160°C with specific pressure of 2.672 MPa for 15 min with 20 and 40% compression ratio levels from initial thickness. After that the samples were conditioned overnight before testing. For compregnation

treatment, the samples were impregnated by 5 and 10% (w/w) of LmwPF and SA solutions separately using –98 kPa vacuum pressure for 15 min then followed by 350 kPa pressure for 4 hours. After that, the samples were hot (80°C) immersed in each impregnating solutions for 3 hours, then immediately compacted using machine at 160°C with a specific pressure of 2.672 MPa for 15 min with 20 and 40% of compression ratio. The samples were also then conditioned overnight prior to testing.

Measurement of specific gravity (SG)

Densified and compregnated wood samples were weighed (Wo) and their volumes were measured (Vo), then oven-dried at 103 ± 2°C for 24 hours to obtain oven-dried weight (W_1). The SG measurements were carried out before and after treatment to record changes in value. The value was calculated according to Eq. 1:

$$SG = \frac{W_1 / V_o}{\rho_{water}} \quad (1)$$

where: W_1- sample weight in oven-dried condition; before and after treatment (g), Vo- sample volume in air-dried condition; before and after treatment (cm^3), ρ_{water}- density of water 4°C (= 1 $g \cdot cm^{-3}$).

Measurement of weight percent gain (WPG)

The WPG was calculated according to Eq. 2:

$$WPG\ (\%) = \frac{W_1 - W_o}{W_o} \times 100 \quad (2)$$

where: W_o- sample weight in oven-dried condition before treatment (g), W_1- sample weight in oven-dried condition after treatment (g).

Measurement of compression-set (C-set)

Compression set is used to determine the thickness variation after densification. The value was measured according to Eq. 3:

$$C\text{-}set\ (\%) = \frac{T_o - T_a}{T_o} \times 100 \quad (3)$$

where: T_o- sample thickness before densification (mm), T_a- sample thickness in oven-dried condition after densification (mm).

Measurement of dimensional stability

Dimensional stability in this study was determined by compression-set recovery (CSR) and thickness swelling (TS) after water soaking process. Densified and compregnated-wood samples were oven-dried at 103 ± 2°C for 24 hours to obtain their oven-dried thickness before swelling. Oven-dried samples were then immersed in water at room temperature for 24 hours and then

oven-dried again at 103 ± 2°C for 24 hours. The thickness in oven-dried condition was measured before and after soaking. The CSR and TS were measured according to Eqs. 4 and 5:

$$\text{CSR (\%)} = \frac{T_{ss}-T_{sb}}{T_o-T_{sb}} \times 100 \quad (4)$$

$$\text{TS (\%)} = \frac{T_{ss}-T_{sb}}{T_{sb}} \times 100 \quad (5)$$

where: To- sample thickness before densification (mm), Tsb- sample thickness in oven-dried condition before swelling (mm), Tss- sample thickness in oven-dried condition after swelling (mm).

Scanning electron microscopy (SEM) observation

SEM images are used to investigate microscopic changes occurred in densified and compregnated samples. The samples were vacuum dried at 40°C for 24 hours and its cross-sections were sputter coated with gold for 120 s and 30 mA, and observed under SEM (JEOL JSM-6510LV, Japan) at 15 kV.

Data analysis

Experimental design used was a completely randomized design with four factors namely wood species, compression ratio, impregnating material, and the concentration of impregnated material solution; all in three levels. Analysis of variance (ANOVA) was performed to evaluate the effect of species, compression ratio, impregnating material, and its concentration on SG and dimensional stability of treated woods. If there are significant differences from each factor and the interactions, it will be followed by Duncan's multiple distance test.

RESULTS AND DISCUSSION

Specific gravity (SG)

The average SG after treatment is presented in Tab. 2. It can be seen that interaction among wood species, impregnating material, and compression ratio has a significant effect on SG at the 5% significance level (Tab. 3).

Tab. 2: Specific gravity of three wood species after treatment.

Treatment category	Wood species					
	Nyatoh		Sepetir		Pisang putih	
	Before	After	Before	After	Before	After
Untreated	0.48 ± 0.06^{de}		0.36 ± 0.03^{a}		0.52 ± 0.02^{efg}	
WR–0–20	0.49 ± 0.07	0.56 ± 0.07^{gh}	0.35 ± 0.05	0.40 ± 0.05^{abc}	0.53 ± 0.01	0.57 ± 0.02^{gh}
SA–5–20	0.48 ± 0.03	0.56 ± 0.03^{gh}	0.35 ± 0.04	0.42 ± 0.04^{abcd}	0.54 ± 0.01	0.59 ± 0.02^{gh}
SA–10–20	0.48 ± 0.05	0.59 ± 0.06^{gh}	0.36 ± 0.03	0.45 ± 0.02^{bcd}	0.54 ± 0.01	0.62 ± 0.02^{hi}
PF–5–20	0.49 ± 0.05	0.56 ± 0.07^{gh}	0.35 ± 0.05	0.40 ± 0.05^{abc}	0.53 ± 0.01	0.57 ± 0.01^{gh}
PF–10–20	0.48 ± 0.04	0.55 ± 0.05^{fgh}	0.31 ± 0.05	0.37 ± 0.05^{a}	0.54 ± 0.02	0.58 ± 0.03^{gh}

WR–0–40	0.47 ± 0.07	0.62 ± 0.08^{hi}	0.37 ± 0.02	0.49 ± 0.04^{def}	0.51 ± 0.01	0.66 ± 0.03^{i}
SA–5–40	0.49 ± 0.06	0.58 ± 0.08^{gh}	0.32 ± 0.05	0.39 ± 0.05^{ab}	0.49 ± 0.06	0.55 ± 0.05^{gh}
SA–10–40	0.46 ± 0.05	0.57 ± 0.05^{gh}	0.33 ± 0.03	0.45 ± 0.03^{bcd}	0.49 ± 0.05	0.59 ± 0.04^{gh}
PF–5–40	0.49 ± 0.05	0.59 ± 0.06^{h}	0.36 ± 0.02	0.46 ± 0.03^{cde}	0.53 ± 0.01	0.59 ± 0.01^{h}
PF–10–40	0.45 ± 0.02	0.55 ± 0.03^{fgh}	0.34 ± 0.01	0.45 ± 0.02^{bcd}	0.51 ± 0.03	0.58 ± 0.03^{gh}

Note: SG values are averages of 15 replicates with standard deviation. Values within a column followed by the same letters are not significantly different at 5% significance level using Duncan's multiple range test.

The highest increase in SG was found in sepetir wood. For all wood species, succinic anhydride (SA) resulted in a higher SG improvement compared to LmwPF, and SG increased with increasing compression ratio level. Result also showed that compregnation and densification treatments could significantly increase the SG of the woods compared with untreated (control). However, SG of the compregnated wood was smaller than that of densified wood. The SG tended to increase slightly with the increase in the concentration of impregnating material solution.

Tab. 3: ANOVA results of each parameters and factors.

Para-meter	**Factors**														
	JK	CM	CC	CR	JK × CM	JK × CC	JK × CR	CM × CC	CM × CR	CC × CR	JK × CM × CC	JK × CM × CR	JK × CC × CR	CM × CC × CR	JK × CM × CC × CR
SG	**	ns	ns	**	ns	ns	ns	**	**	ns	ns	*	ns	ns	ns
WPG	**	**	**	ns	**	**	ns	**	ns	ns	*	ns	ns	ns	ns
C-set	**	**	**	**	**	ns	ns	ns	ns	ns	*	ns	ns	ns	ns
CSR	**	**	**	**	*	ns	*	**	ns	**	ns	*	ns	**	ns
TS	**	**	**	**	**	ns	**	ns	**	ns	ns	**	ns	ns	ns

Note: ns = not significant; * = significantly different at 5% significance level; ** = significantly different at 1% significance level; JK = wood species; CM = impregnating material, CC = concentration, CR = compression ratio.

Generally, it can be said that SG increases after treatment. In case of nyatoh wood there was an increase of 14.13 and 18.83% for 20 and 40% compression ratio, respectively; while in sepetir and pisang putih wood there was 15.58 and 23.06% as well as 8.46 and 14.56%, respectively. Sepetir wood has the highest improvement in SG at both compression ratio and impregnating material, and the values were significantly different from the other species. This phenomenon is related to its anatomical features, i.e. greater void volume dues to larger vessel diameter and more frequent number of the vessels (Augustina et al. 2020). Higher portion of void volume resulted in a higher level of deformation in the cell lumens during compaction. And as the result, the wood is more compacted. This finding is coincided with Darwis et al. (2017). They stated that the increasing SG after densification is mainly influenced by the porosity or proportion of cell cavities. Higher void volume leads to a higher level of deformation in the cell lumens, as well as a large reduction in void volume (Tu et al. 2014, Bao et al. 2017). It also can be convinced by its C-set value. As shown in Fig. 1, sepetir wood had higher C-set value (18.07%) than nyatoh (17.15%) and pisang putih (12.87%) wood.

According to Tab. 2, SG values generated by 20 and 40% compression ratio were 0.52 and 0.54, respectively. These results are related to the increasing number of flattened cells during compression. The same phenomenon was also reported by Inoue et al. (1991). The SG of modified sugi wood increased from 0.36 to 0.50 at 30% compression ratio and doubled at 60% compression ratio. Therefore, there is no doubt that the compregnation will resulted in a significant reduction in lumen diameter of vessels and fibers, thereby reducing the sizeable portion of the void volume.

At 20% compression ratio, the average increase in SG of compregnated and densified woods were 10.68–18.33% and 7.02–12.50%, respectively; and were 13.93–22.31% and 22.73–24.49% at 40% compression ratio. This results indicate that the higher the compression ratio, the more impregnating material that come out of the wood. This phenomenon was supported by the fact that WPG at 40% compression ratio is lower than 20% compression ratio. According to Zhao et al. (2015), a higher compression ratio will result in greater internal stress. The greater internal stresses will push more impregnating materials out of the wood (Lykidis et al. 2019). This resulted in a reduction in deposited and solidified impregnating material in the cell cavity. This phenomenon is also related to the lower C-set generated in compregnated wood compared to densified wood. At 20% compression ratio, the average value of C-set of compregnated and densified wood were 8.82–14.17% and 12.75–17.19%, respectively; while at 40% compression ratio they were 14.17–21.48% and 26.8–28.07%. This can occur because of the variation in the internal stresses that is formed for each compression ratio which is induced by a decrease in humidity (Pelit et al. 2014). The presence of impregnating substances can also prevent deformation in wood.

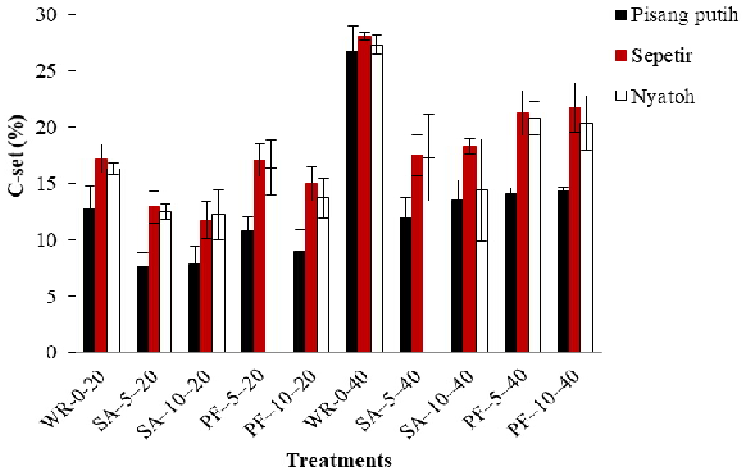

Fig. 1: Compression set of each treatments.

Average SG for compregnated wood using SA as impregnating material (SA-compregnated wood) increased by 10.69–18.33% at 20% compression ratio and 13.93–22.31% at 40% compression ratio, respectively; while those impregnated with LmwPF (LmwPF-compregnated wood) were 6.96–14.36% and 11.12–23.09%, respectively. This phenomenon is also convinced by the WPG (Fig. 2).

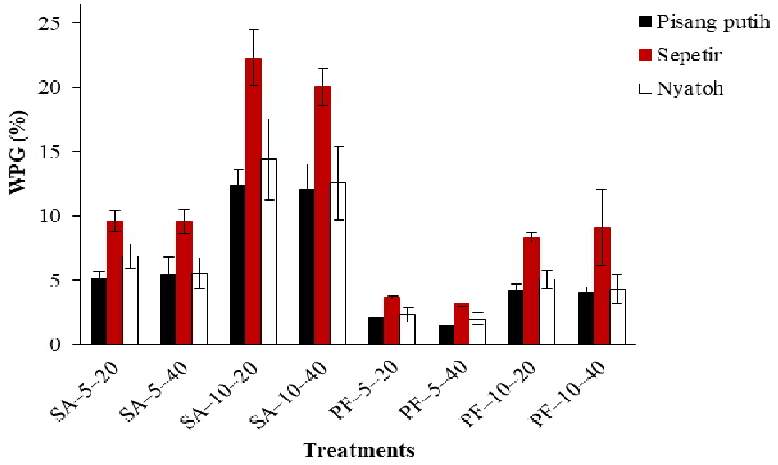

Fig. 2: Weight percent gain of each treatments.

The WPG of the SA-compregnated wood was higher than that of the LmwPF-compregnated wood. It can be said that the changes in microstructure are the result of the SA which covers higher portion of the cell cavity and acted as a blocking agent compared to the LmwPF. According to Chen et al. (2014), modification with SA will result in replacement of the hydroxyl group with a succinic group that is covalently bound. The higher WPG in succinilation is due to the higher molecular weight of SA and adduction of a 4-carbon chain with a carboxyl group to the lignin. Succinilated is also capable of causing the lignin to expand more effectively, making reactive chemicals sites more accessible, and therefore enhancing the rate of modification.

Average SG for the SA-compregnated wood increased by 9.69–17.31% for 5% concentration and 14.93–23.33% for 10% concentration, while those of the LmwPF-compregnated wood increased by 8.59–17.12% and 9.48–20.33%, respectively. The WPG of the SA-compregnated wood increased by 5.45–9.56% and 12.05–20.02% for 5 and 10% concentration, respectively; while those of the LmwPF-compregnated wood were 1.48–3.23% and 4.05–9.10%. This phenomenon indicates that an increase in the impregnating concentration causes an increase in the WPG, which in turn will also result in an increase in SG. The positive correlation between WPG and SG was also confirmed by Nur et al. (2011).

Dimensional stability

Dimensional stability in this study is approached by compression-set recovery (CSR) and thickness swelling (TS) after water soaking process. The CSR and TS of the three wood species with 5 and 10% of LmwPF and SA solutions at 20 and 40% compression ratio are shown in Figs. 3 and 4. It can be seen that sepetir wood generated higher dimensional stability, as indicated by lower the CSR and TS values. CSR and TS increased slightly with an increase of compression ratio. The compregnation resulted in lower CSR and TS than densification. These two values decrease significantly with increasing concentration. This phenomenon was confirmed by the ANOVA results (Tab. 3).

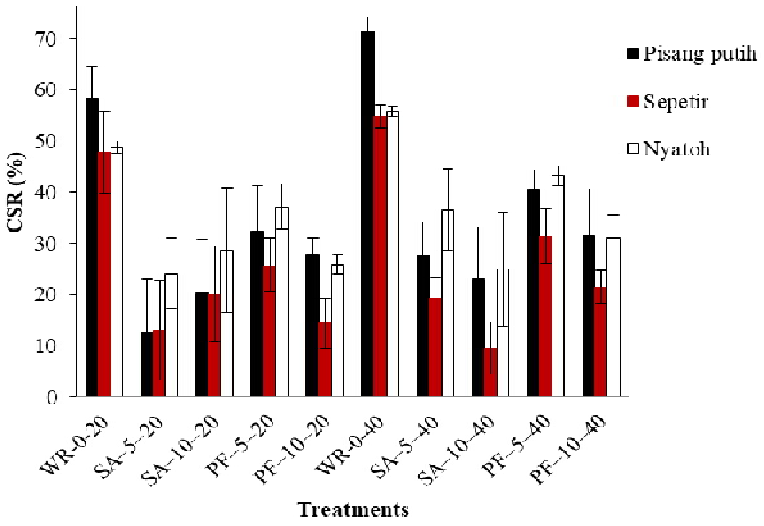

Fig. 3: Compression-set recovery of each treatments.

Average CSR values for nyatoh, sepetir, pisang putih wood were 32.95 and 38.37%, 24.24 and 27.32%, and 30.29 and 38.89% for 20 and 40% compression ratio, respectively; while average TS were 11.17 and 17.10%, 9.92 and 15.58%, and 10.90 and 15.96%, respectively. The lower CSR and TS on sepetir wood are due to increased SG and greater deformation during compression. The higher SG indicates more cells flattening during compression, and consequently increased dimensional stability. The same phenomenon also confirmed by Augustina et al. (2020).

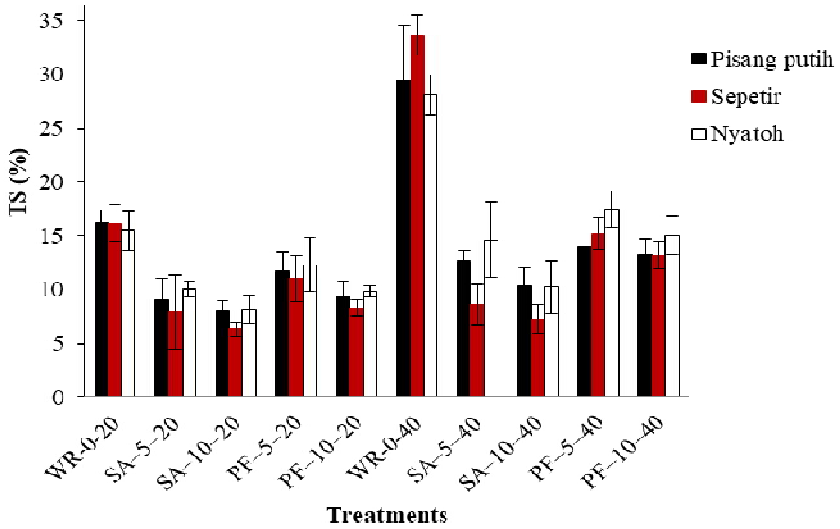

Fig. 4: Thickness swelling of each treatment.

According to Miyoshi et al. (2016), there are 4 different types of cell lumens deformation during compression, namely type I (S-shape cells), type II (cells that have 3-4 projections), type III (cells with protrusion in center or tip), and type IV (elongated shape cells). Sepetir wood has a uniform type of deformation and is categorized as type I and II (Fig. 5). This can lead to permanent and irreversible structural changes and deformations.

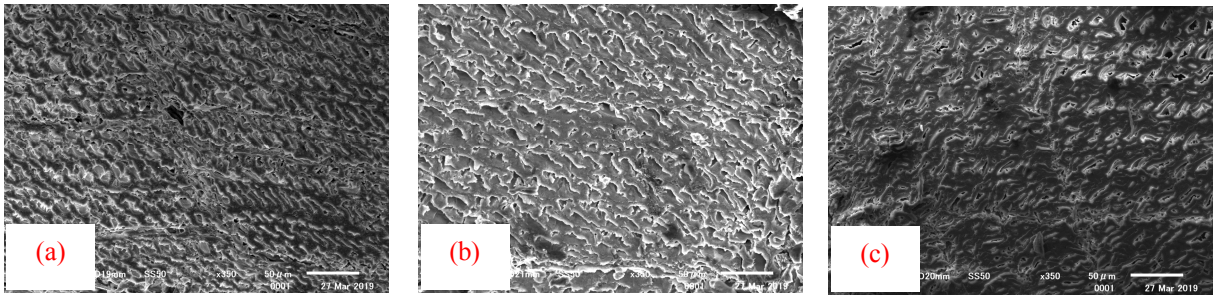

Fig. 5: Type of deformation during compression: a) nyatoh, b) sepetir, and c) pisang putih. Scale bar = 50 µm.

Irreversible swelling occurs due to the breaking of the covalent bonds between hemicellulose and lignin mechanically when the stress exceeds the bond strength (Ohlmeyer and Paul 2010). It was also confirmed by Miyoshi et al. (2016). They stated that the S-shape cells are difficult to swell and tend to increase the dimensional stability of compressed wood. The higher CSR and TS on nyatoh and pisang putih wood are due to higher initial SG which led to uneven distribution of internal stresses during compression. Bao et al. (2017) added that recovery of wood cells depends on distribution of internal stresses.

Average CSR values generated by 20% and 40% compression ratio were 24.24–32.95% and 27.32–38.89%, respectively (Fig. 3); while those of TS were 9.92–11.17% and 15.58–17.10% (Fig. 4). It can be seen that CSR and TS increased with an increase of compression ratio (Tab. 2). A larger compression ratio will produce a greater reaction force inside wood which led the cells to return to its original shape easily. This was especially the case at 40% compression ratio. The same phenomenon was confirmed by Bao et al. (2017) and Darwis et al. (2017). They stated that the THM process induces the deformation of fibers and microfibrils which results in an increase in internal stresses. These stresses allow those fibers and microfibrils to recover during water soaking process, although not 100% recover. It indicated that our treatments provide improvements, especially in dimensional stability.

Average CSR after compregnation and densification treatment at 20% compression ratio were 18.34–28.99% and 47.86–58.28%, respectively; while at 40% compression ratio they were 20.44–33.99% and 54.82–71.49% (Fig. 3). Average TS after compregnation and densification at 20% compression ratio were 8.37–10.09% and 15.5–16.21%, respectively; while at 40% compression ratio they were 11.06–14.35% and 28.10–33.62% (Fig. 4). It can be seen that CSR and TS of compregnated wood are lower compared to those of densified wood. These findings are related to the treatments applied. Bao et al. (2017) and Dos Santos et al. (2018) stated that hydrothermal treatment, especially at temperature above T_g lignin can cause damage to cellulose cross-links, breaking of hemicellulose chains and slight cleavage of lignin that may release the internal stresses. Impregnating materials not only blocks the entry of water into the wood cells by covering the void volume, but also contributes to holding the wood back to its original shape and size (recovery) due to its role as bulking agent. It was also agreed by Ghorbani and Bavaneghi (2016) which stated that impregnating material contributes to reduce the number of hydroxyl group and occupies the intermolecular space in the wood cell wall, thereby decreasing hygroscopicity of wood and consequently increasing the dimensional stability.

The average CSR for the SA-compregnated wood and LmwPF-compregnated wood were 15.51–28.62% and 23.27–34.36%, respectively; while average of their TS were 7.52–10.78% and 11.92–13.66%. It can be seen that both CSR and TS of the SA-compregnated wood are lower than LmwPF-compregnated wood. This phenomenon is correlated with a higher WPG and characteristic of SA which can substitute hydroxyl group with succinic groups. Hill (2006) and Scarica et al. (2018) stated that the application of SA as the impregnating agent can increase stress relaxation because it can act as an internal plasticizer. These facts do support our findings. In case of the LmwPF-compregnated wood, the lower WPG is not sufficient to hold water during the water soaking process. Kajita et al. (2004) stated that LmwPF can easily penetrate into the cell walls, and almost all of them are located in the cell walls and little or no resin visible in the cell lumina.

The average CSR for the SA-compregnated wood at concentrations of 5 and 10% were 16.23–30.40% and 14.80–26.85%, respectively; while for the LmwPF-compregnated wood they were 28.59–40.23% and 17.94–29.69%, respectively. On the other hand, average TS for the SA-compregnated wood at concentration of 5 and 10% were 8.27–12.36% and 6.77–9.20%; while for LmwPF-compregnated wood they were 12.84–14.91% and 10.72–12.42%. It can be seen that in both type of impregnating material, the values of CSR and TS decrease with increasing impregnating concentration. Negative correlation between CSR and impregnating concentration as well as between TS and impregnating concentration can also be described by the WPG (Fig. 6). It was strongly supported by Ghorbani and Bavaneghi (2016). Acetylation affects the spring-back of the board and causes a significant increase, in particular TS and water absorption, along with the increase in WPG.

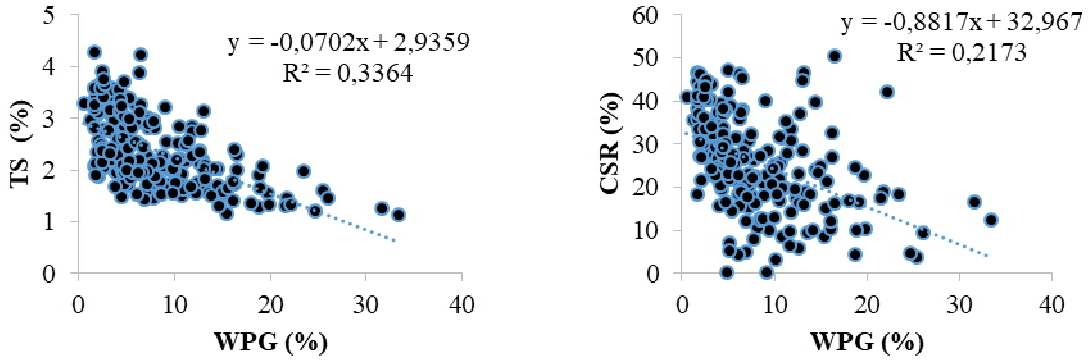

Fig. 6: Correlation between WPG and TS as well as between WPG and CSR.

CONCLUSIONS

The compregnation using LmwPF and SA as impregnating agents can significantly increase the specific gravity (SG) and dimensional stability of the wood. SG of LmwPF- and SA-compregnated wood increased by 10.69–22.31% and 6.96–23.09%, respectively. Application of a higher level of compression ratio will result in better wood characteristics. For 20 and 40% compression ratios, the use of LmwPF and SA as impregnating agents can significantly reduce the spring-back especially the compression-set recovery (CSR) and

thickness swelling (TS) of wood; or in other words, dimensional stability of the wood is significantly improved. CSR after compregnation was 18.34–33.99%, while after densification was 47.86–71.49%. SA-compregnated wood has lower CSR and TS than LmwPF-compregnated wood. Increasing the concentration of the impregnating solution will result in a greater decrease in CSR and TS. The SG and dimensional stability of sepetir-compregnated wood are better than those of nyatoh and pisang putih wood.

ACKNOWLEDGMENTS

The authors are grateful for the support of the Ministry of Research, Technology and Higher Education of the Republic of Indonesia through PMDSU No. 1053/IT3.11/LT/2017.

REFERENCES

1. Augustina, S., Wahyudi, I., Darmawan, W.I, Malik, J., Basri, E., Kojima, Y., 2020: Specific gravity and dimensional stability of boron–densified wood on three lesser–used species from Indonesia. Journal of Korean Wood Science and Technology 48(4): 458–471.
2. Bao, M., Huang, X., Jiang, M., Yu, W., Yu, Y., 2017: Effect of thermos–hydro–mechanical densification on microstructure and properties of poplar wood (*Populus tomentosa*). Journal of Wood Science 63(6): 591–605.
3. Bao, M., Huang, X., Zhang, Y., Yu, W., Yu, Y., 2016: Effect of density on the hygroscopicity and surface characteristics of hybrid poplar compreg. Journal of Wood Science 62: 441–541.
4. Chen, Y., Nichole, M., Stark, Zhiyoung, C., Charles, R., Frihart, Linda, F., Lorenz, R.E.I., 2014: Chemical modification of kraft lignin: effect on chemical and thermal properties. Bioresources 9(3): 5488–5500.
5. Darwis, A., Wahyudi, I., Dwianto, W., Cahyono, T.D., 2017: Densified wood anatomical structure and the effect of heat treatment on the recovery of set. Journal of Indian Academy of Wood Science 14(1): 24–31.
6. Dos-Santos, P.C., Del-Menezzi, C.H.S., 2017: Effect of the densification process on properties of commercial oriented strand boards. European Journal of Wood and Wood Products 76: 1707–1713.
7. Furuta, Y., Aizawa, H., Yano, H., Norimoto, M., 1997: Thermal-softening properties of water-swollen wood: IV. Effects of chemical constituents of the cell wall on the thermal-softening properties of wood. Mokuzai Gakkaishi 43(9): 725–730.
8. Gabrielli, C.P., Kamke, F.A., 2010: Phenol-formaldehyde impregnation of densified wood for improved dimensional stability. Wood Science and Technology 44(1): 95–104.
9. Ghorbani, M., Bavaneghi, F., 2016: Effect of press cycle time on application behavior of board made from chemically modified particles. Drvna Industrija 67(1): 25–31.
10. Hill, C.A.S., 2006: Wood modification: Chemical, thermal, and other processes. Chichester. John Wiley and Sons. Sussex. 249 pp.

11. Inoue, M., Norimoto, M., Otsuka, Y., Yamada, T., 1991: Surface compression of coniferous wood lumber II: Permanent set of compression wood by low molecular weight phenolic resin and some physical properties of the products. Mokuzai Gakkaishi 35(3): 227–233.
12. Kajita, H., Furuno, T., Imamura, Y., 2004: The modification of wood by treatment with low molecular weight phenol-formaldehyde resin: a properties enhancement with neutralized phenolic resin and resin penetration into wood cell walls. Wood Science and Technology 37(5): 349–361.
13. Kamke, F.A., Kutnar, A., 2010: Transverse compression behavior of wood in saturated steam at 150-170°C. Wood and Fiber Science 42(3): 377–387.
14. Kelley, S.S., Timothy, G.R., Glasser, W.G., 1987: Relaxation behavior of the amorphous components of wood. Journal of Materials Science 22(2): 617–624.
15. Khalil, A.H.P.S., Dungani, R., Mohammed, I.A., Hossain, S.Md., Aprilia, S.N.A., Budiarto, E., Rosamah, E., 2014: Determination of the combined effect of chemical modification and compression of Agathis wood on the dimensional stability, termite resistance, and morphological structure. Bioresources 9(4): 6614–6626.
16. Kong, L., Zhao, Z., He, Z., Yi, S., 2017: Effect of steaming treatment on crystallinity and glass transition temperature of *Eucalyptuses grandis* x *E. urophylla*. Results in Physics 7: 914–919.
17. Kutnar, A., Sernek, M., 2007: Densification of wood. Zbornik Gozdarstva In Lesarstva 82: 53–62.
18. Kutnar, A., Kamke, F.A., Sernek, M., 2009: Density profile and morphology of viscoelastic thermal compressed wood. Wood Science and Technology 43(1): 57–68.
19. Lahtela, V., Karki, T., 2014: Effects of impregnation and heat treatment on the physical and mechanical properties of Scots pine (*Pinus sylvestris*) wood. Wood Material Science and Engineering 11(4): 217–227.
20. Lykidis, C., Kotrotsiou, K., Tsichlakis, A., 2019: Reducing set-recovery of compressively densified poplar wood by impregnation–modification with melamine–formaldehyde resin. Wood Material Science and Engineering 15(5): 1–9.
21. Miyoshi, Y., Furutani, M., Furuta, Y., 2016: Swelling behavior of cells in compressed wood. Journal of the Society of Materials Science 65(5): 343–346.
22. Morsing, N., Hoffmeyer, P., 1998: Densification of wood: The influence of hygrothermal treatment on compression of beech perpendicular to gain. Technical University of Denmark. Kgs. Lyngby, 138 pp.
23. Nairn, J.A., 2005: Numerical simulation of transverse compression and densification in wood. Wood and Fiber Science 38(4): 576–591.
24. Navi, P., Sandberg, D., 2012: Thermo hydro mechanical processing of wood. EPFL Press. Lausanne, 280 pp.
25. Nur, I.F.A., Zaidon, A., Rabia'tol, A.M.A., Bakar, E.S., Paridah, M.T., Mohd, H.S., Anwar, U.M.K., 2011: Enhancing the properties of low-density hardwood *Dyera costulata* through impregnation with phenolic resin admixed with formaldehyde scavenger. Journal of Applied Sciences 11: 3474–3481.

26. Ohlmeyer, M., Paul, W., 2010: Optimization of the properties of wood materials by means of thermal modification methods (Work Report No. 2010/2). Hamburg, Germany, 228 pp.
27. Pelit, H., Budakçi, M., Sönmez, A., 2016: Effect of heat post-treatment on dimensional stability and water absorption behaviours of mechanically densified Uludağ fir and Black poplar woods. Bioresources 11(2): 3215–3229.
28. Pelit, H., Sonmez, A., Budakci, M., 2014: Effect of Thermowood® process combined with thermo-mechanical densification on some physical properties of Scot pine (*Pinus sylvestris* L.). Bioresources 9(3): 4552–4567.
29. Pelit, H., Yalçin, M., 2017: Resistance of mechanically densified and thermally post–treated pine sapwood to wood decay fungi. Journal of Wood Science 63(5): 514–522.
30. Rautkari, L., Laine, K., Laflin, M., Hughes, M., 2011: Surface modification of Scots Pine: the effect of process parameters on the through thickness density profile. Journal of Materials Science 46(14): 4780–4786.
31. Sadatnezhad, H.S., Khazaeian, A., Sanberg, D., Tabarsa, T., 2017: Continuous surface densification of wood: A new concept for large-scale industrial processing. Bioresources 12(2): 3122–3132.
32. Scarica, C., Suriano, R., Levi, M., Turri, S., Griffini, G., 2018: Lignin functionalized with succinic anhydride as building block for biobased thermosetting polyester coating. ACS Sustainable Chemical & Engineering 6(3): 3392–3401.
33. Shams, M.I., Kagemori, N., Yano, H., 2006: Compressive deformation of wood impregnated with low molecular weight phenol formaldehyde (PF) resin IV: species dependency. Journal of Wood Science 52: 179–183.
34. Shams, M.I., Yano, H., Endou, K. 2004: Compressive deformation of wood impregnated with low molecular weight phenol formaldehyde (PF) resin I: effects of pressing pressure and pressure holding. Journal of Wood Science 50(4): 337–342.
35. Tabarsa, T., Chui, Y.H., 2000: Characterizing microscopic behavior of wood under transverse compression. Part II. Effect of species and loading direction. Wood and Fiber Science 33(2): 223–232.
36. Tu, D., Su, T., Zhang, T., Fan, W., Zhou, Q., 2014: Thermo-mechanical densification of *Populus tomentosa* ver. *Tomentosa* with low moisture content. Bioresources 9(3): 3846–3856.
37. Wan, H., Kim, M.G., 2006: Impregnation of southern pine wood and strands with low molecular weight phenol-formaldehyde resins for stabilization of oriented strand boards. Wood and Fiber Science 38(2): 314–324.
38. Zhao, Y., Wang, Z., Iida, I., Huang, R., Lu, J., Jiang, J., 2015: Studies on pre-treatment by compression for wood drying I: effect of compression ratio, compression direction and compression speed on the reduction of moisture content in wood. Journal of Wood Science 61(2): 113–119.

IMAM WAHYUDI*, WAYAN DARMAWAN
IPB UNIVERSITY
FACULTY OF FORESTRY AND ENVIRONMENT
DEPARTMENT OF FOREST PRODUCTS
JALAN ULIN KAMPUS DARMAGA
BOGOR 16680
INDONESIA
*Corresponding author: imyudarw16@yahoo.com

SARAH AUGUSTINA
IPB UNIVERSITY
FOREST PRODUCTS SCIENCE AND TECHNOLOGY STUDY PROGRAM
JALAN ULIN KAMPUS DARMAGA
BOGOR 16680
INDONESIA

JAMALUDIN MALIK
FOREST PRODUCTS RESEARCH AND DEVELOPMENT CENTER
JALAN GUNUNG BATU N^{O}. 5
BOGOR 16610
INDONESIA

NAOKI OKANO, OKADA TAIYO, HIKARU KOBORI, YOICHI KOJIMA,
SHIZUOKA UNIVERSITY
FACULTY OF AGRICULTURE
DEPARTMENT OF WOOD BIOMASS UTILIZATION
836 OHYA, SURUGA-KU, SHIZUOKA 422-8529
JAPAN

KAZUSHIGE MURAYAMA
FORESTRY AND FOREST PRODUCTS RESEARCH INSTITUTE
DEPARTMENT OF WOOD-BASED MATERIALS
1 MATSUNOSATO, TSUKUBA, IBARAKI 305-8687
JAPAN

SHIGEHIKO SUZUKI
SHIZUOKA PROFESIONAL UNIVERSITY OF AGRICULTURE
678-1 TOMIGAOKA, IWATA, SHIZUOKA 438-0803
JAPAN

WOOD RESEARCH doi.org/10.37763/wr.1336-4561/66.5.777788
e-ISSN 2729-8906
66(5): 2021 777-788 pp.

EFFICACY OF LINSEED OIL-TREATED WOOD TO IMPROVE HYDROPHOBICITY, DIMENSIONAL STABILITY, AND THERMOSTABILITY

MIHAELA LIU, JIANAN WANG, GUANGLIN XU, XIN WEI TU, XIN YOU LIU, ZHIHUI WU
NANJING FORESTRY UNIVERSITY
CHINA

(RECEIVED NOVEMBER 2020)

ABSTRACT

In this work, linseed oil was impregnated into the wood at room temperature, under vacuum pressure. The properties of linseed oil-treated wood, including dimensional stability, wood moisture absorption, chemical structure, thermostability, and morphological characteristics, were evaluated. Linseed oil displayed good permeability in Ailanthus wood, with weight gains of 30.95% after impregnation. The swelling coefficients of treated wood in the tangential and radial directions decreased by 25.97 to 33.33%, indicating that impregnation improved the dimensional stability of wood. Moreover, linseed oil treatment significantly modified the wood structure, although the FTIR spectra generally remained unchanged. Observation by scanning electron microscopy showed, that linseed oil impregnated into the wood and occluded pits, thereby prevented moisture absorption. This technique can be used in a variety of wood products, such as buildings, furniture, and landscape architecture.

KEYWORDS: Linseed oil treatment, swelling coefficients, thermostability, wood dimensional stability.

INTRODUCTION

Wood is a complex lignocellulose material, its low dimensional stability and durability limits its widespread use. Previous research has led to improvements wood durability, dimensional stability, and hydrophobicity using steam-heat treatment (Wang et al. 2019, Saeed et al. 2016), acetylation and silylation (Ziegler et al. 2008), alkoxysilane modification (Broda et al. 2018), siloxane modification (Giudice et al. 2013), silicone oil heat treatment (He et al. 2019, Qian et al. 2019, Okon et al. 2017), and tricine and bicine modification (Popescu et al. 2020), among many others (Turkoglu et al. 2015). However, thermal treatments may darken the original wood color and attenuate its mechanical properties (Jiang et al. 2020, Sun et al. 2019, Lin et al. 2018, Li et al.

2017, Esteves et al. 2011, Esteves and Pereira 2009, Esteves et al. 2008), whereas chemical treatments may damage the environment. Moreover, many of these modifications are complex and consume large amounts of energy.

Some natural materials are widely used to improve the performance of wood due to their environmentally friendly properties, such as wax, shellac and some vegetable oils (Yang and Liu 2020, Yang et al. 2020, Liu et al. 2020a,b, Dubey et al. 2011, 2012a,b). Linseed oil is produced from the dried ripe seed of the flax plant (*Linum usitatissimum*), which is cultivated for oil and fiber (Yang and Luo 2013). Once exposed to air, the boiled linseed oil can form a siccative but transparent film on a wood surface (Schönemann and Edwards 2011, Lazzari and Chiantore 1999). Linseed oil is environmentally friendly and low-cost with excellent water repellent capacity (Eriksson et al. 2011, Fredriksson et al. 2010). It is commonly applied to conserve archaeological wood (Lucejko et al. 2018). At present, linseed oil is widely utilized for the production of inks, paints, soap, varnishes, and many other products (Arrieta et al. 2017); however, it has not been commonly utilized to enhance the hydrophobicity of wood products.

Following some studies of natural materials impregnated wood dimensional stability (Liu et al. 2020a,b, He et al. 2019), this paper examines the use of linseed oil as an environmentally friendly modifier to increase wood dimensional stability and hydrophobicity. The objectives of this research were to examine *(1)* the effects of linseed oil on wood chemical and physical structures, dimensional stability, and thermostability, and *(2)* the drying mechanisms of linseed oil.

MATERIALS AND METHODS

Sample preparation

Ailanthus (*Ailanthus Desf.*), a commonly cultivated white-colored wood with a similar grain to white oak, was obtained from Qian Heng Mo Zhong company, Sichuan, China. Sapwood specimens with dimensions of 20 × 20 × 20 mm (longitudinal section × radial section × cross-section) and a primal moisture content of 70 ± 5% (mean ± standard error) were prepared and used in the experiments (D4933, 2016). The wood specimens were heat-dried at 103°C before the experiments.

Impregnating the wood with linseed oil

Linseed oil was obtained from Fabryo Company (Brasov, Romania). The impregnation was conducted in a vacuum chamber produced by Shanghai Laboratory Instrumental Works Co., Ltd. (Shanghai, China). Twenty dry specimens were weighed, submerged into linseed oil, and then placed in the vacuum chamber under a pressure of 0.01 MPa and 20°C for 1.5 h. Subsequently, the pressure was allowed to equilibrate to atmospheric level for 1.5 h. The wood specimens were impregnated with linseed oil by vacuuming and reversing the process three times. The wood specimens that were not impregnated with linseed oil were regarded as the control group. Following the treatment, these specimens were naturally dried for 7 days until the linseed oil was cured, dried at 103°C, and then weighed.

Weight percentage gain (WPG)

The specimens were weighed immediately before and after the impregnation. The WPG was determined based on the weight and was calculated by Eq. 1:

$$WPG=\frac{w_w-w_0}{w_0}\times 100\ \% \quad (1)$$

where: w_0 represents the dry weight of specimens before the impregnation (g), and w_w represents the dry weight after the impregnation (g).

Treatment means were compared with a t-test at P = 0.05 in SAS (v. 9.4, SAS Institute, Cary, NC).

Estimation of wood dimensional stability

The swelling was measured following the ASTM D4933-2016 standard. All wood specimens were oven-dried and then placed in a climate chamber at 20°C with 65 % humidity to achieve the equilibrium moisture content (EMC). The dimensions and weights were determined before and following the conditioning. The swelling coefficient was computed with Eq. 2:

$$a=\frac{l_w-l_0}{l_0}\times 100\ \% \quad (2)$$

where: a denotes the swelling coefficient for assessing the longitudinal, tangential, and radial parameters of the specimens, l_w denotes the dimension after conditioning, and l_0 represents the initial dimension of the specimens.

Treatments were compared with t-tests in SAS at p = 0.05.

Moisture absorption

Moisture absorption (MA) experiments were performed following the ASTM D4933: 2016 standard. The wood specimens were placed in a climate chamber under a constant temperature of 20°C with 65% relative humidity to reach the EMC. After conditioning in the climate chamber, the MA was calculated using Eq. 3:

$$MA=\frac{w_a-w_b}{w_b}\times 100\ \% \quad (3)$$

where: w_b and w_a denote the weights before and after the conditioning (g), respectively.

Treatments were compared with t-tests in SAS at p = 0.05.

Chemical structure analysis using FTIR spectroscopy

Attenuated total reflectance infrared (ATR-IR) spectra of the control group and linseed oil-treated wood specimens were collected using a standard FTIR spectrometer (Tensor 27, Bruker, Germany) via direct transmittance at a resolution of 4 cm^{-1} for 32 scans at 500 – 4000

cm^{-1}. The background spectra and the light equipment were aligned immediately before the measurements. The spectra were averaged over six measurements for each treatment before data analysis.

Thermogravimetric analysis

A thermogravimetric analyzer (Netzsch STA449F3, Germany) was employed to measure the degradation characteristics of wood specimens. The untreated control and linseed oil-treated wood powder were placed in a chamber filled with nitrogen and heated at a rate of $10°C \cdot min^{-1}$ until reaching an ultimate temperature of 800°C.

Morphological characteristics

To investigate the potential variations in the physical structures, an environmental scanning electron microscope (SEM) (Quanta 200, FEI Company, the Netherlands) was employed to observe the surface shapes of wood specimens. Increase in electrical conductivity of a sample is the single most common requirement for SEM. In this study, a sputter gold coating (2 nm) was applied on the wood specimens using a Gold Palladium SEM Annular Sputtering target 2" ID × 3" OD × 0.1mm Anatech (SC502-314; Quorum Technologies, Ltd., Watford, UK). Bombarding voltage used for SEM was 20.00 kV.

RESULTS AND DISCUSSION

Weight percentage gain (WPG)

WPG value indicates the net weight of the wood penetrated by linseed oil, as shown in Tab. 1. This depends on the permeability of linseed oil inside the Ailanthus wood. The dry weight of the untreated wood specimens measured 4.497± 0.233 g; however, after impregnating with linseed oil, the dry weight and WPG measured 5.889 ± 0.199 g and 30.95%, respectively.

Wood dimensional stability

Wood dimensional stability is an important factor affecting its utilization and quality, but it depends on tree species, tree age, and age of the wood, among other factors. The radial and tangential swelling coefficients are critical factors to assess the wood dimensional stability because they are more sensitive than those in the longitudinal direction. The linseed oil impregnating treatment significantly improved wood dimensional stability ($P < 0.0001$) in tangential and radial directions but not in a longitudinal direction ($P = 0.1112$) (Fig. 1). The swelling coefficient in the tangential direction of the untreated control measured 3.08%, while the linseed oil-treated wood measured 2.17%.

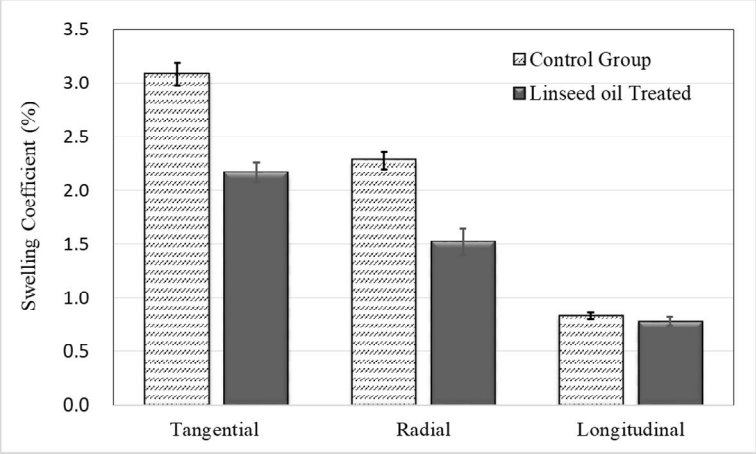

Fig. 1: Swelling coefficients in different directions.

After the treatment with linseed oil, the swelling coefficient in tangential direction decreased by 25.97% compared with the control group. The swelling coefficient of the control group in the radial direction measured 2.28%, while the treated group measured 1.52%. The swelling coefficient of the linseed oil-treated specimens was 33.33 % lower compared with the control group. The control and linseed oil-treated specimens exhibited similar longitudinal swelling coefficients and measured 0.83% and 0.78%, respectively. These observations indicated that the linseed oil treatment can significantly decrease wood swelling coefficients in the radial and tangential directions but not in the longitudinal direction. This is logical as wood tends to shrink and swell in the radial and tangential directions, but not in the longitudinal direction. The increased wood dimensional stability could be attributed to the excellent water repellent property of linseed oil (Humar and Lesar 2013).

Moisture absorption

When the moisture content of wood is under the fiber saturation point (FSP), it can significantly affect wood stability (Yang and Liu 2018). To further elucidate the impact of linseed oil impregnation on wood dimensional stability, the hydrophilicity of wood was evaluated by moisture absorption (MA). The specimens' weights before and following the conditioning in the climate chamber are shown in Fig. 2. After conditioning in the climate chamber, the weights of the control group varied between 4.497 g and 5.033 g before and after conditioning, and the MA was 11.92%. The treated specimens' weights changed and varied from 5.889 g to 6.213 g, and the MA was 5.50%. Linseed oil treatment can reduce water MA Ailanthus wood by 53.86%.

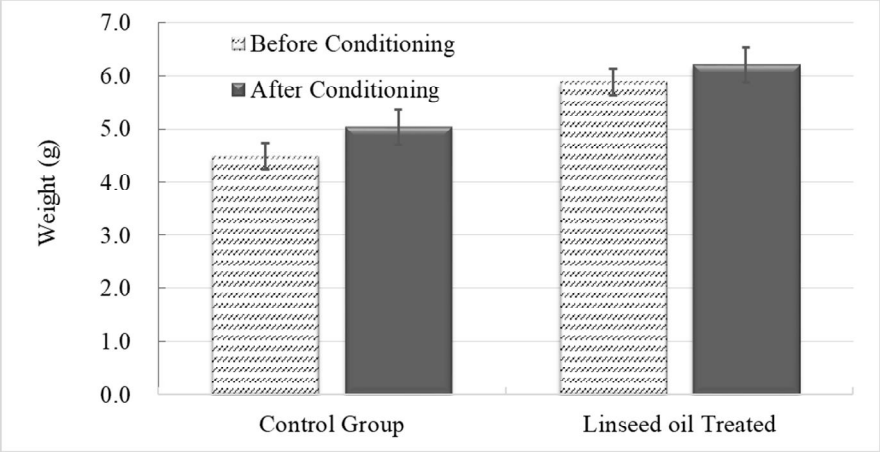

Fig. 2: Weights of the specimens before and after conditioning.

Chemical structure analysis using FTIR spectroscopy

Wood dimensional stability is related to its hydrophilic chemical composition, which generally contains hydroxyl groups and other chemical components. The reduction of these components can improve stability (Jiang et al. 2015). FTIR-ATR spectrometry has been widely employed to reveal chemical changes associated with various treatments. Infrared spectra are sensitive indicators of chemical changes, as demonstrated by previous research in the fields of wood treatments (Basso et al. 2017).

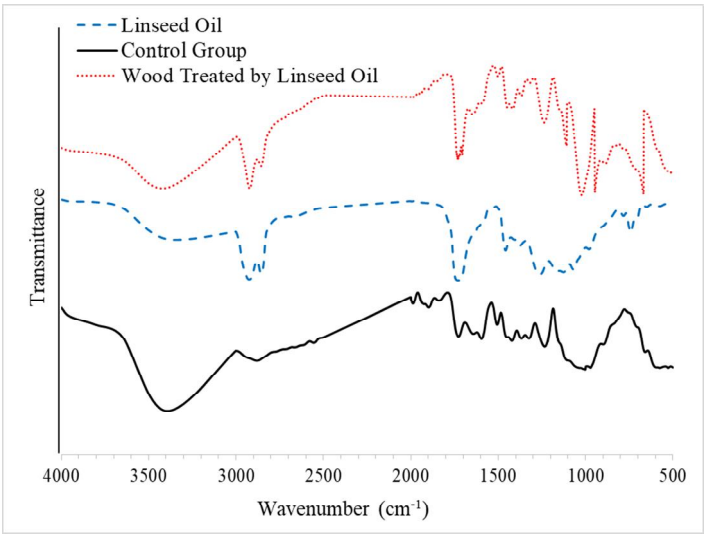

Fig. 3: FTIR spectra of the samples treated by linseed oil.

Fig. 3 presents the FTIR spectra results in the untreated control and the linseed oil-treated specimens. Although the spectra were largely unchanged, the linseed oil treatment modified the chemical structures of the wood specimens. The significant decrease of band intensities at ~3400 cm^{-1} corresponded to −OH stretching. Since linseed oil treatment reduces the relative number of hydroxyl groups (He et al. 2019), it improves the dimensional stability of the wood. Moreover, the band intensity at 1384 cm^{-1} and 2900 cm^{-1} (−CH stretching), and the bands at 1729 cm^{-1} (C=O) and 1604 cm^{-1} (aromatic carbon skeleton stretching vibrations) changed (Liu et al.

2020a,b, He et al. 2019, Esteves et al. 2011). After being treated with linseed oil, another chemical groups did not change. Thus, linseed oil treatment changed some of the chemical groups in the wood, but the composition of the wood remained the same.

Thermostability

The thermal characteristics of wood specimens treated with linseed oil were evaluated using the thermogravimetric (TG) and derivative thermogravimetric (DTG) curves (Fig. 4).

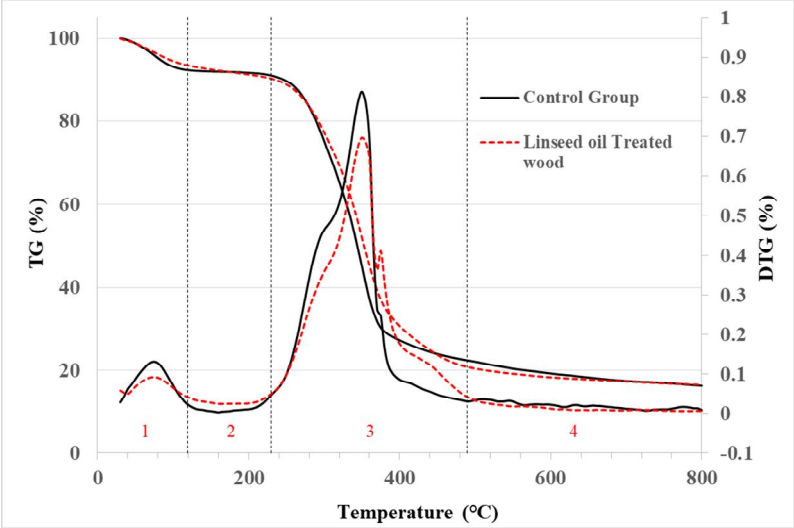

Fig. 4: TG and DTG curves of the wood samples treated.

The TG curve in the first region (marked by "1") represents depolymerization and dehydration. A 6–8% weight reduction was noted in the range of 30 to 120°C in all cases. At this stage, the wood composition does not degrade significantly (He et al. 2019), although the wood's moisture evaporates and some small molecules are degraded. In the range of 120°C to 230°C (marked by "2"), some wood components, such as hemicellulose, may degrade (Esteves and Pereira 2009, Li et al. 2017, 2018) while the chemical bonds of other complex wood components may break. The most mass loss occurred at the temperature of 230°C – 490°C (marked by "3"), accounting for about 70% of the total mass. At this stage, all the structural components of the wood sample underwent thermal degradation. Also, in this region, linseed oil-treated samples reacted differently, with two peaks appearing at 355°C and 375°C. By contrast, at 355°C, the DTG curve of the control samples is more common and has a peak. This spike can be attributed to the breakdown of cellulose (Giuntoli et al. 2009). In region "4," the mass loss of the sample decreases gradually. At this stage, compared with the control group (16.30 wt%), the residue content after linseed oil treatment decreased by 16.59%. The reduction in residue may be due to the degradation of most linseed oil and the inability of some wood components to decompose.

Morphology and mechanism

To evaluate physical structures changes, the SEM micrographs of the treated samples and control group are illustrated in Fig. 5. Results showed that linseed oil treatment significantly

affected the tissue structure of the samples. Pits are the main moisture channels in the wood interior. After linseed oil treatment, some of the pits were occluded, and prevented MA under the environmental conditions, thus improving the dimensional stability of wood. Also, some areas show cured linseed oil (marked by a circle) attached to the internal surface of the wood. Thus, when linseed oil is coated on the inner surface of the wood, it prevents MA and improves the wood dimensional stability.

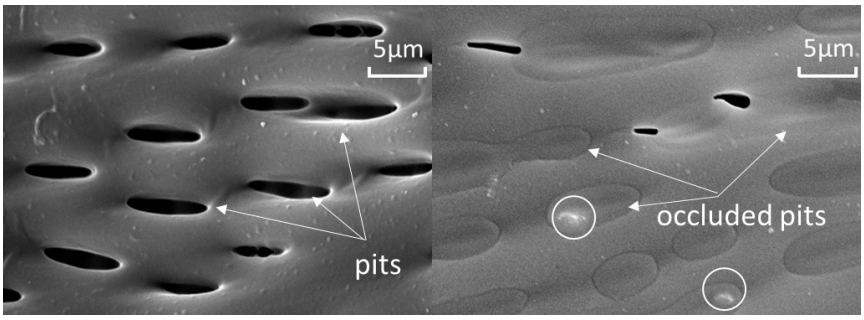

Fig. 5: SEM micrographs of the control group and l treated group.

Linseed oil is mainly composed of linoleic acid (14 – 19%) and linolenic acid (48 – 60%) (Lazzari and Chiantore 1999). The typical mechanism of the linseed oil drying process is hydrocarbon oxidation, which is promoted by the active hydrogen atom at the vinyl position of the molecule (Fig. 6). In linoleic acid and linolenic acid components, one or two methylene groups are located between two unbound double bonds and the formation of hydrogen peroxide is easier to achieve. Then W-type pentadienyl can react with oxygen at both ends to form a hydroperoxide mixture with trans and cis conjugation. Also, the reversibility of oxygen addition leads to the isomerization of W radicals, which can be converted into trans products. The alkoxy radicals produced by the decomposition of hydroperoxides may lead to the formation of oxygen-containing structures, such as alcohols and different carbonyls, or crosslinked products. These radicals are polymerized with other linseed oil molecules. Finally, the crosslinking density of linseed oil increases and a curing film is formed on the inner surface of the wood. As such, the water transport pathway is blocked, resulting in improved wood dimensional stability (Liu et al. 2020a,b, He et al. 2018).

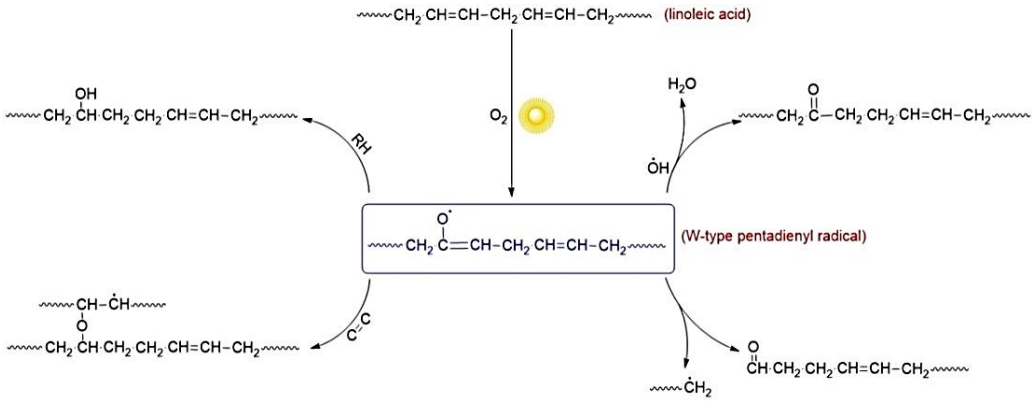

Fig. 6: The drying mechanism of linseed oil (Lazzari and Chiantore 1999).

CONCLUSIONS

Linseed oil impregnation treatment is an effective technique to improve wood stability. Linseed oil has good permeability in the wood and the WPG reached to 30.95% after impregnation. After the treatment with linseed oil, the swelling coefficients of wood in the tangential direction and radial direction decreased by 25.97% and 33.33%, respectively, resulting in improved wood dimensional stability. The moisture absorption of linseed oil-treated wood was reduced by 53.86% under the condition of 20°C and 65% relative humidity. Also, linseed oil treatment changed the structure of the wood to some extent, but the spectrum remained unchanged. In TG analysis the DTG curve of the control samples was more common with a steep peak at 355°C. The samples treated with linseed oil had two decomposition peaks around 355°C and 375°C. Linseed oil impregnates into the wood, occludes pits, and solidifies at the internal wood surface, thereby preventing moisture absorption. This technique can be used in a variety of wood products, such as buildings, furniture, and landscape architecture.

ACKNOWLEDGMENTS

This work was supported by Project from International Cooperation Joint Laboratory for Production, Education, Research and Application of Ecological Health Care on Home Furnishing, the Nanjing Forestry University Foundation for Basic Research (Grant No. 163104127), the National Key R & D Program of China (Grant No. 2016YFD0600704) and the Priority Academic Program Development (PAPD) of Jiangsu Province, China.

REFERENCES

1. Arrieta, M.P., Sampera, M.D., Jiménez-López, M., Aldas, M., López, J., 2017: Combined effect of linseed oil and gum rosin as natural additives for PVC. Industrial Crops and Products 99: 196-204.
2. Basso, M.C., Pizzi, A., Polesel Maris, J., Delmotte, L., Colin, B., Rogaume, Y., 2017: MALDI-TOF, 13C NMR and FTIR analysis of the cross-linking reaction of condensed tannins by triethyl phosphate. Industrial Crops and Products 95: 621–631.
3. Broda, M., Majka, J., Olek, W., Mazela, B., 2018: Dimensional stability and hygroscopic properties of waterlogged archaeological wood treated with alkoxysilanes. International Biodeterioration & Biodegradation 133: 34-41.
4. Dubey, M.K., Pang, S., Walker, J., 2012a: Oil uptake by wood during heat-treatment and post-treatment cooling, and effects on wood dimensional stability. European Journal of Wood and Wood Products 70(1): 183-190.
5. Dubey, M.K., Pang, S., Walker, J., 2012b: Changes in chemistry, color, dimensional stability and fungal resistance of *Pinus radiata* D. Don wood with oil heat-treatment. Holzforschung 66(1): 49-57.

6. Dubey, M. K., Pang, S., Walker, J., 2011: Effect of oil heating age on colour and dimensional stability of heat treated *Pinus radiata*. European Journal of Wood and Wood Products 69(2): 255-262.
7. Eriksson, D., Geladi, P., Ulvcrona, T., 2011: Near-infrared spectroscopy for the quantification of linseed oil uptake in Scots pine (*Pinus sylvestris* L.). Wood Material Science & Engineering 6(4): 170-176.
8. Fredriksson, M., Wadsö, L., Ulvcrona, T., 2010: Moisture sorption and swelling of Norway spruce *Picea abies* (L.) Karst. impregnated with linseed oil. Wood Material Science and Engineering 5(3-4): 135-142.
9. Esteves, B., Graça, J., Pereira, H., 2008: Extractive composition and summative chemical analysis of thermally treated eucalypt wood. Holzforschung 62: 344–351.
10. Esteves, B., Pereira, H., 2009: Wood modification by heat treatment: A review. BioResources 4(1): 370-404.
11. Esteves, B., Videira, R., Pereira, H., 2011: Chemistry and ecotoxicity of heat-treated pine wood extractives. Wood Science and Technology 45(4): 661–676.
12. Giudice, C.A., Alfieri, P.V., Canosa, G., 2013: Decay resistance and dimensional stability of *Araucaria angustifolia* using siloxanes synthesized by sol–gel process. International Biodeterioration & Biodegradation 83: 166-170.
13. Giuntoli, J., De Jong W., Arvelakis, S., Spliethoff, H., Verkooijen, A.H.M., 2009: Quantitative and kinetic TG-FTIR study of biomass residue pyrolysis: Dry distiller's grains with solubles (DDGS) and chicken manure. Journal of Analytical and Applied Pyrolysis 85: 301-312.
14. He, Z.B., Qian, J., Qu, L.J., Yan, N., Yi, S.L., 2019: Effects of tung oil treatment on wood hygroscopicity, dimensional stability and thermostability. Industrial Crops and Products 140: 111647.
15. Humar, M., Lesar, B., 2013: Efficacy of linseed- and tung-oil-treated wood against wood-decay fungi and water uptake. International Biodeterioration & Biodegradation 85: 223-227.
16. Jiang, H., Lu, Q., Li, G., Li, M., Li, J., 2020: Effect of heat treatment on the surface color of rubber wood (*Hevea brasiliensis*). Wood Research 65(4): 633-644.
17. Jiang, J., Li, J., Gao, Q., 2015: Effect of flame retardant treatment on dimensional stability and thermal degradation of wood. Construction and Building Materials 75: 74-81.
18. Lazzari, M., Chiantore, O., 1999: Drying and oxidative degradation of linseed oil. Polymer Degradation and Stability 65: 303-313.
19. Li, T., Cheng, D.L., Avramidis, S., Wålinder, M.E., Zhou, D.G., 2017: Response of hygroscopicity to heat treatment and its relation to durability of thermally modified wood. Construction and Building Materials 144: 671-676.
20. Lin, B.J., Colin, B., Chen, W.H., Pétrissans, A., Rousset, P., Pétrissans, M., 2018: Thermal degradation and compositional changes of wood treated in a semi-industrial scale reactor in vacuum. Journal of Analytical and Applied Pyrolysis 130: 8-18.

21. Liu, M., Tu, Xi., Liu, X., Wu, Z. Lv, Varodi, A., 2020: A comparative study on the effects of linseed oil and shellac treatment on the hygroscopicity, dimensional stability, and color changes of Chinese ash wood. Bioresources 15(4): 8085-8092.
22. Liu, M., Xu, G., Wang, J., Tu, X., Liu, X., Wu, Z., Lv, J., Xu, W., 2020: Effects of shellac treatment on wood hygroskopicity. Dimensional stability and thermostability. Coatings 10(9): 881.
23. Lucejko, J.J., La Nasa, J., Queen, C.M., Braovac, S., Colombini, M.P., Modugno, F., 2018: Protective effect of linseed oil varnish on archaeological wood treated with alum. Microchemical Journal 139: 50-61.
24. Okon, K.E., Lin, F., Chen, Y., Huang, B., 2017: Effect of silicone oil heat treatment on the chemical composition, cellulose crystalline structure and contact angle of Chinese parasol wood. Carbohydrate Polymers 164: 179–185.
25. Popescu, C.M., Jones, D., Kržišnik, D., Humar M., 2020: Determination of the effectiveness of a combined thermal/chemical wood modification by the use of FT-IR spectroscopy and chemometric methods. Journal of Molecular Structure 1200: 127133.
26. Qian, J., Li, J., Wang, Z., Qu, L., Ding, Y., Yi, S., He, Z., 2019: Effects of wax and dimethyl silicone oil mixed impregnation on dimensional stability of two hardwoods. Wood Research 64(1): 165-176.
27. Saeed, M.A., Andrews, G.E., Phylaktou, H.N., Gibbs, B.M., 2016: Raw and steam exploded pine wood: Possible enhanced reactivity with gasification hydrogen. International Journal of Hydrogen Energy 41(37): 16566-16576.
28. Schönemann, A., Edwards, H.G., 2011: Raman and FTIR microspectroscopic study of the alteration of Chinese tung oil and related drying oils during ageing. Analytical and Bioanalytical Chemistry 400(4): 1173-1180.
29. Sun, B.L., Wang, Z., Liu. J., 2019: Study on color and surface chemical properties of *Eucalyptus pellita* wood subjected to thermo-vacuum treatment. Wood Research 64(1): 01-12.
30. Temiz, A., Kose, G., Panov, D., Terziev, N., Alma, M. H., Palanti, S., Akbas, S., 2013: Effect of bio-oil and epoxidized linseed oil on physical, mechanical, and biological properties of treated wood. Journal of Applied Polymer Science 130(3): 1562-1569.
31. Turkoglu, T., Baysal, E., Kurell, I., Toker, H., Ergun, M.E., 2015: The effects of natural weathering on hardness and gloss of impregnated and varnished scots pine and oriental beech wood. Wood Research 60(5): 833-844.
32. Wang, X., Wu, Y., Chen, H., Zhou, X., Zhang, Z., Xu, W., 2019: Effect of surface carbonization on mechanical properties of LVL. BioResources 14(1): 453-463.
33. Yang, X., Luo, J., 2013: The thermo-viscous properties of the linseed oil modified with pentaerythritol. Industrial Crops and Products 41: 437– 441.
34. Yang, L., Liu, H., 2020: Effect of a combination of moderate-temperature heat treatment and subsequent wax impregnation on wood hygroscopicity, dimensional stability, and mechanical properties. Forests 11: 920.

35. Yang, L., Han, T., Fu, Y., 2020: Effect of heat treatment and wax impregnation on dimensional stability of *Pterocarpus macrocarpus* wood. Wood Research 65(6): 963-974.
36. Yang, L., Liu, H., 2018: A review of eucalyptus wood collapse and its control during drying. Bioresources 13(1): 2171-2181.
37. Ziegler, I.M., Tánczos, I., Hórvölgyi, Z., Agoston, B., 2008: Water-repellent acylated and silylated wood samples and their surface analytical characterization. Colloids and Surfaces A: Physicochemical and Engineering Aspects 319(1-3): 204-212.
38. D4933, 2016: Standard guide for moisture conditioning of wood and wood-base materials.

MIHAELA LIU, JIANAN WANG, GUANGLIN XU, XIN WEI TU, XIN YOU LIU*,
ZHIHUI WU*
NANJING FORESTRY UNIVERSITY
CO-INNOVATION CENTER OF EFFICIENT PROCESSING AND UTILIZATION OF FOREST RESOURCES
COLLEGE OF FURNISHING AND INDUSTRIAL DESIGN
ACADEMY OF CHINESE ECOLOGICAL PROGRESS AND FORESTRY STUDIES
LONGPAN NO.159
NANJING
CHINA
*Corresponding author: liu.xinyou@njfu.edu.cn, wzh550@njfu.edu.cn

WOOD RESEARCH doi.org/10.37763/wr.1336-4561/66.5.789805
e-ISSN 2729-8906
66(5): 2021 789-805 pp.

DETERMINING THE COEFFICIENT OF FRICTION OF WOOD-BASED MATERALS FOR FURNITURE PANELS IN THE ASPECT OF MODELLING THEIR SHREDDING PROCESS

MATEUSZ KUKLA, ŁUKASZ WARGUŁA, ALEKSANDRA BISZCZANIK
POZNAN UNIVERSITY OF TECHNOLOGY
POLAND

(RECEIVED NOVEMBER 2020)

ABSTRACT

In order to improve the power selection of the drive unit for the shredding machines, the authors determine the values of friction coefficients used in the cutting force models. These values consider the friction between steel and such wood-based materials as chipboard, MDF and OSB. The tests concern laminated and non-laminated external surfaces and surfaces subjected to cutting processes. The value of the coefficient of friction for the tested materials is in the range: for the static coefficient of friction 0.77-0.33, and for the kinetic coefficient of friction 0.68-0.25. The highest values of the static and kinematic coefficient of friction were recorded for MDF (non-laminated external surface) and they were equal respectively: 0.77 and 0.68. In turn, the smallest values of the discussed coefficients were recorded for chipboard (laminated external wood-base surface), which were at the level of 0.33 and 0.25, resp.

KEYWORDS: Static friction coefficient, kinetic friction coefficient, MDF board, OSB board, chipboard, carpentry waste.

INTRODUCTION

Many processes that use wood and wood-based waste need shredding of these materials. This improves their transport, storage and processing. The re-use of waste wood and wood-based products from production or from the use of products, contributes to reducing both wood waste and deforestation in various geographical areas. At the same time, it is important to use economically efficient machines with a low environmental impact. The increase in consumption worldwide (Blühdorn 2017, Zaharia and Zaharia 2015) contributes to the increase in the amount of waste (Fan and Meng 2020), including: post-consumer waste (Ihnat et al. 2020), used furniture, packaging (Czarnecka-Komorowska and Wiszumirska 2020,

Czarnecka-Komorowska et al. 2018). Processes managing wood-based waste often use shredding machines (Warguła and Kukla 2020, Zhang et al. 2019, Yu et al. 2012), as this facilitates the processes of storage, transport (Reczulski 2015, Gałęzia 2013, Warguła et al. 2020b) and processing, for example: combustion (Rabajczyk 2020, Kajda-Szcześniak and Jaworski 2018, 2019, Spîrchez et al. 2019, Chen 2015), composting (Knitter et al. 2019) including biomass gasification (Sheth and Babu 2010), biochars production (Kosakowski et al. 2020), pellet production (Saosee et al. 2020, Macko and Mroziński 2018, 2019, Ibrahim et al. 2018) and briquettes production (Garrido et al. 2017) or reuse in the production of furniture boards (Ihnát et al. 2017, 2018, Souza et al. 2018).

In these processes, the chippers are mostly mobile machines, powered by combustion engines (Laitila and Routa 2015, Han et al. 2015, Spinelli and Magagnotti 2013). In the case of such machines, it is advantageous to choose a drive unit with no more power than required, as larger internal combustion engines are characterized by an increase in fuel consumption and exhaust gas emissions. This is also important due to the ongoing process, which in essence is not continuous (Warguła et al. 2019). Shredding is usually a periodic-change process in which the machine load results from the frequency of waste delivery (Warguła et al. 2020b). Designing innovative machines shredding wood and wood-based materials is carried out to reduce: environmental impact (Waluś et al. 2018) and operating costs (Warguła and Krawiec 2020). The most popular solutions include the use of: cutting mechanisms, characterized by lower cutting force and increased durability (Guerrini et al. 2019, Macko et al. 2018a,b, Czerniak et al. 2016, Reczulski 2016, 2018), innovative control processes - improving adaptation to conditions of use (Warguła et al. 2020a,d), but also powering engines with fuels alternative to gasoline (LPG and CNG) (Warguła et al. 2020c,e, Dziewiatkowski et al. 2020, Szpica 2018).

Designing machines with a drive unit selected efficiently for the required shredding processes requires precise models of cutting force. These are used, for example, during designing: circular saw (Kopecký et al. 2014, Orłowski et al. 2013, Porankiewicz et al. 2011), a band saw (Chuchała and Orłowski 2018, Orłowski and Ochrymiuk 2017), a chain saw (Kuvik et al. 2017), a large size crusher (Yu et al. 2012), a milling machine (Kopecký et al. 2019, Durkowić et al. 2018, Krauss et al. 2016, Pinkowski et al. 2016, Mandić et al. 2015, Guo et al. 2015, Džinčić et al. 2012). In the event of significant overcapacity, the machine will be characterised by inefficient operation and increased emissions of air pollutants. On the other hand, insufficient power of the drive unit may hinder, and in extreme cases prevent the shredding process (e.g. by blocking the cutting mechanism). The creation of a mathematical model requires knowledge of the values of the coefficients on which it is based, with the greatest accuracy being achieved by experimentally determining the values sought. The results of previous research work on cutting force (Warguła and Kukla 2020) suggest that the shredding process of wood-based panels can essentially be divided into two parts. In the first part, the material is crushed by compacting it. However, the actual part of the process, i.e. cutting, takes place only after the tool has been recessed to a certain depth. This is due to the properties of the cut furniture boards, which are a wood-based material, as schematically presented in Fig. 1. Considering the conclusions from previous studies, it was noted that the cutting process of the discussed wood-based and wooden materials is similar to that of other materials of plant origin. Therefore,

it is reasonable to use available theoretical models of cutting materials of plant origin describing this phenomenon, such as the one described in Eq.1:

$$F = g\sigma + \frac{E}{2} \cdot \frac{h^2}{H} [\tan\beta + \mu\sin^2\beta + \mu'(\mu + \cos^2\beta)], \quad (1)$$

where: F is the pressure force per blade length unit, g is the thickness of the blade, σ is the stress in the material created during cutting, E is Young's modulus of the material to be cut, h is the thickness of the layer of material to be crushed with the knife, H is the total height of the material, β is the angle of application of the knife blade, μ is the coefficient of internal friction, μ' is the coefficient of friction between the knife blade material and the material to be cut (Kanafojski and Karwowski 1976).

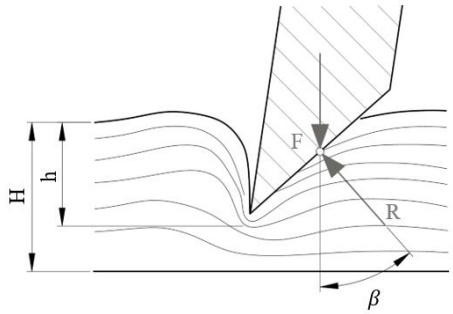

Fig. 1: Force acting on the knife edge at the beginning of the cutting process of plant-based material; H- thickness of the material being cut, h - thickness of the crushed layer, R - reaction force of the material being cut; prepared based on (Kanafojski and Karwowski 1976).

Of course, it is possible to numerically model different values of the friction coefficient μ' corresponding to different values of the cutting depth h. This will allow to take into account the layered structure of the material. This is necessary because each of the layers (in general) may have various properties - including the different values of coefficient of friction.

The main objective of the conducted research is to develop innovative solutions for drive systems of low-power internal combustion chippers for the purpose of shredding wood material and its derivatives, especially wood-based panels. Therefore, it is necessary to precisely define and model the values of forces which must be transferred by cutting mechanisms of machines shredding furniture waste. As a result, this will also translate into the determination of the mechanical power requirements of their drive systems. The proper selection of the drive unit, without too much power reserve, translates into measurable environmental and economic benefits related to the energy saving during the implemented process. This is why it is important to conduct research in the discussed direction. In the presented model (1), only the first component represents a useful force, which is necessary to carry out the cutting process. Due to the large variety of plant-based materials, its value can only be determined based on experiments. Research work is currently under way on this issue. The second segment of Eq. 1 is related to cutting resistances not directly related to the process itself, i.e. crushing of the material, internal friction and friction between the blade and the material being cut. The results presented in this

article are related to the experimental determination of coefficients of the described model. The literature provides values of friction coefficients of wood-based materials (Kazlauskas et al. 2020, Stasiak et al. 2020, Bejo et al. 2000), but does not consider all materials presented in this article and does not consider all surfaces with which the cutting knife may come into contact during the shredding process.

The value of the friction coefficient between: wood-based materials, a wood-based and wood-based materials and/or the cutting tool can depend on many factors. The value of the friction coefficient between two wood-based materials may change, for example, with an increase in contact pressure (an increase in contact pressure causes a decrease in the kinematic and static friction coefficient) (Bejo et al. 2000). Wood moisture contributes to the increase of the static and dynamic friction coefficient (Aira et al. 2014, Seki et al. 2013). The average coefficient of friction between the cemented carbide and the wood surface increased with increasing moisture below the fiber saturation point (FSP). However, an increase in the amount of free water may lead to a more significant decrease in the friction coefficient (Li and Zhang 2019). The arrangement of wood fibers may result in even a twice higher value of the friction coefficient (Aira et al. 2014). The kinematic parameters of the contact, e.g. velocity, also affect the value of the kinetic friction coefficient, however, the available studies for a variety of wood and wood-based materials do not show unequivocal relationships (Li et al. 2013). The value of the dynamic friction coefficient, e.g. during cutting with a steel tool or sintered carbides, can be reduced by applying various types of coatings, e.g. carbon (Karczewski et al. 2012), carbon and titanium (Kaczorowski and Batiry 2008), CrxNy (Djouadi et al. 2000), TiAlN/a-CN (Czarniak et al. 2020) coatings. With the properties of, for example, a cutting tool, the coefficients of dynamic friction of wood-based and wooden materials are affected by their roughness (Xu et al. 2014). The value of the friction coefficient is influenced by many parameters, the authors of the article presented research for a classic tool set in grinders made of tool steel. The speed of the process corresponded to the actual operating conditions of the tested machines, which can range from 40 rpm to 2500 rpm (Huber et al. 2017, Warguła and Kukla 2020, Warguła et al. 2020f) and the ambient temperature similar to that available in the production halls of carpentry workshops.

MATERIALS AND METHODS

Wood-based materials samples preparation

Measurements in this study were carried out for 11 sample types. Using mechanical processing, individual samples of 40 × 15 cm were cut out from boards supplied by commercial suppliers. Depending on the type of board, they differed slightly in thickness, but this parameter does not affect the measurement results.

In the case of a wood-based panel, the external surface was tested in its nominal condition (i.e. the surface condition as the material is immediately after purchase, without any additional treatment likely to change its properties). In the case of MDF, the external surface was tested in its nominal laminated and non-laminated condition. Additionally, experiments were carried out on the surface created after mechanical cutting off of the selected plane of the tested material. In

the case of chipboard, its external and side surfaces were tested in their nominal condition and the surface created after mechanical cutting off part of the material. In addition, the external surface in its nominal condition for the second type of laminated chipboard (porous structure) was also tested. For OSB, the external surface in its nominal condition, the side surface after mechanical cutting of the material and the surface after removal of the cover layer were also tested. In the last case, it was necessary to prepare the surface for testing by partial smoothing. The aim of this treatment was to remove protruding parts of the chips with a grinding wheel (because they were crushed or broken during the tests, making it impossible to carry out the experiment) and not to obtain a smooth surface structure. It was decided to leave the boards nominal thickness so that it is not necessary to cut them wide. The characteristics and determinations of the individual samples are presented in Tab. 1. The markings introduced in Tab. 1 have been consistently maintained throughout the article. The individual surfaces are shown in Fig. 2.

Temperature and humidity affect the results of friction tests (Park et al. 2011). Thus, prepared test samples were conditioned at temperature of 20°C and humidity of 65% so that they reached a moisture content (MC) of 10% ± 0.1%. For this purpose, a climatic chamber was used. The moisture content was checked with a Mettler Toledo moisture analyser during conditioning until the desired value was obtained. The measurement consisted in precise weighing of the sample (± 0.001 g) and simultaneous drying (change of MC from measured value to oven-dry).

Tab. 1: Characteristics and markings of individual samples.

Sample No.	Material type	Surface
1	Chipboard	Laminated external wood-base
2	MDF	Laminated external
3	MDF	Non-laminated external
4	MDF	After mechanical cut
5	Chipboard	Laminated external porous
6	Chipboard	Non-laminated external
7	Chipboard	After mechanical cut
8	Chipboard	Side
9	OSB	After mechanical cut
10	OSB	External
11	OSB	After mechanical removal of the cover layer and smoothing

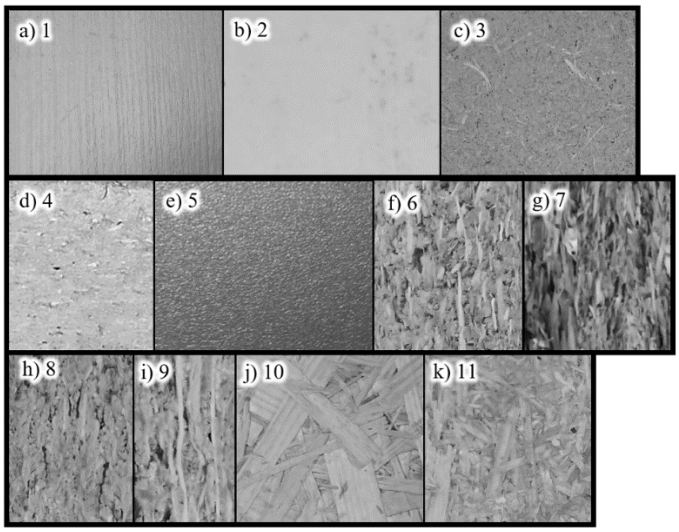

Fig. 2: View of individual tested surfaces; a) sample 1, b) sample 2, c) sample 3, d) sample 4, e) sample 5, f) sample 6, g) sample 7, h) sample 8, i) sample 9, j) sample 10, a) sample 11.

Chipper knives material

A lot of research work can be indicated in the field of surface roughness and topography of contact surfaces, but the exact relationship between surface roughness and friction has not yet been defined (Sedlaček et al. 2009, Meine et al. 2002). Moreover, there are a number of parameters that describe the surface profile. A maximum of 17 parameters are currently being used for this purpose (Meine et al. 2002). So far, however, no single definition of roughness describes the surface profile in a complete way. As a result, quite different surface topographies can have the same roughness value (Meine et al. 2002, Bhushan 1999). However, test results are available to indicate the relationship between roughness and coefficient of friction in dry conditions (without lubricants) (Al-Samarai et al. 2012). Therefore, tests have been performed to determine the surface roughness of cutting plates made of metallic material. However, when interpreting them, the above-mentioned comments should be considered.

The test uses cuboidal plates made of HADOX steel, type 500. It is the same type of material that is used for knives in a cylindrical chipper. The plates were cut out by machining. Before the test, their surface was prepared by rough cleaning with sandpaper and degreasing with a high percentage solution of technical alcohol. The material in this condition corresponds to brand new knives used in chippers. It should be stressed that they are subject to relatively fast wear as a result of the impact character of this type of machines. The condition of the knives' surface may affect the friction coefficient measurements.

The roughness was measured with a Jenoptik IMG Hommel Tester T1000 profilometer using a T1E sensor within a measuring range of 80 μm. The measuring distance was l_t = 4.8 mm and the elementary distance was l_c = 0.8 mm. Five measurements were taken at different places of the prepared plate. The recorded surface profiles are shown in Fig. 3. The collected results concerning: the highest roughness height R_{max}, the highest roughness height according to the measured 10 highest profiles R_z and the mean arithmetic deviation from the mean line R_a are shown in Tab. 2.

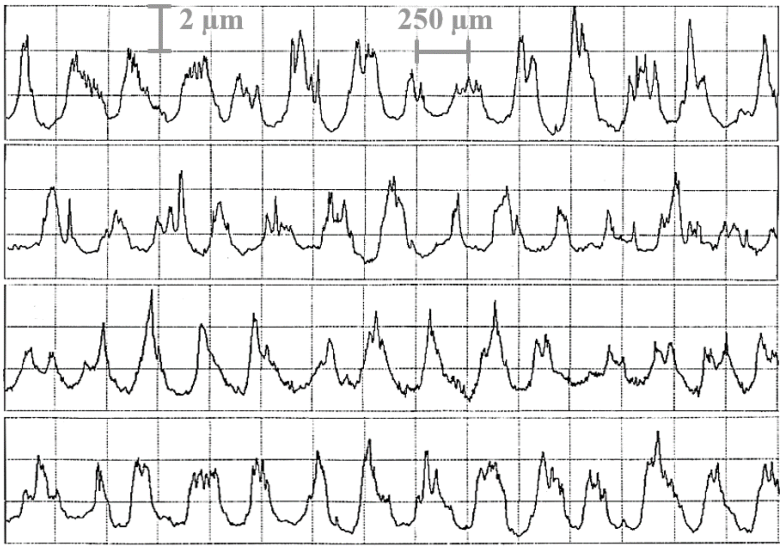

Fig. 3: Selected surface profile shapes of tested metal plates.

Tab. 2: Measured parameters related to the roughness of metal plates.

R_{max} [µm]	R_z [µm]	R_a [µm]
5.48	4.60	0.704
5.77	4.75	0.943
4.37	3.75	0.638
5.01	3.95	0.729
5.03	4.14	0.956

Kinetic friction tests

The research was carried out to determine the coefficient of friction between panels made of wood-based materials and the metal alloy which is used for the production of chipper knives. The determination of the kinetic coefficient of friction took place on a specially prepared station according to the scheme presented in Fig. 4. The tested sample (1) was fixed to the base. A rectangular element made of the used metal alloy (2), which was additionally loaded with mass (3), was placed on it. The total mass of the cuboidal block of the tested metal alloy and the weight was m = 39.5 kg. The hydraulic cylinder (5) was equipped with a force transducer (4), (C9C 1 kN by HBM) which registered this physical value F(t) cooperating with a measuring amplifier (Spider 8 by HBM) and a PC class computer. Hydraulic system cooperating with the actuator allowed to provide a constant value of the actuator's displacement velocity independent of the applied load. The force was applied to the element being moved axially in order to ensure its linear movement, despite this the position of $x(t)$ of the tested element was controlled during the experiment. The actuator's displacement velocity was v = 22 mm·s^{-1}. It was selected in such a way that for set load value, for the largest possible group of materials there was no stip-slick phenomenon.

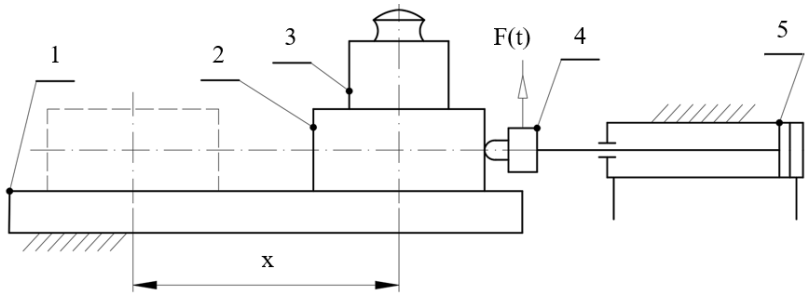

Fig. 4: Scheme of the system for determining the kinetic coefficient of friction; 1 - wood-based panel test sample, 2 - metal alloy test, 3 - mass, 4 - force transducer, 5 - hydraulic cylinder.

In the tests described, the force vs displacement can be presented as one of the three characteristic curve types, shown in Fig. 5. In the case shown in Fig. 5a, there is the stick-slip phenomenon, which is the effect of cyclic overpowering of the force causing the movement and the resistance force of this movement. In this case the maximum friction force F_s was determined from the first extreme of the recorded force. The average friction force F_k was calculated from the sum of the successive minimum and maximum extremes of the measured signal. In the case shown in Fig. 5b, the value of the maximum friction force was determined in a similar way. The average value of the friction force F_k was taken as the arithmetic mean from the measured signal of the friction force course. The sought value F_k for the case from Fig. 5c was determined in the same way, except that for this case it was impossible to define unambiguously the maximum friction force, because the point of occurrence F_s was not a local extreme of the recorded force course. The described test methodology was based on ASTM D2394: 2011.

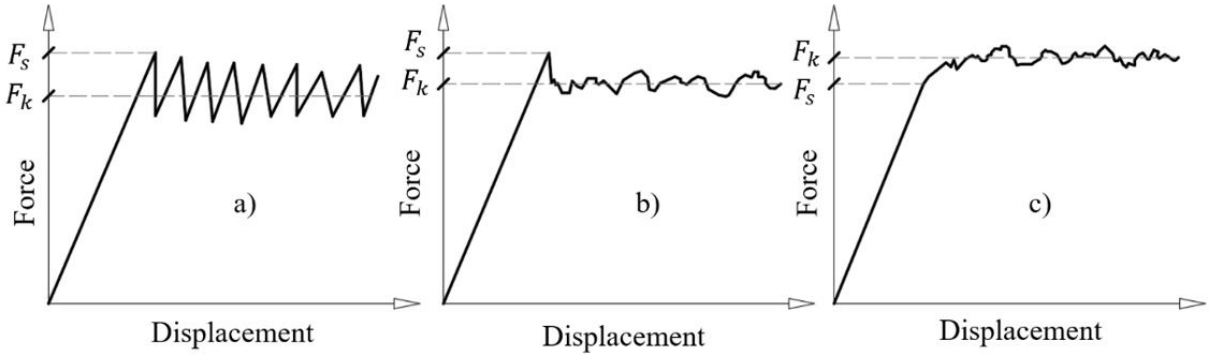

Fig. 5: Nature of the recorded force depending on the friction process; a) the occurrence of the stick-slip phenomenon, b) movement with a clear maximum force value, c) movement without a clear maximum force value.

Based on the determined values: F_s and F_k, static μ_s and kinetic μ_k coefficients of friction were calculated, according to Eqs. 2 and 3:

$$\mu_s = \frac{F_s}{N}, \tag{2}$$

$$\mu_k = \frac{F_k}{N}. \tag{3}$$

In order to analyse the values of these two coefficients, the values of their ratio R have also been determined in accordance with Eq. 4:

$$R = \frac{\mu_s}{\mu_k}. \quad (4)$$

For each of the 11 types of samples 10 experiments were carried out. The arithmetic mean of all measurements for each type of material was taken as the estimator of the static μ_s and kinetic μ_k coefficient of friction values sought. The standard deviation of the arithmetic mean was taken as the estimator error.

RESULTS

The results for a single measurement are shown in Fig. 6, while the selected range for the entire measurement series is shown in Fig. 7. The results of the determined values are shown in the Tab. 3, while their graphical interpretation is shown in Fig. 8.

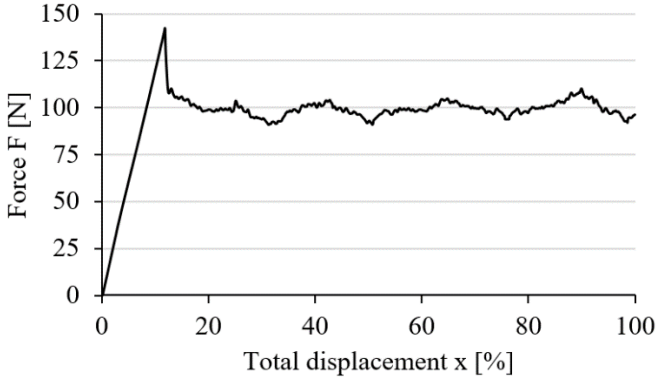

Fig. 6: Selected test result recorded for a single measurement; sample number 2 (MDF, laminated external surface).

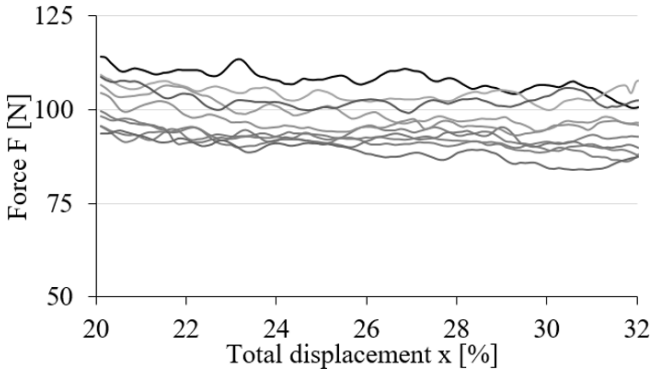

Fig. 7: Set of results of 10 measurement tests for a selected range of experiments (individual colours correspond to successive repetitions); sample number 1 (Wood-based panel, laminated external surface).

Tab. 3: Determined values of static μ_s and kinetic μ_k coefficient of friction and their relationship R; AVG – mean value, SD – standard deviation.

Sample No.	μ_s		μ_k		$R = \mu_k/\mu_s$
	AVG	SD	AVG	SD	
1	0.33	0.02	0.25	0.02	0.75
2	0.38	0.02	0.25	0.01	0.67
3	0.77	0.02	0.68	0.05	0.89
4	0.64	0.02	0.50	0.03	0.79
5	-	-	0.35	0.03	-
6	0.56	0.01	0.46	0.02	0.82
7	0.60	0.01	0.43	0.03	0.72
8	0.55	0.03	0.44	0.04	0.81
9	0.51	0.03	0.38	0.02	0.74
10	0.60	0.06	0.42	0.05	0.70
11	0.62	0.03	0.51	0.04	0.83

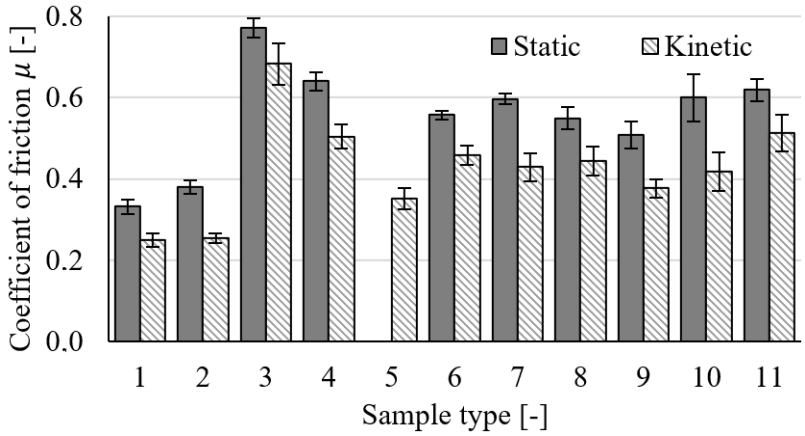

Fig. 8: Results of static μ_s and kinetic μ_k coefficient of friction for individual sample types; error bars are ± standard deviation.

DISCUSSION

The static μ_s and kinetic μ_k coefficient of friction values determined indicate that the former is always greater. Their ratio R is 0.77 on average, with the greatest value equal to 0.89 for sample number 3 and the smallest value equal to 0.67 for sample number 2.

Within MDF samples the lowest coefficients of friction (both static and kinetic) are for the laminated surface. Higher values were noted for the cut surface and the highest values for the non-laminated (side) surface. The increase in the static coefficient of friction μ_s from minimum to maximum for this type of material was 39% and for the kinetic coefficient of friction μ_k it was 51%.

The test results for chipboard are characterized by similar values of friction coefficients in the range of non-laminated surfaces (type 6-8 samples). The biggest difference (8%) in the static μ_s coefficient of friction was observed for samples 7 and 8, and the biggest difference in the kinetic μ_k coefficient of friction (6%) was observed when comparing the results for samples 6 and 7. Due to the nature of the process, it was not possible to determine the static μ_s coefficient of friction for sample number 5, while the kinetic μ_k coefficient of friction was 0.35 and was 18% lower than the next value for this type of material (samples type 5 and 7).

Interestingly, in the case of OSB, the surface created after mechanical cutting of the material had the lowest friction coefficient value. A higher value was recorded for the external surface in its nominal condition, and the highest value of the coefficient of friction was recorded for the internal surface (after removing the top of the material). The difference between the extreme values was 18% for the static coefficient of friction μ_s and 26% for the kinetic coefficient of friction μ_k (type 9 and 11 samples).

Test results for materials with a laminated surface (type 2 and 5 samples) compared to non-laminated surfaces (type 3 and 4 and 6-8 samples respectively) indicate lower values of both coefficients of friction. This is of course due to the different type of material and other parameters of the cooperating surfaces, which however has important implications for the cutting process. The laminate (lower coefficient of friction) may be located only in the small top part of the furniture board's cross-section, while the main part of it consists of a compressed wood-base material (higher coefficient of friction). Therefore, in addition to, for example, the geometry of the blade, the structure of the material itself is also a source of variation in the cutting force value during the process.

The recorded values of static μ_s and kinetic μ_k coefficient of friction and their ratio R can be compared, for example, to tests related to the determination of the coefficient of friction of spruce lumber, for different surface states resulting from the sample preparation method (Park et al. 2011). The range of determined values and in particular the values of the ratio R can be considered to be similar.

CONCLUSIONS

Within the framework of the described research works, the force necessary to displace 11 types of samples from wood-based materials and metal material used for the production of cutting elements for chippers with combustion engines was measured. The samples differed in the type of material and surface condition. Based on the measured force course, static μ_s and kinetic μ_k coefficient of friction and their ratio R were determined, which were subsequently analysed. The data collected will be used, among other things, to model the cutting force during the shredding process of wood-based furniture boards. This will be used to determine the demand for mechanical power of low-power drive systems of chippers with combustion engines, which will allow to propose new technical solutions in this aspect. The main conclusions resulting from the research work can be presented as follows: *(1)* For the accepted parameters of the experiment (movement speed v = 22 mm·s^{-1}, loading mass m = 39.5 kg), an irregular "stick-slip" movement occurred for sample number 10 (OSB external surface layer in nominal condition). *(2)* For the accepted parameters of the experiment (motion velocity v = 22 mm·s^{-1}, loading mass m = 39.5 kg) the recorded movements did not allow to define the maximum friction force, because the point of occurrence F_s (force value at the moment of static/kinetic transition) was not a local extremity of the recorded movements (case from Fig. 5c) for sample number 5 (laminated external porous chipboard). *(3)* The coefficient of friction between the machine knife and the material to be shredded is not constant. This is, among other things, due to: the heterogeneous structure of the material, the surface profile of the material before and

during the shredding process and its composite structure (different materials included in the furniture board and surface modifiers). *(4)* The differences in the value of the friction coefficient may vary from a dozen to several dozen percent. As a result, the demand for the drive torque for the chipper's working mechanism will change during the shredding process. This is important because the working section of this machine is anyway subjected to high dynamic loads of an impact character due to its nature of work.

REFERENCES

1. Aira, J.R., Arriaga, F., Íñiguez-González, G., Crespo, J., 2014: Static and kinetic friction coefficients of Scots pine (*Pinus sylvestris* L.), parallel and perpendicular to grain direction. Materiales de Construcción 64(315): e030, 9 pp.
2. Al-Samarai, R.A., Haftirman, K.R.A., Al-Douri, Y., 2012: The influence of roughness on the wear and friction coefficient under dry and lubricated sliding. International Journal of Engineering Science 3(4): 1-6.
3. ASTM D2394-052011: Standard methods for simulated service testing of wood and wood-base finish flooring.
4. Bejo, L., Lang, E.M., Fodor, T., 2000: Friction coefficients of wood-based structural composites. Forest products journal 50(3): 39-43.
5. Bhushan, B., 1999: Principles and application of tribology. Wiley, New York, 102 pp.
6. Blühdorn, I., 2017: Post-capitalism, post-growth, post-consumerism? Eco-political hopes beyond sustainability. Global Discourse 7(1): 42-61.
7. Chen, S., Li, S., Mu, J., Feng, Y., 2015: Influence of urea formaldehyde resin on the pyrolysis characteristics and gas evolution of waste MDF. Wood Research 60(1): 113-124.
8. Chuchała, D., Orłowski, K., 2018: Forecasting values of cutting power for the sawing process of impregnated pine wood on band sawing machine. Mechanik 2018(8-9): 766-768.
9. Czarnecka-Komorowska, D., Wiszumirska, K., 2020: Sustainability design of plastic packaging for the Circular Economy. Polimery 65(1): 8–17.
10. Czarnecka-Komorowska, D., Wiszumirska, K., Garbacz, T., 2018: Films LDPE/LLDPE made from post–consumer plastics: processing, structure, mechanical properties. Advances in Science and Technology Research Journal 12(3): 134-142.
11. Czerniak, J.M., Macko, M., Ewald, D., 2016: The CutMAG as a new hybrid method for multi-edge grinder design optimisation. Pp 327-337, Novel Developments in Uncertainty Representation and Processing. Springer, Cham.
12. Czarniak, P., Szymanowski, K., Kucharska, B., Krawczyńska, A., Sobiecki, J.R., Kubacki, J., Panjan, P., 2020: Modification of tools for wood based materials machining with TiAlN/a-CN coating. Materials Science and Engineering: B 257: 114540.
13. Djouadi, M.A., Nouveau, C., Beer, P., Lambertin, M., 2000: Cr_xN_y hard coatings deposited with PVD method on tools for wood machining. Surface and Coatings Technology 133: 478-483.

14. Durković, M., Mladenović, G., Tanović, L., Danon, G., 2018: Impact of feed rate, milling depth and tool rake angle in peripheral milling of oak wood on the cutting force. Maderas. Ciencia y tecnología 20(1): 25-34.
15. Dziewiatkowski, M., Szpica, D., Borawski, A., 2020: Evaluation of impact of combustion engine controller adaptation process on level of exhaust gas emissions in gasoline and compressed natural gas supply process. Pp 541-548, Engineering For Rural Development, Jelgava.
16. Džinčić, I., Skakić, D., 2012: Determining the parameters of wood machinability as a function of tangential cutting force during the process of machining wood by routing. Wood Research 57(1): 161-172.
17. Fan, Z., Meng, J., 2020: Classification and treatment of urban domestic garbage in China. In: IOP Conference Series: Earth and Environmental Science 514(3): 032001.
18. Gałęzia, T., 2013: Bilans energetyczny oraz czasochłonność wybranych elementów w łańcuchu technologicznym pozyskiwania biomasy leśnej (Energy balance and time-consumption of selected components in technological chain of forest biomass harvesting). Sylwan 157(6): 419-424.
19. Garrido, M.A., Conesa, J.A., Garcia, M.D., 2017: Characterization and production of fuel briquettes made from biomass and plastic wastes. Energies 10(7): 850.
20. Guerrini, L., Tirinnanzi, A., Guasconi, F., Fagarazzi, C., Baldi, F., Masella, P., Parenti, A., 2019: A Plackett-Burman design to optimize wood chipper settings. Croatian Journal of Forest Engineering 40(1): 81-87.
21. Guo, X., Li, R., Cao, P., Ekevad, M., Cristovao, L., Marklund, B., Grönlund, A., 2015: Effect of average chip thickness and cutting speed on cutting forces and surface roughness during peripheral up milling of wood f lour/polyvinyl chloride composite. Wood Research 60(1): 147-156.
22. Han, S.K., Han, H.S., Bisson, J.A., 2015: Effects of grate size on grinding productivity, fuel consumption, and particle size distribution. Forest Products Journal 65(5-6): 209–216.
23. Huber, C., Kroisleitner, H., Stampfer, K., 2017: Performance of a mobile star screen to improve woodchip quality of forest residues. Forests 8(5): 171.
24. Ibrahim, H.G., Ouiminga, S.K., Yonli, A., Sanogo, O., Daho, T., Koulidiati, J., 2018: Study of temperature fields and heavy metal content in the ash and flue gas produced by the combustion of briquettes coming from paper and cardboard waste. Recycling 3(3): 32.
25. Ihnát, V., Lübke, H., Balbercak, J., Kuňa, V., 2020: Size reduction down cycling of waste wood. Review. Wood Research 65(2): 205-220.
26. Ihnát, V., Lübke, H., Russ, A., Borůvka, V., 2017: Waste agglomerated wood materials as a secondary raw material for chipboards and fibreboards Part I. Preparation and characterization of wood chips in terms of their reuse. Wood Research 62(1): 45-56.
27. Ihnát, V., Lubke, H., Russ, A., Pazitny, A., Boruvka, V., 2018: Waste agglomerated wood materials as a secondary raw material for chipboards and fiberboards: Part II. Preparation and characterization of wood fibers in terms of their reuse. Wood Research 63(3): 431-442.

28. Kaczorowski, W., Batory, D., 2008: Carbon and titanium based layers for wood-based materials. Journal of Achievements in Materials and Manufacturing Engineering 27(2): 187-190.
29. Kaczorowski, W., Batory, D., Szamański, W., Niedzielski, P., 2012: Carbon-based layers for mechanical machining of wood-based materials. Wood science and technology 46(6): 1085-1096.
30. Kajda-Szcześniak, M., Jaworski, T.J., 2019: Analysis of the formation and primary minimization of nitrogen oxides during the combustion of nitrogen-rich post-consumer wood waste. Wood Research 64(4): 589-599.
31. Kajda-Szcześniak, M., Jaworski, T., 2018: Characteristics of the combustion process of woodwork waste in the installation of thermal treatment of municipal solid waste (TPOK). Wood Research 63(1): 15-23.
32. Kanafojski, C., Karwowski, T., 1976: Crop-harvesting machines, in agricultural Machines, Theory and Construction, vol. II, Published for the U.S. Department of Agriculture and the National Science Foundation, Washington, D.C., by the Foreign Scientific Publications Department of the National Centre for Scientific, Technical and Economic Information Warsaw. Pp 55-58, Chapter 2.
33. Kazlauskas, D., Jankauskas, V., Tučkutė, S., 2020: Research on tribological characteristics of hard metal WC-Co tools with TiAlN and CrN PVD coatings for processing solid oak wood. Coatings 10(7): 632.
34. Knitter, M., Czarnecka-Komorowska. D., Czaja-Jagielska, N., Szymanowska-Powalowska, D., 2019: Manufacturing and properties of biodegradable composites based on thermoplastic starch/polyethylene-vinyl alcohol and silver particles. In: Advances in Manufacturing II. Vol. 4 : Mechanical Engineering (ed. Gapinski, B., Szostak, M., Ivanov, V.). Pp 610-624, Springer-Verlag, Berlin.
35. Kopecký, Z., Hlásková, L., Orlowski, K.A., 2014: An innovative approach to prediction energetic effects of wood cutting process with circular-saw blades. Wood Research 59(5): 827-834.
36. Kopecký, Z., Hlásková L., Solař, A., Nesázal P., 2019: Cutting forces quasi-orthogonal CNC milling. Wood Research 64(5): 879-890.
37. Kosakowski, W., Bryszewska, M.A., Dziugan, P., 2020: Biochars from post-production biomass and waste from wood management: Analysis of carbonization products. Materials 13(21): 4971.
38. Krauss, A., Piernik, M., Pinkowski, G., 2016: Cutting power during milling of thermally modified pine wood. Drvna Industrija 67(3): 215-222.
39. Kuvik, T., Krilek, J., Kovác, J., Štefánek, M., Dvorak, J., 2017: Impact of the selected factors on the cutting force when using a chainsaw. Wood Research 62(5): 807-814.
40. Laitila, J., Routa, J., 2015: Performance of a small and medium sized professional chippers and the impact of storagetime on Scots pine (*Pinus sylvestris*) stem wood chips characteristics. Silva Fennica 49(5): 1382.
41. Li, L., Gong, M., Li, D., 2013: Evaluation of the kinetic friction performance of modified wood decking products. Construction and Building Materials 40: 863-868.

42. Li, W.G., Zhang, Z.K., 2019: The effect of micro-pits texture on the coefficient of friction between wood and cemented carbide under different wood moisture content. Wood Research 64(4): 731-742.
43. Macko, M., Mrozinski, A., 2019: Work parameters research of wood pellet machine. In: AIP Conference Proceedings 2077(1): 020038, 8 pp.
44. Macko, M., Mrozinski, A., 2018: Computer aided design of wood pellet machines. Pp 454-461, International Conference on Computer Aided Engineering, Springer.
45. Macko, M., Tyszczuk, K., Śmigielski, G., Flizikowski, J., Mroziński, A., 2018a: The use of CAD applications in the design of shredders for polymers. In: MATEC Web of Conferences 157: 02027.
46. Macko, M., Tyszczuk, K., Śmigielski, G., Mroziński, A., 2018b: Utility of an unitary-shredding method to evaluate the conditions and selection of constructional features during grinding. In: MATEC Web of Conferences 157: 05016, 46 pp.
47. Mandić, M.D., Porankiewicz, B., Danon, G.J., 2015: An attempt at modelling of cutting forces in oak peripheral milling. BioResources 10(3): 5489-5502.
48. Meine, K., Schneider, T., Spaltmann, D., Santner, E., 2002: The influence of roughness on friction: Part I: The influence of a single step. Wear 253(7-8): 725-732.
49. Orłowski, K., Ochrymiuk, T., 2017: A newly-developed model for predicting cutting power during wood sawing with circular saw blades. Maderas. Ciencia y tecnología 19(2): 149-162.
50. Orlowski, K.A., Ochrymiuk, T., Atkins, A., Chuchala, D., 2013: Application of fracture mechanics for energetic effects predictions while wood sawing. Wood Science and Technology 47(5): 949-963.
51. Park, C.Y., Kim, C.K., Kim, H.K., Lee, J.J., 2011: Evaluation of friction properties according to normal force and direction of wood grain in real contact area. Mokchae Konghak 39(5): 437-443
52. Pinkowski, G., Krauss, A., Sydor, M. 2016: The effect of spiral grain on energy requirement of plane milling of Scots pine (*Pinus sylvestris* L.) wood. BioResources 11(4): 9302-9310.
53. Porankiewicz, B., Axelsson, B., Grönlund, A.A., Marklund, B., 2011: Main and normal cutting forces by machining wood of *Pinus sylvestris*. BioResources 6(4): 3687-3713.
54. Rabajczyk, A., Zielecka, M., Małozięć, D., 2020: Hazards resulting from the burning wood impregnated with selected chemical compounds. Applied Science 10(17): 6093.
55. Reczulski, M., 2018: Optimization of the clearance angle in industrial disc chipper. Wood Research 63(2): 295-304.
56. Reczulski, M., 2016: The system wood chipping in disc chipper-problems of uniformity of chips length. Wood Research 61(3): 433-442.
57. Reczulski, M., 2015: Analysis of the construction and operation of system wood chipping and transfer chips. Wood Research 60(4): 671-678.
58. Saosee, P., Sajjakulnukit, B., Gheewala, S.H. 2020: Feedstock security analysis for wood pellet production in Thailand. Energies 13(19): 5126.
59. Sedlaček, M., Podgornik, B., Vižintin, J., 2009: Influence of surface preparation on roughness parameters, friction and wear. Wear 266(3-4): 482-487.

60. Sheth, P.N., Babu, B.V., 2010: Production of hydrogen energy through biomass (waste wood) gasification. International journal of hydrogen energy 35(19): 10803-10810.
61. Seki, M., Sugimoto, H., Miki, T., Kanayama, K., Furuta, Y., 2013: Wood friction characteristics during exposure to high pressure: influence of wood/metal tool surface finishing conditions. Journal of wood science 59(1): 10-16.
62. Souza, A.M., Nascimento, M.F., Almeida, D.H., Silva, D.A.L., Almeida, T.H., Christoforo, A.L., Lahr, F.A., 2018: Wood-based composite made of wood waste and epoxy based ink-waste as adhesive: A cleaner production alternative. Journal of Cleaner Production 193: 549-562.
63. Spinelli, R., Magagnotti, N., 2013: Performance of a small-scale chipper for professional rural contractors. Forest Science and Practice 15(3): 206–213.
64. Spîrchez, C., Lunguleasa, A., Gaceu, L., 2019: Researches on grape husk waste obtained from the winery and its use as pellets for combustion. Wood Research 64(3): 549-556.
65. Stasiak, M., Molenda, M., Bańda, M., Horabik, J., Wiącek, J., Parafiniuk, P., Wajs, J., Gancarz, M., Gondek, E., Lisowski, A., Oniszczuk, T., 2020: Friction and shear properties of pine biomass and pellets. Materials 13: 3567.
66. Szpica, D., 2018: Validation of indirect methods used in the operational assessment of LPG vapor phase pulse injectors. Measurement 118: 253-261.
67. Waluś, K.J., Warguła, Ł., Krawiec, P., Adamiec, J.M., 2018: Legal regulations of restrictions of air pollution made by non-road mobile machinery - the case study for Europe: a review. Environmental Science and Pollution Research 25(4): 3243-3259.
68. Warguła, Ł, Krawiec, P. 2020: The research on the characteristic of the cutting force while chipping of the Caucasian Fir (*Abies nordmanniana*) with a single-shaft wood chipper. IOP Conference Series: Materials Science and Engineering 776: 012012.
69. Warguła, Ł., Krawiec, P., Waluś, K.J., Kukla, M., 2020a: Fuel consumption test results for a self-adaptive, maintenance-free wood chipper drive control system. Applied Science 10(8): 2727.
70. Warguła, Ł., Kukla, M., 2020: Determination of maximum torque during carpentry waste comminution. Wood Research 65(5): 771-784.
71. Warguła, Ł., Kukla, M., Krawiec, P., Wieczorek, B., 2020b: Impact of number of operators and distance to branch piles on wood chipper operation. Forests 11: 598.
72. Warguła, Ł., Kukla, M., Krawiec, P., Wieczorek, B., 2020c: Reduction in operating costs and environmental impact consisting in the modernization of the low-power cylindrical wood chipper power unit by using alternative fuel. Energies 13(11): 2995.
73. Warguła, Ł., Kukla, M., Lijewski, P., Dobrzyński, M., Markiewicz, F., 2020d: Influence of innovative wood chipper speed control systems on exhaust gas emissions and fuel consumption in urban areas. Energies 13: 3330.
74. Warguła, Ł., Kukla, M., Lijewski, P., Dobrzyński, M., Markiewicz, F., 2020e: Influence of the use of liquefied petroleum gas (LPG) systems in wood chippers powered by small engines on exhaust emissions and operating costs. Energies 13(21): 5773.

75. Warguła, Ł., Kukla, M., Lijewski, P., Dobrzyński, M., Markiewicz, F., 2020f: Impact of compressed natural gas (CNG) fuel systems in small engine wood chippers on exhaust emissions and fuel consumption. Energies: 13: 6709.
76. Warguła, Ł., Waluś, J.K., Krawiec, P., 2019: Warunki pracy mobilnych maszyn rozdrabniających drewno w aspekcie innowacyjnych systemów sterowania napędem (Determination of working conditions of mobile chipping wood machines in the aspect of innovative drive control systems). Sylwan 163(9): 765–772.
77. Xu, M., Li, L., Wang, M., Luo, B., 2014: Effects of surface roughness and wood grain on the friction coefficient of wooden materials for wood–wood frictional pair. Tribology Transactions 57(5): 871-878.
78. Zaharia, I., Zaharia, C., 2015: The growth of environmentally sustainable consumerism. Economics, Management and Financial Markets 10(2): 115-120.
79. Zhang, Y., Kusch-Brandt, S., Gu, S., Heaven, S., 2019: Particle size distribution in municipal solid waste pre-treated for bio processing. Resources 8(4): 166.
80. Yu, S.T., Yang, C.M., Ren, C.Q., Luo, G., 2012: Cutting force analysis of large branch crusher based on the finite element. Applied Mechanics and Materials 152: 900-905.

MATEUSZ KUKLA*, ŁUKASZ WARGUŁA, ALEKSANDRA BISZCZANIK
POZNAN UNIVERSITY OF TECHNOLOGY
FACULTY OF MECHANICAL ENGINEERING
INSTITUTE OF MACHINE DESIGN
POZNAŃ
POLAND
* Corresponding author: mateusz.kukla@put.poznan.pl

WOOD RESEARCH doi.org/10.37763/wr.1336-4561/66.5.806820
e-ISSN 2729-8906
66(5): 2021 806-820 pp.

MODELLING OF STEEL-TIMBER COMPOSITE BEAMS: VALIDATION OF FINITE ELEMENT MODEL AND PARAMETRIC STUDY

RUYUAN YANG[1], JIA WAN[2], XIAOFENG ZHANG[3], YOUFU SUN[3]

[1]NANJING TECH UNIVERSITY, CHINA
[2]TAIYUAN UNIVERSITY OF TECHNOLOGY, CHINA
[3]NANJING FORESTRY UNIVERSITY, CHINA

(RECEIVED DECEMBER 2020)

ABSTRACT

In this paper, non-linear finite elements models (FEM) of steel-timber composite (STC) beams have been developed and analyzed using ABAQUS software. In the FEM, the loading conditions of STC beams were simulated, and the nonlinear behaviour of the contact interface between the steel and timber components were incorporated adequately into the FEM. For the yield load, the maximum error between the FE results and the experimental results is 14.85%. The maximum average error of the yield deflection is 12.94%. and of the ultimate load is 16.79%. However, the error of key points was less than 17% (within a reasonable range), which proves that the established finite element model, selected material parameters and contact element model can better simulate the bending performance of STC beams. Finally, a parametric study was carried out by using the verified FEM. It is shown that the FEM developed in this study can replicate adequately the load-deflection response, and the development of stress and plasticity of the bending experiment. Through the parameter study, it can be seen that the distribution density and mechanical properties of the connection between the glulam and H-section steel can affect the mechanical behavior of the whole STC beams.

KEYWORDS: Finite element model (FEM), steel-timber composite, load-deflection response, non-linearity, parametric study.

INTRODUCTION

In order to expand the application of timber structure, in recent years, numerous research projects have been conducted and are currently ongoing to find ways for its wider application in construction through "engineering" of the basic material (Li et al. 2017, 2020). Moreover, timber is also combined with other materials to improve its bearing capacity, such as timber-concrete

composite (TCC) (Schänzlin and Fragiacomo 2017, Daňková et al. 2019, Naud et al. 2019) and other mechanically jointed structures (Yeoh et al. 2011, Khorsandnia et al. 2012, Deam et al. 2008). These composite materials exploit beneficial effects of different materials in different orientations and work as efficient building components in various types of applications. Many researchers reported wide range of numerical analysis and experimental research on the structural performance both short-term and long-term performance of composite materials during the past decades (Fojtik et al. 2020, Yang et al. 2020, Pulngern et al. 2020). Connection and construction methods of composite structure have also been reported by various researchers (Jorge et al. 2011, Leborgne and Gutkowski 2010). In western countries, composite structure has been widely used for its excellent structural performance.

Although there have been a lot of experimental and theoretical studies on the structural performance of composite members with TCC, application on steel-timber composite structure (STC) has not been thoroughly explored in the past. Steel structure offers high strength with a number of beneficial properties but thin-walled steel sections are vulnerable to instability due to buckling. The combination of H-Section steel and glulam by shear connectors can exploit the compressive resistance of timber and can prevent premature failure of the H-section due to torsion and buckling when used as girders. In comparison to bare steel members, STC members have improved stability and bearing capacity, high degree of assembly and low cost of construction and maintenance, which eventually have a relatively positive impact on the environment.

The finite element (FE) numerical simulation is the supplement and extension of the structural experiment. Xu et al. (2015) studied the mechanical performance of steel beam-glulam column composite members through cyclic test and nonlinear finite element (FE) simulations. Liu et al. (2016) developed a three-dimensional (3D) FEM to investigate the structural behaviour of steel-concrete composite beams with Ultra-High Performance Fiber Reinforced Concrete (HSFGB) shear connectors, the accuracy and reliability of the proposed finite element model are validated by comparing their results with available experimental results. Hassanieh et al. (2016, 2017, 2018) investigated the mechanical behaviour of STC connections and beams using a 3D continuum-based FEM, then FEM were validated by experimental tests. It was shown that the FEM can replicate adequately the mechanical behaviour of STC structures tested. Nouri et al. (2019) carried out experimental study on steel-timber composite (STC) beam-to-column connections with double web angles, and nonlinear 3D continuum-based FE simulations were employed to investigate the structural behaviour of this connection.

In current study, the commercial FEM software ABAQUS was used to establish and analyze the 3D FEM of the STC beams, simulate the loading conditions, adopt the reasonable material model and constitutive laws, and simulate the connection mode of H-section steel and glulam. The accuracy and reliability of the proposed FE model were validated by comparing their results with available experimental results. Finally, a parametric study was presented to the flexural behavior of STC beams, and the effects of different types and spacing of shear connectors on the yield load, yield deflection and ultimate bearing capacity of STC beams were considered.

MATERIAL AND METHODS

Outline of four-point bending tests

Fig. 1 shows the sectional dimensions and processing diagram of the STC beam used to verify the FEM. Timber specimen used in the current study was *Larix gmelinii* with lumber dimensions of 3000 × 200 × 40 mm (length × width × height) as the raw material, with a moisture content of 9-12% after drying.

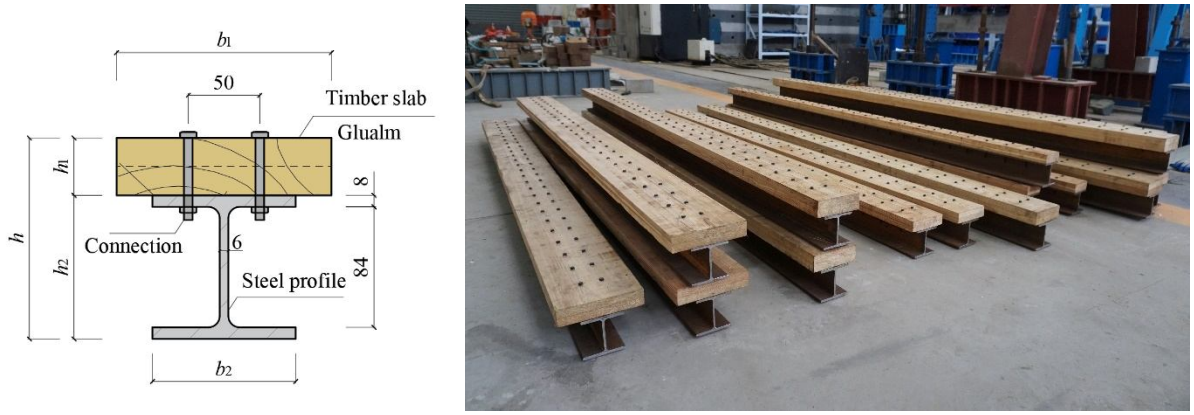

(a) (b)

Fig. 1: Configuration of specimens used in test (all dimensions are in mm): (a) sectional dimensions, (b) perspective view.

Material test was conducted on the raw material following ASTM D143-14: 2014 and basic material properties are shown in Tab. 1. In reference to ANSI A190.1: 2012, glulam slabs consisting of two layers were prepared. Phenol-resorcinol- formaldehyde resin adhesive was used, with a single-side spreading rate of 300 g·m^{-2}, gluing pressure of 1 MPa, lamination time of 3 hours, and curing time of 6 hours. Tests were commenced 7 days after curing.

Tab.1: Basic properties of Larix gmelinii.

Stress direction	f_u (MPa)	μ_{LT}	E (GPa)
Parallel-to-grain compression	50.62	0.3263	13.716
Parallel-to-grain tensile	117.10	0.3214	14.014
Parallel-to-grain shear	9.50	-	-

Note: f_u - ultimate strength (MPa); μ_{LT} - Poisson's ratio of material; and E - elastic modulus (GPa).

Steel profile used in the current research was a hot-rolled steel H-section, which meets relevant standards of GB 50017: 2017 and GB/T50011: 2016 (HW100 × 100 of grade Q235). The thickness of the flange is 8 mm, and that of the web is 6 mm. Laser pilot holes were drilled at relevant positions of the H-section flange and timber, and H-section and glulam holes were accurately aligned (opening diameter 7 mm). The spacing between holes along the span direction was 100 mm, and in transverse direction the spacing was 50 mm. Material test was conducted following ASTM A370-16 (ASTM A370 2016) and basic material properties are shown in Tab. 2.

Tab. 2: Mechanical properties of H steel beam.

f_y (MPa)	f_t (MPa)	f_t/f_y	**Poisson ratio**	E (GPa)
345.79	457.39	1.32	0.29	197.056

Note: f_{yb} - characteristic yield strength of the connector (MPa); and f_{em} - characteristic embedment strength of the *Larix gmelinii* (MPa).

Shear connectors used in the current study of high-strength bolts with a diameter of 6 mm and a grade of 6.8. Material tests confirmed their bending yield strength as 425.4 MPa. The bolts were arranged in double rows with spacing of 100 mm (along the span direction). A 10 × 10 mm washer was used to prevent crushing of the timber, and the bolts were tightened by a torque wrench to provide a post-tensioning force of $0.1f_{uf}$, with f_{uf} being the tensile strength of grade 6.8 bolts.

A total of 18 beam specimens were tested in 6 groups as part of the current study. The total length and span of the specimens were 2700 mm and 2520 mm respectively. The cross-section dimensions of glulam slabs in STC beams were 30 × 150 mm, 40 × 150 mm, 50 × 150 mm, 60 × 150 mm, 40 × 100 mm, 40 × 200 mm respectively. It is worth noting that the size of the H Section and the number of shear connectors were the same in all considered specimens. One of the primary objectives of the current study was to investigate the influence of the thickness and width of glulam slabs on the flexural performance of STC beam. Tab. 3 shows the key parameters of specimens of various groups. The variation of mechanical properties and manufacturing methods of glulam will significantly affect the structural properties of STC beams. Therefore, 3 identical specimens were made and tested for each group of STC beams to ensure the accuracy and repeatability of the test results.

Tab. 3: Key parameters of specimens categorized in 6 groups in the current study.

Group N°.	h_1 (mm)	b_1 (mm)	s (mm)	l (mm)	L (mm)	$b \times h$ (mm)
Group A	30	150	100	2520	2700	150×130
Group B	40	150	100	2520	2700	150×140
Group C	50	150	100	2520	2700	150×150
Group D	60	150	100	2520	2700	150×160
Group E	40	100	100	2520	2700	100×140
Group F	40	200	100	2520	2700	200×140

Note: h_1 - thickness of glulam slabs (mm); b_1 - width of glulam slabs (mm); s - spacing of bolts along the span direction (mm); l - span of STC beams (mm); L - length of STC beams (mm); b - width of STC beams (mm); h - height of STC beams (mm)

The test was carried out in accordance with ASTM D198-15 (ASTM D198: 2015). A distribution beam was used to apply symmetrical loads at two sections 420 mm away from the center line of the specimens. Two loading points were equidistant from the support, which was 1/3 of the span of the beams. Supports were placed at each loading point to avoid stress concentration at the loading point and to prevent local crushing of the timber. All testing arrangements are shown in Fig. 2. In order to measure the settlement of the two ends of the beam and to record the deflection at mid-span, two thimble displacement sensors (model: YHD-25, China) were installed at both ends of the supports, designated as LVDT 1 and

LVDT3. One laser displacement sensor (model: KEYENCE IL-300, Japan) was installed under the mid-span of the beams, designated as LVDT 2.

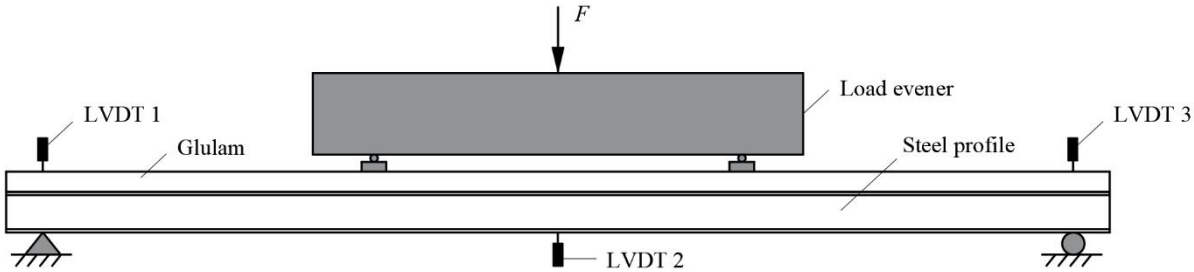

Fig. 2: Set up used for testing STC beams.

Tests were conducted using a microcomputer-controlled electro-hydraulic servo universal testing machine with a capacity of 300 kN and a TDS-530 data acquisition system. The loading regime adopted in the test conforms to ASTM D198-15; the load was applied at a constant rate of 5 $mm \cdot min^{-1}$ until 90% of the ultimate load was reached or some type of damage became obvious.

Finite element model (FEM)

FEM analysis

The FEM of STC beams were established in ABAQUS. Based on the elastoplastic of steel profile and glulam, and the nonlinearity of bolt connection, the numerical simulatio of a four-point bending test was carried out. The STC beam has two symmetrical planes in the four-point bending test. If the out of plane deformation of the steel beam after large deformation was not included (Chybiński and Polus 2019), the model can be treated as a symmetrical model. To reduce the calculation cost, the FEM is 1/4 of the experimental object. In the figure, the red steel plate is the loading steel plate and the support steel plate, the gray part is the glulam beam, the green part is the H-section steel, and the nonlinear element of the simulated bolt connection is located between the glulam and the H-section steel.

The steel profile was simulated by the S4R element, and the shell had 5 integral points along the thickness direction; the glulam was simulated by the C3D8R element. Fig. 3 shows the FE mesh, the element size of the steel profile and glulam was 10 mm, and the mesh size of the loading plate and support plate was larger than that of the steel profile and glulam, which was 25 mm. The vertical interaction between the top surface of the steel profile and the bottom surface of the glulam was simulated by "hard contact", and the tangential action was simulated to Coulomb friction model. The friction coefficient between the steel profile and glulam was set as 0.4. The bolt connection between the steel profile and glulam was simulated by the "connector" in ABAQUS. The nonlinear parameters of the connector were determined by the push-out experimental curves (Yang et al. 2020), and the axial parameters were determined by the axial stiffness of the bolt. The vertical displacement was directly applied on the loading plate to simulate the loading process of bending experiment.

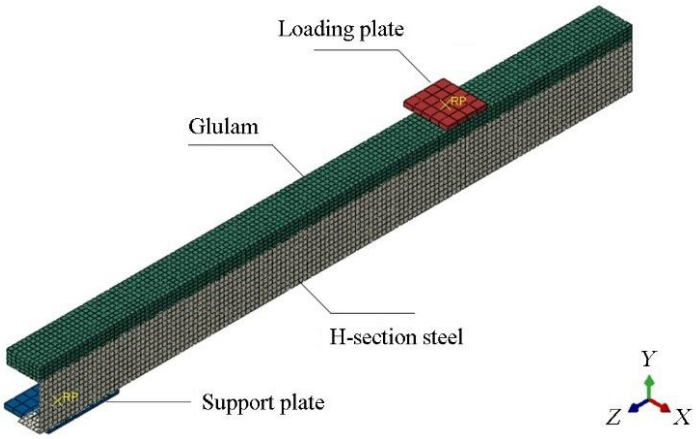

Fig. 3: Mesh grid of FEM.

Constitutive laws of materials

The properties of timber in the FEM were determined by the basic material properties tests. In the bending test of STC beams, the stress characteristics of the upper glulam were mainly the compression along the grain. The timber has better plastic deformation ability under the compression along grain, and the tensile along the grain is brittle failure. For the flexural timber member, because its compression area still has the bearing capacity after exceeding the compression strength, its failure should be limited by its tensile area reaching the tensile strength. In the FE simulation, the ideal elastic-plastic model was used to characterize the compression yield along grain, as shown in Fig. 4. The material properties of steel profile were from the tensile test of the same batch of steel plates. In the FE numerical simulation, the constitutive model of the steel profile was selected as the isotropic trilinear model, as shown in Fig. 5.

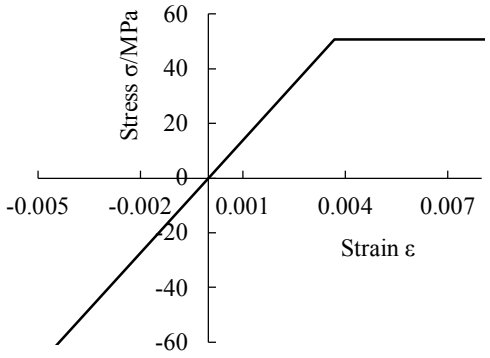

Fig. 4: Elastic-plastic model of timber.

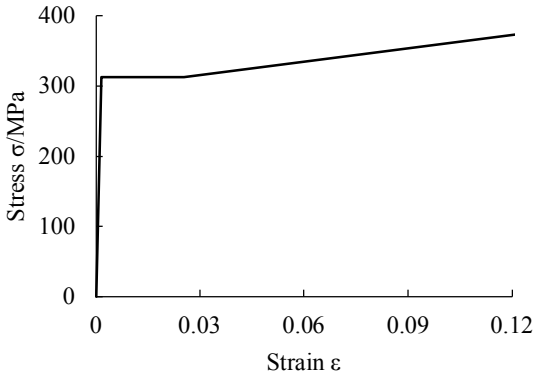

Fig. 5: Trilinear model of steel profile.

Simulation of bolt connection between steel and timber

The H-section steel and glulam in the four-point bending experiment of composite beams were connected by bolts with a diameter of 6 mm. In the FEM, "connector" was used to simulate the tangential and normal mechanical behaviors of bolted connections. The non-linear behavior of the tangent direction of the connector, i.e. the length direction of the STC beam, was determined by the corresponding push-out curves of the glulam with different thickness.

The axial stiffness of the connector was obtained from the conversion of the axial stiffness of the bolt. The position of the connector corresponds to the position of the bolt in the experiment. At the same time, in order to evaluate the influence of the connection between H-section steel and glulam on the mechanical behavior of composite beams, the FEM group of rigid connection was added to compare with the experimental group.

Boundary conditions and loading procedure

The FEM was 1/4 symmetrical for *X* plane and *Z* plane. The symmetrical boundary conditions of *Y*-*Z* plane and *X*-*Y* plane were applied to the symmetrical plane of the *X* plane and *Z* plane respectively. The lower part of the H-section steel was directly placed on the supporting steel plate, and the loading plate of the model was directly placed on the corresponding position of the top surface of the glulam. The contact behavior of loading plate, supporting plate and STC beam was simulated by hard contact, and the tangential behavior was simulated by penalty function. The friction coefficient between the support plate and the lower end of the H-section steel was 0.2, and that between the loading plate and the top of the glulam was 0.4.

The supporting steel plate constrained the translation in the *X* and *Y* directions, released the translation in the *Z* direction, constrained the rotation in the *Y* and *Z* directions, and released the rotation in the *X* direction. The loading steel plate constrained the translation in the *X* direction, and the rotation in the *Y* and *Z* directions, and released the rotation in the *X* direction. The displacement was applied to the loading plate in the *Y* direction (Fig. 6), and was gradually applied to 200 mm in steps of 1 mm.

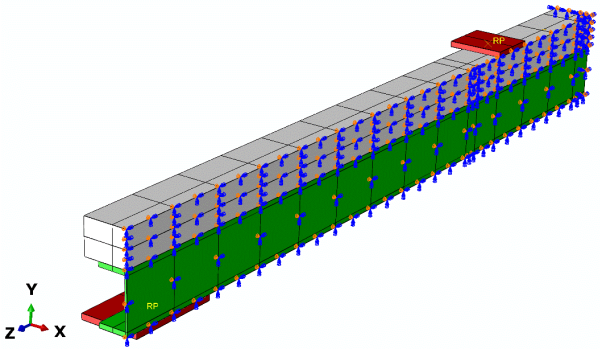

Fig. 6: Boundary condition of FEM.

Validation of FEM

The four-point bending test is a static test, so the solver was selected as the "Static General" in "Standard" during the analysis, regardless of the influence of inertial force. There were 10 groups of FEM. Tab. 4 shows the variable parameter information in each group of models. FE-A to FE-F were the FEM corresponding to the experimental groups; FE-C-150 and FE-C-200 were the FEM with FE-C as the basic model, and bolt spacing changed into 150 mm and 200 mm; FE-SDS was the FEM with self-drilling screw (SDS) as the shear connector; FE-C-Rigid was the rigid connection FEM.

Tab. 4: Summary of FEM information.

Group N°.	h_1 (mm)	b_1 (mm)	Connector type	d (mm)	a_1 (mm)

FE-A	30	150	Bolt	6	100
FE-B	40	150	Bolt	6	100
FE-C	50	150	Bolt	6	100
FE-D	60	150	Bolt	6	100
FE-E	40	100	Bolt	6	100
FE-F	40	200	Bolt	6	100
FE-C-150	50	150	Bolt	6	150
FE-C-200	50	150	Bolt	6	200
FE-SDS	50	150	SDS	5.5	100
FE-C-Rigid	50	150	Rigid connection	-	100

Note: d - nominal diameter of the connector (mm); a_1 - parallel-to-grain connector spacing (mm).

RESULTS AND DISCUSSION

Load-deflection response

Fig. 7 shows the comparison between the FE calculation results of STC beam and the experimental results. Except for the large out of plane deformation in the FE-E, there is deviation between the FE curve and the experimental curves. The change trend of the load-deflection curves of the other FEM is in good agreement with that of the corresponding experimental group. It can be observed that with the increase of the thickness and width of the glulam slab, the difference between the FE group and the experimental group decreases gradually. In the FE-D group, the thickness of glulam slab is the largest, and the difference between the FEM and the experimental results is the smallest, which almost coincides with each other. It is shown that increasing the thickness and width of glulam slab can improve the lateral stiffness of STC beam. Hassanieh et al. (2017) investigated the short-term structural behaviour of STC beams, and they reported the same conclusion. The FEM, selected material parameters and spring element model established in this paper can simulate the bending performance of STC composite beam well. Because the internal defects of the material were not considered in the FEM, the initial stiffness and yield stiffness of the FE curves are slightly higher than the experimental curves. The loading displacement of the FEM is up to 200 mm, while the end displacement of the experimental curves is in the range of 100-150 mm.

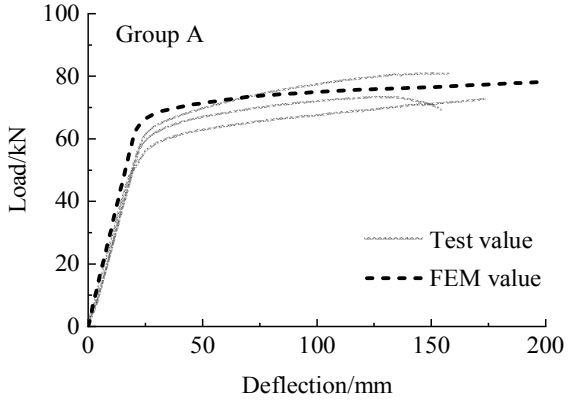

(a) Group A

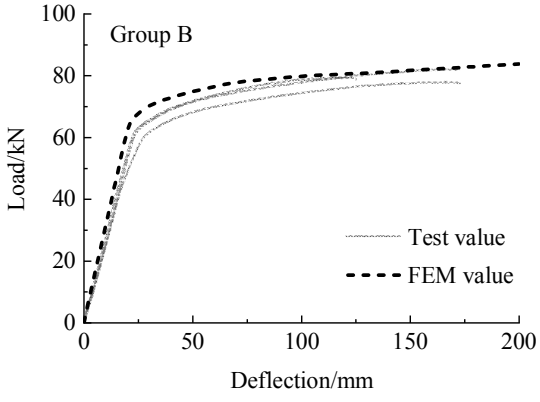

(b) Group B

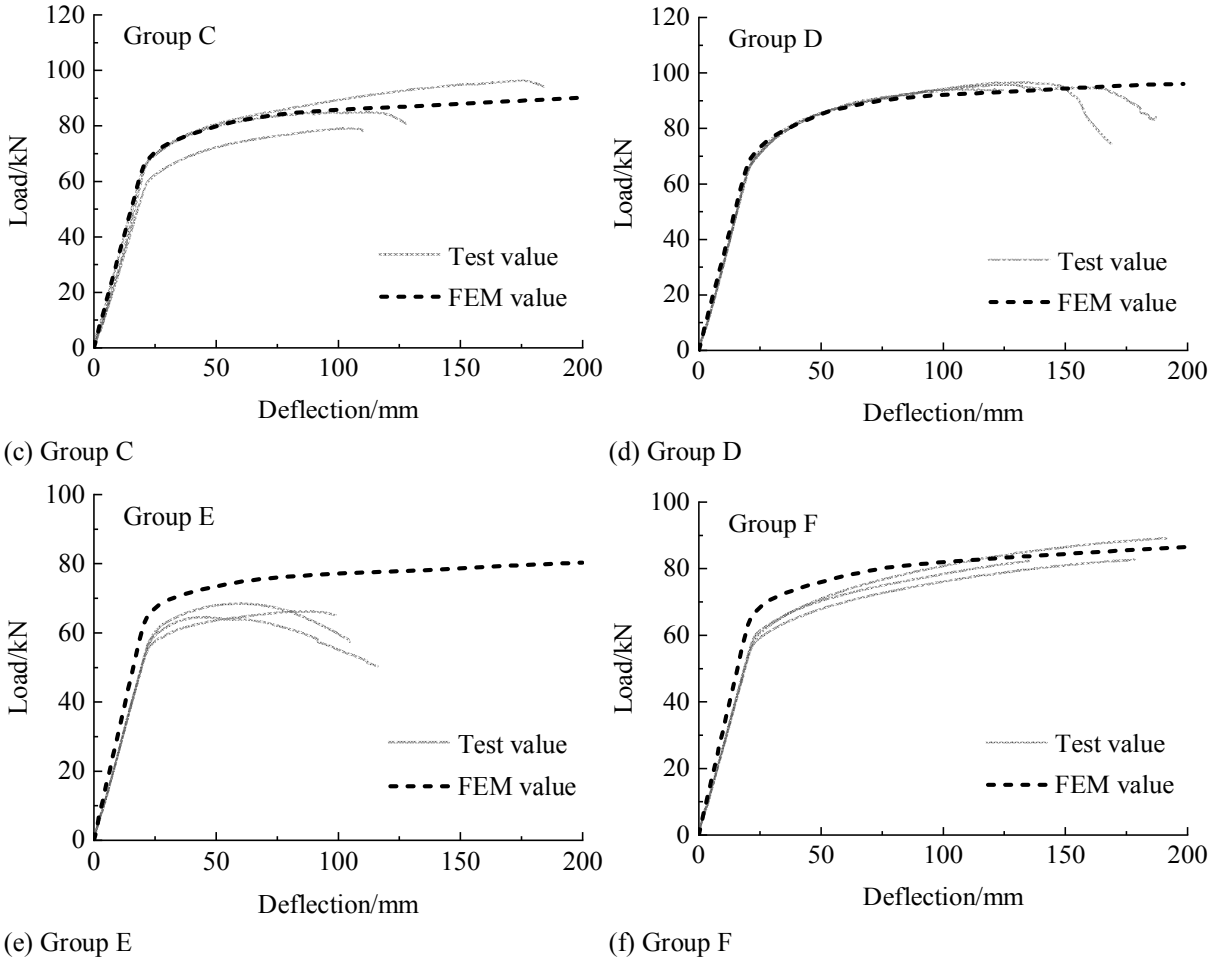

Fig. 7: Comparison between the load-deflection curves of finite element and the experimental.

Tab. 5 shows the comparison between the key points of load-deflection curves of FE-A to FE-D, and the key points of experimental curves. For the yield load, the maximum error between the FE results and the experimental results is 14.85%. The maximum average error of the yield deflection is 12.94%. and of the ultimate load is 16.79%. There are three main reasons for the errors: *(1)* In the FE analysis, 1/4 symmetrical model was selected, the out of plane deformation of STC beams cannot be simulated; *(2)* The defects of the H-section steel and the glulam, the sliding between the loading device and the support at the initial stage of loading were not considered. Therefore, the load-deflection curves of the FEM were generally higher than the experimental curves at the initial stage of loading, and there was no initial sliding phenomenon of the curves. At the later stage of loading, H-section steel and glulam were in the local plastic strengthening stage, and the timber constitutive model used in the FEM cannot accurately simulate the stiffness loss and the complex stress state under the anisotropic condition after the timber enters the strengthening stage; *(3)* At the same time, the nonlinear curves of the bolt connection were different from the load-slip response obtained by the push-out test after the local plastic strengthening stage. Therefore, the ductility and strength of the FEM in the case of large displacement were higher than those of the experimental groups. However, the error of key points was less than 17% (within a reasonable range), which proves that the established finite

element model, selected material parameters and contact element model can better simulate the bending performance of STC beams.

Tab.5: Key points of FEM and test results.

Group	Yield load (kN)		Error (%)	Yield deflection (mm)		Error (%)	Ultimate load (kN)		Error (%)
	Test value	FEM value		Test value	FEM value		Test value	FEM value	
A	56.46	64.84	14.84	21.54	21.03	-2.38	72.85	75.16	3.17
B	58.55	66.72	13.95	22.38	21.24	-5.09	77.81	80.09	2.93
C	65.30	69.84	6.95	21.54	21.29	-1.15	86.61	86.14	-0.54
D	66.61	73.99	11.08	20.30	22.93	12.94	93.92	92.76	-1.24
E	59.68	65.98	10.56	23.49	21.24	-9.59	66.23	77.35	16.79
F	58.71	67.43	14.85	22.37	21.24	-5.04	79.80	82.28	3.11

Note: the ultimate load denotes the load value corresponding to 5 times of the yield deflection. For the test curves, if the 5 times yield deflection exceeds the deflection value corresponding to the peak load, the peak load is used as the ultimate load; Error (%) = [(FEM value − Test value)/ Test value] x 100%.

Development of yield state

The results of FE-D were selected to observe the development of component failure, the stress distribution and plastic yield of H-section steel and glulam with the change of displacement. Fig. 6 shows the experimental and FE results curve of FE-D, in the FE results, 6 points *a*, *b*, *c*, *d*, *e* and *f* were selected, respectively corresponding to the different yield states of the STC beams in the four-point bending experiment. Fig. 7 shows the expansion of yield element of FE-D with displacement.

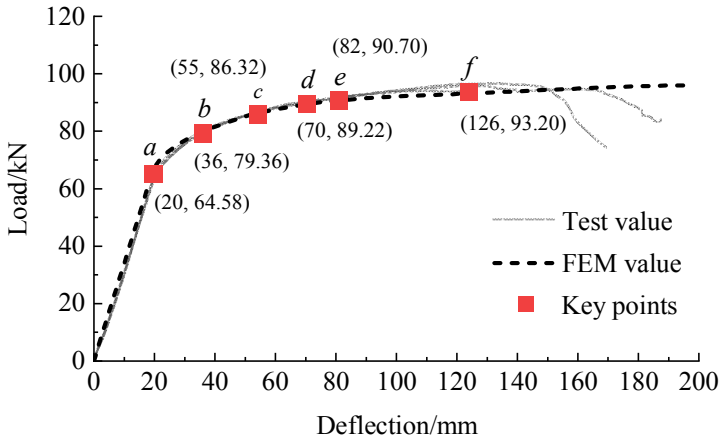

Fig. 6: Key points in the process of stress.

At point "*a*", the deflection is 20 mm, and the load is 64.58 kN. At this time, the material in the bottom flange area of the H-section steel between the loading plates enters the yield state, and the glulam is still in the elastic state; At point "*b*", the deflection is 36 mm, and the load is 79.36 kN. At this time, the yield of the lower flange has developed to the web, and the material yield of the upper flange of the H-section steel appears for the first time, and the glulam is in the elastic state; At point "*c*", the deflection is 55 mm, and the load is 86.32 kN. At this time, the material yield of the lower flange of the H-section steel develops towards the beam length,

the material yield at the web develops along the beam height, and the yield area appears between the loading plates at the top of the glulam for the first time; At point "*d*", the deflection is 70 mm, and the load is 89.22 kN, the yield area of the upper and lower flange of the H-section steel and the web gradually stabilizes, the yield area at the top of the glulam develops towards both sides and depth of the glulam; At point "*e*", the deflection 82 mm, and the load is 90.70 kN, the yield area of the upper flange, lower flange and web of the H-section steel develops slowly, the material yield at the top of the glulam develops along the depth direction, and the material yield area at the bottom of the glulam appears for the first time. At point "*f*", the deflection 126 mm, and the load is 93.20 kN, the yield area of the H-section steel further expands, the yield area between the loading points of the glulam develops along the depth direction, and nearly 60% of the glulam between loading points is in yield state. At this time, it can be seen that most areas of the glulam and H-section between the loading points are in the yield state.

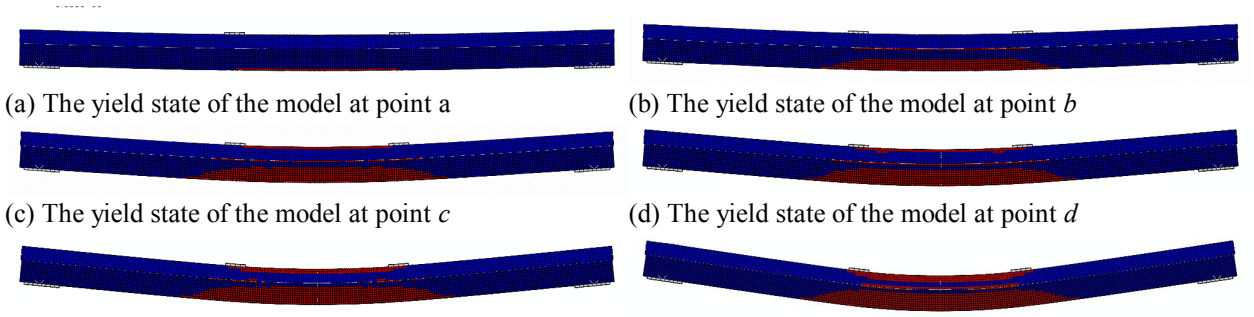

(a) The yield state of the model at point a (b) The yield state of the model at point *b*

(c) The yield state of the model at point *c* (d) The yield state of the model at point *d*

(e) The yield state of the model at point *e* (f) The yield state of the model at point *f*

Fig. 7: Development of yield state for model FE-D during loading.

Parametric study

STC beams involves the combination of two different materials, and its mechanical performance is relatively complex. Many factors will have different degrees of influence on its bending performance. It is not enough to only rely on the long-time and high investment experimental research, and other analysis methods are needed to improve the research accuracy and efficiency. The above has verified the rationality of STC beam FEM. On this basis, the FEM FE-C is selected as the basic model to change the characteristics of shear connector for comparative analysis, to analysis the bending performance of STC beam with these parameters.

In bolt connection, the spacing of bolts was respectively 100 mm, 150 mm and 200 mm. The spacing of the SDS was 100 mm, and the spacing of the rigid connection was 100 mm. The connection properties of bolts with different spacing and SDS were determined by the push-out test (Yang et al. 2020). The rigid connection was realized by setting the tangent and normal attributes of the connector as "Rigid". Tab. 6 shows the FE analysis results of 5 groups of STC beams with different connection characteristics.

As can be seen from Tab. 6, compared with the basic model FE-C, the yield deflection of the rigid connection FEM decreased by -10.85%, the yield load and the ultimate load increased by 12.84% and 6.76% respectively, and the initial stiffness increased by 28.62%; The yield deflection of model FE-SDS decreased by 0.47%, the yield load and the ultimate load increased by 1.09% and 1.29%, and the initial stiffness increased by 3.69%. The yield deflection of

the 150 mm bolt spacing FEM decreased by 1.93%, the yield load and the ultimate load decreased by 0.33% and 1.18%, resp. The yield deflection of the FEM with 200 mm bolt spacing increased by 0.23%, the yield load and the ultimate load decreased by 3.08% and 3.87% resp.

Tab. 6: Key points of FEM with different connections.

Group N°.	ω_y (mm)	Difference (%)	F_y (kN)	Difference (%)	F_u (kN)	Difference (%)	K (kN·mm^{-1})	Difference (%)
FE-C	21.29	-	69.84	-	86.14	-	3.25	-
FE-SDS	21.19	-0.47	70.60	1.09	87.25	1.29	3.37	3.69
FE-C-150	20.88	-1.93	69.61	-0.33	85.12	-1.18	3.29	1.23
FE-C-200	21.34	0.23	67.69	-3.08	82.81	-3.87	3.14	-3.38
FE-C-Rigid	18.98	-10.85	78.81	12.84	91.99	6.79	4.18	28.62

Note: ω_y - yield deflection (mm); F_u - ultimate load, taking the load corresponding to 5 times yield deflection (kN); K - initial stiffness (kN·mm^{-1}); Difference (%) = [(FE value−Experimental value)/ Experimental value] x 100%.

With the increase of bolt spacing, the yield load and the ultimate load decreased, the change of yield deflection was not significant. SDS can increase the yield load and the initial stiffness, but has no significant effect on the yield deflection. The decrease of the yield deflection and the increase of the yield load of the rigid connection are significant. It can be seen that the distribution density and mechanical properties of the connection between the glulam and H-section steel can affect the mechanical behavior of the whole STC beam.

CONCLUSIONS

In current, the finite element (FE) software ABAQUS was used to establish the calculation model and simulate the four-point bending test of steel-timber composite (STC) beams. The results show that the simulated values were in good agreement with the experimental values, and the errors of each key points were in a reasonable range (< 17%). At the same time, the development of yield state and the load-deflection curves of the finite element model (FEM) were in good agreement with the experimental values, which indicates that the established finite element model, the selected material parameters and the contact element models can better simulate the bending performance of STC beams, and provides a FE analysis method for further study of the bending performance of STC beams. Finally, the parametric study was carried out by using the verified FE models, the results show that the distribution density of shear connectors and the mechanical properties of connections can affect the overall mechanical behavior of STC beams. In order to improve the bearing capacity of STC beams in the future, shear connectors with higher stiffness can be considered. At present, the connection form of steel-timber members is still limited, which can be explored and tried in the follow-up research. In addition, the smaller the spacing of connectors, the higher the bearing capacity of STC beams. But in practical application, the utilization rate of materials should also be considered to make the layout of connectors more economical.

ACKNOWLEDGEMENTS

This research is supported by the National First-class Disciplines (PNFD), a Project Funded by the Priority Academic Program Development of Jiangsu Higher Education Institutions (PAPD), and a Project Funded by the Co-Innovation Center of Efficient Processing and Utilization of Forest Resources, Nanjing Forestry University (Nanjing, 210037, China). Any research results expressed in this paper are those of the writer(s) and do not necessarily reflect the views of the foundations. We declare that we do not have any commercial or associative interests, which represent a conflict of interest in connection with the current study.

REFERENCES

1. ANSI A190.1, 2012: Standard for wood products. Structural glued laminated timber.
2. ASTM A370, 2016: Standard test methods and definitions for mechanical testing of steel products.
3. ASTM D143, 2014: Standard test methods for small clear specimens of timber.
4. ASTM D198, 2015: Standard test methods of static tests of lumber in structural sizes.
5. Chybiński, M., Polus, Ł., 2019: Theoretical, experimental and numerical study of aluminium-timber composite beams with screwed connections. Construction and Building Materials 226(30): 317-330.
6. Daňková, J., Mec, P., Šafrata, J., 2019: Experimental investigation and performance of timber-concrete composite floor structure with non-metallic connection system. Engineering Structures 193: 207-218.
7. Deam, B.L., Fragiacomo, M., Buchanan, A.H., 2008: Connections for composite concrete slab and LVL flooring systems. Materials and Structures 41(3): 495-507.
8. Fojtik, R., Kubincova, L., Dubovsky, V., Kozlova, K., 2020: Moisture at contacts of timber-concrete element. Wood Research 65(6): 917-924.
9. GB 50011, 2016: Code for seismic design of buildings. Beijing (in Chinese).
10. GB 50017, 2017: Code for design of steel structure. Beijing (in Chinese).
11. Hassanieh, A., Valipour, H.R., Bradford, M.A., 2016: Experimental and numerical study of steel-timber composite (STC) beams. Journal of Constructional Steel Research 122: 367-378.
12. Hassanieh, A., Valipour, H.R., Bradford, M.A., Sandhaas, C., 2017: Modelling of steel-timber composite connections: Validation of finite element model and parametric study. Engineering Structures 138: 35-49.
13. Hassanieh, A., Valipour, H.R., Bradford, M.A., 2018: Bolt shear connectors in grout pockets: Finite element modelling and parametric study. Construction and Building Materials 176: 179-192.
14. Jorge, L.F.C., Lopes, S.M.R., Cruz, H.M.P., 2011: Interlayer influence on timber-LWAC composite structures with screw connections. Journal of Structural Engineering 137: 618-624.

15. Khorsandnia, N., Valipour, H.R., Crews, K., 2012: Experimental and analytical investigation of short-term behaviour of LVL-concrete composite connections and beams. Construction and Building Materials 37: 229-238.
16. Leborgne, M.R., Gutkowski, R.M., 2010: Effects of various admixtures and shear keys in wood–concrete composite beams. Construction and Building Materials 24(9): 1730-1738.
17. Li, H.T., Wu, G., Zhang, Q.S., Deeks, A., Su, J.W., 2017: Ultimate bending capacity evaluation of laminated bamboo lumber beams. Construction and Building Materials 160: 365-375.
18. Li, Q., Wang, Z.Q., Liang, Z.J., Li, L., Gong, M., Zhou, J.H, 2020: Shear properties of hybrid CLT fabricated with lumber and OSB. Construction and Building Materials 261: 120504.
19. Liu, X.P., Bradford, M., Chen, Q.J., Ban, H., 2016: Finite element modelling of steel–concrete composite beams with high-strength friction-grip bolt shear connectors. Finite Elements in Analysis and Design 108: 54-65.
20. Naud, N., Sorelli, L., Salenikovich, A., Auclair, S.C, 2019: Fostering GLULAM UHPFRC composite structures for multi-storey buildings. Engineering Structures 188: 406-417.
21. Nouri, F., Valipour, H.R., Braford, M.A., 2019: Structural behaviour of steel-timber composite (STC) beam-to-column connections with double angle web cleats subjected to hogging bending moment. Engineering Structures 192: 1-17.
22. Nouri, F., Valipour, H.R., Braford, M.A., 2019: Finite element modelling of steel-timber composite beam-to-column joints with nominally pinned connections. Engineering Structures 201: 109854.
23. Pulngern, T., Chanto, K., Pansuwan, W., Pattaraumpornsak, W., 2020: Effect of lamina thickness on flexural performance and creep behavior of douglas fir glued laminated timber beam. Wood Research 65(5): 715-726.
24. Schänzlin, J., Fragiacomo, M., 2018: Analytical derivation of the effective creep coefficients for timber-concrete composite structures. Engineering Structures 172: 432-439.
25. Xu, B.H., Bouchaïr, A., Racher, P., 2015: Mechanical behavior and modeling of dowelled steel-to-timber moment-resisting connections. Journal of Structural Engineering 141(6): 04014165.
26. Yang, R.Y., Li, H.T., Lorenzo, R., et al, 2020: Mechanical behaviour of steel timber composite shear connections. Construction and Building Materials 258: 119605.
27. Yang, R.Y., Zhang, X.F., Sun, Y.F., Zhou, T.T, Yuan, Q., 2020: Effect of the metallization treatment on the surface properties of *Populus Euphratica*. Wood Research 65(3): 381-394.
28. Yeoh, D., Fragiacomo, M., Franceschi, M.D., Heng, B.K., 2011: State of the art on timber-concrete composite structures: literature review. Journal of Structural Engineering 137(10): 1085-1095.

RUYUAN YANG*
NANJING TECH UNIVERSITY
COLLEGE OF ART & DESIGN
NANJING, CHINA

JIA WAN
TAIYUAN UNIVERSITY OF TECHNOLOGY
COLLEGE OF CIVIL ENGINEERING
TAIYUAN, CHINA

XIAOFENG ZHANG, YOUFU SUN
NANJING FORESTRY UNIVERSITY
COLLEGE OF MATERIALS SCIENCE AND ENGINEERING
NANJING, CHINA
*Corresponding author: ryyang0404@163.com

WOOD RESEARCH doi.org/10.37763/wr.1336-4561/66.5.821832
e-ISSN 2729-8906
66(5): 2021 821-832 pp.

USE OF LOGGING WASTE IN TECHNOLOGIES FOR DEEP CHEMICAL PROCESSING OF WOOD

ALEKSANDR VITITNEV, YURI ALASHKEVICH, ROMAN MARCHENKO,
MIKHAIL ZYRYANOV, ALEKSANDR MOKHIREV
RESHETNEV SIBERIAN STATE UNIVERSITY OF SCIENCE AND TECHNOLOGY
RUSSIAN FEDERATION

(RECEIVED NOVEMBER 2020)

ABSTRACT

The study presents theoretical aspects and modern technologies for processing wood biomass, considers the possibility of obtaining wood chips from felling residues of cutting areas, in particular technological chips that meet the GOST 15815: 1983 “Technological chips. Specifications" standard for use as raw materials in the production of fiberboard. Wood fiber obtained from similar in size and quality indicators according to GOST 15815: 1983 technological chips, pre-treated in a defibrator, was subjected to a refining process at a low concentration, in particular using the developed design of the disks of the refiner of fibrillating action while regulating the main parameters of the process. The resulting wood-fiber mass was characterized by an improvement in the fractional composition of fibers, their size and quality indicators. As a result, improving the quality of the wood-fiber mass provides an increase in the physical and mechanical properties of wood-fiber boards under all other equal production conditions, which excludes the use of binding resins, and may indicate the possibilit of effective processing of logging waste.

KEYWORDS: Wood biomass, felling residue, logging waste, refinement process, wood fiber pulp, refiner disc structure.

INTRODUCTION

Nowadays, when the demand for wood is constantly growing, its integrated utilization is of particular importance. In the coming years, satisfaction of the needs of national economy in timber will be possible through efficient use to the fullest extent possible, by increasing the volume of forest harvesting (Zyryanov et al. 2010). In this regard, the main direction of the timber complex development is to improve utilization of all harvested wood pulp. This requires further improvement of the production profile of forest and woodworking industries,

development in the production of industrial chips, wood boards, plywood, container board and other substitutes for commercial wood (Pirayesh et al. 2013, Lubke et al. 2014, Ihnat et al. 2017, 2018). Improving utilization of wood biomass, involving low-quality, low-value wood, felling residue, logging and wood conversion waste in processing is an issue of high priority (Ihnat et al. 2017, 2020, Ammar et al. 2018, Irle et al. 2018).

However, the problem of processing logging waste has not yet been fully resolved. In practice, they are ploughed in, burned, or simply left for digestion. But recycled wood is a valuable natural raw material that can compensate for the needs in the production of a number of marketable products (Bezrukikh et al. 2014). In our opinion, one of the priority directions of using logging waste in the form of lops, branches, and tops is processing into chips. In turn, technological chips are rather widely used in various industries. With moisture content of at least 40%, it can be a raw material in pulp and paper industry and woodworking industry for the production of container board, technical grades of paper, fiberboard and wood-particle board. Processing of technological chips by power-chemical means enables to produce acids, alcohols, aldehydes, ethers, resin, coal, and gas. Also, technological chips have found application in hydrolysis production (Vasilyev et al. 2001).

Studies (Shyukin et al. 2012, Mokhirev et al. 2014, Mokhirev et al. 2015) have shown that birch wood chips, as well as crushed alder and hazel shrub vegetation, can be an organic filler in the production of wood concrete for industrial premises under construction. Small-sized chips are used as a feed additive, as well as for composting and farm animal and poultry bedding. Fuel chips are intended for combustion in boiler units, apartment stoves and industrial furnaces. For the same purposes, chipped fuel wood is used in briquetted form without adding binders. The fuel briquette production from shredded wood on mobile units is very efficient (Shyukin et al. 2012, Mokhirev et al. 2014, Shegelman 2014).

As a rule, preparation of wood fiber pulp is carried out in several stages of refinement in high-speed disk mills (defibrators, attrition mills, refiners). In the pulp and paper industry, technological chips are subjected to chemical-thermal treatment (boiling chips to produce cellulose), followed by pulp production in refiners. At a certain percentage ratio of cellulose and wood pulp, a certain type of finished product is produced (Borysiuk et al. 2007, Ihnat et al. 2015). Both in the fiberboard production and in the pulp and paper industry, one of the main technological operations is the wood pulp refinement process.

The refinement process is the most important and energy-intensive technological stage of these industries, as a result of which wood fibers acquire certain geometric dimensions, properties, and composition (Laskeev 1967, Alashkevich et al. 2010, Chistova 2010, Bordin et al. 2011, Kerekes 2011, Li et al. 2011, Hua et al. 2012, Zyryanov 2012, Lubke et al. 2014, Gharehkhani et al. 2015, Forouzanfar et al. 2016, Berna et al. 2018, Vititnev 2019, Przybysz et al. 2020), which directly affects the quality of manufactured products (Laskeev 1967, Alashkevich et al. 2010, Chistova 2010, Zyryanov 2012, Ihnat et al. 2015, Tikhonova et al. 2015, Vititnev 2019). Refiner disks are the working body of refiners, design features (Olson et al. 2003, Nabieva 2004, Alashkevich et al. 2010, Li et al. 2011, Vikharev 2019, Vititnev 2019, Cai et al. 2020) of which, along with the main factors of the refinement process (a working gap between the disks, fiber concentration, rotor speed, etc.) are of

paramount importance that determines the effect on wood fibers, their destruction nature, and, respectively, final dimensional and qualitative characteristics and the composition of wood fiber pulp (Gorski et al. 2012). As shown by numerous studies, the scientifically based choice of the refiner disk working surface, depending on the type of processed raw materials and the required quality indicators of wood fiber pulp when regulating the main factors of the refinement process, enables to ensure high efficiency of the refiner and, therefore, efficiency of the entire production (Strand and Mokvist 1989, Nabieva 2004, Bordin et al. 2008, Alashkevich et al. 2010, Chistova 2010, Zyryanov 2012, Vititnev 2019).

The possibility of using technological chips produced from logging waste as raw materials for manufacture of environmentally friendly high-quality products is confirmed by research carried out as part of fiberboard production.

MATERIALS AND METHODS

Materials

In order to analyze the amount and type of waste generated from logging, a preliminary experiment was carried out at 9 logging sites in the Krasnoyarsk Territory, Russian Federation. At these logging sites, felling residues were collected from each felled tree. The number of trees of various species is 140 with the diameter from 16 to 68 cm. The felling residues were divided into branches, large lops, small lops, tops. Chips were produced from each type of felling residues using a chipper. Chips were evaluated for fractional composition and compared with various purpose chips required for production. The qualitative characteristics and chip dimensions are similar to those of the chips produced from logging waste and comply with the standards GOST 15815: 1983. Wood fiber produced from pretreated technological chips in a defibrator of the fiberboard production workshop of Segezha group "Lesosibirskiy LDK No. 1" in the Krasnoyarsk Territory was subjected to a refinement process at low concentration, according to the plan of experimental studies (Vititnev 2019).

Methods

Tab. 1 shows chip characteristics in accordance with GOST 15815: 1983, GOST 17462: 1977 “Forest industry production. Terms and definitions", and TU 13-735: 1983 “Technological chips from small trees and twigs", which were used to evaluate the quality parameters of wood raw materials from felling residues.

Tab. 1: Chip characteristics.

Chip type	Chip length (mm)	Chip thickness (mm)	Cut angle (°)	Bark mass fraction (%)	Rot mass fraction (%)	Purpose
Technological	12-15	< 5	30-60	1.5	0.3	pulp and paper industry
	10-35	< 5	30-60	15	5	fiberboard production
	10-60	< 5	30-60	15	5	wood-particle board production
Fuel	5-50	< 5	-	20	5	combustion
Small-sized	15-30	< 5	-	-	5	feed additive, compost, bedding

At the premises of the laboratory of the Industrial Technology and Machine Engineering Department of Siberian State University, Krasnoyarsk, an original scientifically grounded design of fibrillating refiner discs (Vititnev et al. 2018, RU 2652177) for the wood fiber pulp preparation in the fiberboard production was developed. The main studies of wood fiber pulp refinement process using discs with new design were carried out on an MD single-disk experimental refiner, a unit as close as possible to an industrial refiner, all other production conditions being equal. Fig. 1 shows the geometry of the working surface of the author's refiner disks (RU 2652177) and the traditional double-sided design (Braun and Sparish 2006, RU 2288313).

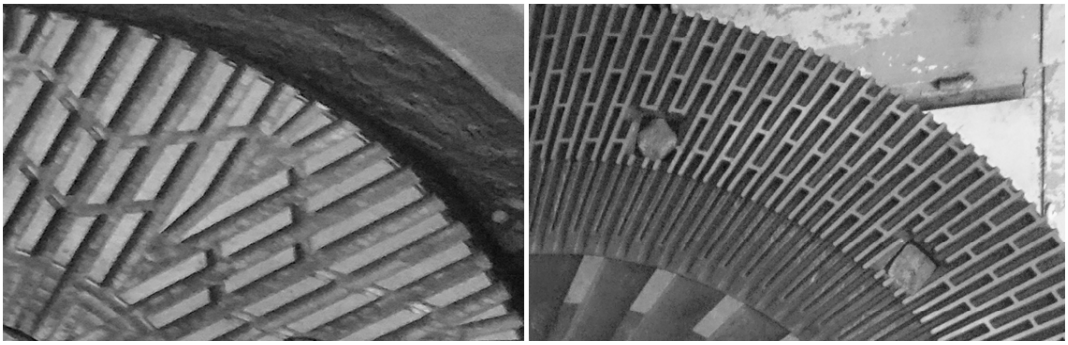

(a) (b)

Fig. 1: Geometry of the working surface of the refiner disks: (a) the author's design, (b) the traditional design.

Subsequently, we evaluated the dimensional and qualitative characteristics (grinding degree – DS; fractional composition – large (F_l), medium (F_m), small (F_f) fractions; average length – L_a and diameter – d_a of fibers, their ratio L_a/d_a) of the produced samples of wood fiber pulp, according to known methods, as well as gluing, casting of wood fiber mat and pressing of finished boards at the enterprise of Segezha group "Lesosibirskiy LDK No. 1", all other fiberboard production conditions being equal. When gluing wood fiber pulp, we used a standard formulation, except for the use of binders, hardening additives in the form of phenol-formaldehyde resins (Mersov 1989, Chistova 2010, Zyryanov 2012, Vititnev 2019).

Grinding degree (DS) of the wood fiber pulp was measured with a special Defibrator-Second device by Defibrator brand (Sweden) commonly used in fiberboard production. Depending on the refinement degree, the pulp can be characterized by different fluid loss (drainage), expressed in seconds in measuring units of the grinding degree DS (Mersov 1989, Chistova 2010, Zyryanov 2012, Lubke et al. 2014, Ihnat et al. 2015, Vititnev 2019).

Wood fiber pulp fractional composition (F_l, F_m, F_f, %). Fiber fractionation was carried out on a FVG-2 fractionator by passing a certain amount of wood fibers through sieves with openings corresponding to the groups of qualitative evaluation (Laskeev 1967, Chistova 2010, Zyryanov 2012). As a result of fractionation, fibers of certain fractions were weighed separately from each sieve, and their weight was expressed as a percentage of the total weight.

Arithmetic mean length (L_a, mm), diameter (d_a, mm) of fibers, their ratio (L_a/d_a). When dividing the wood fiber mass into fractions, the arithmetic mean values of the average

length (L_a), fiber diameter (d_a), their ratio (L_a/d_a), characterizing fiber destruction, intensity of their size change in the longitudinal and transverse directions, were measured, determining specific surface area and fiber flexibility. Geometric parameters were determined by microscopic measurement of at least 100 fibers for each sample using a Hitachi TM-3000 digital microscope at magnification up to 1000x, after which the fibers were categorized into suitable fractions (Laskeev 1967, Chistova 2010, Zyryanov 2012, Ferritsius et al. 2018).

Evaluation of physical and mechanical properties of finished board products was carried out in accordance with the standards GOST 4598: 2018 “Fibre boards by wet way of production. Specifications", EN 622-2: 2004 “Fibreboards. Specifications. Part 2: Requirements for hardboards, NEQ" during tests in accordance with GOST 10633: 2018 “Fiberboards. Test Methods".

The obtained results of experimental studies were processed in the STATISTICA-6 software package and Microsoft Excel 2007 using the Quasi-Newton method; the results reliably describe the investigated wood fiber pulp refinement process using a new design of the refiner disc surface.

RESULTS AND DISCUSSION

Results of the process of producing chips from felling residues

The preliminary experiment results showed that the tree diameter is the factor affecting most significantly the amount of logging waste. The dependency diagram presented in Fig. 2 shows that an increase in the tree trunk diameter to 30-34 cm decreases the content of logging waste from 12% to 9.5%. A further increase in the tree trunk diameter reduces the percentage of logging waste content, which reaches 8.4% with the diameter of 66-68 cm.

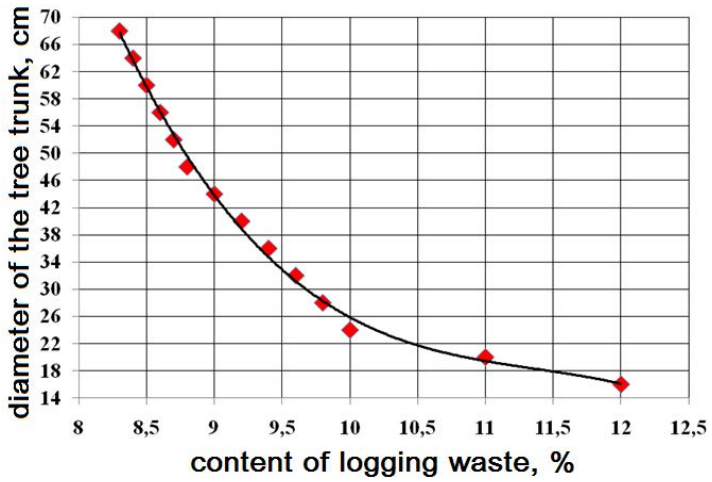

Fig. 2: Dependency of logging waste volume on tree trunk diameter.

The dependency diagram presented in Fig. 3 shows that the volume of lops fluctuates within 3-4.5% of the entire tree volume, branches are 4.5-6.5%, tops are 0.5-1%.

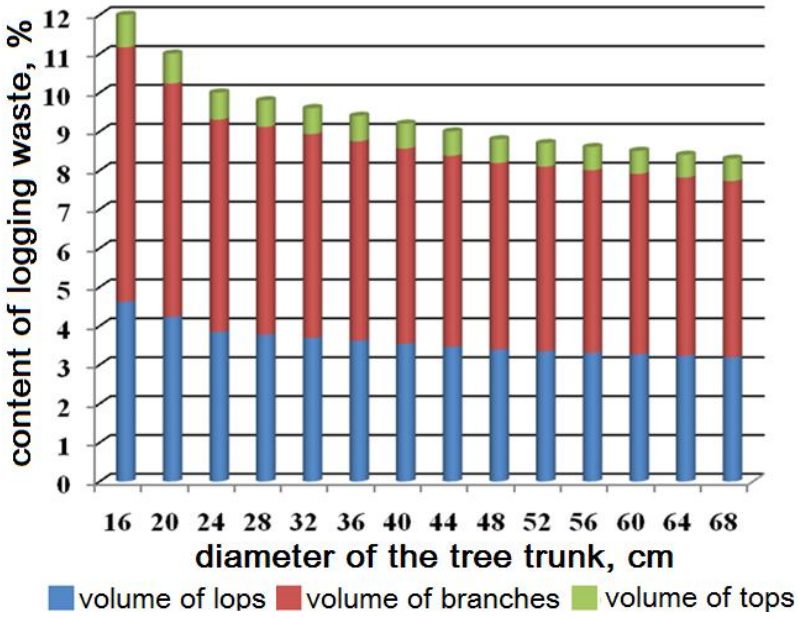

Fig. 3: Dependency of the contents of various logging wastes on tree trunk diameter.

The experiment results presented in Tab. 2 show that technological chips can be produced from: large lops of pine, spruce, birch; pine tops and small lops. Felling and logging waste of the remaining species can be used for small-sized and fuel chips production. This is due to the peculiarity of the microstructure of wood tops, lops, branches and different density of the wood species. The higher the density of the wood and the larger the diameter of the waste, the more technological chips are obtained. With a lower density of wood and the diameter of the waste, chips are obtained in smaller sizes than technological ones.

Tab. 2: Experiment results.

Wood species	Waste type	Diameter (cm)	Chip type
Pine	Tops	5-16	Technological
	Small lops	4-10	Technological
	Large lops	> 10	Technological
	Branches	< 4	Small-sized
Spruce	Tops	5-16	Small-sized
	Small lops	4-10	Small-sized
	Large lops	> 10	Technological
	Branches	< 4	Small-sized
Fir	Tops	5-16	Small-sized
	Small lops	4-10	Small-sized
	Large lops	> 10	Fuel
	Branches	< 4	Small-sized
Birch	Tops	5-16	Fuel
	Small lops	4-10	Small-sized
	Large lops	> 10	Technological
	Branches	< 4	Small-sized

Thus, the research results show that 8-11% of pine and 3-4% of birch and spruce logging waste are suitable for producing technological chips.

Refinement process results

As an example, Figs. 4-5 show graphical dependencies indicating the effect of the working gap between the discs (g) and wood fiber pulp concentration (c) when using the author's design of the refiner disks (RU 2652177) on the change in some dimensional and qualitative characteristics of fibers: grinding degree (DS), average length (L_a), length-to-diameter ratio (L_a/d_a) and the ratio of their fractions: large (F_l), medium (F_m), small (F_s) in the total mass.

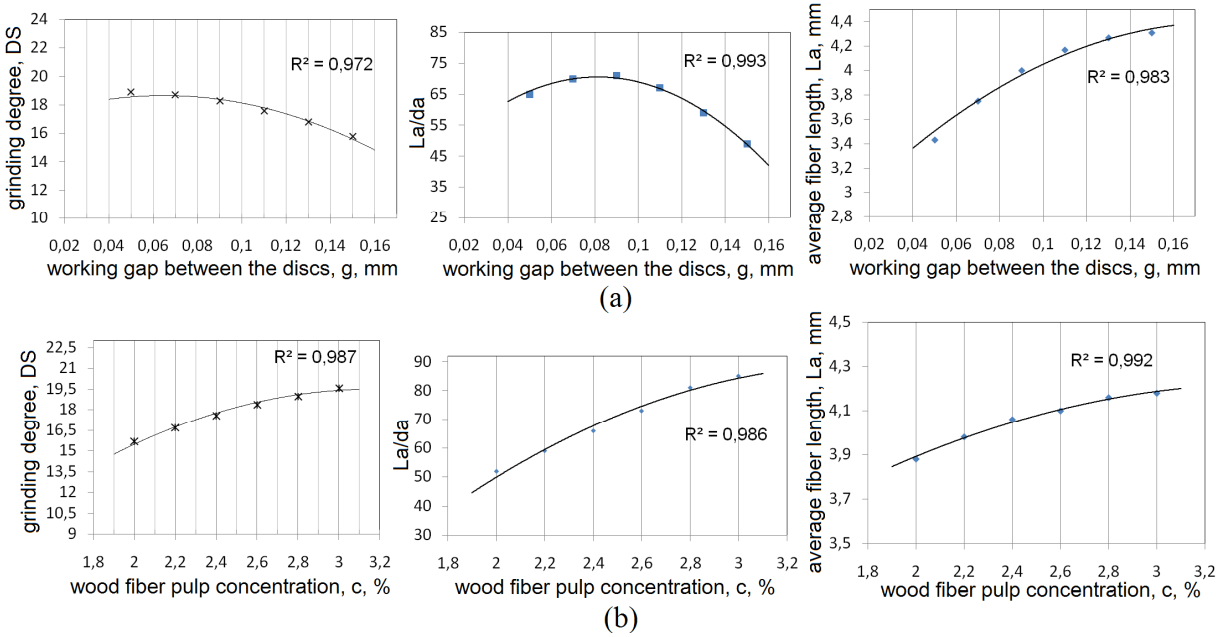

Fig. 4: Dependency of wood fiber pulp qualitative characteristics on refinement process parameters effect: (a) working gap between the discs, (b) wood fiber pulp concentration.

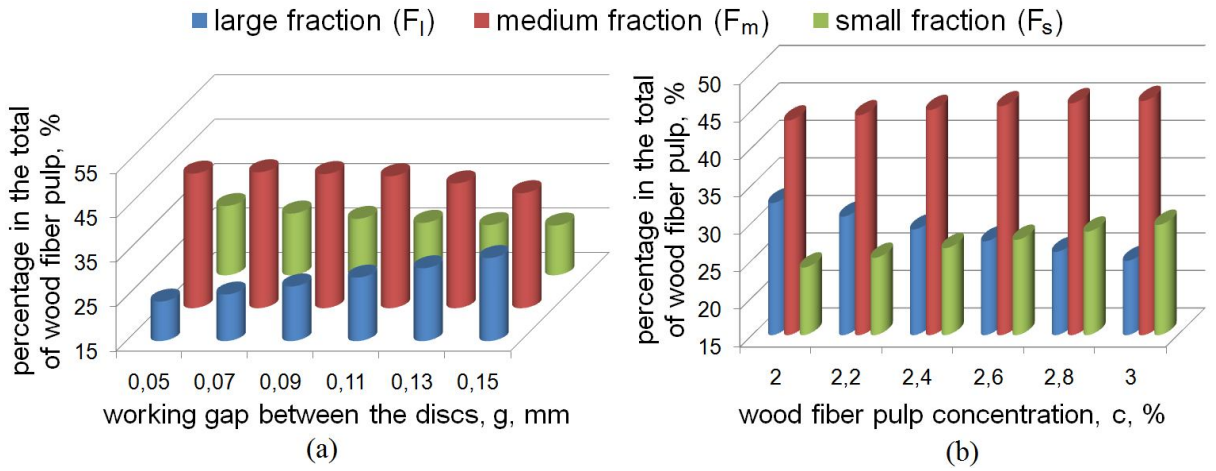

Fig. 5: Dependency of wood fiber pulp fractional composition on refinement process parameters effect: (a) working gap between the discs, (b) wood fiber pulp concentration.

Fig. 6 shows wood fiber before and after refinement (Tab. 3), when using the author's design of the refiner discs (RU 2652177) and the traditional double-sided design (RU 2288313) used in the fiberboard production, all other things being equal.

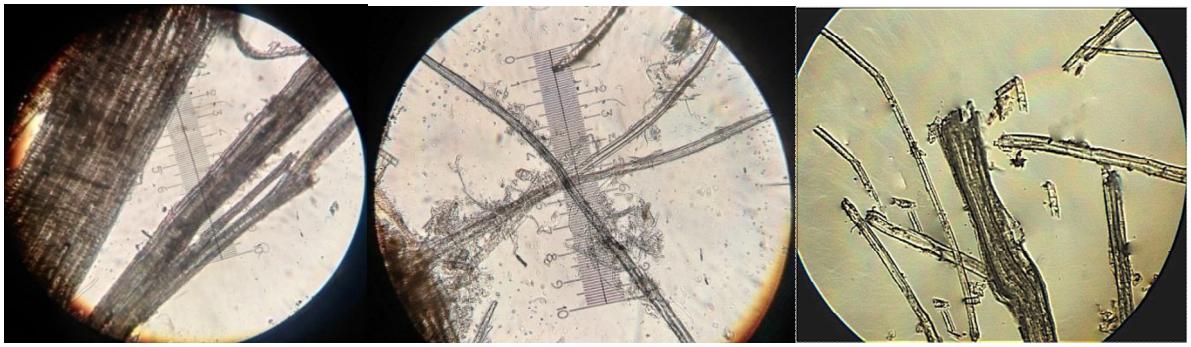

(a) (b) (c)

Fig. 6: Microscopic analysis of the wood fiber pulp (120x magnitude): (a) before refinement, (b) after refinement when using the author's design of the refiner discs and (c) after refinement when using the traditional design of the refiner discs.

Tab. 3: Wood pulp refinement process results when using various types of refiner disc surface.

Wood fiber pulp qualitative characteristics				**Wood fiber pulp fractional composition**			**Fiberboard physical and mechanical properties**	
Grinding degree, DS	Average length of fibers, L_a, (mm)	Average diameter of fibers, d_a, (mm)	Length-to-diameter ratio, L_a/d_a	Large fraction, F_l (%)	Medium fraction, F_m (%)	Small fraction, F_s (%)	Strength, (σ_i), (MPa)	Density (ρ), ($kg \cdot m^{-3}$)
Design of refiner disc RU 2652177								
18	4-4.1	0.05-0.06	70-80	27-28	45-46	27-28	42-44	933-938
Design of refiner disc RU 2288313								
18	5-5.1	0.12-0.13	38-44	28-30	26-27	44-45	32-34	850-862

The photograph presented in Fig. 6a shows that after preliminary processing in a defibrator, the wood fiber mass has a low grinding degree (10 DS) and is mainly the share of large fraction fibers ($F_l \approx 48\%$) — non-ground bundles, coarse insufficiently processed fibers ($L_a \approx 8.57$ mm; $d_a \approx 0.32$ mm; $L_a/d_a \approx 26.6$) with low contents of medium ($F_m \approx 32\%$) and small ($F_s \approx 20\%$) fraction fibers, which requires subsequent grinding in an refiner (Vititnev 2019).

After refinement in a refiner, as shown in Fig. 6b and c, and as per the data presented in Tab. 3, it is worth noting that fractional composition of wood fiber pulp and its qualitative characteristics changed. However, when using the traditional design of discs (Fig. 6c), the predominant formation of fiber small fraction ($F_s \approx 44$-45%) in the total mass and, in general, insufficient flexibility and fibrillation of the fibers is characteristic, as evidenced by the intensity of decrease in their diameter and, as a result, low values of their length-to-diameter ratio. This indicates low efficiency of the refinement process (Chistova 2010, Vititnev 2019), weak interweaving and interaction of fibers in wood fiber mat, and, as a consequence, the need to use additional binding resins when manufacturing fiberboard to ensure its strength characteristics corresponding to the standard GOST 4598: 2018 board of II grade, group B. The author's design of the refiner disks (Fig. 6b) provides high efficiency of the refinement process due to

predominance of the fibrillating effect on the fibers, destroying them through weak bonds. It enables to prepare wood fiber pulp with a predominance of medium fraction ($F_m \approx 46\%$) consisting of well processed and flexible, fibrillated elastic fibers with almost double parameter $L_a/d_a \approx 70\text{-}80$ as a result of intensive reduction in their diameter, which provides increase in strength of the fiberboard products and high quality of its manufacturing in accordance with the requirements of the standard GOST 4598: 2018 board of I grade, group A, without using binder resins (Vititnev 2019).

CONCLUSIONS

The presented research results may indicate the possibility of effective processing of felling and logging waste, the use of technological chips made of it, in particular, of coniferous wood, to produce wood fiber pulp with improved qualitative characteristics in its further preparation process in a refiner using the developed design of fibrillating disc surface. An increase in the size and quality characteristics of wood fiber pulp provides good fiber bonding and structure formation in a board, which makes the use of binder resins unnecessary, significantly improving the process's environmental friendliness and performance.

In general, this will allow to increase the efficiency and percentage of wood biomass use significantly, reduce the shortage of high-quality raw materials for board production, and partially, but rationally, solve the problem of recycling waste generated at logging sites.

ACKNOWLEDGMENTS

The authors express their gratitude to the Center for Collective Use of KSC SB RAS for supporting the research. The research was carried out under the governmental task issued by the Ministry of Education and Science of Russia for the "Technology and Equipment for the Chemical Processing of the Plant Biomass Material" project by the Deep Plant Material Processing Laboratory (FEFE-2020-0016).

REFERENCES

1. Alashkevich, Y. D., Kovalev, V. I., Nabieva, A.A., 2010: Vliyaniye risunka garnitury na protsess razmola voloknistykh polufabrikatov: Monografiya v 2-h chastyakh (Tool pattern effect on the fibrous material milling process: Monograph in two volumes). Vol 1. Siberian State Technological University. Krasnoyarsk, 168 pp.
2. Ammar, M., Mechi, N., Hidouri, A., Elaloui, E., 2018: Fiberboards based on filled lignin resin and petiole fibers. Indian Academy of Wood Science 15(2): 120-125.
3. Berna, J.E.R., Martinez, D.M., Olson, J.A., 2018: A comminution model parametrization for low consistency refining. Powder Technology 328: 288–299.
4. Bezrukikh, Y.A., Medvedev, S.O., Alashkevich, Y.D., Mokhirev, A.P., 2014: Ratsional'noe prirodopol'zovanie v usloviyakh ustoichivogo razvitiya ekonomiki promyshlennykh predpriyatii lesnogo kompleksa (Environmental management in the conditions for

sustainable economic development of industrial forestry complex enterprises). Ekonomika i predprinimatel'stvo (Economics and Entrepreneurship) 12(2): 994-996.
5. Bordin, R., Roux, J.C., Bloch, J.F., 2008: New technique for measuring clearance in low-consistency refiners. Appita Journal 61: 71-77.
6. Borysiuk, P., Nicewicz, D., Pawlicki, J., Klimczewski, M., 2007: The influence of the type and preparation of ligno-cellulose fibres on the properties of MDF. Wood Research 52(4): 79-88.
7. Cai, H., Yuan, ZY., Tong, GL., Zhang, X., Zhang, H., 2020: Comparison of two bar Edge lengths of refining plates on the properties of American old corrugated container pulp during low consistency refining. BioResources 15(1): 347-359.
8. Chistova, N.G., 2010: Pererabotka drevesnykh otkhodov v tekhnologicheskom protsesse polucheniya drevesnovoloknistykh plit (Processing of wood waste in the technological process of producing fiberboard). Doctor of Technical Sciences. Thesis work. Siberian State Technological University. Krasnoyarsk, 415 pp.
9. Ferritsius, O., Ferritsius R., Rundlof, M., 2018: Average fibre length as a measure of the amount of long fibres in mechanical pulps – ranking of pulps may shift. Nordic Pulp & Paper Research Journal 33(3): 468–481.
10. Forouzanfar, R., Vaysi, R., Rezaei, V.T., Hosseini, S.B., Sukhtesaraie, A., 2016: Study on production of fluting paper from poplar pulp mixed with hardwood NSSC pulp. Indian Academy of Wood Science 13(1): 55-63.
11. Gharehkhani, S., Sadeghinezhad, E., Kazi, S.N., Yarmand, H., Badarudin, A., Safei, M.R., Zubir, M.N.M., 2015: Basic effects of pulp refining on fiber properties. A review. Carbohydrate Polymers 115: 785-803.
12. Gorski, D., Morseburg, K., Olson, J., Luukkonen, A., 2012: Fibre and fines quality development in pilot scale high and low consistency refining of ATMP. Nordic Pulp & Paper Research Journal 27(5): 872-881.
13. Hua, J., Chen, G., Xu, D., Shi, S.Q., 2012: Impact of thermomechanical refining conditions on fiber quality and energy consumption by mill trial. BioResources 7(2): 1919-1930.
14. Ihnat, V., Lubke, H., Boruvka, V., Babiak, M., Schwartz, J., 2015: Straw pulp as a secondary lignocellulosic raw material and its impact on properties of insulating fiberboards part II. Preparation of insulated fiberboards with straw fiber content. Wood Research 60(2): 235-245.
15. Ihnat, V., Boruvka, V., Babiak, M., Lubke, H., Schwartz, J., 2015: Straw pulp as a secondary lignocellulosic raw material and its impact on properties of insulating fiberboards part III. Preparation of insulating fiberboards from separately milled lignocellulosic raw materials. Wood Research 60(3): 441-450.
16. Ihnat, V., Lubke, H., Boruvka, V., Russ, A., 2017: Waste agglomerated wood materials as a secondary raw material for chipboards and fibreboards. Part I: Preparation and characterization of wood chips in term of their reuse. Wood Research 62(1): 45-56.
17. Ihnat, V., Lubke, H., Russ, A., Pazitny, A., Boruvka, V., 2018: Waste agglomerated wood materials as a secondary raw material for chipboards and fibreboards part II. Preparation and characterisation of wood fibres in terms of their reuse. Wood Research 63(3): 431-442.

18. Ihnat, V., Lubke, H., Balbercak, J., Kuna, V., 2020: Size reduction downcycling of waste wood. Review. Wood Research 65(2): 205-220.
19. Irle, M., Privat, F., Couret, L., Belloncle, C., Deroubaix, G., Bonnin, E., Cathala, B., 2018: Advanced recycling of post-consumer solid wood and MDF. Wood material science & engineering 14(1): 19-23.
20. Kerekes, R.J., 2011: Force-based characterization of refining intensity. Nordic Pulp & Paper Research Journal 26(1): 14–20.
21. Laskeev, P.K., 1967: Proizvodstvo drevesnoi massy (Wood pulp production). Timber industry, Moscow, 581 pp.
22. Li, B., Li, H.M., Zha, Q.Q., Bandekar, R., Alsaggaf, A., Ni, Y.H., 2011: Review: effects of wood quality and refining process on TMP pulp and paper quality. BioResources 6(3): 3569-3584.
23. Lubke, H., Ihnat, V., Boruvka, V., 2014: Straw pulp as a secondary lignocellulosic raw material and its impact on properties of properties of insulating fiberboards. Part I. Characteristic of straw fibre from the perspective of the mass creation. Wood Research 59(5): 747-755.
24. Mersov, E.D., 1989: Proizvodstvo drevesnovoloknistykh plit (Fiberboard production). Higher School, Moscow, 232 pp.
25. Mokhirev, A.P., Bezrukikh, Y.A. Medvedev, S.O., 2015: Pererabotka drevesnykh otkhodov predpriyatii lesopromyshlennogo kompleksa, kak faktor ustoichivogo prirodopol'zovaniya (Recycling of wood waste from forestry enterprises as a factor of sustainable management of natural resources). Inzhenernyi vestnik Dona (Don Engineering bulletin) 2(2).
26. Mokhirev, A.P., Aksenov, N.V., Sheverev, O.V., 2014: O ratsional'nom prirodopol'zovanii i ekspluatatsii resursov v Krasnoyarskom krae (On the rational management and exploitation of resources in the Krasnoyarsk region). Inzhenernyi vestnik Dona (Don Engineering bulletin) 4(1).
27. Nabieva, A.A., 2004: Otsenka vliyaniya i sovershenstvovaniya tekhnologicheskikh parametrov nozhevykh razmalyvayushchikh mashin (Assessing the efficiency and technological improvement of the knife milling machines). Candidate of Technical Sciences. Thesis work. Siberian State Technological University. Krasnoyarsk, 156 pp.
28. Olson, J.A., Drozdiak, J., Martinez, M., Garner, R., Robertson, A.G., Kerekes, R., 2003: Characterizing fibre shortening in low-consistency refining using a comminution model. Powder Technology 129(1-3): 122-129.
29. Pirayesh, H., Moghadam, I.K., Tichi, A.H., 2013: Some physico-mechanical properties of medium density fiberboards (MDF) based on mixed hardwood particles and chopped sycamore leaves bonded with MDI resin. Indian Academy of Wood Science 10(2): 155–159.
30. Przybysz, P., Dubowik, M., Malachowska, E., Kucner, M., Gajadhur, M., Przybysz, K., 2020: The effect of the refining intensity on the progress of internal fibrillation and shortening of cellulose fibers. BioResources 15(1): 1482-1499.
31. Shegelman, I.R., 2014: Sovershenstvovanie tekhnologicheskogo lesozagotovitel'nogo protsessa s ispol'zovaniem valochno-trelevochnoi mashiny na osnove funktsional'no-tekhnologicheskogo

analiza (The improvement of forestry process with the use of feller-skidder in terms of functional-technological method). Inzhenernyi vestnik Dona (Don Engineering bulletin 3.
32. Shyukin, P.O., Demchuk, A.V., Budnik, P.V., 2012: Povyshenie effektivnosti pererabotki vtorichnykh resursov lesozagotovok na toplivnuyu shchepu (Improving the efficiency of processing secondary resources of logging into fuel chips). Inzhenernyi vestnik Dona (Don Engineering bulletin) 3.
33. Strand, B.C., Mokvist A., 1989: The application of comminution theory to describe refiner performance. Journal of Pulp and Paper Science 15(3): 100–105.
34. Tikhonova, E., Irle, M., Lecourt, M., 2015: Revisiting hardboard properties from the fiber sorting point of view. Holzforschung 69(5): 627–632.
35. Vasilyev, S.B., Patyakin, V.I., Shegelman, I.P., 2001: Tekhnika i tekhnologiya proizvodstva shchepy v lespromkhoze (Technique and technology for wood chips production in timber industry). PetrSU (Petrozavodsk State University). Petrozavodsk, 100 pp.
36. Vikharev, S., 2019: Research of a fibrous layer at refining in the refiners. IOP Conf. Series: Earth and Environmental Science 316: 012080.
37. Vititnev, A.Y., 2019: Sovershenstvovaniye protsessa razmola voloknistykh polufabrikatov v proizvodstve drevesnovoloknistykh plit (Improving the fibrous semi-finished material milling in the fiberboard production process). Candidate of Technical Sciences. Thesis work. Reshetnev Siberian State University. Krasnoyarsk, 152 pp.
38. Zyryanov, M.A., Shvetsov, V.A, Chistova, N.G., 2010: Pererabotka drevesnykh otkhodov v proizvodstve drevesnovoloknistykh plit (Recycling of wood waste in fiberboard production). Vestnik Kras GAU (Krasnoyarsk State Agrarian University Bulletin) 4: 288-291.
39. Zyryanov, M.A., 2012: Poluchenie polufabrikatov v odnu stupen' razmola dlya proizvodstva drevesnovoloknistykh plit mokrym sposobom (Producing semi-finished materials in one milling stage for fiberboard production using the moist method). Candidate of Technical Sciences. Thesis work. Siberian State Technological University. Krasnoyarsk, 171 pp.

ALEKSANDR VITITNEV*, YURI ALASHKEVICH, ROMAN MARCHENKO,
MIKHAIL ZYRYANOV, ALEKSANDR MOKHIREV
RESHETNEV SIBERIAN STATE UNIVERSITY OF SCIENCE AND TECHNOLOGY
DEEP PLANT MATERIAL PROCESSING LABORATORY
KRASNOYARSKII RABOCHII PROSPECT 31
660037 KRASNOYARSK
RUSSIAN FEDERATION
*Corresponding author: sanekvititnev@yandex.ru

WOOD RESEARCH doi.org/10.37763/wr.1336-4561/66.5.833843
e-ISSN 2729-8906
66(5): 2021 833-843 pp.

COMPARATIVE PROTEOMIC ANALYSIS OF THE THICK-WALLED RAY FORMATION PROCESS OF *HALOXYLON AMMODENDRON* IN THE GURBANTUNGGUT DESERT, CHINA

CHAOBIN ZHOU
ZUNYI NORMAL COLLEGE
CHINA

JUNJIE DING
XINJIANG ACADEMY OF AGRICULTURAL AND RECLAMATION SCIENCE
CHINA

XIAOJING HU
XINJIANG AGRICULTURAL UNIVERSITY
CHINA

WEI GONG
SICHUAN AGRICULTURAL UNIVERSITY
CHINA

(RECEIVED DECEMBER 2020)

ABSTRACT

Thick-walled ray cells of *Haloxylon ammodendron* were first reported by Zhou and Gong in 2017, but their formation mechanism remains unknown. In this study, we performed a proteomic analysis of ray cell wall formation in the xylem. *H. ammodendron* in Shihezi exhibits a thicker ray cell wall than that in Jinghe. During the process of cell wall biosynthesis in the xylem of *H. ammodendron*, the nonspecific lipid-transfer protein and beta expansin EXPB2.1 (*Mirabilis jalapa*) first loosen the cell wall, and this step is followed by extension and expansion. Subsequently, xyloglucan endotransglycosylase/hydrolase 1 cleaves and links the xyloglucan chains. Photosystem I P700 apoprotein A1, reversibly glycosylated polypeptide 1 and GDP-mannose-3′,5′-epimerase are involved in the cellulose, hemicellulose and pectin biosynthesis processes in the cell wall by providing components or energy. Finally, the proteins involved in phenylpropanoid biosynthesis promote lignification of the ray cell wall and complete the biosynthetic process of the cell wall.

KEYWORDS: Xylem special character, isobaric tag for relative and absolute quantitation, differentially expressed proteins, phenylpropanoid biosynthesis, ray cell.

INTRODUCTION

Haloxylon ammodendron is an important afforestation species in the arid desert regions in both Asia and Africa. Previous studies have found that the xylem of *H. ammodendron* has ray tissues, that these tissues are uniseriate or multiseriate with a height of 53.80 μm - 434.85 μm and a width of 7.60 μm - 87.15 μm, that the wall of ray cells is clearly thickened in the xylem of *H. ammodendron*, and that the wall thickness of the ray cell can reach 2.85 μm - 3.08 μm, which is 3 - 6 times the thickness of axial parenchyma, slightly higher than that of fibre (2.64 μm - 2.97 μm) (Zhou and Gong 2017), and markedly higher than that of fibre in *Salix psammophila* (a xerophytic deciduous shrub in Kubuqi Desert, China) (Zhou et al. 2017). In general, ray tissue is composed of parenchyma cells, and the wall thickness of ray cells is markedly thinner than that of fibre cells in most species (Plavcová and Jansen 2015). However, thick-walled ray cells have been found in the parenchyma of some species, such as *Melia azedarach* and *Symbolanthus macranthus* (Carlquist and Grant 2005). The mechanical properties of tissues with thickened walls are enhanced (Alves and Angyalossy-Alfonso 2002, Xi 2018). Therefore, research on the regulatory proteins (genes) involved in the cell wall formation process will be important for both understanding the environmental adaptability of xylem characteristics and improving the wood quality in plantations.

With the development of genomics and molecular genetics, research on plant cell wall formation has achieved good progress in recent years. Studies have mainly focused on *Arabidopsis thaliana* (Taylor et al. 2003), *Populus trichocarpa* (Suzuki et al. 2006), *Picea sitchensis* (Bong.) Carr. (Fernandes et al. 2011), and *Gossypium hirsutum* (Pear et al. 1996). Although many studies have investigated cell wall biosynthesis, the content and structure of the cell wall components vary among species and tissues, which leads to diversity and complexity in the cell wall composition (Burton et al. 2010). Therefore, the biosynthetic pathway of the cell wall in specific tissues of different species remains to be studied.

Thus, the proteomic characteristics of the process of ray cell wall formation in *H. ammodendron* were studied. GO annotation analysis combined with KEGG pathway enrichment and other bioinformatics methods was performed to explore the differentially expressed proteins and metabolic pathways related to ray cell wall formation in this plant.

MATERIALS AND METHODS

Sample location and sampling

The climate and growth characteristics of *H. ammodendron* plantations in the sampling area were described by Zhou and Gong (2017). At the end of June 2017, samples were collected at the Jinghe (82°53′35″E, 44°36′10″N) and Shihezi (86°14′44″E, 45°00′34″N) Desert Research and Experimental Station of Shihezi University in the Gurbantunggut Desert, Xinjiang, China. The identification of *H. ammodendron* was performed according to the morphology using

a website (http://www.iplant.cn/info/Haloxylon%20ammodendron) built by the Institute of Botany, Chinese Academy of Sciences. Perennial branches of *H. ammodendron* with a diameter of approximately 1 cm were collected. The bark, phloem and cambium were scraped from the branches, and a blade sterilized with anhydrous ethanol was used to scrape the xylem. The samples were wrapped in aluminium foil, placed in liquid nitrogen, rapidly cooled, transported to the laboratory and stored in a refrigerator at -80°C.

Observation and measurement of the wall thickness of ray cells

Observations under a light microscope and measurements of the wall thickness of ray cells of *H. ammodendron* were performed as described by Zhou and Gong (2017).

Scanning electron microscopy (SEM)

The xylem of *H. ammodendron* was cut into blocks of 1 x 1 x 1 cm, air dried and polished to a smooth surface. The samples were dehydrated using a graded ethanol series and dried using the liquid CO_2 critical point method. The sample was soaked in 98% H_2SO_4 for 5 min. The sample was attached to conductive tape, metal spraying was performed for 200 s, and the sample was then observed by SEM.

Proteomic analysis

Protein extraction

Samples (1 g-2 g) with 10% polyvinylpolypyrrolidone (PVPP) were ground into powder in liquid nitrogen, and protein was then extracted by adding 5-fold volumes of 10% trichloroacetic acid (TCA)/acetone. Each sample included three biological replicates.

Protein digestion

After determination of the protein concentration using the Bradford assay and SDS-PAGE, the protein solution (100 μg) with 8 M urea was diluted 4-fold with 100 mM triethylammonium bicarbonate (TEAB). Trypsin Gold (Promega, Madison, WI, USA) was used to digest the proteins at a protein : trypsin ratio of 40 : 1 overnight at 37°C.

Peptide labelling

The peptides were dissolved in 30 μL of 0.5 M TEAB with vortexing. The isobaric tag for relative and absolute quantitation (iTRAQ) labelling reagents were brought to ambient temperature, and these reagents were then transferred and mixed with the proper samples. Peptide labelling was performed using the iTRAQ Reagent 8-plex Kit according to the manufacturer's protocol.

Peptide fractionation

The peptides were separated on a Shimadzu LC-20AB HPLC Pump system coupled with a high-pH RP column.

High performance liquid chromatography

Each fraction was resuspended in buffer A (2% acetonitrile (CAN) and 0.1% free folate (FA) in water) and centrifuged at 20000 rpm for 10 min. The supernatant was loaded onto a C18 trap column at 5 $\mu L \cdot min^{-1}$ for 8 min using the autosampler of an LC-20AD nano-HPLC instrument (Shimadzu, Kyoto, Japan).

Mass spectrometry analysis

The peptides separated by nano-HPLC were subjected to tandem mass spectrometry Q EXACTIVE (Thermo Fisher Scientific, San Jose, CA, USA) for data-dependent acquisition (DDA) detection by nanoelectrospray ionization. The parameters for MS analysis are listed as follows: electrospray voltage, 1.6 kV; precursor scan range, 350 $m \cdot z^{-1}$ - 1600 $m \cdot z^{-1}$ at a resolution of 70000 in the Orbitrap; MS/MS fragment scan range, >100 $m \cdot z^{-1}$ at a resolution of 17500 in the HCD mode; normalized collision energy setting, 27%; dynamic exclusion time, 15 s; automatic gain control (AGC) for full MS target and MS2 target, 3E6 and 1E5, respectively; and number of MS/MS scans following one MS scan, 20 most abundant precursor ions above a threshold ion count of 20000.

Tab. 1: Mascot search parameters.

Item	**Value**
Type of search	MS/MS ion search
Enzyme	Trypsin
Fragment mass tolerance	0.05 Da
Mass values	Monoisotopic
Variable modifications	Oxidation (M), iTRAQ8plex (Y)
Fixed modifications	Carbamidomethyl (C), iTRAQ8plex (N-term), iTRAQ8plex (K)
Peptide mass tolerance	20 ppm
False discovery rate (FDR)	< 0.01
Fold change	> 1.2
P value from the significance test	< 0.05

Bioinformatics

For peptide data analysis, raw mass data were processed using Mascot 2.3.02 (Matrix Science, London) against a database. The search parameters are shown in Tab. 1. Blast2GO software was used for the Gene Ontology (GO) analysis of differentially expressed proteins. A database (http: www.genome.jp/kegg/) was used for the KEGG pathway enrichment analysis of the differentially expressed proteins and detected the most significant pathways.

RESULTS

Wall thickness of ray cells in the xylem of *Haloxylon ammodendron*

The ray cell walls in the xylem of *H. ammodendron* showed an obviously thick wall structure (Fig. 1), and the wall thickness of *H. ammodendron* ray cells in Jinghe (2.85 ± 0.42 μm) was significantly lower than that in Shihezi (3.08 ± 0.44 μm) ($p < 0.01$).

Differentially expressed proteins

In total, 6767 peptides and 3076 proteins were identified with an FDR of 1%. Repeat experiments defined differentially expressed proteins with a 1.2-fold change ($P < 0.05$). A total of 795 and 421 proteins were identified as upregulated and downregulated in Shihezi, respectively.

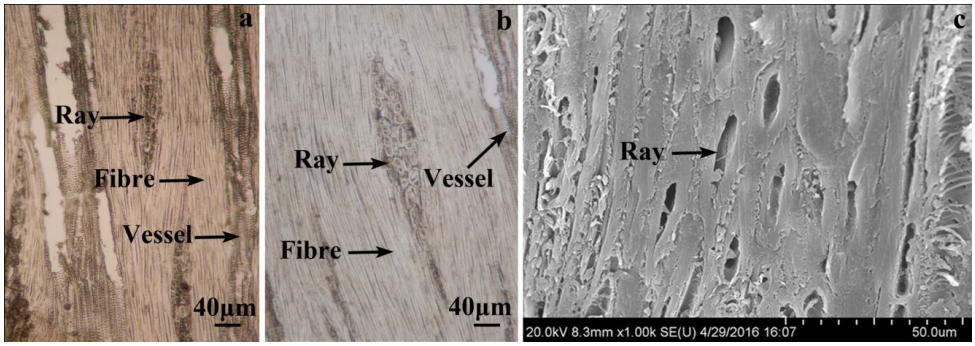

Fig. 1: Anatomical characteristics of Haloxylon ammodendron rays (SEM) in tangential sections: a) Jinghe, b), Shihezi, c) SEM. The arrows show ray cells with thick walls.

Among the upregulated differentially expressed proteins, a total of 55 proteins, including beta expansin EXPB2.1 (*Mirabilis jalapa*), glucan endo-1,3-beta-D-glucosidase (*Beta vulgaris* subsp. *vulgaris*), hypothetical protein JCGZ_24101 (*Jatropha curcas*), pectin acetylesterase family protein (*Theobroma cacao*), and polyphenol oxidase (*Spinacia oleracea*), were related to loosening, cellulose/hemicellulose and pectin in the process of ray cell wall formation in the *H. ammodendron* xylem (Fig. 2).

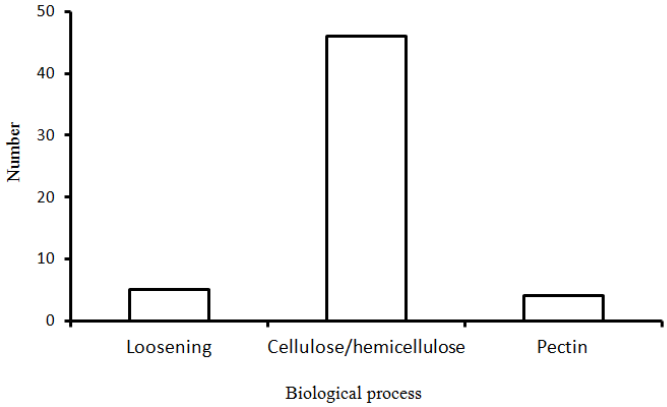

Fig. 2: Differentially expressed proteins related to ray cell wall formation in the Haloxylon ammodendron xylem.

Pathway annotation of the identified proteins

To better understand the pathways involving the differentially expressed proteins during the formation of ray cell walls in the xylem of *H. ammodendron*, we performed pathway annotation analysis of the differentially expressed proteins based on the KEGG database. The results showed that a total of nine pathways were related to ray cell wall synthesis in the xylem of *H.*

ammodendron, such as phenylpropanoid biosynthesis, photosynthesis, glycolysis/gluconeogenesis, carbon metabolism, starch and sucrose metabolism, and metabolic pathways (Tab. 2).

DISCUSSION

The proteome related to ray cell wall formation in the xylem of *H. ammodendron* from the Gurbantunggut Desert was studied. A total of 3,076 proteins were identified, and among these, 795 and 421 proteins were significantly upregulated and significantly downregulated, respectively, in *H. ammodendron* from Shihezi, which harboured ray cells with a greater cell wall thickness than the ray cells of *H. ammodendron* in Jinghe. Among the metabolic pathways involving the differentially expressed proteins, phenylpropanoid biosynthesis, photosynthesis, glycolysis/gluconeogenesis, carbon metabolism, starch and sucrose metabolism, metabolic pathways, plant hormone signal transduction, cysteine and methionine metabolism and amino sugar and nucleotide sugar metabolism were found to be related to ray cell wall synthesis (Tab. 2).

Tab. 2: Significantly enriched pathways related to cell wall formation in the Haloxylon ammodendron xylem.

Number	Pathway	Differentially expressed proteins with pathway annotations (1041)	Pathway ID
1	Photosynthesis	25 (2.4%)	ko00195
2	Starch and sucrose metabolism	36 (3.46%)	ko00500
3	Phenylpropanoid biosynthesis	34 (3.27%)	ko00940
4	Metabolic pathways	378 (36.31%)	ko01100
5	Amino sugar and nucleotide sugar metabolism	29 (2.79%)	ko00520
6	Glycolysis/gluconeogenesis	39 (3.75%)	ko00010
7	Plant hormone signal transduction	7 (0.67%)	ko04075
8	Cysteine and methionine metabolism	18 (1.73%)	ko00270
9	Carbon metabolism	71 (6.82%)	ko01200

Among the metabolic pathways, five differentially expressed proteins were associated with cell wall loosening, the biosynthesis of cellulose and hemicellulose involved 46 differentially expressed proteins, and four differentially expressed proteins were found to be involved in pectin biosynthesis (Fig. 2).

Lipid transfer proteins can transfer lipids between membranes and might be involved in cell wall relaxation (Yeats and Rose 2008). In this study, a protein (protein ID of XP_021763617.1) named probable nonspecific lipid-transfer protein AKCS9-like (*Citrus sinensis*) was upregulated in the ray cell walls of the xylem of *H. ammodendron* in Shihezi (with a higher ray cell wall thickness), and this protein might be involved in the process of cell wall loosening.

Expansin is a protein that loosens the cell walls of plants and participates in the process of cell wall expansion (Zhang et al. 2018). Expansin consists of four subfamilies: α-expansin (EXPA), β-expansin (EXPB), expansin-like A (EXLA) and expansin-like B (EXLB) (Kende et al. 2004). In our study, we found that β-expansin EXPB2.1 was upregulated in the ray cell walls

of *H. ammodendron* in Shihezi, which indicated that this protein is involved in the loosening process of the ray cell wall in the xylem of *H. ammodendron*.

Cell wall expansion depends on xyloglucan degradation or xyloglucan-cellulose hydrolysation, and xyloglucan endotransglycosylase (XET) plays an important role in this process (Darley et al. 2001). XETs were first identified and described by Fry et al. (1992) and Nishitani and Tominaga (1992). The main activity of XETs is transglycosidase activity, which catalyses the cleavage of the xyloglucan chain and moves the half chain to the nonreducing terminal of the second xyloglucan chain (Sulova et al. 1998). The cleavage (degradation) of cell wall xyloglucan promotes cell wall loosening, growth and cellulose accumulation (Park et al. 2004). Previous studies have shown the potential transformation and relaxation ability of XET in cell walls, and the expression and activity of XET are significantly correlated with the expansion area of the cell (Fry et al. 1992, Xu et al. 1996). Xyloglucan endotransglycosylase/hydrolase 1, which belongs to the plant hormone signal transduction pathway, is upregulated in the ray cell walls in the xylem of *H. ammodendron* in Shihezi. Xyloglucan endotransglycosylase/hydrolase 1, somatic embryogenesis receptor kinase 1-like precursor and kinase protein with tetratricopeptide repeat domain isoform 1 catalyse various biochemical processes from brassinosteroid biosynthesis to cell elongation (Tab. 3).

Reversibly glycosylated polypeptide 1 is involved in the transport of sugar into the Golgi cavity and the biosynthesis of noncellulosic polysaccharides (Saxena and Brown 1999). In this study, reversibly glycosylated polypeptide 1 was found to be involved in amino sugar and nucleotide sugar metabolism and was upregulated in Shihezi (ratio of 1.28).

GDP-mannose-3′,5′-epimerase (GME) catalyses the conversion of GDP-D-mannose to GDP-L-galactose (Ma et al. 2014), which is a structural component of agar and cell wall polysaccharides (Siow et al. 2013). GME is involved in ascorbic acid biosynthesis in the Smirnoff-Wheeler pathway (Smirnoff and Wheeler 2000), and the first step is the GME-catalysed formation of GDP-D-mannose (Wolucka and Van Montagu 2003). Ascorbic acid, an antioxidant and cofactor of enzymes, plays an important role in the photosynthesis and biosynthesis of cell wall components (Conklin and Barth 2004). In this study, GME was shown to be involved in metabolic pathways and was upregulated in the ray cell walls of *H. ammodendron* in Shihezi.

Tab. 3: Differentially expressed proteins in the plant hormone signal transduction pathway.

Protein ID	Mass	Mean Ratio	NCBI nr Description
KMT14924.1	24371.44	0.78	Somatic embryogenesis receptor kinase 1-like precursor [*Glycine max*]
KMT01268.1	56957.73	0.7	PREDICTED: probable serine/threonine-protein kinase At4g35230 [*Prunus mume*]
XP_010695172.1	54916.24	0.87	Kinase protein with tetratricopeptide repeat domain isoform 1 [*Theobroma cacao*]
XP_021754164.1	54688.02	1.11	Kinase protein with tetratricopeptide repeat domain isoform 1 [*Theobroma cacao*]
XP_021774662.1	57370.1	1.02	PREDICTED: probable serine/threonine-protein kinase At4g35230 [*Prunus mume*]
KMT19882.1	31419.18	0.98	Hypothetical protein VITISV_036640 [*Vitis vinifera*]
XP_021838893.1	31624.29	1.36	Xyloglucan endotransglycosylase/hydrolase 1

			[*Neolamarckia cadamba*]

Beta-1,4-glucanase, encoded by the KORRIGAN gene, is involved in cellulose biosynthesis (Szyjanowicz et al. 2004). However, little is known about the functions of KORRIGAN EGase (KOR). This study revealed that beta-1,4-glucanase participates in starch and sucrose metabolism and was upregulated in the ray cell walls of *H. ammodendron* in Shihezi.

In conclusion, during the process of ray cell wall biosynthesis in the xylem of *H. ammodendron*, it can be hypothesized that various proteins, including the predicted nonspecific lipid-transfer protein-like protein At5g64080-like (*Vitis vinifera*), the predicted probable nonspecific lipid-transfer protein AKCS9-like (*C. sinensis*) and beta expansin EXPB2.1 (*M. jalapa*), first cause cell wall loosening, extension and expansion, and xyloglucan endotransglycosylase/hydrolase 1 then cleaves and links xyloglucan chains. Subsequently, photosystem I P700 apoprotein A1, reversibly glycosylated polypeptide 1 and GDP-mannose-3′,5′-epimerase are involved in cellulose, hemicellulose and pectin biosynthesis in the cell wall by providing components or energy. Finally, the proteins involved in phenylpropanoid biosynthesis promote the lignification of ray cell walls and complete the biosynthetic process of cell walls.

Notably, this study revealed that the upregulated proteins corresponded to a significantly increased ray cell wall thickness. The regulatory proteins or genes related to thickening of the ray cell walls in *H. ammodendron* can be further explored to determine their functions, and the genes can be applied to the improvement of timber plantations, which is important for both identifying the effect of a specific xylem component on the environment and improving the mechanical properties of wood in timber plantations.

CONCLUSIONS

(1) The wall thicknesses of ray cells of *H. ammodendron* in Jinghe and Shihezi were 2.85 ± 0.42 μm and 3.08 ± 0.44 μm, respectively ($p < 0.01$). *(2)* During the process of ray cell wall biosynthesis in the xylem of *H. ammodendron*, it can be assumed that nonspecific lipid-transfer protein-like proteins and beta expansin EXPB2.1 (*Mirabilis jalapa*) first loosen the cell wall, and this step is followed by extension and expansion. Subsequently, xyloglucan endotransglycosylase/hydrolase 1 cleaves and links the xyloglucan chains, and photosystem I P700 apoprotein A1, reversibly glycosylated polypeptide 1 and GDP- mannose-3′,5′-epimerase are then involved in cellulose, hemicellulose and pectin biosynthesis in the cell wall by providing components or energy. Finally, the proteins involved in phenylpropanoid biosynthesis promote lignification and complete the biosynthetic process of ray cell walls.

ACKNOWLEDGEMENTS

This study was funded by the National Natural Science Foundation of China (grant numbers 31500471 and 31660196).

REFERENCES

1. Alves, E., Angyalossy-Alfonso, V., 2002: Ecological trends in the wood anatomy of some Brazilian species. 2. Axial parenchyma, rays and fibres. IAWA Journal 23: 391–418.
2. Burton, R.A., Gidley, M.J., Fincher, G.B., 2010: Heterogeneity in the chemistry, structure and function of plant cell walls. Nature Chemical Biology 6: 724–732.
3. Carlquist, S., Grant, J.R., 2005: Wood anatomy of gentianaceae, tribe helieae, in relation to ecology, habit, systematics, and sample diameter. Brittonia 57: 276–291.
4. Conklin, P., Barth, C., 2004: Ascorbic acid, a familiar small molecule intertwined in the response of plants to ozone, pathogens and the onset of senescence. Plant Cell and Environment 27: 959–970.
5. Darley, C.P., Forrester, A.M., McQueen-Mason, S.J., 2001: The molecular basis of plant cell wall extension. Plant Molecular Biology 47: 179–195.
6. Fernandes, A.N., Thomas, L.H., Altaner, C.M., Callow, P., Forsyth, V.T., Apperley, D.C., Kennedy, C.J., Jarvis, M.C., 2011: Nanostructure of cellulose microfibrils in spruce wood. Proceedings of the National Academy of Sciences of the United States of America 108: E1195–E1203.
7. Fry, S.C., Smith, R.C., Renwick, K.F., Martin, D.J., Hodge, S.K., Matthews, K.J., 1992: Xyloglucan endotransglycosylase, a new wall-loosening enzyme activity from plants. Biochemcal Journal 282: 821–828.
8. Kende, H., Bradford, K.J., Brummell, D.A., Cho, H.T., Cosgrove, D.J., Fleming, A.J., Gehring, C., Lee, Y., McQueen-Mason, S., Rose, J.K.C., Voesenek, A.C.J., 2004: Nomenclature for members of the expansin superfamily of genes and proteins. Plant Molecular Biology 55: 311–314.
9. Ma, L.C., Wang, Y.R., Liu, W.X., Liu, Z.P., 2014: Overexpression of an alfalfa GDP-mannose 3, 5-epimerase gene enhances acid, drought and salt tolerance in transgenic *Arabidopsis* by increasing ascorbate accumulation. Biotechnology Letters 36: 2331–2341.
10. Nishitani, K., Tominaga, R., 1992: Endoxyloglucan transferase, a novel class of glycosyltransferase that catalyzes transfer of a segment of xyloglucan molecule to another xyloglucan molecule. Journal of Biological Chemistry 267: 21058–21064.
11. Park, Y.W., Baba, K., Furuta, Y., Iida, I., Sameshima, K., Arai, M., Hayashi, T., 2004: Enhancement of growth and cellulose accumulation by overexpression of xyloglucanase in poplar. FEBS Letters 564: 183–187.
12. Pear, J.R., Kawagoe, Y., Schreckengost, W.E., Delmer, D.P., Stalker, D.M., 1996: Higher plants contain homologs of the bacterial celA genes encoding the catalytic subunit of cellulose synthase. Proceedings of the National Academy of Sciences of the United States of America 93: 12637–12642.
13. Plavcová, L., Jansen, S., 2015: The role of xylem parenchyma in the storage and utilization of nonstructural carbohydrates (Chapter 8). In: Functional and Ecological Xylem Anatomy (ed Hacke, U.). Pp 209- 234, Cham, Springer.
14. Saxena, I.M., Brown, R.M.Jr., 1999: Are the reversibly glycosylated polypeptides implicated in plant cell wall biosynthesis non-processive β-glycosyltransferases? Trends

Plant Science 4: 6–7.
15. Siow, R-S., Teoh, S., Teo, S-S., Shukor, M.Y. bin Abd, Phang, S-M., Ho, C-L., 2013: Molecular cloning and characterization of GDP-mannose-3′,5′-epimerase from *Gracilaria changii*. Journal of Applied Phycology 25: 1309–1318.
16. Smirnoff, N., Wheeler, G.L., 2000: Ascorbic acid in plants: biosynthesis and function. Critical Reviews in plant Sciences 35: 291–314.
17. Sulova, Z., Takacova, M., Steele, N.M., Fry, S.C., Farkas, V., 1998: Xyloglucan endotransglycosylase: evidence for the existence of a relatively stable glycosyl-enzyme intermediate. Biochemcal Journal 330: 1475–1480.
18. Suzuki, S., Li, L., Sun, Y.H., Chiang, V.L., 2006: The cellulose synthase gene superfamily and biochemical functions of xylem-specific cellulose synthase-like genes in *Populus trichocarpa*. Plant Physiology 142: 1233–1245.
19. Szyjanowicz, P.M.J., McKinnon, I., Taylor, N.G., Gardiner, J., Jarvis, M.C., Turner, S.R., 2004: The irregular xylem 2 mutant is an allele of korrigan that affects the secondary cell wall of *Arabidopsis thaliana*. Plant Journal 37: 730–740.
20. Taylor, N.G., Howells, R.M., Huttly, A.K., Vickers, K., Turner, S.R., 2003: Interactions among three distinct CesA proteins essential for cellulose synthesis. Proceedings of the National Academy of Sciences of the United States of America 100: 1450–1455.
21. Wolucka, B., Van Montagu, M., 2003: GDP-mannose 3', 5'-epimerase forms GDP-L-gulose, a putative intermediate for the de novo biosynthesis of vitamin C in plants. Journal of Biological Chemistry 278: 47483–47490.
22. Xi, E.H., 2018: Dynamic relationship between mechanical properties and chemical composition distribution of wood cell walls. Wood Research 63: 179–192.
23. Xu, W., Campbell, P., Vargheese, A.K., Braam, J., 1996: The Arabidopsis XET-related gene family: environmental and hormonal regulation of expression. Plant Journal 9: 879–889.
24. Yeats, T.H., Rose, J.K.C., 2008: The biochemistry and biology of extracellular plant lipid-transfer proteins (LTPs). Protein Science 17: 191–198.
25. Zhou, C.B., Gong, W., 2017: Effect of provenance and climate on xylem anatomy of *Haloxylon ammodendron* (C.A. Mey) bunge in the Gurbantunggut desert, China. Applied Ecology and Environmental Research 15: 1309–1321.
26. Zhou, X.Q., Wang, Y.R., Wang, L., Lv, J.X., Zhao, R.J., Yao, L.H., Chen, Z.J., 2017: Cell wall structure and mechanical properties of *Salix psammophila*. Wood Research 62: 1–12.

CHAOBIN ZHOU
ZUNYI NORMAL COLLEGE
INSTITUTE OF BIOLOGY AND AGRICULTURE SCIENCE & TECHNOLOGY
PINGAN ROAD, XINPU NEW DEVELOPMENT ZONE, ZUNYI CITY
GUIZHOU PROVICE
563006 CHINA

JUNJIE DING
XINJIANG ACADEMY OF AGRICULTURAL AND RECLAMATION SCIENCE
SHIHEZI CITY, XINJIANG PROVICE
832000 CHINA

XIAOJING HU
XINJIANG AGRICULTURAL UNIVERSITY
URUMQI CITY, XINJIANG PROVICE
830000 CHINA

WEI GONG*
SICHUAN AGRICULTURAL UNIVERSITY
CHENGDU CITY, SICHUAN PROVICE
611130 CHINA
*Corresponding author: gongwei@sicau.edu.cn

WOOD RESEARCH doi.org/10.37763/wr.1336-4561/66.5.844858
e-ISSN 2729-8906
66(5): 2021 844-858 pp.

EXPERIMENTS AND RELIABILITY ANALYSIS ON FRAME-TO-SHEATHING JOINTS IN LIGHT WOOD FRAMED SHEAR WALLS

HONGLIANG ZUO, JING DI
NORTHEAST FORESTRY UNIVERSITY
CHINA

(RECEIVED DECEMBER 2020)

ABSTRACT

To exploit the spruce-pine-fir (SPF) panel and the parallel strand bamboo (PSB) panel used in light wood framed shear wall and investigate the lateral behaviors of frame-to-sheathing joints in light wood framed shear wall with different characteristics, the experimental investigation and reliability analysis were carried out under monotonic load. The test configurations included joints with perpendicular-to-framing-grain load or parallel-to-framing-grain load, with SPF sheathing panel or PSB sheathing panel and with nail or screw. The results suggested that nailed joints with PSB panel occurred ductile failure but other joints occurred brittle failure. Moreover, the ultimate bearing capacity and the elastic stiffness of the joints under perpendicular load were higher than that of the joints under parallel load. The use of PSB panel and screw increased the ultimate bearing capacity of the joints. Furthermore, based on Johansen yield theory and experimental results, the reliability analysis was carried out through first-order reliability methods. The results showed that the SPF-nail joints, the PSB-nail joints, and PSB-screw joints achieved the reliability requirements.

KEYWORDS: Frame-to-sheathing joint, monotonic load test, lateral performance, reliability analysis, light wood framed shear wall.

INTRODUCTION

Light wood frame construction is widely used due to its advantages of better seismic performance and construction flexibility (Dobrila and Premrov 2003). Light wood framed shear walls are the primary components of light wood structural systems, which mainly resist the lateral forces from earthquakes and wind loads (Guíñez et al. 2019, Seim et al. 2016). Generally, a light wood framed shear wall is composed of a timber frame that is sheathed with panels using fasteners. The lateral force resistance performance of the wall mainly depends on the skin effect of the sheathing panels, which is due to the fastened joints between the sheathing panels and

bottom plates, studs respectively (Tekic et al. 2019). Accordingly, the frame-to-sheathing joints have a significant influence on the load carrying capacity and over all structural performance of the light wood framed shear walls (Dorn et al. 2013, Sartori and Tomasi 2013).

The joints in light wood framed shear walls with different sheathing like ply-woods, OSBs and GFBs have been considered in the past studies (Casagrande et al. 2020, Hassanieh and Valipour 2020). Recently there has been a renewed interest in using bamboo in light wood frame construction, and their results indicated that bamboo-based panel can be used as construction elements (Varela et al. 2013, Wang et al. 2017). Zhi Li et al. (2015) investigated the mechanical models and capacity equations for nail connectors used in light wood framed shear walls with cross-prefabricated ply-bamboo sheathing panels. The equations to predict the bearing capacity of timber-bamboo nail joints was obtained from the theoretical and experimental study. So far, most of the experiments have mainly focused on frame-to-sheathing nailed joints (Liu et al. 2018, Jockwer et al. 2018, Judd and Fonseca 2005), and less attention has been paid to the joints with screws and other sheathing panels. Parallel strand bamboo (PSB) is a potential building material which integrating social, economic and ecological benefits. It is well known as bio-composites which was made from original bamboos and shaped through complex processes (Guo et al. 2018, Wang et al. 2019). Furthermore, spruce-pine-fir (SPF) has been used by humanity for thousands of years because this natural fiber material meets the requirements of structural application, in terms of high ratio of strength to weight, low production cost, and ease of manufacturing (Dias et al. 2018, Sartori and Tomasi 2013, Bader et al. 2018). But, the PSB panel and the SPF panel has not well been exploited and utilized in light wood framed structure.

Thus, to effectively use PSB panels and SPF panels as sheathing panels in light wood frame structures, a new type of end narrow panels reinforced light wood frame shear wall was considered, which was intend to improve the lateral performance of walls by setting PSB sheathing panels or SPF sheathing panels at the ends of the wall. Existing studies clearly revealed that the behavior of a wall is mostly governed by the performance of frame-to-sheathing joints (Li et al. 2015). Therefore, the performances of the joints between different panels and framing elements were experimental studied under various conditions in this paper. Since PSB sheathing panels are relatively hard compared with conventional sheathing panels, proper fastener should be studied first. Based on constructability with conventional carpentry, common nails and screws were selected as the connectors between sheathing panels and framing elements. In order to obtain the design value of bending yield moment of the fasteners, the three-points bending tests were conducted. Moreover, the lateral performance of frame-to-sheathing joints was investigated by monotonic tests. This study offers a theoretical and experimental support for the application of PSB panels and SPF panels in light wood framed shear walls.

The goal of the research presented in this paper was to experimentally characterize the mechanical behavior, in terms of bearing capacity and stiffness, of frame-to-sheathing joints in light wood frame shear walls. In order to the reliability analysis of frame-to-sheathing joints, the experimental data obtained in this research were necessary to compare with design values obtained from Eurocode 5 (2004). Reliability index of the strength limit state of such joints were computed by first-order reliability methods. The application and design suggestions of the joints with different characteristics in light wood framed shear wall were discussed.

MATERIAL AND METHODS

Material specifications

The material and specifications used in the test joints were selected according to GB50005 (2017) and ASTM D1761 (2012). The details of the specimens are shown in Tab. 1. For this study, spruce-pine-fir (SPF) had a density of 420 kg·m^{-3} and parallel strand bamboo (PSB) with a density of 1100 kg·m^{-3}. The moisture content of the SPF and PSB were 13% and 6% respectively during the tests.

Tab. 1: Material specifications of the test wall.

Element	Material	Specifications
Framing	SPF	Cross-sectional dimensions: 38 mm × 89 mm
Sheathing panel	PSB	b = 100 mm, h = 300 mm, t = 10 mm
	SPF	b = 100 mm, h = 300 mm, t = 10 mm
Fastener	Nail	d_n =2.5 mm, l =50 mm
	Screw	d_e =2.5 mm, l =50 mm

Notes: b- width; h- height; t- thickness; l- length of a fastener; d_n- diameter of a nail; d_e- effective diameter of a screw; SPF - spruce, pine, fir; PSB- parallel strand bamboo.

Specimen design and fabrication

The parameters of the test joints are shown in Tab. 2, in this research, 80 specimens were manufactured and tested to investigate the behavior of the frame-to-sheathing joints considering the following aspects: *(1)* loading direction, *(2)* sheathing panel type, and *(3)* fastener type. Two different loading types of frame-to-sheathing joints were tested under monotonic loads: representative of bottom plate to sheathing and stud to sheathing joints, joints loading perpendicular to timber grain direction of SPF frame and parallel to timber grain direction of SPF frame, respectively (Fig. 1). There was a predrilled hole in every joint at location on the fastener. The diameter of predrilled hole was 2.5mm.

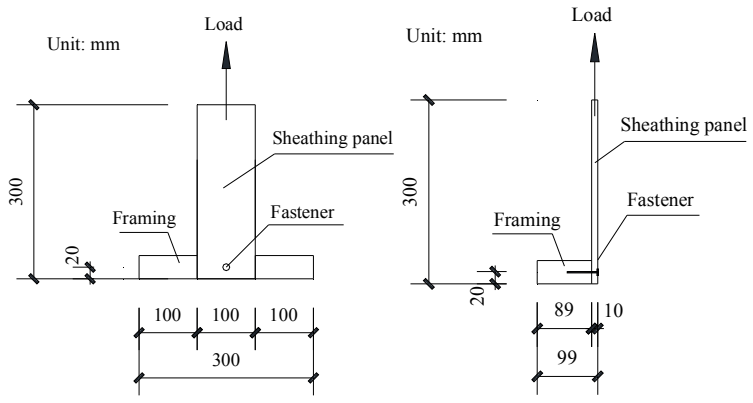

a)

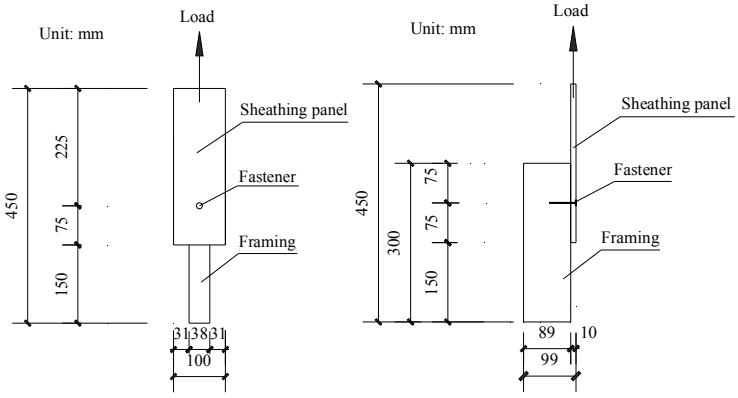

b)

Fig. 1: Details of the test specimens: (a) loading perpendicular to the grain of the framing, (b) loading parallel to the grain of the framing.

Tab. 2: Test matrix of the test.

Loading direction	Test group	Sheathing panel type	Fastener type	Number of tests
Perpendicular	CSN	SPF panel	Nail	10
	CSS		Screw	10
	CPN	PSB panel	Nail	10
	CPS		Screw	10
Parallel	PSN	SPF panel	Nail	10
	PSS		Screw	10
	PPN	PSB panel	Nail	10
	PPS		Screw	10

Experimental testing procedure

Bending yield moment of fasteners were tested according to ASTM F1575-03 (2013). The load was applied to the nail at the center between the two bearing points, and the rate of loading was 6.25 mm·min^{-1}.

The steel jigs used for frame-to-sheathing joints are shown in Fig. 2. Monotonic lateral tests of joints were performed under deformation control with a loading rate of 2.54 mm·min^{-1} for nail joints in accordance with the ASTM D1761 (2012).

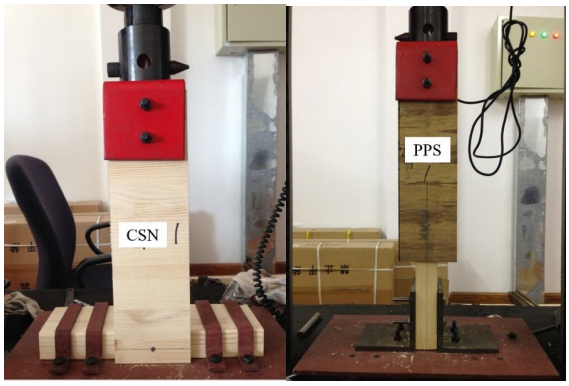

a) *b)*

Fig. 2: Experimental setup of the joints: (a) loading perpendicular to the grain of the framing, (b) loading parallel to the grain of the framing.

Several parameters were obtained and calculated from the tests. The ultimate bearing capacity P_{max} and the corresponding displacement Δ_{Pmax} were obtained from tests. According to the load-displacement curve, it can be seen that the load-displacement curve of joints at the initial stage of loading was greatly affected by the loading direction, so the elastic stiffness was defined as Eq. 1:

$$K_e = \frac{0.4P_{max} - 0.2P_{max}}{\Delta_{0.4P_{max}} - \Delta_{0.2P_{max}}} \quad (N \cdot mm^{-1}) \tag{1}$$

Reliability analysis model

The reliability analysis carried out in this study used first-order reliability methods (FORM) (Folz et al. 1989). To determine the reliability index and the failure probability, the failure of the joint is defined by the limit-state function as follows:

$$Z = g(\mathbf{x}) \tag{2}$$

where: x denotes the vector of random variables.

Eq. 2 separates the failure domain from the safe domain (Nikolaidis et al. 2004, Zhang et al. 2018) as shown in Fig. 3.

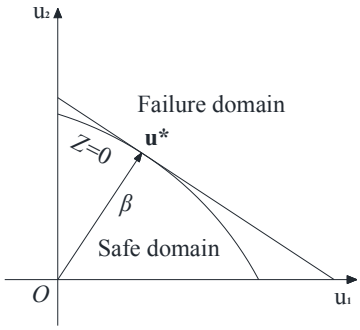

Fig. 3: FORM approximations for a component problem.

The failure probability of joints can be expressed as follows:

$$P_f = \int_{g(\mathbf{x})\le 0} g(\mathbf{x})d\mathbf{x} = \Phi(-\beta) = 1 - \Phi(\beta) \tag{3}$$

(5)

The reliability index of joints can be expressed as follows:

$$\beta = \frac{\mu_z}{\sigma_z} = \frac{g(\mathbf{u}^*) + \sum_{i=1}^{n} \frac{\partial g(\mathbf{u}^*)}{\partial x_i}(\mu_{x_i} - u_i^*)}{\sqrt{\sum_{i=1}^{n} \left[\frac{\partial g(\mathbf{u}^*)}{\partial x_i}\right]^2 \sigma^2_{x_i}}} \tag{4}$$

where: u^* is located on the limit-state surface, and has minimum distance from the origin in the standard normal space.

Due to the maximum load carrying capacity of joints are mostly governed by the bending performance of fasteners, and the large variability in the mechanical properties of wood and bamboo, the analysis main focus on the fastener element. Therefore, the limit-state function is written as:

$$Z = g(\mathbf{x}) = R_{test} - R_{theory} \tag{5}$$

where: $x = \{R_{test}, M_{y,d}\}^T$ is the vector of random variables, $M_{y,d}$ is the design value of bending yield moment of fasteners, R_{test} is the ultimate bearing capacity of joints, R_{theory} is the bearing capacity of joints calculated according to Eurocode 5.

In the absence of large set of experimental data, a normal distribution for maximum load carrying capacity of the joints and bending yield moment of the fasteners were assumed (Shadravan and Ramseyer 2018, Dobrila and Premrov 2003). Durations of load effects were not included in the calibration procedure for the system modification factor.

Design value of bending yield moment of fastener

The characteristic value of bending yield moment of fasteners was calculated according to:

$$M_{y,k} = \mu - 1.645\sigma \qquad (\text{N·mm}) \tag{6}$$

where: μ is the mean of bending yield moment for fastener obtained from tests, σ is the standard deviation of bending moment for fastener.

The design value of bending yield moment of fasteners was calculated according to Eq. 7:

$$M_{y,d} = \frac{M_{y,k}}{\gamma_M} \qquad (\text{N·mm}) \tag{7}$$

where: γ_M is the partial factor for fastener, according to Eurocode 5 (2004) γ_M =1.3.

The characteristic value and design value of bending yield moment for each group of fasteners are provided in Tab. 3.

Tab. 3: The characteristic value and design value of the fasteners.

Common nail				**Screw**			
μ (N·mm)	σ (N·mm)	$M_{y,k}$ (N·mm)	$M_{y,d}$ (N·mm)	μ (N·mm)	σ (N·mm)	$M_{y,k}$ (N·mm)	$M_{y,d}$ (N·mm)
2232.66	116.25	2041.42	1570.33	4909.67	277.64	4452.96	3425.35

Design formulas for joint

In accordance with the observations obtained by the research reported in this paper, the failure can be classified into brittle and ductile failure modes. All of joints, except the nailed joints with PSB sheathing panel, were brittle failure modes. The nailed joints with PSB sheathing panel were ductile failure modes. Base on the Johansen theory, the joints occurred brittle failure according to the failure mode ‘‘d’’. Instead, the specimens occurred ductile failure according to the failure mode “ f “.

For the test joints occurred brittle failure mode the characteristic load carrying capacity according to Eurocode 5 (2004) was calculated as:

$$R_{\text{theory,k}} = 1.05\frac{f_{\text{h1,k}} t_1 d_e}{2+\beta_h}\left[\sqrt{2\beta_h(1+\beta_h)+\frac{4\beta_h(2+\beta_h)M_{\text{y,Rk}}}{f_{\text{h1,k}} t_1^{\,2} d_e}}-\beta_h\right]+\frac{F_{\text{ax,Rk}}}{4} \quad \text{(N)} \quad (8)$$

where: t_1 is the thickness of the sheathing panel, $f_{\text{hi,k}}$ is the characteristic embedment strength in timber member i, d_e is the effective diameter of fastener, $M_{\text{y.Rk}}$ is the characteristic fastener yield moment, β_h is the ratio between the embedment strength, $\beta_h = f_{\text{h2,k}}/f_{\text{h1,k}}$, $F_{\text{ax,Rk}}$ is the characteristic axial withdrawal capacity of the fastener.

For the test joints occurred ductile failure mode the characteristic load carrying capacity according to Eurocode 5 (2004) was calculated as:

$$R_{\text{theory,k}} = 1.15\sqrt{\frac{2\beta_h}{1+\beta_h}}\sqrt{2M_{\text{y,Rk}} f_{\text{h1,k}} d_e}+\frac{F_{\text{ax,Rk}}}{4} \quad \text{(N)} \quad (9)$$

The characteristic embedding strength for the SPF timber with predrilled hole was calculated according to Eurocode 5 (2004) as follows:

$$f_{\text{hs}} = 0.082\left(1-0.01 d_{\text{e}}\right)\rho_{\text{k}} \quad (\text{N}\cdot\text{mm}^{-2}) \quad (10)$$

where: ρ_{k} is density of the timber, ρ_{k} =420 kg.m^{-3}.

The characteristic embedding strength for the PSB sheathing was calculated according to Eurocode 5 (2004) as follows:

$$f_{\text{hp}} = 30 d_{\text{e}}^{-0.3} t^{0.6} \quad (\text{N}\cdot\text{mm}^{-2}) \quad (11)$$

where: t is thickness of the PSB sheathing panel.

The characteristic withdrawal capacity of the common nail was calculated according to Eurocode 5 (2004) as follows:

$$F_{ax,Rnk} = \begin{cases} f_{ax,k} dt_{pen} \\ f_{ax,k} dt + f_{head,k} d_h^{\,2} \end{cases} \quad (N) \tag{12}$$

$$f_{ax,n} = 20 \times 10^{-6} \rho_k^{\,2} \quad (N \cdot mm^{-2}) \tag{13}$$

$$f_{head,n} = 70 \times 10^{-6} \rho_k^{\,2} \quad (N \cdot mm^{-2}) \tag{14}$$

where: $f_{ax,n}$ is the characteristic pointside withdrawal strength, $f_{head,n}$ is the characteristic heads pull-through strength, d is the nail diameter, t_{pen} is the pointside penetration length or the length of the threaded part in the pointside member, t is panel thickness, d_h is the nail head diameter.

The characteristic withdrawal capacity for the screw was calculated according to Eurocode 5 (2004) as follows:

$$F_{ax,Rsk} = f_{ax,k} d_e l_{ef} k_d \quad (N) \tag{15}$$

$$f_{ax,k} = 0.52 d_e^{\,-0.5} l_{ef}^{\,-0.1} \rho_k^{\,0.8} \quad (N \cdot mm^{-2}) \tag{16}$$

$$k_d = min \begin{cases} \frac{d_e}{8} \\ 1 \end{cases} \tag{17}$$

where: $f_{ax,k}$ is the characteristic withdrawal strength perpendicular to the grain, d_e is the effective diameter of screw, l_{ef} is the penetration length of the threaded part.

The characteristic value and design value of elements in joints were calculated according to Eurocode 5 (2004) and the results are given in Tab. 4. The calculated data were used in the subsequent reliability analysis.

Tab. 4: Calculated results of joints.

	Embedding strength ($N \cdot mm^{-2}$)		**Withdraw strength** (N)		**Lateral load capacity of joints** (N)			
	SPF	PSB	Nail	Screw	SPF-nail	PSB-nail	SPF-screw	PSB-screw
Characteristic value	33.579	90.728	352.800	743.183	528.614	901.643	768.341	1062.567
Design value	25.830	69.790	271.385	571.679	436.299	693.562	644.560	865.555

RESULTS AND DISCUSSION

Failure modes

The ultimate failure modes of the joint between SPF sheathing and SPF frame are shown in Fig. 4. The ultimate failure modes of the joint between PSB sheathing and SPF frame are shown in Fig. 5. There were two ultimate failure modes of joints with SPF panel in monotonic tests: *(1)* bending of fastener and *(2)* brittle failure of SPF sheathing panel. On the other hand, there were

three ultimate failure modes of joints with PSB sheathing in monotonic tests: *(1)* nail yielding followed by withdrawal of nail from the wood member, and *(2)* brittle failure of screw. The main damage patterns of joints with SPF panel was brittle failure of SPF sheathing panel, whereas, in joints with PSB panel, was failure of fastener.

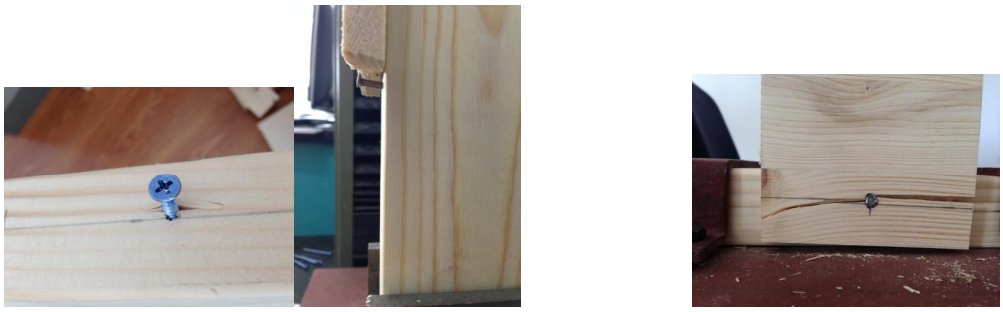

a) *b)*

Fig. 4: Failure modes of the joints with SPF sheathing: (a) bending of fastener, (b) brittle failure of SPF sheathing panel.

a) *b)*

Fig. 5: Failure modes of the joints with PSB sheathing: (a) bending of fastener, (b) brittle failure of screw.

Load-displacement relationships

The average curves for different joints were obtained and compared in Fig. 6. According to Fig. 6, the curves under the parallel load test had obvious horizontal section. This is due to the weak shear resistance between the framing fibers parallel to grain, resulting in the slippage of the fasteners parallel to grain (Li et al. 2015). The fiber grain direction perpendicular to the load direction can better limit the displacement of the fastener, so the load displacement curve under the vertical load test had no horizontal section.

The joints with SPF sheathing panel had relatively low level of strength and stiffness, and after reaching the force peak value at a displacement level of 8-12 mm, a sudden impairment of strength was observed due to the tear of the SPF sheathing panel. Even though the experimental results showed good performance in terms of the strength and stiffness of screwed joints with PSB sheathing panel, the ductility properties of this joint seem very poor. In the case of nailed joints with PSB sheathing panel, the strength capacity was lower than screwed one, but shown a more ductile behavior.

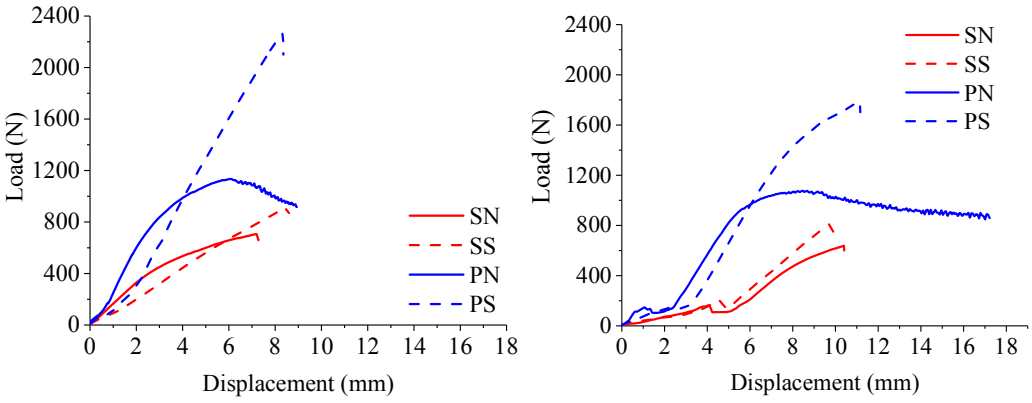

Fig. 6: Load-displacement curves of the test specimens: (a) perpendicular test, (b) parallel test.

The mean, standard deviation, and coefficient of variation of the parameters for each group of joints are shown in Tab. 5. The following discussion presents the major conclusions, which can be drawn based on the results of Tab. 5.

Tab. 5: Parameters of the lateral behavior of the joints.

	P_{max} (N)			Δ_{Pmax} (mm)			K_e (N·mm^{-1})		
	Mean	SD	CoV (%)	Mean	SD	CoV (%)	Mean	SD	CoV (%)
CSN	702.64	139.28	19.82	7.28	1.39	19.09	171.90	29.57	17.20
CPN	1204.59	205.20	17.04	6.94	1.21	17.44	361.86	81.37	22.48
CSS	900.98	174.37	19.35	8.42	1.51	17.93	139.36	26.30	18.88
CPS	2264.54	369.43	16.31	8.34	1.30	15.59	333.29	45.85	13.76
PSN	633.64	125.01	19.73	10.39	2.40	23.10	123.79	10.93	8.83
PPN	1026.95	159.79	15.56	8.68	1.54	17.74	263.56	49.27	18.69
PSS	805.26	141.59	17.58	9.70	1.63	16.80	136.86	25.89	18.92
PPS	1782.53	321.59	18.04	11.16	1.76	15.77	290.83	57.11	19.63

Effects of the loading direction

According to Tab. 5, the loading direction had a significant effect on the monotonic lateral behaviors of the joints. In contrast, the bearing capacity of the joints under perpendicular load was significantly higher than that under parallel load, which is due to the full utilization of the compressive strength perpendicular to grain of the framing element under the perpendicular load. Under the parallel load, the fastener exerts a concentrated force on the surrounding wood fibers parallel to grain to make it tear, resulting in less resistance. Due to the large slip of the fastener under the parallel load, the displacement at the ultimate bearing capacity and the elastic stiffness of the joints under the parallel load were higher than those under the perpendicular load.

Effects of the panel type

Compared with the joints with the SPF sheathing panel, the bearing capacities of the joints with the PSB sheathing panel were significantly increased. The ultimate bearing capacity of

the joints with PSB panel was 62% -150% higher than that of the joints with PSB panel, which is because the compressive strength and tensile strength of SPF panel are significantly higher than those of SPF panel. The fasteners in the joints with PSB panel can give full play to their bending and shear strength, so that the damage of the joints with PSB panel is ultimately the damage of the fastener. However, since the tearing of the SPF panel precedes the bending of the fasteners, the mechanical properties of the fasteners in the joints with SPF panel cannot be fully utilized. The elastic stiffness of the joints with PSB panel was 110% higher than that of the joints with SPF panel. This is because the density and hardness of PSB panel are significantly higher than that of SPF panel, and the contact between PSB panel and the fastener is rigid. Due to the small stiffness and large deformation of SPF panel, the elastic stiffness of the joints with SPF panel was relatively small. Accordingly, it could be observed that the improvements of the lateral behavior of the frame-to-sheathing joints increased with the use of PSB sheathing panel. This is attributed to the fact that a greater material performance of PSB panel leads to all materials into full play.

Effects of the fastener type

The conclusion can be obtained that the bearing capacity of the screwed joints was higher than that of nailed joints. In the joints with PSB panel, the ultimate bearing capacity of joints using nail was increased by 87% by using screw. In the joints with SPF panel, the use of screw increased the ultimate bearing capacity of joints using nail by approximately 28%. The reason is that the bending strength of screw is higher than that of nail. On the other hand, there was a correlation between the enhancement effect of the screw on the joint and the panel performance. Among the screwed joints, the improvements of the bearing capacity for the screwed joints with the PSB sheathing panel were more remarkable than those of the screwed joints with the SPF sheathing panel. Because the bending strength and stiffness of the two types of fastener are similar, the type of fastener had little influence on the elastic stiffness of the joints, which was about 10%. Moreover, the elastic stiffness of the screwed joints was slightly lower than that of the nailed joints in perpendicular tests, whereas in parallel tests, screwed joints showed higher elastic stiffness. The primary reason for this effect is that the bending capacity and the withdraw capacity of the screws significantly higher than that of the nails.

Evaluation of lateral performance

The reliability index and the failure probability of joints were calculated and the results are given in Tab. 6. The comparison of the reliability index for joints are shown in Fig. 7.

Tab. 6: Reliability index and failure probability of joints.

	CSN	CPN	CSS	CPS	PSN	PPN	PSS	PPS
β	1.8968	2.4839	1.4504	3.0823	1.5608	2.0733	1.1095	2.3006
P_f	0.0289	0.0065	0.0735	0.0010	0.0593	0.0191	0.1336	0.0107

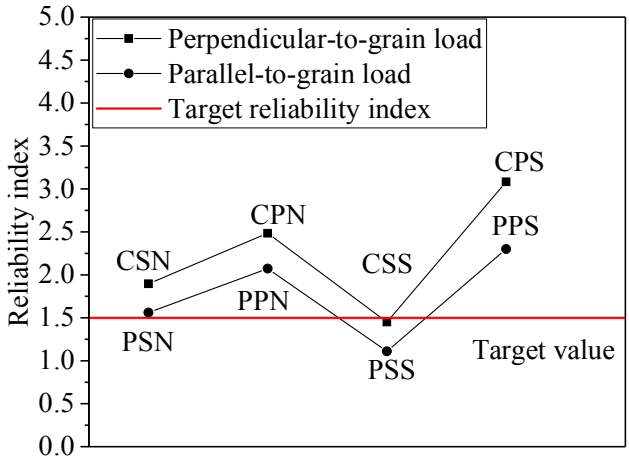

Fig. 7: Reliability index of joints.

Based on the calculated reliability index the influence of the varied parameters can be evaluated. According to the results and observations from Tab. 6, higher reliability index, which means lower failure probability, were achieved for the joint occurred ductile failure. The reliability index of the joints occurred brittle failure in perpendicular tests was higher than that in parallel tests. The primary reason for this is the influence of the loading direction on the lateral performance of the joints is not considered in the design. In addition, the joints under the parallel load generally only play the role of transfer, not the main lateral-bearing part. The joints under the perpendicular load are the main lateral-bearing elements in the light wood framed shear wall. Therefore, the reliability index of joints under perpendicular load should achieve the safety requirements. Since the light wood framed shear wall is composed of many joints, too low reliability index will lead to insecurity of the structure, while too high reliability index will lead to waste of materials and brittle failure. Generally, the reliability index of joints is within the range of β = 1.5 to β = 2.0 (Smardzewski 2009, Schick and Seim 2019). However, the reliability index of the new type joints is within the range of β = 1.11 to β = 3.08. It is suggested that although the lateral design value can calculate according to the Eurocode 5 (2004), the design methods still need further study and modify to achieve the specific reliability level. The target reliability index β = 1.50 was adopted for the assessment of probabilistic results in order to verify the applicability of design method.

By comparing the reliability index obtained from the calculation with β = 1.5, it can be concluded that the lateral strength design values of the joints obtained by the Eurocode design method can meet the minimum reliability requirements, except the SPF-screw joints. In addition, the reliability index of the joints with PSB panel was significantly higher than that of the joints with SPF panel. Therefore, it is recommended to use PSB-screw joints in structures with high reliability and strength requirements. Because the SPF panel has a higher strength-to-weight ratio and lower cost than PSB panel, SPF-nail joints can be used in non-important parts of the structure, which can not only provide resistance, but also reduce the self-weight of the structure to reduce the earthquake effects.

CONCLUSIONS

Experimental investigation and reliability analysis were conducted in order to study the influencing factors on the lateral performance of frame-to-sheathing joints under monotonic load, including those of loading direction, sheathing panel type and fastener type. The experimental results of the 80 frame-to-sheathing joints were reported and discussed. Additionally, the bending experiments of fasteners were conducted in order to obtain the design value of bending yield moment. Moreover, the reliability analysis used first-order reliability methods of the joints was developed for further studies. At last, the practical application suggestions of different joints were provided. Based on the results of these studies, the following conclusions can be stated: *(1)* Based on the experimental data and reliability analysis, the results suggested that the joints with PSB sheathing panel can be applied in light wood framed shear wall as mainly bearing elements. The joints with SPF sheathing panel can be applied in light wood framed shear wall as non-important parts of the light wood framed shear wall. *(2)* Based on the Johansen yield theory and reliability analysis, the reliability index of the joints in perpendicular tests was higher than that in parallel tests. The reliability index of joints with PSB panel was higher than that with SPF panel. The reliability index of lateral design value of joints calculated by Eurocode is within the range of 1.11 to 3.08. The reliability index of joints under perpendicular load met the minimum reliability requirements, except the SPF-screw joints. In order to meet the specific requirements of structural design code, the further modifications of the design method of the frame-to-sheathing joints with different sheathing panel are necessary. *(3)* The lateral capacity and the elastic stiffness of the frame-to-sheathing joints under perpendicular load were higher than those of the frame-to-sheathing joints under parallel load. The lateral capacity and the elastic stiffness of the frame-to-sheathing joints with PSB sheathing panel were higher than those of the frame-to-sheathing joints with SPF sheathing panel. The lateral capacity of the frame-to-sheathing screwed joints were higher than that of the frame-to-sheathing nailed joints. The type of fastener had little influence on the elastic stiffness of the joints period.

ACKNOWLEDGMENTS

The authors gratefully acknowledge the financial support provided by the Science Foundation of Heilongjiang Province (LH2020E009) and the Special Project for Double First-Class - Cultivation of Innovative Talents (000/41113102).

REFERENCES

1. ASTM D1761, 2012: Standard test methods for mechanical fasteners in wood.
2. ASTM F1575-03, 2013: Standard test method for determining bending yield moment of nails.

3. Bader, M., Nemeth, R., 2018: The effect of the relaxation time on the mechanical properties of longitudinally compressed wood. Wood Research 63(3): 383-98.
4. Folz, B., Foschi R.O., 1989: Reliability-based design of wood structural systems. Journal of Structural Engineering 115(7):1666-1680.
5. Casagrande, D., Bezzi, S., D'Arenzo, G., Schwendner, S., Polastri, A., Seim, W., Piazza, M., 2020: A methodology to determine the seismic low-cycle fatigue strength of timber connections. Construction and Building Materials 231: 117026-117045.
6. Dias, A.M.P.G., Kuhlmann, U., Kudla, K., Mönch, S., Dias, A.M.A., 2018: Performance of dowel-type fasteners and notches for hybrid timber structures. Engineering Structures 171: 40-46.
7. Dobrila, P., Premrov, M., 2003: Reinforcing methods for composite timber frame–fiberboard wall panels. Engineering Structures 25(11): 1369-1376.
8. Dorn, M., de Borst, K., Eberhardsteiner, J., 2013: Experiments on dowel-type timber connections. Engineering Structures 47: 67-80.
9. EN 1995-1-1, 2004: Eurocode 5: Design of timber structures. Part 1-1: General- Common rules and rules for buildings.
10. GB50010-2017, 2017: Code for design of timber structures.
11. Guíñez, F., Santa María, H., Almazán, J.L., 2019: Monotonic and cyclic behaviour of wood frame shear walls for mid-height timber buildings. Engineering Structures 189: 100-110.
12. Guo, Y., Shiliu, Z., Yuxia, Ch., Shengquanliu, Q., 2018: Contrastive analysis of screw withdrawal resistance between bamboo oriented strand board and conventional particleboard. Wood Research 63(6): 1071-80.
13. Jockwer, R., Fink, G., Köhler, J., 2018: Assessment of the failure behaviour and reliability of timber connections with multiple dowel-type fasteners. Engineering Structures 172: 76-84.
14. Judd, J.P., Fonseca, F.S., 2005: Analytical model for sheathing-to-framing connections in wood shear walls and diaphragms. Journal of Structural Engineering 131(2): 345-352.
15. Li, Z., Xiao, Y., Wang, R., Monti, G., 2015: Studies of nail connectors used in wood frame shear walls with ply-bamboo sheathing panels. Journal of Materials in Civil Engineering 27(7): 0401-4216.
16. Liu, Y., Xiong, H., Kang, J., 2018: Seismic evaluation of wood frame construction based on nail connection deflection status. Wood Research 63(6): 979-92.
17. Nikolaidis, E., Ghiocel, D.M., Singhal, S., 2004: Engineering design reliability handbook. CRC Press. Boca Raton, 289 pp.
18. Sartori, T., Tomasi, R., 2013: Experimental investigation on sheathing-to-framing connections in wood shear walls. Engineering Structures 56: 2197-2205.
19. Schick, M., Seim, W., 2019: Overstrength values for light frame timber wall elements based on reliability methods. Engineering Structures 185(11): 230-242.
20. Seim, W., Kramar, M., Pazlar, T., Vogt, T., 2016: OSB and GFB as sheathing materials for timber-framed shear walls: comparative study of seismic resistance. Journal of Structural Engineering 142(4).
21. Shadravan, S., Ramseyer, C.C., 2018: Investigation of wood shear walls subjected to lateral load. Structures 16: 82-96.

22. Smardzewski, J., 2009: The reliability of joints and cabinet furniture. Wood Research 54(1): 67-76.
23. Tekic, Z., Kozaric, L., Purcar, M.V., Lukic, S., 2019: Load-bearing capacity of metal connector plates depending on location and geometry of the nail. Wood Research 64(4): 677-90.
24. Varela, S., Correal, J., Yamin, L., Ramirez, F., 2013: Cyclic performance of glued laminated *Guadua* bamboo-sheathed shear walls. Journal of Structural Engineering 139(11): 2028-2037.
25. Wang, R., Xiao, Y., Li, Z., 2017: Lateral loading performance of lightweight GluBam shear walls. Journal of Structural Engineering 143(6).
26. Wang, X., Zhou, A., Chui, Y.H., 2019: Experimental investigation of mode II fracture properties of parallel strand bamboo composite by end notched flexure test. Bioresources 14(1): 1579-90.
27. Zhang, X., Shahnewaz, M., Tannert, T., 2018: Seismic reliability analysis of a timber steel hybrid system. Engineering Structures 167: 629-638.

HONGLIANG ZUO, JING DI*
NORTHEAST FORESTRY UNIVERSITY
SCHOOL OF CIVIL ENGINEERING
NO.26 HEXING ROAD
HARBIN
CHINA
*Corresponding author: djjy1118@outlook.com

WOOD RESEARCH doi.org/10.37763/wr.1336-4561/66.5.859874
e-ISSN 2729-8906
66(5): 2021 859-874 pp.

INTERNATIONAL COMPETITIVENESS OF THE FURNITURE MANUFACTURING – LESSON FROM THE SELECTED EU COUNTRIES

EMILIA GRZEGORZEWSKA
WARSAW UNIVERSITY OF LIFE SCIENCES - SGGW
POLAND

MARIANA SEDLIAČIKOVÁ
TECHNICAL UNIVERSITY IN ZVOLEN
SLOVAK REPUBLIC

DENIS JELAČIĆ
UNIVERSITY OF ZAGREB
CROATIA

(RECEIVED FEBRUARY 2021)

ABSTRACT

This study aims to compare and evaluate the international competitiveness of the furniture industry in the selected European Union (EU) countries using chosen result-oriented indicators. The results found that countries with the highest levels of international competitiveness of the furniture industry included Poland, Romania and Italy. In contrast, the comparative advantage of Germany, which is the largest furniture exporter in the EU, was not as significant. No comparative advantage in the furniture trade was observed in France and United Kingdom, which is confirmed by the negative values of the Relative Trade Advantage (RTA) index and by unfavorable values of the export specialization index. The results presented in the article expand the existing knowledge in the area of assessing the international competitiveness of the largest furniture exporters.

KEYWORDS: Furniture manufacturing, international competitiveness, result-oriented indicators, EU countries.

INTRODUCTION

The variety of approaches used to define and measure international competitiveness has so far resulted in the lack of a formalized theory of international competitiveness. In the empirical

literature there are many definitions of competitiveness that cover different levels of aggregation and various areas of activity (Ajitabh and Momaya 2004, Dima et al. 2018). Competitiveness can be looked at different levels: country level (Rabar and Cvek 2019), industry level (Buturac et al. 2018) and firm level (Ajitabh and Momaya 2004, Rugman and Oh 2008). While investigating the phenomenon of national competitiveness, the focus should not be on economy as a whole, but on certain industries and industrial segments (Cho and Moon 2000).

The complexity of the issues relating to competitiveness requires a variety of methods for assessment. Balassa (1979) index is one of the well-known result-oriented indicators in the literature and has been modified by many authors (Vollrath 1991, Laursen 2015). However, as emphasizes Sirgmets et al. (2019), indicators for competitiveness should be used in combination with other indicators to provide a complete assessment. Many studies using the result-oriented indicators to evaluate competitiveness of industries have been elaborated. This also applies to the forest-based sectors, including furniture industry.

The most cited study was elaborated by Han et al. (2009), who evaluated the competitiveness of Chinese wooden furniture against the background of selected countries. Based on this research it can be concluded that China has experienced a transition from comparative disadvantage into a high comparative advantage over the period and has maintained a strong position in this labor-intensive industry. However, it still falls behind traditionally strong competitors such as Italy and Germany in terms of quality and unit price. It is also experiencing a growing challenge from lower-income countries such as Poland and Vietnam. Studies to assess the market success and the competitiveness of wood-based industries were conducted among others by Zhang et al. (2012), Zhelev (2013), Klos and Fabisiak (2013), Bojnec and Fertő (2014), Barta and Kovats (2015), Kersan-Škabić (2014), Hajdúchová et. al. (2016), Sedliačiková et al. (2016), Vu et al. (2019) and Grzegorzewska et al. (2020).

China plays an important role in the international furniture trade (Han et al. 2009, Cao et al. 2004, Xiong et al. 2017). However, the furniture industry is also an important element of the EU economy, and the European Community plays a special role in the global furniture market. This is evidenced by the high position of certain EU countries in the world ranking of furniture manufacturers and exporters. According to the data from the International Trade Centre, in 2018, EU28 countries generated 37% of the global furniture exports value. Therefore, the main goal of the article was to conduct an analysis and assess the comparative advantages in the foreign trade in the furniture industry products of selected EU countries, to show changes taking place in this area, as well as to identify countries characterized by the smallest and the highest level of international competitiveness in furniture production. In addition, the article indicates the factors determining the level of international competitiveness of the furniture industry in selected EU countries and refers to the results of earlier empirical studies.

MATERIAL AND METHODS

The competitiveness research included a group of ten EU member states, which in 2018 were characterized by the largest share of the furniture export value in the value of the global export of these products. Germany, Italy, Poland, Czech Republic, Netherlands, France, United Kingdom, Spain, Denmark and Romania. In total, in 2018, these countries generated 29% of the global export value, which confirms their important role in the international trade in the furniture industry products. The years 2009-2018 were analyzed in the research. The primary source of the research material was the International Trade Centre database.

A review of the research concerning international competitiveness in the wood and furniture industry, as well as a theoretical overview of empirical studies on assessing competitiveness with regard to the forest industry conducted by Gordeev (2020) reveals that in the majority of the cases, result-oriented indicators were employed to evaluate the comparative advantages of the foreign trade. Due to the fact that indicators should be used in combination, to minimize the shortcomings of each single indicator. On the basis of the literature review a system of indicators evaluating the trade competitiveness of the sector and its commodities was adopted:

The Import Penetration Rate

The Import Penetration Rate (MP) compares the value of imports and the supply on the internal market. The MP indicator is recorded as follows (OECD 2011, Fronczek 2017):

$$MP = \frac{M}{Q - X + M} \tag{1}$$

where: M is import, X is export, and Q is production.

The Specialization Indicator

The Specialization Indicator (SI) is the relation between the share of a product (or products) in the export of country and the share of this product (or products) in the world export. The values above 1 suggest a specialization in export. This indicator takes the following form (Pawlak 2013):

$$SI_k = \frac{X_{ik}}{X_k} : \frac{X_{iw}}{X_w} \tag{2}$$

where: X_{ik} is export of product i in country k, X_k is total export of goods in country k, X_{iw} is export product i worldwide, and X_w is total export of goods worldwide.

The Coverage Ratio

The Coverage Ratio (CR), also known as Export/Import Coverage Ratio, is the relation between the value of export of a product (group of products) and the value of its import. The values above 100 mean export specialization of a product or group of products. This indicator CR takes the following form (Kubala and Firlej 2019):

$$CR_{ik} = \frac{X_{ik}}{M_{ik}} \cdot 100\% \quad (3)$$

where: X_{ik} is export of product *i* in country *k*, and M_{ik} is import of product i in country *k*.

The Relative Revealed Comparative Export Advantage Index

One of the modifications of the well-known RCA indicator is the Relative Revealed Comparative Export Advantage Index (XRCA) described by Eq. 4 (Pawlak 2013, Frohberg and Hartmann 1997). The XRCA indicator is the relation of two quotients. The first is the ratio of export of a product (or group of products) in the country k to the export of this product (or group of products) in the country m. The second is the ratio of total export of goods in both countries (excluding the analyzed product or group of products). Values above 1 mean a comparative advantage in the product category. In turn, the values below 1 suggest a comparative disadvantage (Pawlak 2013).

$$XRCA_{ik} = \frac{X_{ik}}{X_{im}} : \frac{\sum_{j,j\neq i} X_{jk}}{\sum_{f,f\neq i} X_{fm}} \quad (4)$$

where: *X* is export, *i*, *j* are product categories, and *k*, *m* are countries.

The Relative Import Penetration Index

The Relative Import Penetration Index (MRCA) is the relation of two quotients. The first is the ratio of import of a product (or group of products) in the country *k* to the imports of this product (or group of products) in the country *m*. The second is the ratio of total import of goods in both countries (excluding the analyzed product or group of products) (Pawlak 2013, Frohberg and Hartmann1997) (Eq. 5). The values of MRCA indicator below 1 indicate a comparative advantage. In turn, the values above 1 mean a comparative disadvantage.

$$MRCA_{ik} = \frac{M_{ik}}{M_{im}} : \frac{\sum_{j,j\neq i} M_{jk}}{\sum_{j,j\neq i} M_{jm}} \quad (5)$$

where: *M* is import, *i*, *j* are product categories, and *k*, *m* are countries.

The Relative Trade Advantage Index

The Relative Trade Advantage Index (RTA) is the difference between the XRCA and the MRCA (Pawlak 2013, Frohberg and Hartmann 1997):

$$RTA_{ik} = XRCA_{ik} - MRCA_{ik} \quad (6)$$

The positive values of RTA suggest a comparative advantage in each product (or group of products). While negative values indicate no competitive advantage (Pawlak 2013, Frohberg and Hartmann 1997).

RESULTS AND DISCUSSION

Data from the International Trade Centre confirmed that in 2009 Germany was the largest furniture exporter in the EU (Tab. 1). The export value of the furniture industry amounted to EUR 10.9 billion (Fig. 1a). This value represented 21.5% of the EU export (Tab. 2). Italy was second in the ranking of furniture exporters in the EU. The export value of the furniture industry products reached EUR 9.3 billion, which accounted for 18.2% of the EU export.

Tab. 1: Export, import and trade balance of the furniture industry in the selected EU countries for 2009 and 2018 (billion EUR).

Country	Export				Import				Trade balance	
	2009	2018	D*	V**	2009	2018	D	V	2009	2018
World	104.7	218.3	208.5	23.6	106.8	210.7	197.3	20.4	-2.1	7.6
EU28	50.9	83.8	164.6	16.5	48.5	80.7	166.4	14.7	2.4	3.1
Germany	10.9	15.8	145.0	11.4	11.2	18.4	164.3	16.3	-0.3	-2.6
Italy	9.3	12.4	133.3	9.8	2.4	3.6	150.0	11.5	6.9	8.8
Poland	5.6	12.6	225.0	26.5	1.3	3.3	253.8	24.6	4.3	9.3
Czech Republic	1.9	4.8	252.6	31.5	1.1	3.1	281.8	31.1	0.8	1.7
Netherlands	1.6	4.2	262.5	28.9	2.8	6.1	217.9	18.9	-1.2	-1.9
France	3.0	3.5	116.7	7.2	6.8	10.2	150.0	13.5	-3.8	-6.7
United Kingdom	1.7	3.4	200.0	25.3	6.3	10.0	158.7	8.7	-4.6	-6.6
Spain	1.9	3.2	168.4	22.7	2.6	4.1	157.7	17.1	-0.7	-0.9
Denmark	1.8	2.6	144.4	14.2	1.2	2.1	175.0	15.1	0.6	0.5
Romania	1.1	2.5	227.3	27.6	0.4	1.0	250.0	24.6	0.7	1.5

*D - dynamics (%), **V - coefficient of variation (%).

Poland was also a significant furniture exporter. In the next place among the furniture industry exporters was France. In 2009, the value of the furniture exports from this country was at the level of EUR 3.0 billion, which constituted 2.9% of the export value of this industry generated by all countries and 5.9% of the EU export. Among the EU countries, the aforementioned four countries played a particularly important role in generating the furniture trade value. In total they generated over 55% of export value. The export value of the furniture industry products of each of the remaining countries was below EUR 2.0 billion, and their share in creating the export value of the EU member states ranged from 2.1% (Romania) to 3.8% (Czech Republic).

In the years from 2009 to 2018, the global furniture industry exports more than doubled and amounted to EUR 218.3 billion at the end of the analyzed period. Of this amount, EUR 83.8 billion was generated in EU countries (64.6% more than in 2009), which constituted 38.4% of the world furniture export (Tab. 2).

Nevertheless, Italy and Germany, together with Poland were still at the forefront of the largest furniture exporters (Fig. 1a). Particularly noteworthy is the evident increase in the importance of the Czech furniture industry in this area, which resulted in its promotion from the 5th to 4th position in this ranking. In the studied period, the highest level of the coefficient of

variation of the furniture industry export value, which indicates the relative variability of this characteristic, was observed in Czech Republic (31.5%), and the smallest (below 10%) variation in the furniture export value took place in France (7.2%) and Italy (9.8%).

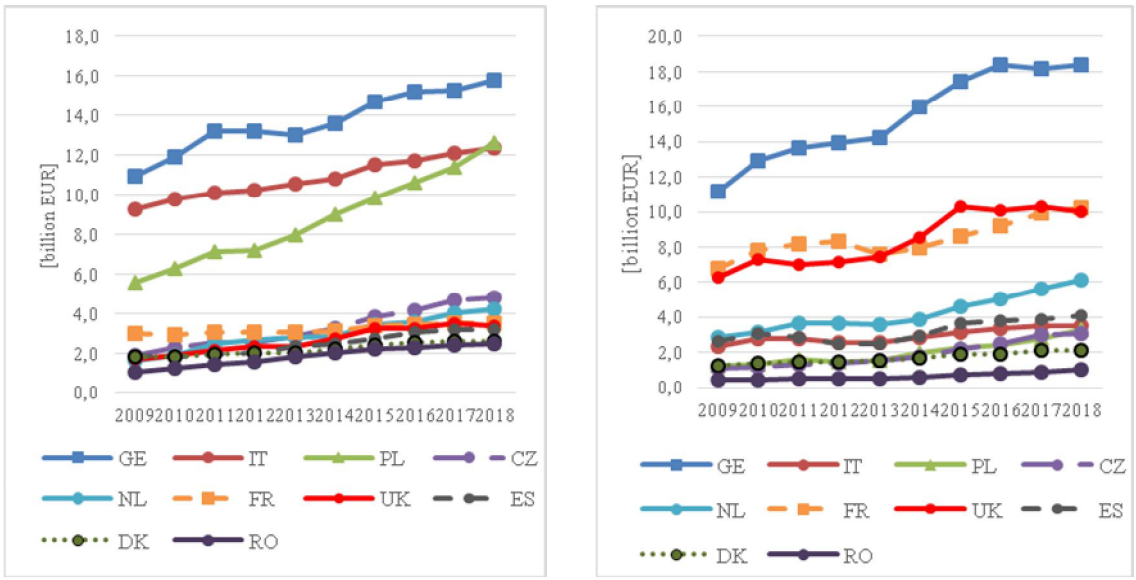

(a) *(b)*

Fig. 1: The changes in foreign trade of furniture industry in the selected EU countries for 2009-2018: (a) The furniture export value (billion EUR); (b) The furniture import value (billion EUR).

In 2009, the global furniture import was at the level of EUR 106.8 billion, marginally higher than the export, which caused a trade deficit in this area of products (Tab. 1). Of this amount, EUR 48.5 billion (45.4%) was generated by the EU member states. Among the analyzed countries, Germany was the largest importer in this period. The furniture value that came to this country from abroad amounted to EUR 11.2 billion (Fig. 1b), which accounted for 23.1% of the EU import. France and United Kingdom were next on the list of importers. The importance of the remaining countries in creating the value of furniture imports in the EU was considerably smaller. This was particularly the case for new EU member states, i.e. Poland, Czech Republic and Romania.

In 2009, among the analyzed countries, the highest positive trade balance was observed in Italy. A clearly export-oriented character was also noted in the case of the Polish furniture industry. The value of products intended for foreign markets was four times higher than the value of foreign furniture on the Polish market. In the years from 2009 to 2018, the global furniture import increased by 97.3% and amounted to EUR 210.7 billion. The export growth rate was significantly higher, which resulted in a positive furniture trade balance. On the other hand, in the EU member states, the dynamics of the furniture industry products import value was similar to the value of their export. Thus, the trade surplus was at a similar level as in 2009.

In 2018, Poland and Italy once again recorded the highest positive furniture trade balance. The gap between these countries has evidently narrowed. This situation was caused by favorable economic trends in Poland as well as by the dynamic development of the furniture industry,

which was manifested by a significant increase in the production, accompanied by a smaller increase in the domestic demand, among others. This led to a significant increase in the value of exported products. Out of the ten largest exporters among the analyzed EU countries, the Czech Republic (EUR 1.7 billion), Romania (EUR 1.5 billion) and Denmark (EUR 0.5 billion) also showed a positive furniture trade balance, although the surplus of exports over imports was significantly lower than in Poland and Italy.

Tab. 2: The share of the export and import values of the furniture industry of the selected countries in the world and EU for 2009 and 2018 (%).

Country	2009	2018	DF*	V**	2009	2018	DF	V
	Share of furniture exports in world exports				Share of furniture exports in EU exports			
EU28	48.6	38.4	-10.2	10.4	100.0	100.0	0.0	0.0
Germany	10.4	6.9	-3.5	15.5	21.5	18.8	-2.7	5.8
Italy	8.8	5.7	-3.1	18.0	18.2	14.8	-3.4	8.7
Poland	5.3	5.8	0.5	8.7	10.9	15.0	4.1	9.2
Czech Republic	1.8	2.2	0.4	17.7	3.8	5.7	1.9	14.7
Netherlands	1.5	1.9	0.4	9.8	3.2	5.0	1.8	16.0
France	2.9	1.6	-1.3	21.7	5.9	4.2	-1.7	12.5
United Kingdom	1.6	1.6	0.0	5.6	3.3	4.1	0.8	9.6
Spain	1.8	1.5	-0.3	10.1	3.7	3.9	0.2	7.3
Denmark	1.7	1.2	-0.5	13.6	3.5	3.1	-0.4	5.7
Romania	1.0	1.1	0.1	6.2	2.1	3.0	0.9	15.0
	Share of furniture imports in world imports				Share of furniture imports in EU imports			
EU28	45.4	38.6	-6.8	11.7	100.0	100.0	0.0	0.0
Germany	10.5	8.7	-1.8	10.2	23.1	23.3	0.2	8.2
Italy	2.2	1.7	-0.5	17.3	4.9	4.4	-0.5	5.7
Poland	1.2	1.5	0.3	17.8	2.6	3.6	1	12.4
Czech Republic	1.1	1.5	0.4	19.1	2.3	3.8	1.5	20.3
Netherlands	2.6	2.9	0.3	11.8	5.8	7.6	1.8	8.9
France	6.4	4.8	-1.6	17.7	14.1	12.6	-1.5	7.1
United Kingdom	5.9	4.7	-1.2	11.2	13.0	12.4	-0.6	5.0
Spain	2.5	1.9	-0.6	18.9	5.4	5.0	-0.4	13.0
Denmark	1.2	1.0	-0.2	11.1	2.6	2.7	0.1	2.3
Romania	0.4	0.5	0.1	18.3	0.9	1.3	0.4	16.1

*DF – difference (p.p.), ** V – coefficient of variation (%).

The conducted analyses demonstrate that in 2009, the highest comparative advantage in the furniture trade was generated by manufacturers and exporters from Poland, Romania and Italy. This is evidenced by the values of the relative revealed comparative export advantage index (XRCA) and relative trade advantage index (RTA), as well as the value of the export/import coverage ratio (CR), which exceeds 100%, indicating a positive turnover in the trade of this group of products (Tabs. 3 and 4). In Poland, the value of revenues from furniture exports exceeded the amount of the incurred import expenses 4 times. Meanwhile, the surplus of exports over imports in Italy and Romania was respectively over 3 and 2 times higher. The export/import coverage ratio in these countries equaled 389.89 and 247.65%, resp. (Tab. 3). Additionally, the highest level of implemented export specialization was noted in Poland, Romania and Italy, measured by the value of the SI index. At the beginning of the analyzed period, the values of

the export specialization indicators in these countries were equal to 4.78, 3.14 and 2.68, resp. The positive and relatively high value of the RTA index achieved by these countries is also noteworthy. Denoting the difference between the XRCA and MRCA indicators, the RTA index also takes into account the export and import situation of the country. Among the ten largest furniture exporters, Poland obtained the highest competitive advantage in this area. In 2009, the mean value of the RTA index was equal to 5.2 (Tab. 4), with the Polish furniture exporters having the highest advantage with respect to Ireland and Malta. These are small countries, which show a relatively low share of the furniture industry production value in the total industry value as well as a relatively low economic labor productivity.

Favorable competitive situation in the furniture trade was also observed in Romania and Italy – on average, the RTA index was equal to 3.1 and 2.7, respectively (Tab. 4). In 2009, a relatively high level of competitiveness in the furniture industry was also noted in the Czech Republic and Denmark, as demonstrated by the values of the relative revealed comparative export advantage index (mean value – 2.4 and 2.8, resp.), as well as the values of the coverage ratio which exceeded 100% (170.3 and 144.1%, resp.). Studies have shown that the Czech and Danish furniture industries were characterized by a favorable competitive situation, which is also confirmed by the RTA values greater than zero (1.4 and 1.3, resp.).

Tab. 3: Selected competitiveness indices of the furniture industry for the selected EU countries.

Country	2009			2018			V*		
	MP	SI	CR	MP	SI	CR	MP	SI	CR
Germany	0.63	1.14	97.71	0.76	0.90	85.80	6.61	12.70	6.34
Italy	0.17	2.68	389.89	0.26	2.00	347.44	12.80	13.21	6.07
Poland	0.55	4.78	443.06	1.45	4.24	386.14	30.90	8.02	7.97
Czech Republic	2.46	2.00	170.26	3.57	2.10	155.72	11.70	5.20	8.04
Netherlands	0.65	0.44	57.14	1.03	0.63	68.19	15.79	12.35	9.24
France	0.64	0.77	44.30	0.75	0.55	34.67	5.32	13.33	7.05
United Kingdom	0.53	0.55	26.44	0.63	0.62	34.33	5.95	9.15	9.31
Spain	0.34	0.98	70.93	0.61	0.83	79.80	23.36	7.57	12.69
Denmark	0.88	2.30	144.13	1.39	2.12	121.19	15.74	5.78	5.04
Romania	0.62	3.14	247.65	1.65	2.79	243.77	33.28	4.49	10.84

*V – coefficient of variation.

It should be emphasized that the comparative advantage of German manufacturers in the furniture trade was not as substantial as in the case of the aforementioned countries. Although in 2009 Germany was the largest furniture manufacturer and exporter among all EU countries, it was also among the leading importers of furniture industry products. In the beginning of this period, the export specialization index (SI) of this country was equal to 1.1; however, the export/import coverage ratio (CR) was lower than 100%, which confirmed the lack of a significant advantage over partners in this area. This view is also confirmed by the values of the comparative advantage of export and import indices, which are above 1. However, the RTA indicator was only marginally above zero.

No comparative advantage in the furniture trade was observed in the cases of France and the Netherlands. Negative values of the RTA index were noted there, along with an unfavorable

situation in the development of the SI and CR indicators, which confirmed the lack of export specialization of these countries in the international exchange of the furniture industry products.

Tab. 4: The values of XRCA, MRCA and RTA indices for the selected EU countries.

Country	Value	2009			2018		
		XRCA	MRCA	RTA	XRCA	MRCA	RTA
Germany	max	8.5	2.1	6.9	32.7	2.0	31.2
	min	0.2	0.5	-1.7	0.2	0.7	-1.6
	mean	1.4	1.2	0.2	2.4	1.2	1.2
	st. deviation	1.7	0.4	1.7	6.1	0.4	6.0
Italy	max	20.4	1.0	19.7	74.5	1.0	73.7
	min	0.5	0.3	-0.2	0.4	0.3	-0.2
	mean	3.3	0.6	2.7	5.5	0.6	4.9
	st. deviation	4.0	0.2	4.0	13.9	0.2	13.9
Poland	max	37.4	1.5	36.3	150.6	1.7	149.4
	min	0.9	0.4	-0.1	0.7	0.6	-0.2
	mean	6.0	0.8	5.2	11.1	1.0	10.1
	st. deviation	7.4	0.3	7.4	28.2	0.3	28.1
Czech Republic	max	15.1	1.9	13.7	79.0	2.4	77.2
	min	0.4	0.5	-1.2	0.4	0.8	-1.3
	mean	2.4	1.1	1.4	5.8	1.4	4.4
	st. deviation	3.0	0.3	3.0	14.8	0.5	14.7
Netherlands	max	3.3	1.3	2.3	22.7	1.7	21.5
	min	0.1	0.3	-1.1	0.1	0.6	-1.4
	mean	0.5	0.7	-0.2	1.7	1.0	0.7
	st. deviation	0.6	0.2	0.7	4.3	0.3	4.2
France	max	5.7	2.2	4.0	6.0	2.2	4.2
	min	0.1	0.6	-1.9	0.1	0.7	-2.0
	mean	0.9	1.3	-0.3	0.9	1.3	-0.4
	st. deviation	1.1	0.4	1.2	1.3	0.4	1.1
United Kingdom	max	4.1	2.0	2.5	7.5	2.1	5.8
	min	0.1	0.5	-1.8	0.1	0.6	-1.7
	mean	0.7	1.1	-0.5	1.1	1.2	-0.1
	st. deviation	0.8	0.4	0.8	1.6	0.4	1.5
Spain	max	7.3	1.6	6.1	31.0	1.5	29.9
	min	0.2	0.4	-1.2	0.2	0.5	-1.1
	mean	1.2	0.9	0.3	2.3	0.9	1.4
	st. deviation	1.4	0.3	1.4	5.8	0.3	5.7
Denmark	max	17.5	2.8	15.4	80.3	3.0	78.1
	min	0.4	0.7	-1.9	0.4	1.0	-2.0
	mean	2.8	1.6	1.3	5.9	1.8	4.1
	st. deviation	3.4	0.5	3.4	15.0	0.6	14.9
Romania	max	24.1	1.4	23.0	102.0	1.5	100.9
	min	0.6	0.4	-0.4	0.5	0.5	-0.4

	mean	3.9	0.8	3.1	7.5	0.9	6.6
	st. deviation	4.8	0.3	4.7	19.1	0.3	19.0

In 2018, comparative advantages in the furniture trade were generated by all countries covered by the analysis, with the exception of France and United Kingdom. Polish furniture manufacturers were once again the most competitive in this respect. In Poland, the value of revenues from the furniture exports exceeded the amount of the incurred import expenses almost four times. The CR index of this country equaled 386.14%, whereas the coefficient of variation in the analyzed period was below 10%, which confirms its slight variability. In addition, the Polish furniture industry was characterized by the highest relative comparative advantage of export (mean value of XRCA = 11.1) and the overall comparative furniture trade advantage (mean value of RTA = 10.1). Polish furniture enterprises have the advantages of low labor costs, favorable geographical position, and a high demand for its products. Poland was competitive both in the area of export as well as the entire international furniture exchange with respect to all EU countries, except for Lithuania and Estonia. These countries were characterized by the largest average share of the furniture production value in relation to the value of the domestic industry production, which confirmed the important role of the furniture industry in the total industry. The importance of furniture export in relation to the total value of the exported goods was also significant. At the same time these countries were characterized by a lower value of furniture production per employee. In the analyzed group of the largest furniture manufacturers, Poland obtained the highest levels of the RTA index with respect to France (6.53), United Kingdom (5.51), the Netherlands (5.60), Germany (3.76) and Spain (3.69). This confirms the significant comparative advantage of Poland in relation to the above-mentioned countries in terms of furniture trade.

In 2018, the surplus of exports over imports in Italy and Romania was respectively over 3 and 2 times higher. The export/import coverage ratio in these countries was 347.44% and 243.77%, respectively. Additionally, the high level of implemented export specialization was noted in Romania and Italy, measured by the value of the SI index. The values of the export specialization indicators in these countries were equal to 2.79 and 2.00, resp. Positive trends were also observed in the mean value the RTA index, the values of which were at the level of 6.6 and 4.9, respectively. These countries demonstrated the highest comparative advantage in the furniture trade in relation to France, United Kingdom, the Netherlands and Germany, with Romania achieving the most favorable results. On the other hand, negative RTA indicators were confirmed for Lithuania, Estonia and Poland. The Czech Republic and Denmark showed also a relatively high level of competitiveness in the furniture industry. This is confirmed by the average values of the XRCA index for export (5.8 and 5.9, respectively) as well as the values of the CR index, i.e. the ratio of export to import, which exceeded 100% (155.72 and 121.19%, resp.). In addition, the mean values of the RTA index were more favorable (4.4 and 4.1, resp.).

Research shows that Poland, Romania and Italy were among the countries with the highest levels of international competitiveness in the furniture industry. During the analyzed period, the RTA and the XRCA showed an upward trend, which implies an improvement in the international competitiveness of the furniture production in these countries and confirms

specialization in net export. Italy and Poland are characterized by a relatively high share of the furniture industry production value in the overall value of industrial production. They are also distinguished by a significant value and volume of furniture production; however, a large number of business entities and a relatively high level of employment, production per company and per employee, place these countries slightly above the average among the EU28 countries. Both Italy and Poland have a long furniture tradition. Moreover, Italian furniture has a good reputation among global customers due to its unique design, among others. On the other hand, Poland took the advantage of the proximity to the Western European market and has become an export-oriented furniture producer (Han et al. 2009). The competitiveness of the Polish furniture industry results from the relatively large sale volumes of such products on the external market, often under the brand names of foreign importers. The Polish furniture industry sells 90% of its products abroad (Grzegorzewska and Stasiak-Betlejewska 2014) and has the highest trade volume of any low-technology manufacturing industry (Grzegorzewska and Więckowska 2016). The high comparative advantages of Poland regarding finished wood products were also found in many empirical studies (Han et al. 2009, Augustyniak and Mińska-Struzik 2018, Grzegorzewska et al. 2020). In addition, Ratajczak (2009) found that the Polish comparative advantages increase with the level of the wood products processing.

An important competitor among the European countries is also Romania. Due to industry large investments in new technologies the furniture production and export have increased (Burja and Mărginean 2013). A relatively high level of competitiveness in the furniture industry was also demonstrated by the Czech Republic and Denmark, which is confirmed by the favorable values of the competitiveness indicators. Similar results were presented by Bojnec and Fertő (2014), according to whom the selected EU13 countries (i.e. Poland, the Czech Republic, Romania) show comparative advantage in the trade of finished wood products, including furniture. The authors reported that wood processing plays a significant role in increasing wood product differentiation as well as the value-added of products processed from wood, which indicates improvement in the international competitiveness of the forestry industry sector. Research confirmed that the other EU13 countries are also competitive on the wood-based market (Zhelev 2013). However, the competitiveness indicators for those countries are lower than for Poland, the Czech Republic or Romania.

In contrast, the comparative advantage of the German manufacturers in the furniture trade was not as evident as in the case of the aforementioned countries. In 2018, Germany was still a leader in the ranking of European furniture manufacturers and exporters; however, it was also among the leading importers of the furniture industry products. Unfavorable values of the export specialization index (SI = 0.90) and the export/import coverage ratio (CR = 85.80%) were noted. Nevertheless, the comparative advantage of the German furniture trade increased over the analyzed period, although this increase was not significant – the mean value of the RTA index increased from 0.2 to 1.2. At the end of the analyzed period, the lack of comparative advantage in the furniture trade was observed in France and United Kingdom. These countries were characterized by unfavorable values of the export specialization index (< 1) and the export/import coverage ratio (< 100%).

The average competitiveness position on the global timber and furniture market was also confirmed by Dieter and Englert (2007) and Vu et al. (2019). Moreover, Neykov et al. (2019) demonstrated the lower efficiency of the wood-based industries in Germany using the DEA method. Germany has been characterized by reduced investments and innovations in the furniture industry for a long time. Among the important factors affecting this situation is the reduction in the domestic demand as well as an increased pressure from foreign imports, particularly from Asia. That is why the German furniture manufacturers decided to partially outsource to Poland, which to a certain extent enabled stabilization of the production and increased competitiveness (Vu et al. 2019, Osses et al. 2013, Brenneke 2009). Nonetheless, relatively cheap workforce and low furniture production costs in the Eastern European, Asian or Latin American countries result in lower level of competitiveness of the German furniture manufacturers (Vu et al. 2019). No comparative advantage in the furniture trade was observed in France and United Kingdom. These countries were characterized by unfavorable values of the export specialization index. In addition, the relative import penetration index (MRCA) was higher than the relative revealed comparative export advantage index (XRCA), which resulted in negative values of the RTA index. The negative international competitiveness values for the wood processing industries in United Kingdom were also confirmed by Vu et al. (2019).

In addition, it should be noted that the results presented in this article are consistent with the study reported by Han et al. (2009), which emphasized that Poland and Italy exhibited a remarkably strong comparative advantage, whereas Germany showed a moderate comparative advantage. This means that over a decade, several largest furniture exporters in the EU have maintained, and sometimes even improved, their level of international competitiveness in the field of international furniture trade. However, the weak competitiveness of the wood processing industries in some EU countries can be seen in the fact that the competitive advantage is visible in favorable prices and not in manufacturing complex products with high value added (Bohaček et al. 2020, Ihnat et al. 2018). Business and development, which are purely based on the strategy of low costs and cheap final products, are increasingly less sustainable for enterprises, which aspire towards improvement of competitiveness (Milićević et al. 2017).

The presented research has some limitations. First of all, the data relating to the furniture industry were presented cumulatively for all products. Therefore, in subsequent studies, the analysis of competitiveness should be broadened by expanding the scope to include individual categories of furniture. Furthermore, it would be justified to analyze non-European countries, which are important players on the global furniture market and compare their level of competitiveness in the field of furniture production with the EU countries. Nonetheless, the research results presented in the article expand the existing knowledge and enable certain gaps in the area of assessing the international competitiveness of the largest furniture exporters to be filled. The conducted research may also be a source of information for furniture manufacturers, the entire furniture industry as well as the national governments, since one of their most important tasks is to support highly export-oriented industries. This significant influence of government financial and nonfinancial support on companies and industries performance with mediating role of the competitive position was particularly emphasized by Songling et al. (2018).

CONCLUSIONS

Countries with the highest levels of international competitiveness of the furniture industry included Poland, Romania and Italy. Furthermore, the indicators of competitiveness showed an upward trend, which implies an improvement in the international competitiveness of the furniture production carried out in these countries. The positive and relatively high value of the RTA index achieved by these countries is noteworthy. In 2018, the average values of this indicator for Poland, Romania and Italy were 10.1, 6.6 and 4.9, respectively. Also, the values of the SI index and CR index were very favorable.

In contrast, the comparative advantage of Germany, which is the largest furniture exporter in the EU, was not as significant. Unfavorable values of the export specialization index (SI = 0.90) and the export/import coverage ratio (CR = 85.80%) were noted. Nevertheless, the comparative advantage of the German furniture trade increased over the analyzed period, although this increase was not significant – the mean value of the RTA index increased from 0.2 to 1.2. Relatively cheap workforce and low furniture manufacturing costs in Eastern European countries contribute to a decrease in the level of competitiveness of the German furniture industry. In 2018, the lack of comparative advantage in the furniture trade was observed in France and United Kingdom. These countries were characterized by unfavorable values of the SI indicator and the CR indicator.

It was emphasized that in subsequent studies, the analysis of competitiveness should be broadened by expanding the scope to include individual categories of furniture. In addition, it seems appropriate to analyze non-European countries, which are important players on the global furniture market and compare their level of competitiveness in the field of furniture production with the EU countries.

ACKNOWLEDGMENTS

The authors are grateful for the support of the National Science Centre Poland, Grant No. 2019/03/X/HS4/01342, Slovak project agency APVV – projects APVV-18-0520, APVV-18-0378, APVV-17-0456 and APVV-17-0583, agency KEGA – project KEGA 005TU Z-4/2020 and project LignoPro – ITMS: 313011T720.

REFERENCES

1. Ajitabh, A., Momaya, K., 2004: Competitiveness of firms: Review of theory, frameworks and models. Singapore Management Review 26(1): 45-61.
2. Augustyniak, D., Mińska-Struzik, E., 2018: The competitiveness of Polish furniture exports. Drewno 61(202): 21-38.

3. Balassa, B., 1979: The changing pattern of comparative advantage in manufactured goods. The Review of Economics and Statistics 61(2): 259-266.
4. Barta, B., Kovats, J., 2015: Short note added value among the furniture manufacturing SMES. Wood Research 60(6): 1017-1024.
5. Bohaček, Š., Pažitný, A., Halaj, M., Balberčák, J., Kuňa, V., 2020: Freeze-thaw pretreatment of poplar sapwood dust. Wood Research 65(6): 905-916.
6. Bojnec, Š., Fertő, I., 2014: Forestry industry trade by degree of wood processing in the enlarged European Union countries. Forest Policy and Economics 40: 31-39.
7. Brenneke, G.E., 2009: European sector monitor of the wood/furniture industry. Arbeit und Leben Bielefeld e.V. Bielefeld, Germany, 89 pp.
8. Burja, V., Mărginean, R., 2013: The furniture industry in Romania and the European Union – A comparative approach. Revista Economica 65(4): 107-120.
9. Buturac, G., Lovrinčević, Z., Mikulić, D., 2018: Export competitiveness of the Croatian food industry. Argumenta Oeconomica 2(41): 135-155.
10. Cao, X.Z., Hansen, E.N., Xu, M.Q., Xu, B.M., 2004: China's furniture industry today. Forest Products Journal 54: 14-23.
11. Cho, D., Moon, H., 2000: From Adam Smith to Michael Porter: Evolution of competitiveness theory. World Scientific Publishing Co. Pte. Ltd., Singapore, 323 pp.
12. Dieter, M., Englert, H., 2007: Competitiveness in the global forest industry sector: An empirical study with special emphasis on Germany. European Journal of Forest Research 126: 401-412.
13. Dima, A.M., Begu, L., Vasilescu, M.D., Maassen, M.A., 2018: The relationship between the knowledge economy and global competitiveness in the European Union. Sustainability 10(6): 1706.
14. Frohberg, K., Hartmann, M., 1997: Comparing measure of competitiveness. (Discussion Paper No. 2). IAMO, Halle, Germany, 17 p.
15. Fronczek, M., 2017: Import penetration rate in view of a new concept of measuring foreign trade. Argumenta Oeconomica 1(38): 285-297.
16. Gordeev, R.V., 2020: Assessing competitiveness of forest industry: Theoretical and empirical aspects. Journal of Siberian Federal University. Humanities & Social Sciences 13(4): 443-452.
17. Grzegorzewska, E., Sedliačiková, M., Drábek, J., Behún, M., 2020: Evaluating the international competitiveness of Polish furniture manufacturing industry in comparison to the selected EU countries. Acta Facultatis Xylologiae Zvolen 62(2): 149-164.
18. Grzegorzewska, E., Stasiak-Betlejewska, R., 2014: The influence of global crisis on financial liquidity and changes in corporate debt of the furniture sector in Poland. Drvna Industrija 65(4): 315-322.
19. Grzegorzewska, E., Więckowska, M., 2016: Selected aspects of innovation in the furniture industry – Empirical research findings. Drewno 59(198): 147-161.
20. Hajdúchová, I., Sedliačiková, M., Halaj, D., Krištofík, P., Musa, H., Viszlai, I., 2016: Slovakian forest-based sector in the context of globalization. BioResources 11(2): 4808-4820.

21. Han, X., Wen, Y., Kant, S., 2009: The global competitiveness of the Chinese wooden furniture industry. Forest Policy and Economics 11(8): 561-569.
22. Ihnát, V., Lübke, H., Russ, A., Pažitný, A., Borůvka, V., 2018: Waste agglomerated wood materials as a secondary raw material for chipboard and fibreboard. Part II. Preparation and characterization of wood fibres in terms of their reuse. Wood Research 63(3): 431-442.
23. International Trade Centre, 2020: Trade statistics for international business development http://trademap.org.
24. Kersan-Škabić, I., 2014: Croatian wood industry – clusters, competitiveness and perspectives of development in the framework of European Union membership. Poslovna Izvrsnost 7(2): 55-77.
25. Klos, R., Fabisiak, B., 2013: Possibilities of reliability theory application in the process of furniture design. Wood Research 58(1): 113-122.
26. Kubala, S., Firlej, Ch., 2019: Assessment of Poland's competitive position in trade in fur skins and their products against a background of the EU countries. Zagadnienia Ekonomiki Rolnej Problems of Agricultural Economics 4(361): 129-143.
27. Laursen, K., 2015: Revealed comparative advantage and the alternatives as measures of international specialization. Eurasian Business Review 1(5): 99-115.
28. Milićević, S., Nikolić, M., Cvetanović, S., 2017: The competitiveness of wood processing industry in the Republic of Serbia during the period 1995-2015. Industrija 45(3): 131-150.
29. Neykov, N., Kitchoukov, E., Antov, P., Savov, P., 2019: Efficiency analysis of the Bulgarian forestry and forest-based industry: a DEA approach. Proceedings of International Conference on Innovations in Science and Education. Pp 228-235, Prague.
30. Osses, T., Kies, U., Schulte, A., 2013: Regional shifts of employment growth in the European wood-based panel and furniture industries. International Forestry Review 15: 464-469.
31. Pawlak, K., 2013: International competitive ability of the agri-food sector in the European Union. Poznan University of Life Sciences Press, Poznan, 491 pp.
32. Rabar, D., Cvek, D., 2019: Measuring the macroeconomic performance of the Croatian economy: An empirical efficiency analysis approach. Proceedings of XV Interdisciplinary Management Research Conference. Pp 1167-1187, Opatija, Croatia.
33. Ratajczak, E., 2009: Foresight in the wood science and industry – research development scenarios in Poland till 2020. Drewno 52(182): 143-136.
34. Rugman, A.M., Oh, C.H. 2008: The international competitiveness of Asian firms. Journal of Strategy and Management 1(1): 57-71.
35. Sedliačiková, M., Hajdúchová, I., Krištofík, P., Viszlai, I., Gaff, M., 2016: Improving the performance of small and medium wood-processing enterprises. BioResources 11(1): 439-450.
36. Sirgmets, R., Teder, M., Kaimre, P., 2019: The structural changes and competitiveness of the forest and wood Sector in the Baltic Countries within 1999-2016. Baltic Forestry 25(1): 97-104.
37. Songling, Y., Ishtiaq, M., Anwar, M., Hamid, A., 2018: The role of government support in sustainable competitive position and firm performance. Sustainability 10(10): 3495.

38. Vollrath, T.L., 1991: A theoretical evaluation of alternative trade intensity measures of revealed comparative advantage. Weltwirtschaftliches Archives 2(127): 265-280.
39. Vu, T.T.H., Tian, G., Khan, N., Zada, M., Zhang, B., Nguyen, T.V., 2019: Evaluating the international competitiveness of Vietnam wood processing industry by combining the variation coefficient and the entropy method. Forests 10: 901.
40. Xiong, X.Q., Guo, W.J., Fang, L., Zhang, M., Wu, Z.H., Lu, R., Miyakoshi, T., 2017: Current state and development trend of Chinese furniture industry. Journal of Wood Science 63: 433-444.
41. Zhang, J., Ebbers, H., Mulder, R., 2012: Competitiveness of Chinese industries: A comparison with the EU. Review of European Studies 4: 203-209.
42. Zhelev, P., 2013: Analysis of the international competitiveness of the Bulgarian furniture industry. Trakia Journal of Sciences 11: 227-236.

EMILIA GRZEGORZEWSKA*
WARSAW UNIVERISITY OF LIFE SCIENCES – SGGW
DEPARTMENT OF TECHNOLOGY AND ENTREPRENEURSHIP IN WOOD INDUSTRY
NOWOURSYNOWSKA 159 02-776 WARSAW
POLAND
*Corresponding author: emilia_grzegorzewska@sggw.edu.pl

MARIANA SEDLIAČIKOVÁ
TECHNICAL UNIVERSITY IN ZVOLEN
FACULTY OF WOOD SCIENCES AND TECHNOLOGY
DEPARTMENT OF ECONOMICS, MANAGEMENT AND BUSINESS
T. G. MASARYKA 24, SK-960 01 ZVOLEN
SLOVAKIA

DENIS JELAČIĆ
UNIVERSITY OF ZAGREB
FACULTY OF FORESTRY
INSTITUTE OF PRODUCTION ORGANISATION
HR-10000 ZAGREB
CROATIA

WOOD RESEARCH doi.org/10.37763/wr.1336-4561/66.5.875890
e-ISSN 2729-8906
66(5): 2021 875-890 pp.

WOOD-BASED SANDWICH PANELS: A REVIEW

PEIXING WEI[1], JINXIANG CHEN[1], YUE ZHANG[2], LIJUN PU[2]
[1]SOUTHEAST UNIVERSITY NANJING
CHINA
[2]JIANGSU VOCATIONAL COLLEGE OF AGRICULTURE AND FORESTRY
CHINA

(RECEIVED DECEMBER 2020)

ABSTRACT

A sandwich panel with a high ratio of strength to weight is commonly used in aerospace, construction, packaging and other fields. Using a renewable material such as wood to make sandwich panels can achieve a perfect unity of material and structure. In view of the lack of systematic analyses of wood-based sandwich panels, this work reviewed the development of wood-based sandwich panels. Based on the core structure, these panels can be divided into hollow-core structures and solid-core structures. With the emergence of new materials and new technologies, new wood-based sandwich products had been created. However, the current research only focused on the manufacturing, and the related novel design was still lacking. This work put forward a research idea of bionic design based on the integration of structure and function and pointed out the research direction for wood-based sandwich panels.

KEYWORDS: Wood-based sandwich panel, hollow-core structure, solid-core structure, property, application.

INTRODUCTION

Although the principle of a sandwich structure might have been applied much earlier, its concept was not clearly put forward until the middle of the 19th century (Fairbairn 1849). In general, sandwich panels were a kind of structural material composed of two high-strength stiff layers (facings) and one low-density layer (core) (Birman and Kardomateas 2018). The surface layer can bear the in-plane load and bending moment, which can be made from steel (Nilsson et al. 2017), wood (Kljak and Brezovic 2007), fibre reinforced concrete (O'Hegarty et al. 2019) or concrete (O'Hegarty and Kinnane 2020), and other materials (Boldis et al. 2016); the core layer mainly serves to transmit the load, and its function is to maintain the distance between the two layers and increase the inertia moment and bending stiffness of the panel (Noor et al. 1996,

Zenkert 1995). The configurations of the core included corrugated core, plastically formed core, honeycomb cell core, and so on (Noor et al. 1996). Owing to low density of the core material, the sandwich panel can greatly reduce its dead weight under the same bearing capacity (Sandeep and Srinivasa 2020).

During World War II, the United Kingdom first used sandwich-structured plywood to manufacture mosquito bombers. At the same time, the United States (US) invented a sandwich structure with two reinforced plastic surface layers and one lower density core layer (Feichtinger 1989). Since the 1950s, the US Forest Products Laboratory studied on wood sandwich panels and had been in the leading position over the world for a long time (Vinson 2005). The surface materials of sandwich panels used in aircraft manufacturing were mainly plywood and pulp fibre in the early stage, and their cores were made of cork, balsa wood, and synthetic materials such as cellulose acetate. Later, aluminium alloy, titanium, and stainless steel were used for the surface layer and core layer of sandwich panels in aerospace (Noor et al. 1996). With the development of industrial synthetic materials, sandwich panels turned to using synthetic materials (Gibson and Ashby 1997).

In recent years, the ecological problems caused by petrochemical energy consumption and resource overexploitation have become serious, such as the frequent occurrence of extreme climates and the unprecedented challenges of human living environment. To reduce resources' consumption and environmental pollution, human beings urgently seek renewable and eco-friendly materials for daily life (Bekhta et al. 2013, Labans and Kalniņs 2014, Lakreb et al. 2015, Li et al. 2016, Asdrubali et al. 2017, Susainathan et al. 2017, Mirski et al. 2018, Mohammadabadi et al. 2018). As a renewable and degradable natural material, wood is a real low-carbon material (Robertson et al. 2012, Shao 2012, Vogtländer et al. 2014). Sandwich structures made of wood materials can give full play to the advantages of material and structure, and thus they are a kind of structural material with a great prospect (Negro et al. 2011, Monteiro et al. 2018).

Recent research in core materials of wood-based sandwich panels covered low-density wood fibre (Fernandez-Cabo et al. 2011, Zhang et al. 2012), plywood (Labans and Kalniņs 2014, Susainathan et al. 2017), wood strips (Li et al. 2016), cork (Lakreb et al. 2015), wooden dowel lattice (Jin et al. 2015), corrugated cardboard (Russ et al. 2013, McCracken and Sadeghian 2018), and 3D-shaped wood strand (Mohammadabadi et al. 2018). However, there is so far no systematic summary in this field. Therefore, this paper summarized the structure, properties, application and existing problems of wood-based sandwich panels, and proposed some research directions to better use sandwich structure and wood resource.

Structures and properties of wood-based panels

Structures of wood-based panels

Based on the different core configurations, wood-based sandwich panels can be classified into hollow-core structures and solid-core structures. There were six types of hollow-core structures: honeycomb core (Hao et al. 2020) (Fig.1a), I-shaped core (Labans and Kalniņs 2014) (Fig. 1b), interlocking lattice core (Chen and Tsai 1996, Han and Tsai 2003, Li et al. 2013, Klímek et al. 2016) (Fig. 1c), corrugated core (Srinivasan et al. 2008, Banerjee and

Bhattacharyya 2011) (Fig. 1d), moulded core (Way et al. 2016) (Fig. 1e), and pyramid lattice core (Yang et al. 2018) (Fig. 1f). The solid-core structures were relatively simple, namely, the core layer was composed of different light materials (Kawasaki and Kawai 2006, Hiziroglu 2012, Lakreb et al. 2015) (Fig. 1g,h,i).

Obviously, the hollow-core structures were undoubtedly more cost-effective than the solid-core structures. However, solid-core structures with a high porosity or a low density were also adopted in engineering application under the consideration of thermal and sound insulation.

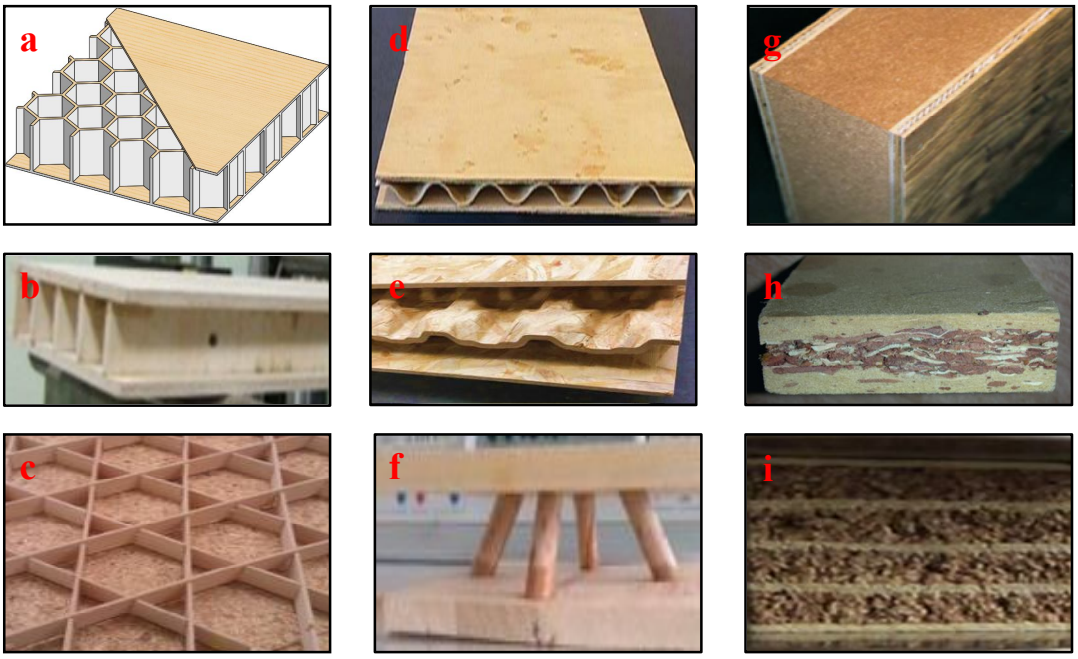

Fig. 1: Typical wood-based sandwich panels: a) honeycomb core; b) I-shaped core; c) interlocking lattice core; d) corrugated core; e) moulded core; f) pyramid lattice core; g) single-layer fiber core; h) single-layer strand core; i) multi-layer fiber core.

Structural properties of typical wood-based sandwich panels

Compressive properties of the wood honeycomb panel

Researchers have carried out many studies on honeycomb panels (Ramohalli 1983, Evans 1991, Chen 1994, Renji et al. 1996, Herup and Palazotto 1998, Horrigan et al. 2000, Okada and Kortschot 2002, Grove et al. 2006, Burlayenko and Sadowski 2010, Stocchi et al. 2014, Abbadi et al. 2015, Gunes and Arslan 2016, Balcı et al. 2017, Crupi et al. 2018, Ha et al. 2019, Gao et al. 2020), but it was limited in wood honeycomb panels. Xu (2007) prepared wood sandwich panels with different wood surface layers and paper honeycomb cores and carried out a comparative study (Fig. 2). It was found that there were five types of failure modes under lateral compression, namely, global instability, shear wrinkling, interfacial debonding, panel rupture, and panel buckling. The deformation mechanisms and lateral compressive strengths were different which depended on the surface materials.

Panel No.	Face sheet	Thickness of face sheet (mm)	Core	Thickness of core (mm)
A	Paper	0.31	Paper core	9.53
B	Sapele veneer	0.50	Paper core	9.53
C	Sapele veneer	0.50	Paperboard	10.52
D	Plywood	2.22	Paperboard	10.52
E	MDF	2.46	Paperboard	10.52

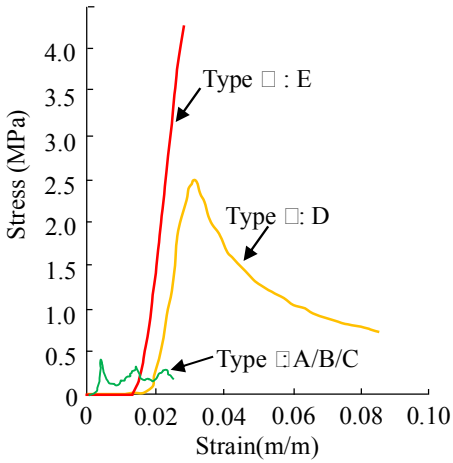

Fig. 2: Stress-strain relationship of wood honeycomb panels under lateral loading.

Creep behaviour of the wood honeycomb panel

There are few studies on the creep properties of paper-based honeycomb cores. Yan's research team from University of Toronto studied the creep properties of wood honeycomb panels with different material combinations. In their research, two kinds of honeycomb cores (Fig. 3a,b) and three kinds of surface layers (hardboard, medium density fibreboard (MDF), and plywood) were used to make wood honeycomb panels (Chen et al. 2011, Chen and Yan 2012). The results showed that the creep behaviour of the sandwich panel was closely related to the type of honeycomb core, the thickness of core and surface layer, and the surface material. To better combine the wood honeycomb panel with the hardware, Sambrew et al. (2010) proposed a concept of strengthening the edge of the wood honeycomb core and designed the edge reinforced wood honeycomb panel (Fig. 3c). This structure could effectively improve the compression and creep properties of wood honeycomb panels.

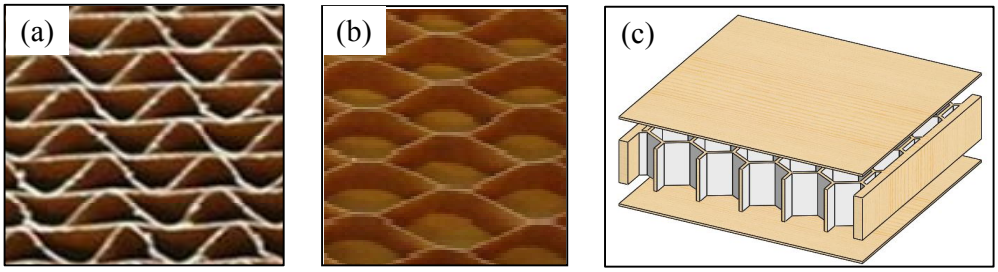

Fig. 3: Wood-based honeycomb panel: a) Corrugated honeycomb core; b) expanded honeycomb core; and c) wood-based honeycomb panel with edging reinforcement.

Applications of wood-based sandwich panels

Development and application of wood-based sandwich panels for furniture

With the continuous reduction of forest resource, to save resource and reduce dead weight has become an important issue in furniture industry (Labans and Kalniņs 2014). Using honeycomb structure in furniture can greatly save wood resource and also avoid the large deformation which often occurred for commercial wood composites. At present, honeycomb composite with a thickness of 20 mm above in furniture were widely used in Europe.

Traditionally, the honeycomb panel used in furniture was a frame honeycomb panel. Until 2005, lightweight frameless honeycomb panel manufacturing equipment and technology were created, which helped to realize industrialization and automation of wood honeycomb panels.

Jarusombuti et al. (2009) made a composite sandwich panel using local bamboo and straw resource in Thailand for the furniture industry. By testing the physical and mechanical properties of the samples, it was found that the composite sandwich panel can completely meet the requirements of indoor particleboard. Similarly, Hiziroglu (2012) developed a wood sandwich panel with eastern cedar (*Juniperus virginiana* L.) strands as the core layer and commercially produced Southern pine fibers as the surface layer. With the increase of density, the bending property increased, but the dimensional stability decreased.

MDF can easily deform while used for furniture components. To solve this problem, Büyüksari et al. (2012) proposed a wood-based sandwich panel, in which the MDF was the core layer and the hot-pressed wood veneer was the surface layer. Through tests on the physical and mechanical properties, it was found that the bending performance of the panel can be improved by increasing the temperature and pressure and the pressure had a great influence on the expansion rate of the water absorption thickness. Thus, to adjust the different combinations of temperature and pressure can make sandwich products meet the structural properties.

Development and application of wood-based sandwich panels for building

Compared with other commercial wood-based panels, wood-based sandwich panels had advantage in thermal insulation. Also, the sound absorption coefficient was almost zero, which was far lower than that of fibreboard. The research team from Kyoto University (Kawasaki et al. 1998, Kawasaki et al. 1999, Kawasaki and Kawai 2006) developed a sandwich panel with low-density fibreboard as the core layer for the thermal insulation wall or floor. Although Fernandez-Cabo et al. (2011) proposed a similar sandwich panel structure, their starting points for solving the problems were different. In Japan, Kawasaki et al. (2003) focused on the in-plane shear stiffness of sandwich panels. However, Fernandez-Cabo et al. (2011) examined the flexural response of sandwich panels subjected to wind loads. Labans and Kalni ņs (2014) developed a new type of I-shaped wood sandwich panel for construction. Under the condition of meeting the same stiffness as commercial plywood, the optimal design and experimental verification of this new type of wood sandwich panel were carried out. The results showed that, through reasonable design, a benefit building material with a low density and excellent mechanical properties can be obtained.

Development and application of wood-based sandwich panels for packaging

Paper-based honeycomb materials have been widely used in packaging industry owing to their advantages of high strength to weight ratio, good stiffness, good cushioning and vibration absorption performance, and environmental protection. According to the principle of a sandwich structure, the advantages of various materials can be fully utilized by using wood materials as the surface layer and paper honeycombs as the core layer. Through experimental verification, the physical and mechanical properties of these honeycomb sandwich materials are greatly improved (Xu 2007).

The creep of packaging materials often occurred during transportation which resulted in voids in container and led to an increase of the products' damage rate. For wood-based sandwich panels, creep originated from two reasons. One was the creep of the upper and lower surface layers, and the other was the shear deformation of the core layer. Xu (2007) studied the creep properties of sandwich materials with different combinations. However, the limitation was that the sandwich panels were regarded as homogeneous material, and in fact the wood honeycomb sandwich panel was an anisotropic material, which led to a large error. In addition, due to the problems associated with the test cycle, the short-term creep performance was used to predict the long-term creep properties of sandwich materials. Whether this prediction was correct needed to be examined.

Development trend of wood-based sandwich panels

Combined with other materials, wood with natural defects can be avoided. Thus, the study of wood composites has become a popular topic (Rao 2003, Yeniocak et al. 2016).

Wood-plastic composite (WPC) sandwich panels

WPCs have been widely utilized in construction, packaging, transportation and furniture products (Binhussain and El-Tonsy 2013). To improve the mechanical properties of WPCs, researchers have performed much research (Ou et al. 2010, Zolfaghari et al. 2013). Based on the sandwich structure, structure design of WPCs was carried out to improve mechanical properties (Vitale et al. 2016, Hao et al. 2018).

Tungjitpornkull and Sombatsompop (2009) studied the sandwich panel formed by the surface layer of wood/PVC composites and the core layer of glass fibre (GF)/PVC. It was found that the delamination of GF and PVC led to a decrease in the mechanical properties. To solve this problem, Mongkollapkit et al. (2010) studied the influence of the orientation angle of the GF and the viscosity index of the PVC and dicarboxylic acid on delamination. Hao et al. (2018) studied sandwich-structured WPCs composed of wood flour/high-density polyethylene and linear low-density polyethylene. The results showed that the bending strength and impact strength of the sandwich panel increased by 42% and 77%, respectively, while the water absorption rate was significantly reduced. However, the linear low-density PVC core layer did not cause a material change in the creep and relaxation characteristics of the panel, which led to an increase in the linear thermal expansion coefficient.

Edgars et al. (2017) designed two kinds of sandwich panels (Fig. 4). The bending tests showed that the flexural modulus of the sandwich panel with a corrugated GF reinforced resin core layer was 4180 MPa, the flexural strength was 22.6 MPa, and the density was 235 $kg \cdot m^{-3}$. The flexural modulus of the sandwich panel with plywood stiffeners and a foam core was 6200 MPa, the bending strength was 26.1 MPa, and the density was 325 $kg \cdot m^{-3}$. These two kinds of sandwich panels had the characteristics of light weight and high strength.

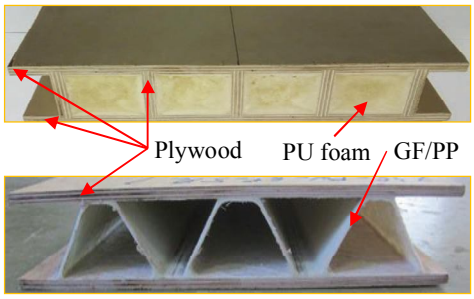

Fig. 4: Two types of lightweight and high-strength sandwich panels. Upper: sandwich panels with plywood stiffeners and a foam core; Bottom: sandwich panels with a corrugated GF/PP core.

Fibre reinforced wood-based sandwich panels

Yang et al. (2014) prepared a new type of composite wall panel using GF reinforced plastic (FRP) impregnated with vinyl resin and paulownia wood as the core material through vacuum induction moulding process. With the decrease in the height-thickness ratio, the ultimate bearing capacity of the specimens under axial compression increased. Fang et al. (2014) prepared a sandwich-structured bridge deck with glulam as the core material and GF reinforced composite (GFRP) as the surface layer (Fig. 5a) and carried out a bending performance test of a GFRP-glulam sandwich beam. Xiong et al. (2014) carried out a three-point bending test on a poplar sandwich composite panel (Fig. 5b) made by a pultrusion process. Wu et al. (2015) used GF reinforced composite as the surface layer and lattice web and paulownia wood as the core and chose the vacuum induction moulding process to prepare a paulownia wood sandwich beam with a lattice web panel interface (Fig. 5c). Wang et al. (2017) studied the bending properties of a paulownia wood sandwich panel (Fig. 5c) strengthened by a lattice web. Zou et al. (2017) proposed a new type of lattice web reinforced lightweight wood sandwich bridge deck (GFRP and balsa wood) (Fig. 5c).

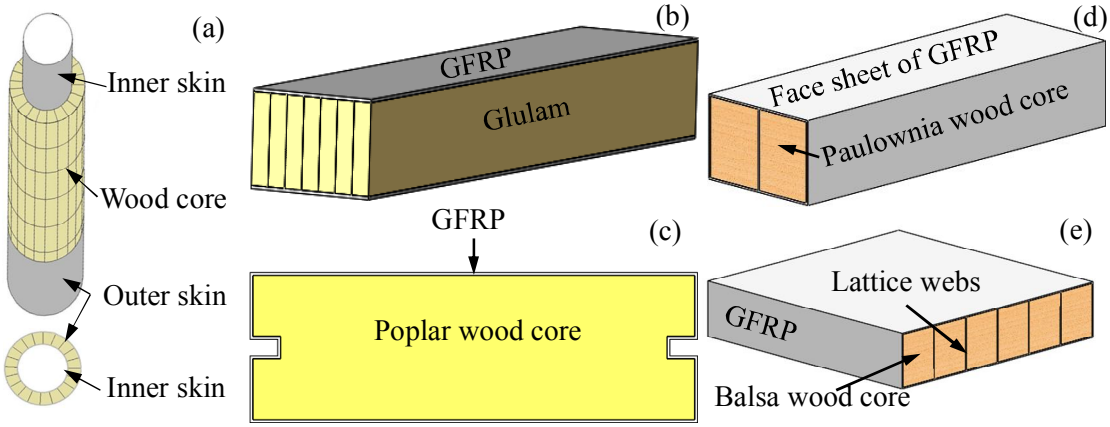

Fig. 5: Fibre reinforced wood-based sandwich panels.

Steel-wood composite sandwich panels

Due to its light-weight of wood, researchers have explored the feasibility of steel-wood composite for structural applications. For example, Teng et al. (2009) studied the flexural

bearing capacity and ductility performance of cold-formed thin-walled steel and OSB composite floors; Han et al. (2010) and Li et al. (2008) studied the bending performance of profiled steel sheets and bamboo plywood composite floors, and found that they had a good combination effect. Poplar plywood had good bending performance and impact resistance as a structural cover panel (Zhao et al. 2010). Wood materials were generally used for the surface layers of sandwich panels, and steel was used for the core layer.

Wei et al. (2017) carried out finite element simulations and experimental research on the stress analysis of steel-wood sandwich panels. The core layer yielded first and then the panel yielded, and finally the debonding occurred. And bonding failure was the direct reason for the failure of this sandwich panel.

Bamboo-wood composite sandwich panels

Gao et al. (2010) designed three kinds of bamboo-wood composite sandwich walls (Fig. 6). The thermal insulation and sound insulation of three kinds of composite walls were tested. The results showed that the thermal insulation and sound insulation of the a-type wall was the worst, but it can be substantially improved by adding rock wool (type c); the thermal insulation and sound insulation of the wall exhibited no obvious changes after the interior wall panel was replaced by a gypsum board (type b).

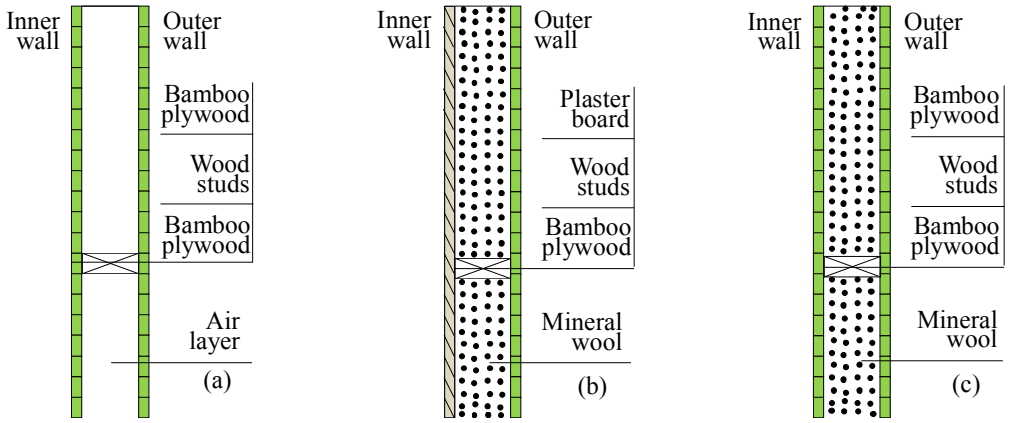

Fig. 6: Bamboo-wood sandwich wall: (a) bamboo plywood-overlaid hollow wall; (b) plaster board-overlaid sandwich wall; and (c) bamboo plywood-overlaid sandwich wall.

Zhou (2017) prepared a multifunctional composite wall (Fig. 7b) using a 33 mm-thick hollow-core particleboard (Fig. 7a). The core layer was an air layer separated by wood strips of different thicknesses (23 mm and 74 mm), and then a 9 mm gypsum board and plywood were applied on the surface of the particleboard (Fig. 7b). Jiang et al. (2017) improved the structure and proposed the use of small diameter bamboo as a reinforcement material to improve the main physical and mechanical properties of hollow-core particleboard (Fig. 7c). Then, resorcinol phenol formaldehyde adhesive was coated on the surface of the original bamboo-reinforced particleboard, and laminated veneer or plywood was installed on the surface of the particleboard to form a sandwich board structure. The results showed that bamboo had a substantial effect on the properties of hollow-core particleboard, and the mechanical properties and dimensional

stability are greatly improved.

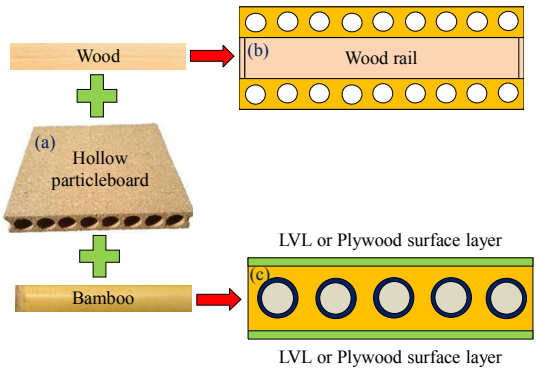

Fig. 7: Bamboo-wood sandwich panel.

Other wood-based sandwich panels

Renewable lightweight materials can be used to reduce carbon emissions and achieve sustainable development. Wood, an ancient material, can be compounded with other materials to form a lightweight and high-strength structure. Burnett and Kharazipour (2018) created a sandwich structure with a core layer made from popcorn particles and a surface layer of poplar plywood (Fig. 8). This sandwich panel can achieve the performance of traditional wood composites such as fibreboard and particleboard, and thus it may be used in the furniture industry. Susainathan et al. (2017) prepared wood composite sandwich panels using two kinds of plywood with different blank structures and four different surface materials (aluminium, GF reinforced resin, carbon fibre reinforced resin and flax reinforced resin) and studied the failure mechanism of quasi-static bending and low-speed impact performance (Susainathan et al. 2018). This kind of wood-based sandwich panel can not only give full play to the advantages of light wood, but also the strength of composite materials.

Fig. 8: Popcorn-wood sandwich panel.

CONCLUSIONS

Wood-based sandwich panels were a special kind of sandwich panels, which had an advantage of light weight and high strength. In addition, they also had the resource advantage that other materials such as metal and plastic did not have. Scientific planting and logging can realize a continuous supply of wood resource. Therefore, according to the literature search, it was evident that research on wood sandwich panels had obviously increased and accelerated. In this paper, the structural characteristics, applications, and development trends of wood sandwich panels were summarized: *(1)* Wood sandwich panels can be divided into hollow-core structures and solid-core structures. The hollow-core structures included corrugated structure, honeycomb

structure, lattice structure, interlocking structure, and so on. The solid core structures mainly used wood, light fibreboard, particleboard, and crop straw fibres as the core material, and the structure was relatively simple. *(2)* According to the literature, researchers not only improved their structures of sandwich panels but also used new materials. The sandwich structure was formed by wood composite or mixed use of plywood, fibreboard, and particleboard. And even wood materials were combined with plastics, steel, bamboo, fibre reinforced materials, and so on. *(3)* Researchers focused on the development of new products. However, there was a lack of basic research on the design theory and failure mechanisms. Although there were many kinds of wood-based sandwich panels, most of them were still in the research stage of preparation, structural parameters, physical and mechanical properties, and engineering application and dynamics research have not been carried out. *(4)* Hollow-core wood sandwich panels had the advantage of light weight and high strength, but their insulation and sound insulation effects were not good due to poor sealing. And the poor compressive and shear properties of solid-core wood sandwich panels also limited their applications. Thus, the integration of structure and function is the basic principle for the development of new wood-based sandwich panels. *(5)* In future research, the bionic design concept should be applied to the structural design of wood-based sandwich panels to effectively improve the physical and mechanical properties. For example, according to the beetle coleoptera structure (honeycomb-column structure), the core layer structure of a wood-based sandwich panel can be first prepared, and then the straw fibre or wood fibre can be filled into the honeycomb, which can not only improve the mechanical properties of the wood sandwich panel, but also improve its physical properties such as thermal and sound insulation.

ACKNOWLEDGMENTS

This work is financially by Jiangsu Planned Projects for Postdoctoral Research Funds (2018K121C), and Qing Lan Project of Jiangsu Province (2019).

REFERENCES

1. Abbadi, A., Tixier, C., Gilgert, J., Azari, Z., 2015: Experimental study on the fatigue behaviour of honeycomb sandwich panels with artificial defects. Composite Structures 120: 394-405.
2. Asdrubali, F., Ferracuti, B., Lombardi, L., Guattari, C., Evangelisti, L., Grazieschi, G., 2017: A review of structural, thermo-physical, acoustical, and environmental properties of wooden materials for building applications. Building and Environment 114: 307-332.
3. Banerjee, S., Bhattacharyya, D., 2011: Optimal design of sandwich panels made of wood veneer hollow cores. Composites Science and Technology 71(4): 425-432.
4. Balcı, O., Çoban, O., Bora, M.Ö., Akagündüz, E., Yalçin, E.B., 2017: Experimental investigation of single and repeated impacts for repaired honeycomb sandwich structures. Materials Science and Engineering A 682: 23-30.

5. Bekhta, P., Korkut, S., Hiziroglu, S., 2013: Effect of pretreatment of raw material on properties of particleboard panels made from wheat straw. Bioresources 8(3): 4766-4774.
6. Binhussain, M.A., El-Tonsy, M.M., 2013: Palm leave and plastic waste wood composite for out-door structures. Construction and Building Materials 47: 1431-1435.
7. Birmana, V., Kardomateas, G.A., 2018: Review of current trends in research and applications of sandwich structures. Composites Part B 142: 221-240.
8. Boldis, M., Gasparik, M., Gaff, M., Ruman, D., 2016: Compression set of PU foam mattresses with self-clamping joints and sandwich structure. Wood Research 61(6): 1003-1016.
9. Burlayenko, V.N., Sadowski, T., 2010: Effective elastic properties of foam-filled honeycomb cores of sandwich panels. Composite Structures 92(12): 2890-2900.
10. Büyüksari, Ü., Hiziroglu, S., Akkılıç, H., Ayrılmış, N., 2012: Mechanical and physical properties of medium density fiberboard panels laminated with thermally compressed veneer. Composites Part B 43(2): 110-114.
11. Burnett, M., Kharazipour, A., 2018: Mechanical behaviour of a lightweight, three-layered sandwich panel based on the raw material maize. Holzforschung 72(1): 65-70.
12. Chen, R.S., 1994: Effect of curing process on mechanical properties of honeycomb-core sandwich plates. Composites Engineering 4(4): 445-458.
13. Chen, H.J., Tsai, S.W., 1996: Analysis and optimum design of composite grid structures. Journal of Composite Materials 30(4): 503-534.
14. Chen, Z., Yan, N., Deng, J., Smith, G., 2011: Flexural creep behavior of sandwich panels containing kraft paper honeycomb core and wood composite skins. Materials Science and Engineering A 528(16-17): 5621-5626.
15. Chen, Z., Yan, N., 2012: Investigation of elastic moduli of kraft paper honeycomb core sandwich panels. Composites Part B 43(5): 2107-2114.
16. Crupi, V., Kara, E., Epasto, G., Guglielmino, E., Aykul, H., 2018: Theoretical and experimental analysis for the impact response of glass fibre reinforced aluminium honeycomb sandwiches. Journal of Sandwich Structures and Materials 20(1): 42-69.
17. Evans, K.E., 1991: The design of doubly curved sandwich panels with honeycomb cores. Composite Structures 17(2): 95-111.
18. Edgars, L., Kaspars, Z., Kaspars, K., 2017: Structural performance of wood-based sandwich panels in four-point bending. Procedia Engineering 172: 628-633.
19. Fang, H., Han, J., Liu, W.Q., Zhu, L., 2014: Experiment on bending capacity and structural design of GFRP - *Pseudotsuga taxifolia* glulam bridge deck. Journal of Architecture and Civil Engineering 31(3): 58-63.
20. Fairbairn, W., 1849: An account of the construction of the Britannia and Conway tubular bridges. John Weale, London, UK.
21. Fernandez-Cabo, J.L., Majano-Majano, A., San-Salvador Ageo, L., Ávila-Nieto, M., 2011: Development of a novel façade sandwich panel with low-density wood fibres core and wood-based panels as faces. European Journal of Wood and Wood Products 69: 459-470.
22. Feichtinger, K.A., 1989: Test methods and performance of structural core materials-1. Static properties. Journal of Reinforced Plastics and Composites 8(4): 334-357.

23. Gao, X., Zhang, M.M., Huang, Y.D., Sang, L., Hou, W.B., 2020: Experimental and numerical investigation of thermoplastic honeycomb sandwich structures under bending loading. Thin-Walled Structures 155: 106961.
24. Gao, L., Wang, Z., Chang, L., 2010: Heat and sound insulation performance of prefabricated bamboo-wood wall. China Wood Industry 24(1): 26-28.
25. Gibson, L.J., Ashby, M.F., 1997: Chapter 9: the design of sandwich panels with foam cores. In book: Pp 345-386, Cellular solids. Cambridge University Press, UK.
26. Gunes, R., Arslan, K., 2016: Development of numerical realistic model for predicting low-velocity impact response of aluminium honeycomb sandwich structures. Journal of Sandwich Structures and Materials 18(1): 95-112.
27. Grove, S.M., Popham, E., Miles, M.E., 2006: An investigation of the skin/core bond in honeycomb sandwich structures using statistical experimentation techniques. Composites Part A 37(5): 804-812.
28. Ha, N.S., Lu, G.X, Xiang, X.M., 2019: Energy absorption of a bio-inspired honeycomb sandwich panel. Journal of Materials Science 54(8): 6286-6300.
29. Han, D.Y., Tsai, S.W., 2003: Interlocked composite grids design and manufacturing. Journal of Composite Materials 37(4): 287-316.
30. Han, T.S., Li, Y.S., Zhang, W.L., Shen, H.Y., 2010: Study on flexural performance of thin-walled steel-bamboo plywood composite slabs. Forest Engineering 26(3): 54-57.
31. Hao, X.L., Zhou, H.Y., Xie, Y.J., Mu, H.L., Wang, Q.W., 2018: Sandwich-structured wood flour/HDPE composite panels: Reinforcement using a linear low-density polyethylene core layer. Construction and Building Materials 164: 489-496.
32. Hao, J.X., Wu, X.F., Oporto, G., Liu, W.J., Wang, J.X., 2020: Structural analysis and strength-to-weight optimization of wood-based sandwich composite with honeycomb core under three-point flexural test. European Journal of Wood and Wood Products 78: 1195-1207.
33. Herup, E.J., Palazotto, A.N., 1998: Low-velocity impact damage initiation in graphite/epoxy/Nomex honeycomb-sandwich plates. Composites Science and Technology 57(12): 1581-1598.
34. Hiziroglu, S., 2012: Some properties of sandwich type composite panels manufactured from eastern redcedar. Composites Part B 43(8): 3288-3292.
35. Horrigan, D.P.W, Aitken, R.R., Moltschaniwskyj, G., 2000: Modelling of crushing due to impact in honeycomb sandwiches. Journal of Sandwich Structures and Materials 2(2): 131-151.
36. Jarusombuti, S., Hiziroglu, S., Bauchongkol, P., Fueangvivat, V., 2009: Properties of sandwich-type panels made from bamboo and rice straw. Forest Products Journal 59(10): 52-57.
37. Jin, M., Hu, Y., Wang, B., 2015: Compressive and bending behaviours of wood-based two-dimensional lattice truss core sandwich structures. Composite Structures 124: 337-344.

38. Jiang, J., Lu, X.N., Shen, H.Y., 2017: Characterization of original bamboo reinforced extruded particleboards (BRP) and stability design for its longitudinal compression. China Forest Products Industry 44(9): 28-32.
39. Kawasaki, T., Zhang, M., Kawai, S., 1998: Manufacture and properties of ultra-low-density fiberboard. Journal of Wood Science 44(5): 354-360.
40. Kawasaki, T., Zhang, M., Kawai, S., 1999: Sandwich panel of veneer-overlaid low-density fiberboard. Journal of Wood Science 45(4): 291-298.
41. Kawasaki, T., Hwang, K., Komatsu, K., Kawai, S., 2003: In-plane shear properties of the wood-based sandwich panel as a small shear wall evaluated by the shear test method using tie-rods. Journal of Wood Science 49(3): 199-209.
42. Kawasaki, T., Kawai, S., 2006: Thermal insulation properties of wood-based sandwich panel for use as structural insulated walls and floors. Journal of Wood Science 52(1): 75-83.
43. Kljak, J., Brezovic, M., 2007: Influence of plywood structure on sandwich panel properties: Variability of veneer thickness ratio. Wood Research 52(2): 77-88.
44. Klímek, P., Wimmer, R., Brabec, M., Sebera, V., 2016: Novel sandwich panel with interlocking plywood kagome lattice core and grooved particleboard facings. BioResources 11(1): 195-208.
45. Labans, E., Kalniņs, K., 2014: Experimental validation of the stiffness optimization for plywood sandwich panels with rib-stiffened core. Wood Research 59(5): 793-802.
46. Lakreb, N., Bezzazi, B., Pereira, H., 2015: Mechanical behavior of multilayered sandwich panels of wood veneer and a core of cork agglomerates. Materials and Design 65: 627-636.
47. Li, J.H., Hunt, J.F., Cai, Z.Y., Zhou, X.Y., 2013: Bending analyses for 3D engineered structural panels made from laminated paper and carbon fabric. Composites Part B 53(5): 17-24.
48. Li, J.H., Hunt, J.F., Gong, S.Q., Cai, Z.Y., 2016: Simplified analytical model and balanced design approach for light-weight wood-based structural panel in bending. Composite Structures 136: 16-24.
49. Li, Y.S., Shan, W., Huang, Z.B., Ge, B.D., Wu, Y., 2008: Experimental study on mechanical behavior of profiled steel sheet-bamboo plywood composite slabs. Journal of Building Structures 29(1): 96-102.
50. McCracken, A., Sadeghian, P., 2018: Corrugated cardboard core sandwich beams with bio-based flax fiber composite skins. Journal of Building Engineering 20: 114-122.
51. Monteiro, S., Martins, J., Magalhães, F.D., Carvalho L., 2018: Lightweight wood composites: challenges, production and performance. In book: Lignocellulosic composite materials. Springer.
52. Mongkollapkit, N., Kositchaiyong, A., Rosarpitak, V., Sombatsompop, N., 2010: Mechanical and morphological properties for sandwich composites of wood/PVC and glass fiber/PVC layers. Journal of Applied Polymer Science116(6): 3427-3436.
53. Mohammadabadi, M., Yadama, V., Yao, L., Bhattacharyya, D., 2018: Low-velocity impact response of wood-strand sandwich panels and their components. Holzforschung 72(8): 681-689.

54. Mirski, R., Dziurka, D., Banaszak, A., 2018: Properties of particleboards produced from various lignocellulosic particles. BioResources 13(4): 7758-7765.
55. Negro, F., Cremonini, C., Zanuttini, R., Properzi, M., Pichelin, F., 2011: A new wood-based lightweight composite for boatbuilding. Wood Research 56(2): 257-266.
56. Noor, A.K., Burton, W.S., Bert, C.W., 1996: Computational models for sandwich panels and shells. Applied Mechanics Reviews 49(3): 155-200.
57. Nilsson, P., Al-Emrani, M., Atashipour S.R., 2017: Transverse shear stiffness of corrugated core steel sandwich panels with dual weld lines. Thin-Walled Structures 117: 98-112.
58. Ou, R.X., Zhao, H., Sui, S.J., Song, Y.M., Wang, Q.W., 2010: Reinforcing effects of Kevlar fiber on the mechanical properties of wood-flour/high-density-polyethylene composites, Composites Part A 41(9): 1272-1278.
59. Okada, R., Kortschot, M.T., 2002: The role of the resin fillet in the delamination of honeycomb sandwich structures. Composites science and technology 62(14): 1811-1819.
60. O'Hegarty, R., West, R., Reilly, A., Kinnane, O., 2019: Composite behaviour of fibre-reinforced concrete sandwich panels with FRP shear connectors. Engineering Structures 198: 1-15.
61. O'Hegarty, R., Kinnane, O., 2020: Review of precast concrete sandwich panels and their innovations. Construction and Building Materials 233: 117145.
62. Ramohalli, K., 1983: Thermochemical response of honeycomb sandwich panels. Journal of fire sciences 1(5): 379-395.
63. Rao, J.P., 2003: Developing situation and prospects on wood-based composites. Journal of Fujian College of Forestry 23(3): 284-287.
64. Renji, K., Nair, P.S., Narayanan, S., 1996: Modal density of composite honeycomb sandwich panels. Journal of Sound and Vibration 195(5): 687-699.
65. Robertson, A., Lam, F., Cole, R., 2012: A comparative cradle-to-gate life cycle assessment of mid-rise office building construction alternatives: laminated timber or reinforced concrete. Buildings 2(3): 245-270.
66. Russ, A., Schwartz, J., Boháček, Š., Lübke, H., Ihnát, V., Pažitný, A., 2013: Reuse of old corrugated cardboard in constructional and thermal insulating boards. Wood Research 58(3): 505-510.
67. Sambrew, S., Semple, K., Smith, G., 2010: Edge reinforcement of honeycomb sandwich panels. Forest Products Journal 60(4): 382-389.
68. Shao, Z.P., 2012: Fracture mechanics of plant fibre (wood and bamboo). Science Press, China.
69. Srinivasan, N., Jayaraman, K., Bhattacharyya, D., 2008: Profile production in multi-veneer sheets by continuous roll forming. Holzforschung 62(4): 453-460.
70. Susainathan, J., Eyma, F., De Luycker, E., Cantarel, A., Castainie, B., 2017: Manufacturing and quasi-static bending behavior of wood-based sandwich structures. Composite Structures 182: 487-504.
71. Susainathan, J., Eyma, F., De Luycker, E., Cantarel, A., Castainie, B., 2018: Experimental investigation of impact behavior of wood-based sandwich structures. Composites Part A 109: 10-19.

72. Sandeep, S.H., Srinivasa, C.V., 2020: Hybrid sandwich panels: A review. International Journal of Applied Mechanics and Engineering 25(3): 64-85.
73. Stocchi, A., Colabella, L., Cisilino, A., Alvarez, V., 2014: Manufacturing and testing of a sandwich panel honeycomb core reinforced with natural-fiber fabrics. Materials and Design 55: 394-403.
74. Teng, X.F., Cao, B.Z., Xu, C., Lu, L.L., Sun, G.D., Cao, R., 2009: Experimental research on cold formed steel OSB floor. Journal of Jilin Institute of Architectural and Civil 26(2): 1-5.
75. Tungjitpornkull, S., Sombatsompop, N., 2009: Processing technique and fiber orientation angle affecting the mechanical properties of E-glass fiber reinforced wood/PVC composites. Journal of Materials Processing Technology 209(6): 3079-3088.
76. Vinson, J.R., 2005: Sandwich structures: past, present, and future. Springer.
77. Vogtländer, J.G., van der Velden, N.M., van der Lugt, P., 2014: Carbon sequestration in LCA, a proposal for a new approach based on the global carbon cycle: cases on wood and on bamboo. The International Journal of Life Cycle Assessment 19(1): 13-23.
78. Vitale, J.P., Francucci, G., Xiong, J., Stocchi, A., 2017: Failure mode maps of natural and synthetic fiber reinforced composite sandwich panels. Composites Part A 94: 217-225.
79. Way, D., Sinha, A., Kamke, F.A., Fujii, J.S., 2016: Evaluation of a wood-strand molded core sandwich panel. Journal of Materials in Civil Engineering 28(9): 04016074.
80. Wang, Y., Fang, H., Liu, W.Q., Qi, Y.J., 2017: Experimental research on the flexural properties of paulownia wood core composite sandwich panel reinforced by lattice webs. Industrial Construction 47(8): 170-174.
81. Wei, B.N., Xu, H.M., Li, T., 2017: Experiment and finite element analysis on reliability of balsa sandwich panels. Journal of Guangxi University (Natural Science Edition) 42(1): 142-147.
82. Wu, Z.Y., Fang, H., Liu, W.Q., Zhu, L., Qi, Y.J., 2015: Experimental study on flexural behavior of paulownia wooden core sandwich composite beam reinforced with lattice web. Fiber Reinforced Plastics/Composites (10): 53-57.
83. Xu, Z.Y., 2007: Properties of the composite material of sandwich construction with wooden faceplate and a paper honeycomb core. Nanjing Forestry University, China.
84. Xiong, W., Qi, Y.J., Liu, W.Q., Shi, D., 2014: Experimental study on flexural performance of pultruded composite sandwich bridge decks. Fiber Reinforced Plastics/Composites 12: 97-100.
85. Yang, D.X., Hu, Y.C., Fan, C.S., 2018: Compression behaviors of wood-based lattice sandwich structures. BioResources 13(3): 6577-6590.
86. Yang, S.L., Liu, W.Q., Fang, H., Wang, L., 2014: Experiment study of composite wall boards with GFRP face sheets and a paulownia wood core. Industrial Construction 44(10): 30-35.
87. Yeniocak, M., Goktas, O., Ozen, E., Gecgel, A., 2016: Improving mechanical and physical properties of particleboard made from vine (*Vitis vinifera* L.) prunings by addition reinforcement materials. Wood Research 61(2): 265-274.

88. Zenkert, D., 1995: An introduction to sandwich construction. Chamelon Press, London, UK.
89. Zhao, L., Liu, L.Q., Zheng, X.Y., Sun, D.X., 2010: Performance study of Yiyang structure plywood under uniform load. Sichuan Building Science 36(1): 22-25.
90. Zhang, Y., Yu, Z.M., Shan, F.R., Shang, J.B., 2012: Characteristic and prediction model of vertical density profile of fiberboard with fiberboard with "pretreatment-hot pressing" united technology. Wood Research 57(4): 613-630.
91. Zolfaghari, A., Behravesh, A.H., Adli, A., 2013: Continuous glass fiber reinforced wood plastic composite in extrusion process: mechanical properties. Materials and Design 51: 701-708.
92. Zou, F., Fang, H., Qi, Y.J., Liu, W.Q., 2017: Preparation and flexural analysis of balsa wood core sandwich composite bridge deck reinforced by lattice webs. Fiber Reinforces Plastics/Composites (3): 44-48.
93. Zhou, T.J., 2017: Study on anti-corrosion performance of ginkgo branch and functional performance of wall materials. Nanjing Forestry University, China.

PEIXING WEI, JINXIANG CHEN*
SOUTHEAST UNIVERSITY
SCHOOL OF CIVIL ENGINEERING
NO.2 SOUTHEAST UNIVERSITY ROAD
NANJING
CHINA 210096
*Corresponding author: chenjpaper@yahoo.co.jp

YUE ZHANG, LIJUN PU
JIANGSU VOCATIONAL COLLEGE OF AGRICULTURE AND FORESTRY
SCHOOL OF LANDSCAPE ARCHITECTURE
NO 19 WENCHANG EAST ROAD
JURONG, JIANGSU
CHINA 212400

WOOD RESEARCH doi.org/10.37763/wr.1336-4561/66.5.891899
e-ISSN 2729-8906
66(5): 2021 891-899 pp.

SHORT NOTES

APPLICATION OF MINERAL FILLER IN MEDIUM DENSITY FIBERBOARD (MDF) AND ITS EFFECT ON MATERIAL PROPERTIES AS A FUNCTION OF PARTICLE SIZE

TOMASZ OZYHAR
OMYA INTERNATIONAL AG
SWITZERLAND

(RECEIVED DECEMBER 2020)

ABSTRACT

The addition of inorganic filler material in medium density fiberboard (MDF) and the effect on material properties as a function of particle size was examined. Medium density fiberboard was manufactured in a laboratory scale environment to a target raw density of 750 kgm^{-3}. Wood fibers were replaced by using calcium carbonate at 3 and 10 wt.% using fillers with weighted median particle sizes of d_{50} = 2.0 μm and d_{50} = 30 μm, respectively. Urea formaldehyde resin was used as binder in all MDF. The influence of filler addition on the modulus of elasticity, bending and tensile strength, dimensional stability and liquid permeability was investigated. The results demonstrate the effect of filler content and its dependence on particle size. The addition of filler with d_{50} = 30 μm does not have any influence on material properties up to a filler content of 10 wt.%. Using the finer filler with d_{50} = 2.0 μm at 10 wt.% filler, the quantity significantly increases the water adsorption and swelling behavior and reduces the strength properties of the MDF.

KEYWORDS: Dimensional stability, liquid permeability, mechanical properties, medium density fiberboard (MDF), mineral filler, particle size, urea formaldehyde.

INTRODUCTION

Medium density fiberboard (MDF) usually consists of wood as the main raw material, complemented by typically 3 to 15% of a thermoset adhesive (solid resin based on dry mass of wood) and, depending on the final composition, selected additional additives such as hardener, water repellents, dies and inks, etc. (Rowell 2012). In contrast, inorganic minerals are rarely used in this kind of application and have received little attention. Limited studies on the use of inorganic minerals in engineered wood base panels have focused predominantly on improving the fire resistance properties by incorporating inorganic minerals such as aluminum trihydrate

(ATH) (Hashim et al. 2005, Redwan et al. 2015), nanoclay (Zahedsheijani et al. 2012) or expanded vermiculite (Wang et al. 2016). At the same time, the application of mineral fillers, especially calcium carbonate as a cost competitive material to replace cellulose fiber, with the goal to reduce manufacturing cost, is well known in the paper industry (Hubby and Gill 2016). Considering the obvious similarities in the structure of MDF and paper, it is somehow striking that a similar concept, i.e. the potential utilization of calcium carbonate as a filler to partially replace wood fibers has not been investigated in detail until now. Only recently, the use of a mineral additives as a partial substitute for wood material in MDF and particle board was suggested in Ozyhar 2020 and Ozyhar et. al 2020. While the authors have investigated the influence of calcium carbonate addition on basic material properties in relation to addition quantity, the effect from particle size on properties including the mechanical strength or water absorption, remains unanswered. However, particle size of the mineral filler is a known factor which have been shown to be critical to strength development in paper (Bown 1998, Hubby and Gill 2016).

The following study was aimed to create a basic understanding regarding the potential for use of an inorganic filler as a partial replacement for wood fibers in MDF. Specifically, the main goal was to evaluate the influence of calcium carbonate addition on the material properties of MDF as a function of particle size.

MATERIAL AND METHODS

Materials

Fresh wood fibers, obtained from pine wood chips, were used for MDF manufacturing. These were broken down in a refiner at 9 bar for 3 to 4 min. The sieve analysis of the fiber material measured by fractioning through sieve analysis in an air jet sieve Alpine e200 LS of HOSOKAWA ALPINE AG, Germany, revealed that 97% were smaller than 2.0 mm, 86% smaller than 1.0 mm and 33% smaller than 0.2 mm, respectively. Two ground calcium carbonate (GCC) fillers with differing particle sizes were used. A finer filler with weighted median particle size d_{50} = 2.0 µm and surface area of 2.7 m^2 (FGCC) and a coarser filler with weighted median particle size d_{50} = 30.0 µm and surface area of 1.2 m^2 (CGCC). A formaldehyde resin, Kaurit 350 supplied by BASF AG and a hydrophobing agent, Hydrowax 138 supplied by SASOL GmbH were used in this study.

Methods

Four different MDF variants were manufactured by replacing the respective amount of wood fibers by weight using calcium carbonate fillers with filler quantities of 3 and 10 wt.% and the different particle sizes, fine (FGCC) and coarse (CGCC), respectively. MDF with a target density of 750 $kg \cdot m^{-3}$ was manufactured in a laboratory scale environment by mixing the fibers in a paddle mixer with 10 wt.% urea formaldehyde resin and 0.5 wt.% hydrophobing agent (based on wood fibers). Calcium carbonate was added in powder form to the paddle mixer and mixed with the fiber after the urea formaldehyde resin had been applied to fiber. MDF with target density of 750 $kg \cdot m^{-3}$ was manufactured in laboratory scale environment by mixing the fibers in

a paddle mixer with 10 wt.% urea formaldehyde resin and 0.5 wt.% hydrophobing agent (based on wood fibers). The fiber/filler mix was then pressed into a 460 x 440 mm^2 solid board of 17.5 mm thickness at a temperature of 220°C using a press time factor of 12 $s \cdot mm^{-1}$. The boards were then sanded to dimensions of 400 x 380 mm^2 and final thickness of 16 mm.

Internal bond strength (IB), bending strength (BS) and modulus of elasticity in bending (MOE), water absorption (WA) and thickness swelling (TS) behavior after 24h and the raw density were determined on the samples acclimatized at 20ºC and relative humidity of 65% following the procedures described in DIN EN 310 (1993), DIN EN 317 (1993), DIN EN 319 (1993) and DIN EN 323 (1993). In addition, liquid permeability was determined on 4 samples for each variant following the test method described in Ozyhar et. al (2020).

RESULTS AND DISCUSSION

To ensure homogeneity between the filler addition and the fibers, resin was added to the fibers prior to adding the filler to guarantee the adherence of the filler to the fibers. The filler distribution in the fiber matrix was investigated visually using SEM images, with specific interest on any potential agglomeration of particles that could influence locally the material strength and other properties. The uniform distribution of calcium carbonate filler in the wood fiber matrix, as shown in Fig. 1, eliminates the potential influence of uneven filler distribution or agglomeration on the material properties.

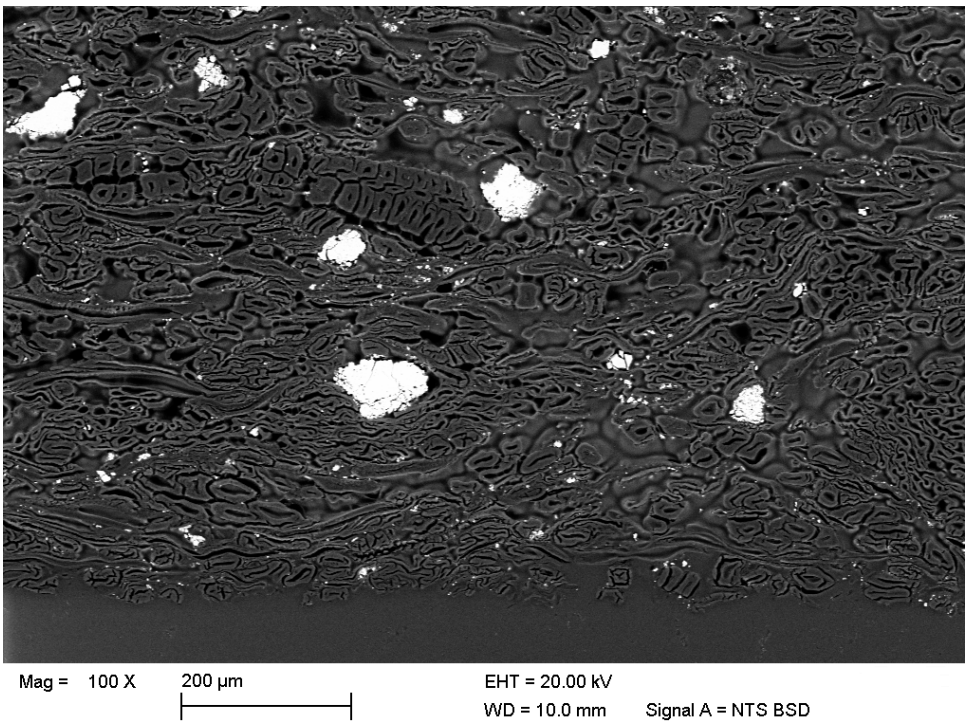

Fig. 1: Scanning electron micrograph (SEM) of cross section of medium density fiberboard (MDF) with addition of 10 wt.% of coarse calcium carbonate (CGCC) as filler.

Filler effect on mechanical properties

The influence of calcium carbonate addition as a filler material in MDF on the material properties measured is summarized in Tab. 1. The results demonstrate that filler content has an effect on the material properties and there is a dependence on the particle size.

Tab. 1: Material properties of medium density fiberboard (MDF) with 3 and 10 wt.% of calcium carbonate as filler.

Material property		Sample nomenclature				
		0% filler	3% filler		10% filler	
		Reference MDF	FGCC	CGCC	FGCC	CGCC
Raw density (kg·m^{-3})	$\bar{x}$ (CV%)	770 (2.2)	767 (1.8)	778 (1.8)	763 (2.3)	761 (3.0)
	n (-)	10	10	10	10	10
BS (Nmm^{-2})	$\bar{x}$ (CV%)	3.77 (7.1)	30.8 (4.9)	30.7 (3.6)	30.4 (5.0)	35.6 (5.3)
	n (-)	6	6	6	6	6
IB (Nmm^{-2})	$\bar{x}$ (CV%)	1.66 (4.2)	1.59 (5.3)	1.62 (3.5)	1.23 (5.5)	1.67 (3.0)
	n (-)	10	10	10	10	10
MOE (Nmm^{-2})	$\bar{x}$ (CV%)	3310 (5.6)	3327 (3.7)	3253 (3.4)	2902 (4.6)	3030 (4.9)
	n (-)	6	6	6	6	6
WA (%)	$\bar{x}$ (CV%)	20.6 (11.4)	24.0 (11.4)	22.4 (5.0)	31.5 (7.3)	24.8 (7.3)
	n (-)	10	10	10	10	10
TS (%)	$\bar{x}$ (CV%)	6.1 (9.1)	6.4 (5.5)	6.1 (2.8)	8.3 (4.4)	6.5 (3.7)
	n (-)	10	10	10	10	10
Permeability (10^{-13}·m^2)	$\bar{x}$ CV(%)	2.2 (15.4)	2.0 (10.3)	2.0 (30.4)	3.5 (28.0)	3.3 (13.4)
	n (-)	4	4	4	4	4

Note: $\bar{x}$ - arithmetic mean, CV - coefficient of variation, n - number of specimens, FGCC - fine ground calcium carbonate, CGCC - coarse ground calcium carbonate, BS - bending strength, IB - internal bond strength, MOE - modulus of elasticity, WA - water adsorption, TS - thickness swelling.

The relationship becomes most evident for the mechanical properties bending and internal bond strength (Figs. 2a,b). Addition of CGCC filler does not have a significant effect on the strength properties up to a filler content of 10 wt.%. However, strength properties are affected significantly at loading levels of 10 wt.% when using FGCC indicating that effect from filler content depends on particle size.

It is suggested that the mechanical strength behavior seen is directly related to the surface area of the particles and the adhesive bond formation between wood fibers, directly related to

strength. The FGCC has a surface area more than double that of the CGCC, 2.7 m^2g^{-1} and 1.2 m^2g^{-1}, respectively.

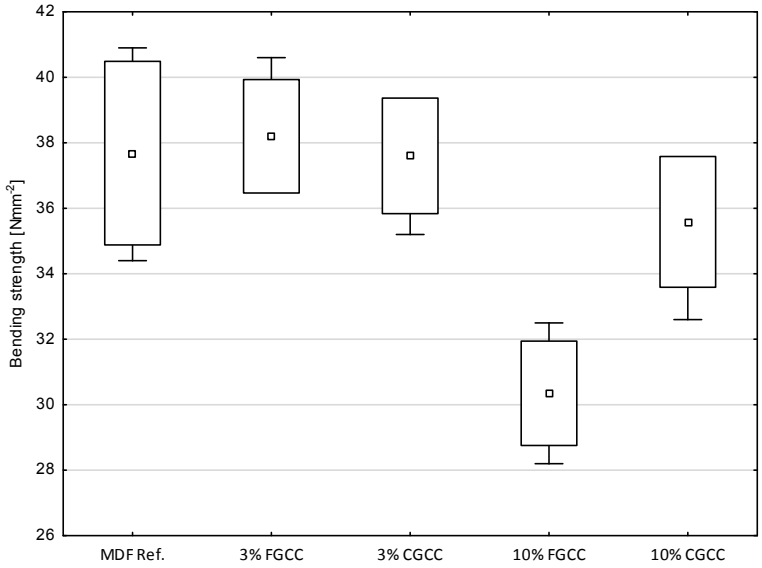

a)

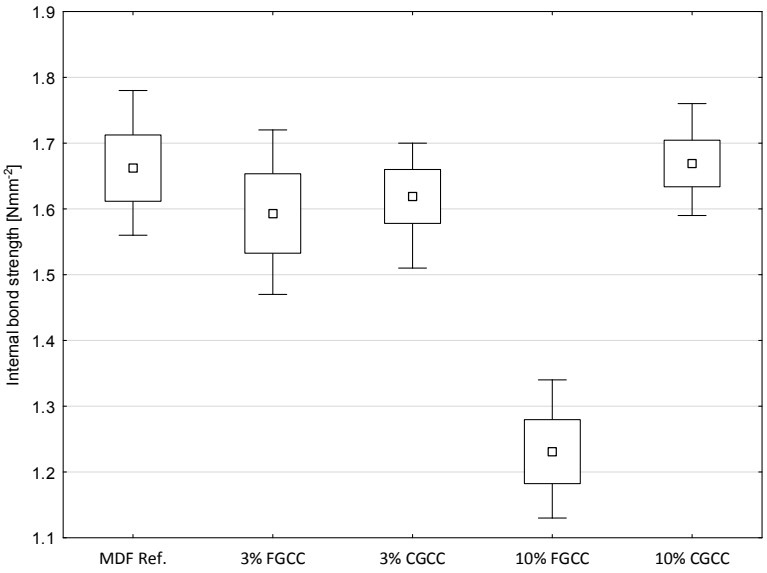

b)

Fig. 2: a) Bending strength and b) internal bond strength as function filler content and filler particle size. Whiskers show minimum and maximum values, square in box displays arithmetic mean value, box boundaries display mean +/- 0.95 conf. interval. MDF. Ref. (medium density fiberboard without filler addition); FGCC and CGCC refer to fine and coarse ground calcium carbonate, resp.

The FGCC particles are believed to affect the adhesive bond formation to a much higher extent firstly by reducing the surface available on the wood fibers for bond formation and mechanically disturbing the wood fibers themselves. Secondly, the FGCC particles adsorb and "consume" more resin per unit mass with increasing surface area thus reducing the available resin for fiber bond formation.

The high surface area, in combination with an expected negative effect on UF curing associated with alkaline surface pH of calcium carbonate is believed to be the main reason for decline in strength seen with decreasing particle size. The negative effect of increased pH on curing kinetics of UF and bond formation have been demonstrated previously (Johns and Niazi 1980, Pizzi 2003).

Filler effect on physical properties

The effect of filler addition on the dimensional stability of MDF is clearly demonstrated by the thickness swelling measurement (Fig. 3a).

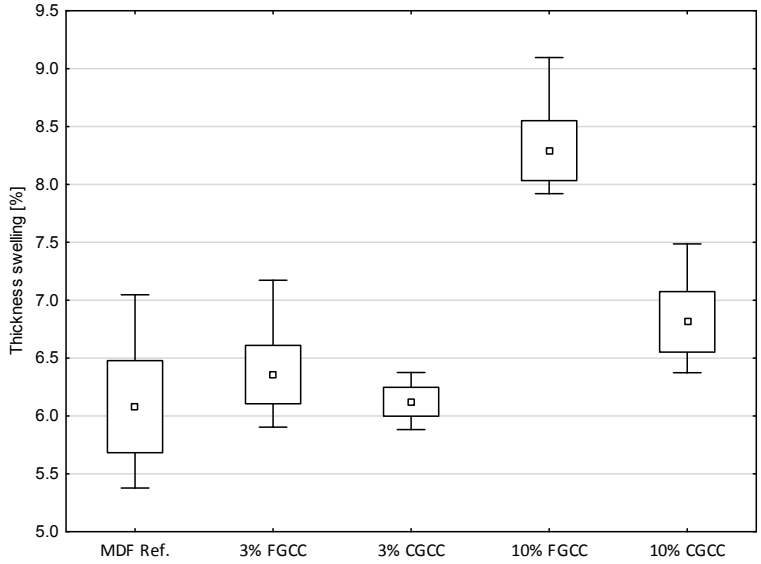

a)

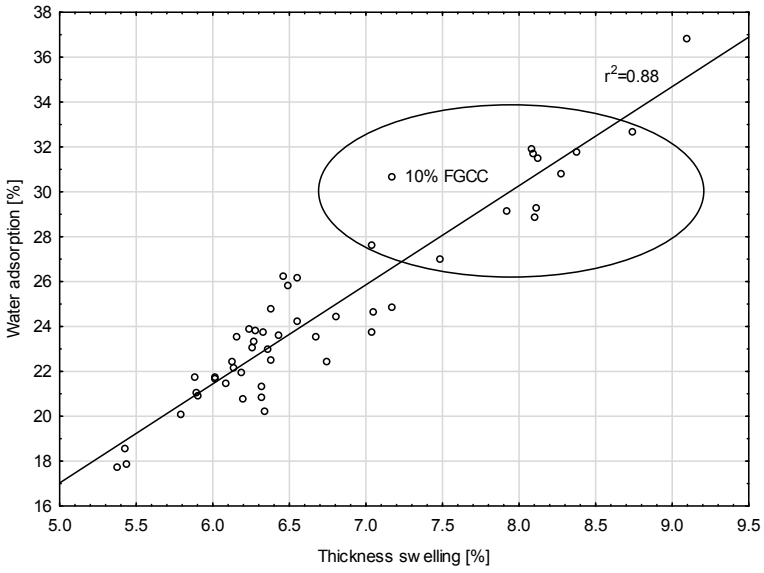

b)

Fig. 3: Thickness swelling of MDF with addition of calcium carbonate as function of filler-content and particle size. Whiskers show minimum and maximum values, square in box displays arithmetic mean value, box boundaries display mean +/- 0.95 conf. interval. b) Relationship between water adsorption and swelling behavior for caused by calcium carbonate addition.

MDF. Ref. (medium density fiberboard without filler addition); FGCC and CGCC refer to fine and coarse ground calcium carbonate, resp.

Only at the higher loading level is there any change in TS. The small increase in thickness measured at 10 wt.% for the CGCC is not statistically significant, therefore, no effect on thickness swelling is concluded for this sample. Fine GCC filler, on the other hand, when applied at 10 wt.%, increases the corresponding TS significantly. The TS is, therefore, effected by the filler content percentage and depends on the particle size. Fig. 3b shows the water adsorption following an almost linear trend in relation to the thickness swelling. The results show that by adding FGCC filler to MDF the water uptake increases and correlates closely with increasing thickness swelling.

The findings are contradictory to what expected by replacing 10% of hydrophobic wood fibers with inorganic material, i.e. decreased swelling due to less hydrophobic material available. This is likely due to the increased liquid permeability of the MDF at a filler addition level of 10 wt.% (Fig. 4).

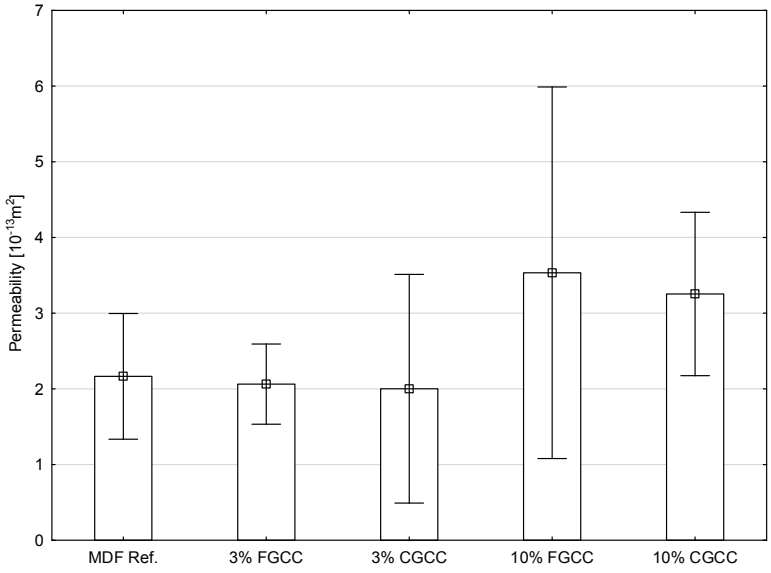

Fig. 4: Permeability of medium density fiberboards with 3 and 10 wt.% calcium carbonate addition as filler. Whiskers show conf. interval at 0.95 level, square in box displays arithmetic mean value. MDF. Ref. (medium density fiberboard without filler addition); FGCC and CGCC refer to fine and coarse ground calcium carbonate, resp.

An increased water uptake was expected for MDF panels at 10 wt.% filler content based on liquid permeability values measured using hexadecane, a method known to determine liquid permeability in paper materials (Ridgway and Gane 2003). The higher permeability values of the MDF with the higher filler addition when compared with control panel, can be explained by the packing density of the fiber-filler furnish and the much higher density of the filler. Having a higher density, calcium carbonate occupying less volume increases the theoretical porosity and consequently the permeability at constant volume and mass of panel.

CONCLUSIONS

The results of this study prove that the addition of calcium carbonate (GCC) as a filler in MDF has an effect on the material properties studied here. Filler quantity and particle size play an important role. The results demonstrate that the filler with weighted median particle size (d_{50}) of 30 µm of up to 10 wt.% can be added to MDF without effecting the material properties. However, addition of GCC filler consisting of small particles with particle size $d_{50} \leq 2$ µm has a significant effect on all material properties leading to a decrease in the mechanical properties and an increase in the water adsorption and swelling thickness, believed to be caused by increased permeability.

ACKNOWLEDGMENTS

The author would like to express his deepest gratitude to Mr. Weber and Mr. Direske from Institut für Holztechnologie Dresden (IHD) for supervising of manufacturing of MDF samples and determination of material properties. Special thanks go to Dr. Ridgway for performing the permeability measurements and reviewing the manuscript.

REFERENCES

1. Bown, R., 1998: Particle size, shape and structure of paper fillers and their effect on paper properties. Paper Technology (39): 44-48.
2. DIN EN 310, 1993: Wood-based panels. Determination of modulus of elasticity in bending and of bending strength.
3. DIN EN 317, 1993: Particleboards and fiberboards. Determination of swelling in thickness after immersion in water .
4. DIN EN 319, 1993: Particleboards and fiberboards. Determination of tensile strength perpendicular to the plane of the board.
5. DIN EN 323, 1993: Wood-based panels. Determination of density.
6. Hashim, R., How, L.S., Kumar, R.N., Sulaiman, O., 2005: Some of the properties of flame retardant medium density fiberboard made from rubberwood and recycled containers containing aluminum trihydroxide. Bioresources Technology 96: 1826-31.
7. Hubbe, M.A., Gill, R.A., 2016: Fillers for papermaking: A review of their properties, usage practices, and their mechanistic role. BioResources 11: 2886-2963.
8. Johns, W.E., Niazi, K.A., 1980: Effect of pH and buffering capacity of wood on the relation time of urea formaldehyde resin. Wood and Fiber Science 12: 255-263.
9. Ozyhar, T., 2020: Application of mineral filler in surface layer of three-layer particle board and its effect on material properties as a function of filler content. International Wood Products Journal 11(3): 109-114.

10. Ozyhar, T., Depnering, T., Ridgway, C., Welker, M., Schoelkopf, J., Mayer, I., Thoemen, H., 2020: Utilization of inorganic mineral filler material as partial replacement for wood fiber in medium density fiberboard (MDF) and its effect on material properties. European Journal of Wood and Wood Products 78(1): 75–84.
11. Redwan, A.M., Badri, K.H., Tarawneh, M., 2015: The effect of aluminium hydroxide (ATH) on the mechanical properties and fire resistivity of palm-based fibreboard prepared by pre-polymerization method. Advanced Materials Research 1087: 287-292.
12. Pizzi, A., 2003: Urea–formaldehyde adhesives. In: Handbook of adhesive technology, second edition, revised and expanded. Eds. Pizzi A., Mittal, K.L. Pp 613-631, CRC Press, New York, NY.
13. Ridgway, C.J., Gane, P.A.C., 2003: Bulk density measurement and coating porosity calculation for coated paper samples. Nordic Pulp & Paper Research Journal 18: 24–31.
14. Rowell, R.M., 2012: Handbook of wood chemistry and wood composites. 2nd Edition. Pp 321-413, CRC Press, Boca Raton.
15. Wang, J., Wang, F., Gao, Z., Zheng, M., Sun, J., 2016: Flame retardant medium-density fiberboard with expanded vermiculite. BioResources. 11: 6940-6947.

*TOMASZ OZYHAR
OMYA INTERNATIONAL AG
RESEARCH AND DEVELOPMENT SERVICES
FROSCHACKERSTRASSE 6
EGERKINGEN
SWITZERLAND
*Corresponding author: tomasz.ozyhar@omya.com